Dispersion relations for extinction of acoustic and electromagnetic waves

Sohl, Christian

2007

Dispersion Relations for Extinction of Acoustic and Electromagnetic Waves

Christian Sohl

Licentiate Thesis
Electromagnetic Theory

Lund University
Lund, Sweden
2007

Department of Electrical and Information Technology
Electromagnetic Theory
Lund University
P.O. Box 118, S-221 00 Lund, Sweden

Series of licentiate and doctoral theses
No. 69
ISSN 1402-8662

This thesis is prepared with LaTeX 2_ε
Printed in Sweden by Tryckeriet i E-huset, Lund University
Lund, August 2007

When I am judging a theory, I ask myself whether, if I were God, I would have arranged the world in such a way.

Albert Einstein

"The New Quotable Einstein", Chapter XVII

Abstract

This thesis deals with physical limitations on scattering and absorption of acoustic and electromagnetic waves. A general dispersion relation for the extinction cross section of such waves is derived from the holomorphic properties of the scattering amplitude in the forward direction. The result states that for a given volume, there is only a limited amount of scattering and absorption available in the entire frequency range. The dispersion relation is shown to be valuable for a broad range of problems in theoretical physics involving wave interaction with matter over a frequency interval.

The theory of broadband extinction of electromagnetic waves is also applied to a large class of causal and reciprocal antennas to establish physical realizability and upper bounds on bandwidth and directive properties. The results are compared with classical limitations based on eigenfunction expansions, and shown to provide sharper inequalities and, more importantly, a new fundamental understanding of antenna dynamics solely based on static properties. In modeling of metamaterials, the theory implies that for a narrow frequency band, engineered composite materials may possess extraordinary characteristics, but tradeoffs are necessary to increase its bandwidth.

Sammanfattning (in Swedish)

Avhandlingen behandlar fysikaliska begränsningar på spridning och absorption av akustiska och elektromagnetiska vågor. En dispersionsrelation för utsläckningstvärsnittet för akustisk och elektromagnetisk vågrörelse härleds från analytiska egenskaper på spridningsamplituden i framåtriktningen. Slutsatsen är att det för en given växelverkande volym endast finns en begränsad mängd spridning och absorption att tillgå i hela frekvensspektrum. Dispersionsrelationen visar sig vara ett värdefullt verktyg för en bred samling problem i teoretisk fysik med koppling till växelverkan av vågrörelse med materia över ett frekvensintervall.

Teorin för elektromagnetiska vågors utsläckning tillämpas också på en stor klass av kausala och reciproka antenner för att fastställa realiserbarhet och övre begränsningar på bandbredd och riktningsberoende egenskaper. Resultaten jämförs med klassiska begränsningar baserade på egenfunktionsutvecklingar, och där visar resultaten ge såväl skarpare olikheter på antennprestanda som en ny fundamental förståelse för antenners dynamik endast i termer av statiska egenskaper. För materialmodellering medför teorin att artificiella material mycket väl kan uppvisa en överdådig karakeristik för ett smalt frekvensintervall, men att kompromisser är nödvändiga för att öka deras bandbredd.

List of included papers

This thesis consists of a General Introduction and the following scientific papers:

I. C. Sohl, M. Gustafsson, and G. Kristensson. Physical limitations on broadband scattering by heterogeneous obstacles. Technical Report LUTEDX/(TEAT-7151)/1–25/(2006), Lund University. Accepted for publication in *Journal of Physics A: Mathematical and Theoretical* **40**, 11165–11182, 2007.

II. C. Sohl, M. Gustafsson, and G. Kristensson. Physical limitations on metamaterials: Restrictions on scattering and absorption over a frequency interval. Technical Report LUTEDX/(TEAT-7154)/1–11/(2007), Lund University.

III. C. Sohl, M. Gustafsson, and G. Kristensson. The integrated extinction for broadband scattering of acoustic waves. Technical Report LUTEDX/(TEAT-7156)/1–10/(2007), Lund University.

IV. M. Gustafsson, C. Sohl, and G. Kristensson. Physical limitations on antennas of arbitrary shape. Technical Report LUTEDX/(TEAT-7153)/1–36/(2007), Lund University. First part of this paper is published in *Proceedings of the Royal Society A: Mathematical, Physical & Engineering Sciences* **463**, 2589–2607, 2007.

V. C. Sohl, M. Gustafsson, and G. Kristensson. A survey of isoperimetric limitations on antennas. Technical Report LUTEDX/(TEAT-7157)/1–9/(2007), Lund University. Also published by 19th International Conference on Applied Electromagnetics and Communications (ICECom 2007), Dubrovnik, Croatia, September 24–26, 2007.

VI. C. Sohl, C. Larsson, M. Gustafsson, and G. Kristensson. A scattering and absorption identity for metamaterials — experimental results and comparison with theory. Technical Report LUTEDX/(TEAT-7158)/1–9/(2007), Lund University.

Papers II, III and VI are submitted for publication in scientific journals.

Other publications by the author

The following scientific papers are excluded from the thesis:

VII. C. Sohl, M. Gustafsson, and G. Kristensson. Bounds on metamaterials in scattering and antenna problems. 2nd European Conference on Antennas and Propagation (EuCAP 2007), Edinburgh, United Kingdom, November 11–16, 2007.

VIII. M. Gustafsson, C. Sohl, and G. Kristensson. Physical limitations on scattering and absorption of antennas. 2nd European Conference on Antennas and Propagation (EuCAP 2007), Edinburgh, United Kingdom, November 11–16, 2007.

IX. C. Sohl, M. Gustafsson, and G. Kristensson. Physical limitations on broadband scattering. URSI International Symposium on Electromagnetic Theory (EMTS 2007), Ottawa, Canada, July 26–28, 2007.[1]

X. C. Sohl, M. Gustafsson, and G. Kristensson. Physical limitations on G and B for antennas. URSI International Symposium on Electromagnetic Theory (EMTS 2007), Ottawa, Canada, July 26–28, 2007.

XI. M. Gustafsson, C. Sohl, and G. Kristensson. Physical limitations on D/Q for antennas. URSI International Symposium on Electromagnetic Theory (EMTS 2007), Ottawa, Canada, July 26–28, 2007.

XII. G. Kristensson, C. Sohl, and M. Gustafsson. New physical limitations in scattering and antenna problems. URSI International Symposium on Electromagnetic Theory (EMTS 2007), Ottawa, Canada, July 26–28, 2007.

[1] Awarded with a Young Scientist Award at the URSI International Symposium on Electromagnetic Theory (EMTS 2007), Ottawa, Canada, July 26–28, 2007.

Summary of included papers

The main thread of this thesis is a forward dispersion relation for the extinction of acoustic and electromagnetic waves. The included papers focus on various consequences of this summation rule applied to scattering theory, material modeling and antenna problems.

Paper I

This paper deals with physical limitations on scattering and absorption of electromagnetic waves over a frequency interval. The direct scattering problem addressed here is plane-wave illumination of a bounded obstacle of arbitrary shape. The scatterer is modeled by a general set of linear and passive constitutive relations including both heterogeneous and anisotropic material models. A forward dispersion relation for the extinction cross section is derived in terms of the static polarizability dyadics, and various isoperimetric bounds are presented for scattering and absorption over a frequency interval. The theoretical results are exemplified by numerical simulations with excellent agreement.

The author of this dissertation carried out most of the analysis and the numerical simulations.

Paper II

This paper is an application of the physical limitations on scattering and absorption in Paper I. The paper focuses on temporally dispersive material models which attain negative values of the real part of the permittivity and/or the permeability, *i.e.*, metamaterials. It is concluded that for a single frequency, metamaterials may possess extraordinary properties, but with respect to a frequency interval such materials are no different from any other naturally formed substances as long as causality is obeyed. As a consequence, if metamaterials are used to lower the resonance frequency, this is done at the expense of an increasing Q-factor of the resonance. The theory is illustrated by numerical simulations for a stratified sphere and a prolate spheroid using the classical Lorentz and Drude dispersion models.

The author of this dissertation carried out most of the analysis and is responsible for the numerical simulations.

Paper III

This paper focuses on a forward dispersion relation for the combined effect of scattering and absorption of acoustic waves. The derivation is similar to the one for the electromagnetic waves in Paper I, but additional challenges are introduced when extending the summation rule to acoustic waves. The effect of both permeable and

impermeable boundary conditions are presented, and it is concluded that the forward dispersion relation is applicable to the Neumann and transmission problems, whereas the analysis fails for the Dirichlet and Robin boundary conditions. The theory is exemplified by both permeable and impermeable scatterers with homogeneous and isotropic material properties.

The author of this dissertation carried out a major part of the analysis.

Paper IV

This paper addresses physical limitations on bandwidth, realized gain, Q-factor, and directivity for antennas of arbitrary shape. Based on the forward dispersion relation in Paper I, the product of bandwidth and realizable gain is shown to be bounded from above by the eigenvalues of the long wavelength high-contrast polarizability dyadics. These dyadics are proportional to the antenna volume and easily determined for geometries of arbitrary shape. Ellipsoidal antenna volumes are analyzed in detail and numerical results for some generic antenna geometries are presented. The theory is verified against the classical Chu limitations, and shown to yield sharper bounds for the ratio of the directivity and the Q-factor for non-spherical geometries.

The author of this dissertation contributed both to the analysis and the numerical examples.

Paper V

This paper provides additional theoretical and numerical results on the physical limitations on antennas in Paper IV. In particular, the interplay between directive properties and bandwidth is discussed when metamaterials are introduced in the antenna design. Numerical simulations of a monopole antenna with a finite ground plane are presented and shown to be in astonishing agreement with the theoretical bounds.

The author of this dissertation carried out most of the analysis.

Paper VI

This paper presents measurement results on the combined effect of scattering and absorption of electromagnetic waves by a fabricated sample of metamaterial. This engineered composite material, designed as a planar array of capacitive and inductive coupled resonators, is commonly referred to in the literature as a negative permittivity metamaterial. Recent bounds on material modeling presented in Paper II are reviewed and compared with the outcome of the measurements. The experimental results are shown to be in good agreement with the theory.

The author of this dissertation carried out a major part of the analysis.

Preface

This thesis for the degree of Licentiate in Engineering summarizes two years of research I have conducted at the Dept. of Electrical and Information Technology, and formerly the Dept. of Electroscience, within Lund University, Sweden. Although I started the doctoral studies in February 2005, most of the results presented here were obtained during the fall 2006 and spring 2007. In fact, this particular research field in the borderland between classical electrodynamics and general wave mechanics has turned out to be a true grain of gold offering many stimulating problems. Some open questions that will be addressed in the future are pointed out in the General Introduction and the included papers.

Sölvesborg, July 2007 Christian Sohl

Acknowledgments

I would like to express my deepest gratitude to my supervisors Mats Gustafsson and Gerhard Kristensson for invaluable guidance and support during the past two years. I am particularly grateful for our pleasant collaboration and their good taste in choosing stimulating research problems. Mats has been a true source of inspiration and I sincerely admire his great intuition in our many delightful discussions on physical problems. Despite the many duties, Gerhard has always offered me time, and his excellent theoretical skills has been a major reason for me to leave modern physics and join the Electromagnetic Theory group. I also thank Christer Larsson for fruitful discussions and collaboration on metamaterials, and Carl-Gustaf Svensson for generous hospitality in connection with the extinction measurements at Saab Bofors Dynamics, Linköping, 19 April, 2007. I am also grateful to Klas Malmqvist for solving the pitiable financial problems I encountered during the employment freeze at Lund University in February 2005.

I also thank Anders Karlsson for discussions on the T-matrix approach as well as reading and criticizing some of the manuscripts, Anders Melin for sharing his impressive knowledge in mathematics, Anders Derneryd for discussions on antennas from an industrial point of view, Daniel Sjöberg for assistance with LaTeX, Elsbieta Szybicka for solving many practical problems, Richard Lundin for sharing his excellence in teaching, Sten Rikte for introducing me to classical electrodynamics in 2004, Lars Hedenstjerna for constructing a plate capacitor for polarizability measurements, and Leif Karlsson and Erik Jonsson for general computer assistance. I am also grateful to Alireza Kazemzadeh, Peter Johannesson, and Kristin Persson for providing a stimulating atmosphere as a doctoral student, and the former colleague Christian Engström for sharing the authors interest in mathematics.

The financial support of this thesis by the Swedish Research Council is gratefully acknowledged. Travel grants from Sigfrid and Walborg Nordkvist's foundation for participation in the European School of Antennas *MIMO Communication Systems and Antennas* in Stockholm, September 5–9, 2005, and *Computational EM for Antenna Analysis* in Torino, September 19–23, 2005, are also acknowledged.

Last, but not least, I would like to thank family and friends, especially my parents Lena and Per, for monitoring me from doing too much research.

Contents

General Introduction

Christian Sohl

... "There's the King's Messenger. He's in prison now, being punished: and the trial doesn't even begin till next Wednesday: and of course the crime comes last of all."

"Suppose he never commits the crime?" said Alice.

Lewis Carroll

"Through the Looking Glass", Chapter V

1 Introduction

Since the introduction of the Kramers-Kronig relations in Refs. 7 and 25 concerning propagation of light in lossy dielectric media, dispersion relation techniques have been applied successfully to several fields of physics to establish information about the nature of particle collisions and wave interaction with matter.[1] The underlying idea of dispersion relations is that certain physical amplitudes with experimental significance are boundary values of holomorphic functions of one or more complex variables. The holomorphic nature of these amplitudes are closely connected with the principle of causality in the form of time ordered events. In fact, there are at least two remarkable features of dispersion relations: i) they provide a consistency check if the quantities involved are either measured or calculated, and ii) they may be used to verify whether a given physical model or an experimental outcome is causal or not.

The objective of this General Introduction is to illustrate the importance of causality for propagation of acoustic and electromagnetic waves. Several applications to material modeling and scattering problems are presented. Linear systems obeying causality are also crucial in various fields of electrical engineering such as network theory and broadband circuit design, see Refs. 5 and 11. Dispersion relations with a somewhat different causality condition in terms of local commutativity of field operators also play a fundamental role in quantum field theory, see Refs. 37 and 38.

2 Causality and holomorphic properties

This section introduces some elementary properties of linear time-translational invariant systems obeying primitive causality. In particular, the damped harmonic oscillator in classical mechanics is analyzed, and the Kramers-Kronig relations for light propagation in a dielectric medium are derived. The exposition on the damped harmonic oscillator follows the outline in Ref. 35 and Problem 3.39 in Ref. 37, whereas Refs. 19 and 20 have been valuable for the preparation of the Kramers-Kronig relations. Other important references are Refs. 17, 27, 28, 34, 42 and 47.

[1] Dispersion relations should not be confused with the connection between energy and momentum, or wave propagation in time and space, which also bear the same name in wave mechanics. Neither should the term be confused with dispersion models for temporally dispersive matter, *e.g.*, the Lorentz model in classical electrodynamics, see Sec. 2.6.

2.1 Elementary considerations

Consider an arbitrary physical system subject to an external time-dependent action or input $f(t)$, to which the system responds by producing a cause or output $x(t)$. The internal properties of the system are unspecified except for the following general assumptions:

$\alpha)$ the output $x(t)$ is a linear functional of the input $f(t)$, *i.e.*,

$$x(t) = \int_{-\infty}^{\infty} g(t,t')f(t')\ \mathrm{d}t',$$

where the kernel $g(t,t')$ is the impulse response of the system at time t when subject to an input at time t';

$\beta)$ the internal properties of the system are independent of time,[2] *i.e.*, $g(t,t') = g(t-t')$, or equivalently, if the input $f(t)$ is advanced or delayed by some time interval, the same shift in time interval occurs for the output $x(t)$;

$\gamma)$ the system is subject to time-ordered events in the sense that the output $x(t)$ cannot precede the input $f(t)$, *i.e.*, $g(\tau) = 0$ for $\tau < 0$.

The conditions $\alpha)$, $\beta)$ and $\gamma)$ refer to linearity or superposition, time-translational invariance, and primitive causality, respectively. In contrast to primitive causality, there is also a relativistic causality condition which states that no signal can propagate with velocity greater than the speed of light in vacuum. However, the relativistic causality condition is less general than the primitive since it depends on the existence of a limiting velocity. Only the primitive causality condition is therefore addressed in this thesis. Furthermore, non-linear equations of motion are excluded due to the complication of finding appropriate functionals modeling such systems. Non-linear systems may also possess self-excitation.

The three conditions $\alpha)$, $\beta)$ and $\gamma)$ have far-reaching consequences on the Fourier transform of $g(t)$, *i.e.*,

$$G(\omega) = \int_{0}^{\infty} g(\tau)\mathrm{e}^{\mathrm{i}\omega\tau}\ \mathrm{d}\tau. \tag{2.1}$$

The convergence of (2.1) is guaranteed if, for example, $g(\tau)$ is absolutely integrable on the real axis. However, this assumption can be relaxed be introducing the class of temperate distributions, see Ref. 18. Throughout this thesis, it is assumed that $g(\tau)$ vanishes sufficiently rapid at infinity such that (2.1) is well-defined. Under the assumption of absolute integrability, the fact that $g(\tau)$ only has support on the positive real axis implies that (2.1) defines a holomorphic function in the upper half of the ω-plane. The idea is made plausible by observing that the exponential function in (2.1) significantly improves the convergence of the Fourier integral for $\mathrm{Im}\,\omega > 0$. The holomorphic properties of $G(\omega)$, or equivalently, the presence of no singularities in the upper half of the ω-plane, is thus seen to be a direct consequence

[2] Throughout this thesis, no distinction in notation is made between the one and two variable functions $g(t,t')$ and $g(\tau)$, where $\tau = t - t'$.

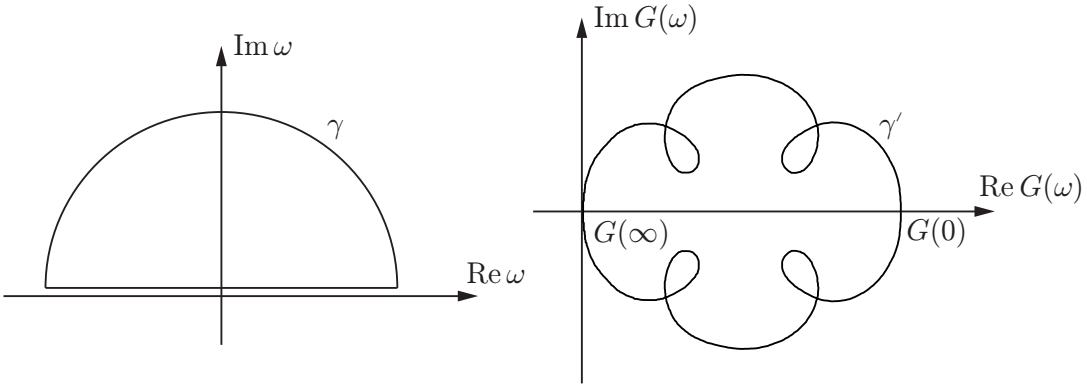

Figure 1: Contours in the complex ω-plane (left figure) and the complex $G(\omega)$-plane (right figure) in the proof of Meĭman's theorem.

of the causality condition.[3] Also note that by complex conjugating both sides of (2.1) and invoking that $g(\tau)$ is real-valued, one obtains for $\mathrm{Im}\,\omega \geq 0$,

$$G(-\omega^*) = G^*(\omega), \tag{2.2}$$

where an asterisk denotes the complex conjugate. The cross symmetry (2.2) implies that the real part of $G(\omega)$ is even and the imaginary part of $G(\omega)$ is odd with respect to the imaginary axis. In particular, $G(\omega)$ take real values on the imaginary axis.

Passivity or energy dissipation often implies restrictions on the imaginary part of $G(\omega)$. Extended to the upper half of the ω-plane, the passivity condition states that, see Ref. 15,

$$\mathrm{Im}(\omega G(\omega)) \geq 0. \tag{2.3}$$

In particular, (2.3) implies that $\mathrm{Im}\,G(\omega) \geq 0$ for $\omega > 0$ and $\mathrm{Im}\,G(\omega) \leq 0$ for $\omega < 0$. Note that (2.3) is consistent with (2.2) in the sense that if the passivity condition holds for $\mathrm{Re}\,\omega > 0$, the cross symmetry implies that it is also valid for $\mathrm{Re}\,\omega < 0$. A function like $G(\omega)$ which is holomorphic in the upper half of the ω-plane and there satisfies (2.3) is called a Herglotz function. A general representation of Herglotz functions in terms of a Riemann-Stieltjes integral is presented in Ref. 35.

The following theorem presented in Ref. 27 establishes some important properties of $G(\omega)$ under the assumption of strict passivity, *i.e.*, $\mathrm{Im}\,G(\omega) > 0$ for $\omega > 0$.[4] The theorem resembles Levinson's theorem for the bound states of the Schrödinger equation as the roots of the Jost function, see Refs. 34 and 40.

Meĭman's theorem. *Under the assumption of strict passivity, i.e.,* $\mathrm{Im}\,G(\omega) > 0$ *for* $\omega > 0$, $G(\omega)$ *is non-zero in the upper half of the* ω*-plane, and does not take real values at any finite point in that half-plane except on the imaginary axis, where it decreases monotonically from a positive value to zero at* $\omega = \mathrm{i}\infty$.

[3] In the lower half of the ω-plane, the integral in (2.1) diverges. In general, $G(\omega)$ has singularities in this region and can be defined there only as the holomorphic continuation of (2.1) from the upper half-plane.

[4] The proof of Meĭman's theorem can however be extended to include $\mathrm{Im}(\omega G(\omega)) \geq 0$.

Proof. For any real-valued constant ϑ, the function $G(\omega) - \vartheta$ is holomorphic in the upper half of the ω-plane, and the argument principle in Ref. 1 yields that

$$\frac{1}{2\pi \mathrm{i}} \oint_{\gamma} \frac{\mathrm{d}G(\omega)}{\mathrm{d}\omega} \frac{\mathrm{d}\omega}{G(\omega) - \vartheta} = \frac{1}{2\pi \mathrm{i}} \oint_{\gamma'} \frac{\mathrm{d}G(\omega)}{G(\omega) - \vartheta} \tag{2.4}$$

is equal to the number of roots of $G(\omega) - \vartheta$ within γ', *i.e.*, the number of points at which $G(\omega) = \vartheta$. Here, the curve γ' is defined by the map $\gamma' = G(\gamma)$ of the contour on the left hand side of Fig. 1. This map has the property that the infinite semicircle is mapped onto $G(\infty) = 0$, and $\omega = 0$ is mapped onto another real-valued point $G(0) > 0$.[5] Since, by assumption, $\operatorname{Im} G(\omega) > 0$ for $\omega > 0$, and therefore $\operatorname{Im} G(\omega) < 0$ for $\omega < 0$, the axes $\omega < 0$ and $\omega > 0$ on the left hand side of Fig. 1 are mapped onto curves (symmetrically distributed with respect to the real axis) which entirely lie in the lower and upper half parts of the $G(\omega)$-plane, respectively. Thus, it follows that γ' on the right hand side of Fig. 1 does not intersect the real axis for any finite real-valued ω except at $G(0)$.

The argument principle now yields that (2.4) is equal to unity if $0 < \vartheta < G(0)$ and zero otherwise, or equivalently, in the upper half of the ω-plane, $G(\omega)$ takes the value ϑ once only if $0 < \vartheta < G(0)$. On the other hand, if $\vartheta > G(0)$, $G(\omega)$ is nowhere equal to ϑ. Since $G(\omega)$ does not have a maximum or minimum on the imaginary axis, and by contradiction attain some values at least twice, it follows that $G(\omega)$ decreases monotonically from $G(0) > 0$ at $\omega = \mathrm{i}0$ to zero at $\omega = \mathrm{i}\infty$.[6]

In the presence of a singularity at $\omega = 0$, this point must be excluded from the integration contour by a small semicircle of vanishing radius.[7] □

Sofar, only single-input single-output systems with a scalar notation have been addressed. For multiple-input multiple-output systems, $f(t)$ and $x(t)$ are replaced by vector-valued functions, and the kernel corresponding to the impulse response $g(\tau)$ becomes dyadic-valued. In Paper III, a single-input single-output system is used for scattering of acoustic waves, whereas the appropriate formulation for electromagnetic waves in Papers I–II and IV–VI is based on the multiple-input multiple-output notation. For convenience, in this General Introduction, both acoustic and electromagnetic waves are discussed in a single scalar notation.

2.2 The damped harmonic oscillator

An example of a passive system which satisfies the conditions α), β) and γ) above is given by the damped harmonic oscillator. This system provides a simple, yet accurate, model employed in many branches of physics involving wave phenomena, *cf.*, the Lorentz model in Papers I and II for the interaction of electromagnetic

[5] The fact that $G(0) > 0$ follows by sending $\omega \to 0+$ in (2.23) or (2.25) and invoking the assumption of strict passivity.

[6] Recall that the Riemann-Lebesgue lemma implies that $G(\omega) \to 0$ as $|\omega| \to \infty$ in the upper half of the ω-plane if $g(\tau)$ is absolutely integrable, see Refs. 3 and 41.

[7] For real-valued ω, only singularities in $G(\omega)$ located at $\omega = 0$ are addressed in this thesis. The assumption of a singularity at origin is motivated by the conductivity model in classical electrodynamics, see Sec. 2.6.

waves with temporally dispersive matter. The equation of motion for the damped harmonic oscillator, when subject to an external driving force $f(t)$ per unit mass, reads

$$\ddot{x} + 2\gamma\dot{x} + \omega_0^2 x = f(t), \tag{2.5}$$

where x denotes its displacement from equilibrium, and dots refer to time derivatives. Furthermore, $\gamma \geq 0$ and $\omega_0 > 0$ are the damping constant and natural frequency of the oscillator, respectively.

The energy balance for the oscillator is obtained by multiplying (2.5) with $\dot{x}$ and integrating from $-\infty$ to t, *viz.*,

$$E(t) + 2\gamma \int_{-\infty}^{t} \dot{x}^2(t') \, \mathrm{d}t' = \int_{-\infty}^{t} f(t')\dot{x}(t') \, \mathrm{d}t', \tag{2.6}$$

where $E(t) = \dot{x}^2(t)/2 + \omega_0^2 x^2(t)/2$ is the energy of the oscillator at time t. In (2.6), it has been assumed that the oscillator is at rest as $t \to -\infty$. For $\gamma \geq 0$, the left hand side of (2.6) is non-negative, and it follows that

$$\int_{-\infty}^{t} f(t')\dot{x}(t') \, \mathrm{d}t' \geq 0. \tag{2.7}$$

The condition (2.7) is a direct consequence of passivity or energy dissipation, see Refs. 24 and 31.

The solution of (2.5) for the free oscillator with $f(t) = 0$ is straightforward, *viz.*,

$$x_0(t) = \mathrm{e}^{-\gamma t}\big(a_1 \mathrm{e}^{-\mathrm{i}(\omega_0^2 - \gamma^2)^{1/2} t} + a_2 \mathrm{e}^{\mathrm{i}(\omega_0^2 - \gamma^2)^{1/2} t}\big), \tag{2.8}$$

where $\gamma \neq \omega_0$, and the complex-valued constants a_1 and a_2 are determined from initial conditions. For an overcritical damping, $\gamma > \omega_0$, the two terms in (2.8) are exponential functions with negative exponents, whereas the solution for $\gamma < \omega_0$ takes the form of a damped harmonic oscillation. For the critical damping $\gamma = \omega_0$, the solution of (2.5) reads $x_0(t) = \mathrm{e}^{-\gamma t}(a_1 t + a_2)$.[8] From a physical point of view, the passivity condition $\gamma \geq 0$ is seen to be crucial for preventing a displacement of the oscillator which increases exponentially with time. Recall that $1/\gamma$ is the lifetime or characteristic time scale over which the damping takes place.

According to the superposition principle, a general solution of (2.5) is given by (2.8) and the corresponding particular solution when the external driving force is present on the right hand side of (2.5). In order to determine this heterogeneous solution, assume that $f(t)$ can be represented by, *e.g.*, the Fourier integral (also the Laplace transform is applicable)

$$f(t) = \frac{1}{2\pi} \int_{-\infty}^{\infty} F(\omega) \mathrm{e}^{-\mathrm{i}\omega t} \, \mathrm{d}\omega.$$

[8] For $\gamma = \omega_0$, the oscillator passes the equilibrium at most one time, and has at most one extreme value (depending on the initial conditions).

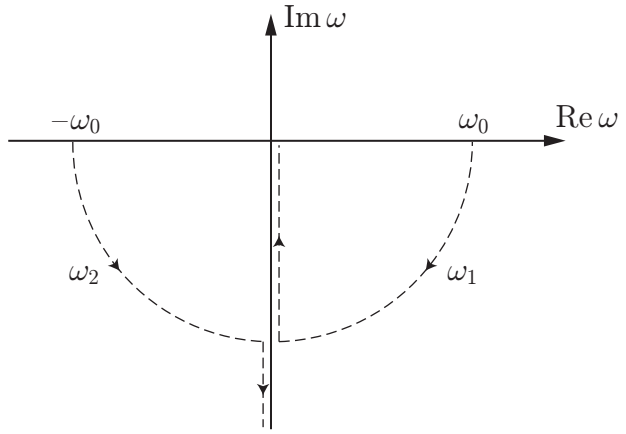

Figure 2: Trajectories for the singularities $\omega_{1,2}$ as function of increasing γ.

Taking the Fourier transform of both sides in (2.5), and invoking the convolution theorem, implies

$$x(t) = \frac{1}{2\pi}\int_{-\infty}^{\infty} G(\omega)F(\omega)\mathrm{e}^{-\mathrm{i}\omega t}\,\mathrm{d}\omega = \int_{-\infty}^{\infty} g(t-t')f(t')\,\mathrm{d}t', \tag{2.9}$$

where $G(\omega) = -1/(\omega-\omega_1)(\omega-\omega_2)$ is the frequency response of the oscillator, and $\omega_{1,2} = -\mathrm{i}\gamma \pm (\omega_0^2-\gamma^2)^{1/2}$ are the roots of the polynomial $\omega^2 + 2\mathrm{i}\gamma\omega - \omega_0^2 = 0$.[9] The paths described by the singularities $\omega_{1,2}$ in the ω-plane as $\gamma \in [0,\infty)$ increases are depicted in Fig. 2. Note that the singularities coincide for the critical damping $\gamma = \omega_0$, and that they divide in such a manner that one of them approaches $-\mathrm{i}\infty$ as $\gamma \to \infty$, while the other tends to $\omega = 0$.

Since $G(\omega)$ is the Fourier transform of $g(\tau)$, the problem to represent the solution of (2.5) as a linear functional is hence reduced to evaluate the Fourier integral

$$g(\tau) = \frac{1}{2\pi}\int_{-\infty}^{\infty} \frac{-1}{(\omega-\omega_1)(\omega-\omega_2)}\mathrm{e}^{-\mathrm{i}\omega\tau}\,\mathrm{d}\omega. \tag{2.10}$$

This is conveniently done by means of residue calculus, see Ref. 1, for which the damping $\gamma > 0$ again plays an important role.[10] For $\tau < 0$, (2.10) supports a closure (in the form of an infinite semicircle) of the contour for $\mathrm{Im}\,\omega > 0$ which does not contribute to the integral. Since $\mathrm{Im}\,\omega_{1,2} < 0$, the singularities in $G(\omega)$ are located in the lower half of the ω-plane, and the Cauchy integral theorem implies that $g(\tau) = 0$ for $\tau < 0$. But this property is merely the primitive causality condition introduced in Sec. 2.1. Hence, the damped harmonic oscillator with $\gamma > 0$ is an example of a linear time-translational invariant system obeying passivity and primitive causality. For $\tau > 0$, the appropriate region for closure is the lower half of the ω-plane. In this

[9] For real-valued ω, the passivity condition $\gamma \geq 0$ is equivalent to (2.3).

[10] For $\gamma = 0$, the integrand in (2.10) is singular at $\omega = \pm\omega_0$, and should in this case be interpreted as a Cauchy principal value integral. Excluding the singularities on the real axis with small semicircles of vanishing radii yields $g(\tau) = \sin(\omega_0\tau)/\omega_0$ irrespectively of the sign of τ.

case, the method of residues yields

$$\frac{1}{2\pi}\oint \frac{-1}{(\omega-\omega_1)(\omega-\omega_2)}\mathrm{e}^{-\mathrm{i}\omega\tau}\,\mathrm{d}\omega = \mathrm{i}\sum_{i=1,2}\operatorname*{Res}_{\omega=\omega_i}\frac{1}{(\omega-\omega_1)(\omega-\omega_2)}\mathrm{e}^{-\mathrm{i}\omega\tau}. \tag{2.11}$$

The additional minus sign on the right hand side of (2.11) is due to the negative orientation of the contour integral.

A partial decomposition of $1/(\omega-\omega_1)(\omega-\omega_2)$, and invoking the definition of the residue at $\omega=\omega_i$ as the coefficient in front of $1/(\omega-\omega_i)$ in the Laurent series expansion, yields, for $\omega_1\neq\omega_2$ (or equivalently $\gamma\neq\omega_0$),

$$\operatorname*{Res}_{\omega=\omega_i}\frac{1}{(\omega-\omega_1)(\omega-\omega_2)}\mathrm{e}^{-\mathrm{i}\omega\tau} = \frac{(-1)^{i+1}}{\omega_1-\omega_2}\mathrm{e}^{-\mathrm{i}\omega_i\tau}, \qquad i=1,2. \tag{2.12}$$

For $\omega_1=\omega_2$ (or equivalently the critical damping $\gamma=\omega_0$), the residue on the left hand side of (2.12) is equal to $-\mathrm{i}\tau\mathrm{e}^{-\gamma\tau}$ (recall that if $f(\omega)=g(\omega)/(\omega-\bar{\omega})^n$ for some positive integer n, where g is holomorphic at $\omega=\bar{\omega}$, then $\operatorname{Res}_{\omega=\bar{\omega}} f(\omega) = g^{(n-1)}(\bar{\omega})/(n-1)!$). Hence, for $\tau>0$, (2.10) and (2.11) imply

$$g(\tau) = \mathrm{e}^{-\gamma\tau}\frac{\sin((\omega_0^2-\gamma^2)^{1/2}\tau)}{(\omega_0^2-\gamma^2)^{1/2}}, \tag{2.13}$$

which is the impulse response of the oscillator, *i.e.*, its motion due to a Dirac delta excitation. The impulse response (2.13) is also valid for the critical damping as $\gamma\to\omega_0$, in which case $g(\tau)\to\tau\mathrm{e}^{-\gamma\tau}$ for $\tau>0$. This result coincides with the one obtained when inserting the residue $-\mathrm{i}\tau\mathrm{e}^{-\gamma\tau}$ into (2.11). Note that the oscillator frequency $(\omega_0^2-\gamma^2)^{1/2}$ and the characteristic time scale $1/\gamma$ are related to the real and imaginary parts of the singularities $\omega_{1,2}$, respectively, whereas the sum of the moduli of the residua is given by the amplitude $(\omega_0^2-\gamma^2)^{1/2}\mathrm{e}^{-\gamma\tau}$.

The displacement for the damped harmonic oscillator with $\gamma>0$ is finally obtained by inserting $g(\tau)$ into (2.9), *viz.*,

$$x(t) = \frac{1}{(\omega_0^2-\gamma^2)^{1/2}}\int_{-\infty}^{t}\mathrm{e}^{-\gamma(t-t')}\sin((\omega_0^2-\gamma^2)^{1/2}(t-t'))f(t')\,\mathrm{d}t'. \tag{2.14}$$

The upper limit of integration at time t clearly illustrates the idea in Sec. 2.1 that the displacement $x(t)$ only depends on the external driving force $f(t')$ for $t'<t$ with the entire history of $f(t')$ included. Recall that the impulse response $g(\tau)$ also can be derived using the Green function techniques in Ref. 39.

2.3 The Abraham-Lorentz equation of motion

A more complicated situation occurs for a charged particle when the phenomenological damping term $2\gamma\dot{x}$ in (2.5) is replaced by the radiation reaction, *i.e.*, the recoil effect of the charged particle on itself. In this case, the Abraham-Lorentz model[11] in Ref. 20, which corresponds to the simplest possible radiation reaction

[11] Also termed the Abraham-Lorentz-Dirac model since it was generalized by P. A. M. Dirac in Ref. 8 to account for the effects of special relativity.

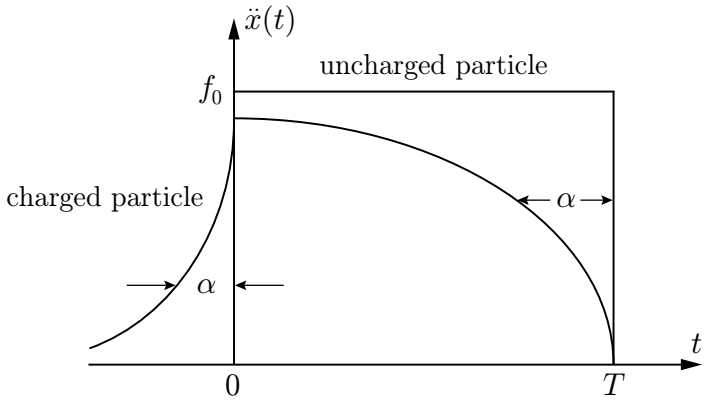

Figure 3: Illustration of the self-acceleration and the associated violation of primitive causality for a charged particle.

consistent with energy conservation, yields a term in (2.5) proportional to the third time derivative of $x(t)$, *viz.*,

$$-\alpha\dddot{x} + \ddot{x} + \omega_0^2 x = f(t), \tag{2.15}$$

where $\alpha > 0$ denotes the proportionality factor.[12] The physical interpretation of the radiation reaction is the recoil effect as a consequence of momentum carried away from the particle.

The equation of motion (2.15) now implies that $G(\omega)$ instead is determined by the roots ω_i of the polynomial $-\mathrm{i}\alpha\omega^3 - \omega^2 + \omega_0^2 = 0$. From Vieta's formulae, or the fundamental theorem of algebra, it follows that these roots satisfy $\omega_1+\omega_2+\omega_3 = \mathrm{i}/\alpha$, or equivalently, at least one of them are located in the upper half of the ω-plane. Thus, $G(\omega)$ is meromorphic rather than holomorphic in that region. In fact, from the discussions in Refs. 35 and 36, it is clear that the solution of (2.15) is either violating causality or passivity; a solution to (2.15) which satisfies passivity is necessary non-causal and, as a consequence, admits self-acceleration, *i.e.*, the particle starts to accelerate a time interval of order α before the external driving force $f(t)$ is applied. Another unpleasant consequence of (2.15) is the runaway solution for $\omega_0 = 0$, in which case passivity is violated and the acceleration $\ddot{x}(t) = \ddot{x}(0)\mathrm{e}^{t/\alpha}$ of a free particle increases exponentially with time. These difficulties also persist in the Abraham-Lorentz-Dirac model consistent with special relativity. For an introduction to the physical origin of the radiation reaction, see also Ref. 14.

To illustrate the phenomenon of self-acceleration, consider a free, charged particle subject to the following external driving force per unit mass: $f(t) = f_0$ for $0 < t < T$, and zero otherwise.[13] Then (2.15) with $\omega_0 = 0$ reads

$$-\alpha\dddot{x} + \ddot{x} = f(t). \tag{2.16}$$

[12] More explicitly, $\alpha = \mu_0 q^2/6\pi m c_0$, where q and m denote the charge and mass of the particle, and μ_0 and c_0 are the vacuum permeability and velocity of light in free space, respectively. For the electron, $\alpha = 6 \cdot 10^{-24}\,\mathrm{s}$, which is the typical time it takes for light to travel across an electron.

[13] This is merely the solution to Problem 11.19 in Ref. 14.

The general solution of (2.16) is continuous in time (just integrate (2.16) from $t-\varepsilon$ to $t+\varepsilon$ and send $\varepsilon \to 0+$) although $f(t)$ is discontinuous. Imposing the continuity condition at $t=0$ and $t=T$ implies that either the runaway solution for $t>T$ or the self-acceleration for $t<0$ can be eliminated, but not both of them. By preserving passivity, and thereby preventing an acceleration which increases exponentially with time for $t>T$, the solution of (2.16) becomes

$$\ddot{x}(t) = \begin{cases} f_0\left(1-\mathrm{e}^{-T/\alpha}\right)\mathrm{e}^{t/\alpha}, & t<0 \\ f_0\left(1-\mathrm{e}^{(t-T)/\alpha}\right), & 0<t<T \\ 0, & t>T \end{cases}. \tag{2.17}$$

The solution (2.17) is seen to violate primitive causality in the sense that the particle starts to accelerate a time interval of order α (recall however that α is a small number) before the external driving force $f(t)$ is applied, see Fig. 3. These absurd implications are not entirely understood nearly a century ago after the proposal of the Abraham-Lorentz model. Similar non-causal effects for Condon's model on optical activity in classical electrodynamics are addressed in Ref. 26.

2.4 The origin of dispersion relations

The holomorphic properties of $G(\omega)$ established in Sec. 2.1 are now used to derive a common starting point for many classical dispersion relations. For this purpose, consider the following Cauchy integral with the point ω located inside a closed contour in the upper half of the ω-plane:

$$G(\omega) = \frac{1}{2\pi\mathrm{i}} \oint \frac{G(\omega')}{\omega'-\omega}\,\mathrm{d}\omega'. \tag{2.18}$$

Specify the contour by the real axis and an infinite semicircle in the upper half of the ω-plane, and assume that $G(\omega')$ vanishes sufficiently rapid at infinity. Then, for any point $\omega+\mathrm{i}\varepsilon$, where ω and ε are real-valued,

$$G(\omega) = \lim_{\varepsilon\to 0+} \frac{1}{2\pi\mathrm{i}} \int_{-\infty}^{\infty} \frac{G(\omega')}{\omega'-\omega-\mathrm{i}\varepsilon}\,\mathrm{d}\omega'. \tag{2.19}$$

The integrand in (2.19) is recognized as the formula for the principal part distribution, *i.e.*,

$$\lim_{\varepsilon\to 0+} \frac{1}{\omega'-\omega-\mathrm{i}\varepsilon} = \mathcal{P}\left(\frac{1}{\omega'-\omega}\right) + \mathrm{i}\pi\delta(\omega'-\omega), \tag{2.20}$$

where $\mathcal{P}$ denotes Cauchy's principal value. The interpretation of the delta distribution on the right hand side of (2.20) is the contribution from a small semicircle on the real axis enclosing the singularity at $\omega'=\omega$, see Fig. 4. This contour is similar to the integration path in Fig. 2 in Paper I, where the singularity is located at $\omega'=0$.

Under the assumption that $G(\omega')$ is sufficiently well-behaved at origin to interchange the Cauchy principal value and the limit $\varepsilon \to 0+$, (2.20) inserted into (2.19)

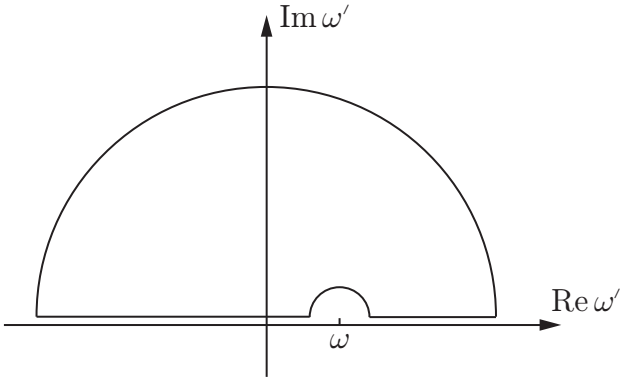

Figure 4: Integration contour in (2.18) for $\omega > 0$. The radii of the small and large semicircles approach zero and infinity, respectively.

yields[14]

$$G(\omega) = \frac{1}{\mathrm{i}\pi}\mathcal{P}\int_{-\infty}^{\infty} \frac{G(\omega')}{\omega' - \omega}\,\mathrm{d}\omega'. \tag{2.21}$$

The relation (2.21) is recognized as the Hilbert transform in Ref. 41. It can be split into the first and second Plemelj formulae by applying the real and imaginary parts on both sides of (2.21). By using the cross symmetry (2.2), *i.e.*, the fact that $\mathrm{Re}\,G(\omega')$ and $\mathrm{Im}\,G(\omega')$ are even and odd in ω', respectively, one obtains the following transform pair which only involves integration over the positive real axis:

$$\mathrm{Re}\,G(\omega) = \frac{2}{\pi}\mathcal{P}\int_0^{\infty} \frac{\omega'\,\mathrm{Im}\,G(\omega')}{\omega'^2 - \omega^2}\,\mathrm{d}\omega' \tag{2.22}$$

$$\mathrm{Im}\,G(\omega) = -\frac{2\omega}{\pi}\mathcal{P}\int_0^{\infty} \frac{\mathrm{Re}\,G(\omega')}{\omega'^2 - \omega^2}\,\mathrm{d}\omega' \tag{2.23}$$

Recall that the Plemelj formulae are a direct consequence of passivity and primitive causality.

The two formulae in (2.22) and (2.23) imply each other, so it is sufficient to only keep one of them. For our purpose, (2.22) provides the necessary tool for the analysis of extinction of acoustic and electromagnetic waves in Papers I and III. In fact, (2.22) and (2.23) are the starting point of many classical dispersion relations, including the forward and non-forward dispersion relations for scattering of waves and particles in Sec. 3. The Plemelj formulae can also be used to derive dispersion relations for various functions of $G(\omega)$ satisfying (2.2), since the sums, products, and compositions of holomorphic functions also are holomorphic, *cf.*, the dispersion relation for the reciprocal of $G(\omega)$ in Sec. 2.6 (recall that $G(\omega)$ is nowhere zero in the upper half of the ω-plane due to Meĭman's theorem on p. 5.) Note that also the

[14]Here, the Cauchy principal value integral (2.21) is defined as

$$\mathcal{P}\int_{-\infty}^{\infty} \frac{G(\omega')}{\omega' - \omega}\,\mathrm{d}\omega' = \lim_{\epsilon\to 0+}\left(\int_{-\infty}^{\omega-\epsilon} + \int_{\omega+\epsilon}^{\infty}\right)\frac{G(\omega')}{\omega' - \omega}\,\mathrm{d}\omega'.$$

frequency response $G(\omega) = -1/(\omega-\omega_1)(\omega-\omega_2)$ for the damped harmonic oscillator in Sec. 2.2 satisfies (2.22) and (2.23).

Another interesting relation for real-valued ω is obtained by considering the contour integral of $\omega' G(\omega')/(\omega'^2+\omega^2)$ with respect to the real axis and an infinite semicircle in the upper half of the ω'-plane (*i.e.*, the same contour as in Fig. 4 except for the small semicircle centered at $\omega' = \omega$). Under the assumption that the contribution from the infinite semicircle vanishes, the method of residues yields (recall that if $f(\omega)$ is holomorphic and has a simple singularity at $\omega = \bar{\omega}$, then $\mathrm{Res}_{\omega'=\bar{\omega}} f(\omega) = \lim_{\omega\to\bar{\omega}}(\omega-\bar{\omega})f(\omega)$)

$$\int_{-\infty}^{\infty} \frac{\omega' G(\omega')}{\omega'^2+\omega^2}\,\mathrm{d}\omega' = 2\pi\mathrm{i}\operatorname*{Res}_{\omega'=\mathrm{i}\omega} \frac{\omega' G(\omega')}{\omega'^2+\omega^2} = \mathrm{i}\pi G(\mathrm{i}\omega), \tag{2.24}$$

where $\omega > 0$. The real part of the integral in (2.24) vanishes since $\mathrm{Re}\, G(\omega')$ is even in ω'. Thus, since also the integrand $\omega' \,\mathrm{Im}\, G(\omega')/(\omega'^2+\omega^2)$ is even in ω',

$$G(\mathrm{i}\omega) = \frac{2}{\pi}\int_0^{\infty} \frac{\omega' \,\mathrm{Im}\, G(\omega')}{\omega'^2+\omega^2}\,\mathrm{d}\omega'. \tag{2.25}$$

Integrating both sides in (2.25) with respect to $\omega \in [0,\infty)$ finally yields the summation rule

$$\int_0^{\infty} G(\mathrm{i}\omega)\,\mathrm{d}\omega = \int_0^{\infty} \mathrm{Im}\, G(\omega)\,\mathrm{d}\omega, \tag{2.26}$$

where it has been assumed that $G(\omega)$ is sufficiently regular to interchange the order of integration in the ω and ω' variables. The relation (2.26) can also be derived by a direct application of Cauchy's integral theorem to a quarter circle contour in the first quadrant of the ω-plane. The interpretation of (2.26) is that it relates the values of $G(\omega)$ on the upper half of the imaginary axis to those of $\mathrm{Im}\, G(\omega)$ on the real axis. Provided that the integral on the left hand side is convergent, (2.26) suggest that $\mathrm{Im}\, G(\omega)$ is integrable rather than square integrable as presented in Titchmarsh's theorem below.

In some cases, it is more natural to establish conditions on the asymptotic behavior of the frequency response $G(\omega)$ for real-valued ω, instead of assuming that $G(\omega)/(\omega'-\omega)$ vanishes when integrating over a large semicircle or any other similar contour obtained via holomorphic continuation. For this purpose, the ideas in this section are restated in a form appropriate for $G(\omega)$ when it is square integrable. From Parseval's theorem (also termed Plancherel's theorem in Ref. 10) it then follows that

$$\int_{-\infty}^{\infty} |G(\omega)|^2\,\mathrm{d}\omega = 2\pi\int_0^{\infty} |g(\tau)|^2\,\mathrm{d}\tau < C,$$

where C is a constant. Introduce $\omega = \omega' + \mathrm{i}\omega''$, where ω' and ω'' are real-valued, and recall that $G(\omega'+\mathrm{i}\omega'')$ is the Fourier transform of $\mathrm{e}^{-\omega''\tau}g(\tau)$ evaluated at ω'. For $\omega'' > 0$, another application of Parseval's theorem yields

$$\int_{-\infty}^{\infty} |G(\omega'+\mathrm{i}\omega'')|^2\,\mathrm{d}\omega' = 2\pi\int_0^{\infty} \mathrm{e}^{-2\omega''\tau}|g(\tau)|^2\,\mathrm{d}\tau < 2\pi\int_0^{\infty} |g(\tau)|^2\,\mathrm{d}\tau,$$

which implies that $G(\omega)$ belongs to the Hardy class H^2, see Refs. 9 and 12, *i.e.*,

$$\int_{-\infty}^{\infty} |G(\omega' + \mathrm{i}\omega'')|^2 \, \mathrm{d}\omega' < C. \tag{2.27}$$

This is an important result illuminated in a set of theorems in Ref. 41, collectively referred to as Titchmarsh's theorem.

Titchmarsh's theorem. *If $G(\omega)$ is square integrable on the real axis, the following three conditions are equivalent:*

i. the inverse Fourier transform of $G(\omega)$ vanishes for $\tau < 0$, i.e.,

$$g(\tau) = \frac{1}{2\pi} \int_{-\infty}^{\infty} G(\omega) \mathrm{e}^{-\mathrm{i}\omega\tau} \, \mathrm{d}\omega = 0, \quad \tau < 0;$$

ii. $G(\omega)$ is, for almost all ω', the limit as $\omega'' \to 0+$ of the function $G(\omega' + \mathrm{i}\omega'')$, which is holomorphic in the upper half of the ω-plane, and there satisfies (2.27)*;*

iii. the real and imaginary parts of $G(\omega)$ satisfy any of (2.22) *and* (2.23)*.*

The equivalence in Titchmarch's theorem is understood to hold in the sense that each of the conditions are both necessary and sufficient for the others to be true. Loosely speaking, the theorem states that for a frequency response vanishing sufficiently rapid at infinity, the following statements are mainly one single property expressed in three different ways: i) having a Fourier transform which vanishes on the negative real axis, ii) being holomorphic in the upper half of the ω-plane, and iii) obeying a dispersion relation.

2.5 Dispersion relations with one subtraction

The requirement of square integrability in Titchmarsh's theorem is often violated in physical problems. In fact, for passive systems with square integrable (or finite energy) input $f(t)$, there exists a constant C such that the output $x(t)$ satisfies

$$\int_{-\infty}^{\infty} |x(t)|^2 \, \mathrm{d}t \leq C \int_{-\infty}^{\infty} |f(t)|^2 \, \mathrm{d}t.$$

In fact, for many systems, conservation of energy implies that C is bounded from above by unity. Irrespectively of the value of C, it follows from Parseval's theorem that

$$\int_{-\infty}^{\infty} |X(\omega)|^2 \, \mathrm{d}\omega = \int_{-\infty}^{\infty} |G(\omega)|^2 |F(\omega)|^2 \, \mathrm{d}\omega \leq C \int_{-\infty}^{\infty} |F(\omega)|^2 \, \mathrm{d}\omega,$$

where $X(\omega)$ denotes the Fourier transform of $x(t)$. Thus, $G(\omega)$ is bounded rather than square integrable on the real axis. Although Titchmarsh's theorem is not directly applicable in this case, $G(\omega)$ is still holomorphic in the upper half of the ω-plane.

As pointed out in the previous paragraph, a common situation occurs when $G(\omega)$ is bounded. Then, for an arbitrary point $\bar{\omega}$ in the upper half of the ω-plane, Titchmarsh's theorem can be applied to $(G(\omega) - G(\bar{\omega}))/(\omega - \bar{\omega})$, which indeed is square integrable. Under the assumption that $G(\omega)$ is differentiable at $\bar{\omega}$, (2.21) implies

$$G(\omega) = G(\bar{\omega}) + \frac{\omega - \bar{\omega}}{\mathrm{i}\pi} \mathcal{P} \int_{-\infty}^{\infty} \frac{G(\omega') - G(\bar{\omega})}{\omega' - \bar{\omega}} \frac{\mathrm{d}\omega'}{\omega' - \omega}, \tag{2.28}$$

which is known as a dispersion relation with one subtraction. This relation is particularly useful when $\bar{\omega} = 0$ or $|\bar{\omega}| \to \infty$. In the latter case with $G_\infty = \lim_{|\omega| \to \infty} G(\omega)$,

$$G(\omega) = G_\infty + \frac{1}{\mathrm{i}\pi} \mathcal{P} \int_{-\infty}^{\infty} \frac{G(\omega')}{\omega' - \omega} \, \mathrm{d}\omega',$$

where $\mathcal{P} \int_{-\infty}^{\infty} \mathrm{d}\omega'/(\omega' - \omega) = 0$ has been used. Dispersion relations with more than one subtraction, suitable for the asymptotic behavior $G(\omega) = \mathcal{O}(\omega^n)$ as $\omega \to \infty$ where n is a positive integer, are addressed in Ref. 35.

2.6 The Kramers-Kronig relations

Also the Kramers-Kronig relations (named after the contemporary discoveries by R. de L. Kronig and H. A. Kramers in Refs. 7 and 25), modeling the propagation of light in a homogeneous and lossy dielectric medium, originate from (2.22) and (2.23). To illustrate this, introduce the permittivity $\epsilon(\omega)$ relative to free space, and set $G(\omega) = \epsilon(\omega) - \epsilon_\infty$, where $\epsilon_\infty = \lim_{\omega \to \infty} \epsilon(\omega)$ for real-valued ω denotes the instantaneous response of the medium.[15] Then $G(\omega)$ satisfies (2.2), and, under the assumption of strict passivity, $\operatorname{Im} \epsilon(\omega) > 0$ for $\omega > 0$, it follows from Meĭman's theorem on p. 5 that $\epsilon(\omega)$ only is real-valued on the imaginary axis among all finite points in the upper half of the ω-plane. On the imaginary axis, the modulus of $\epsilon(\omega) - \epsilon_\infty$ decreases monotonically as ω tends to infinity.[16]

Physical reasons in Ref. 20 suggest that for this particular frequency response, $\operatorname{Re} G(\omega) = \mathcal{O}(\omega^{-2})$ and $\operatorname{Im} G(\omega) = \mathcal{O}(\omega^{-3})$ as $\omega \to \infty$ along the real axis. However, the conductivity model and the Debye model[17] vanish slower at infinity than suggested in Ref. 20, but still sufficiently fast to be square integrable. For the conductivity model, $\operatorname{Re} G(\omega) = 0$ and $\operatorname{Im} G(\omega) = \mathcal{O}(\omega^{-1})$, while for the Debye model, $\operatorname{Re} G(\omega) = \mathcal{O}(\omega^{-2})$ and $\operatorname{Im} G(\omega) = \mathcal{O}(\omega^{-1})$ as $\omega \to \infty$. Thus, (2.22) and (2.23) yield, in the absence of a conductivity term, the following constraints on physical

[15] The present analysis is not restricted to isotropic media; instead, the formulae presented here also hold in the anisotropic case for the Rayleigh quotients of the permittivity dyadic $\boldsymbol{\epsilon}(\omega)$. It should also be mentioned that $\epsilon(\omega)$ can be replaced by the permeability $\mu(\omega)$ in the expressions below.

[16] This conclusion is merely the first part of the statement in Problem 7.24 in Ref. 20.

[17] The conductivity model is defined by the additive term $\mathrm{i}\varsigma/\omega\epsilon_0$, while the Debye model reads $\epsilon(\omega) = \epsilon_\infty + (\epsilon_\mathrm{s} - \epsilon_\infty)/(1 - \mathrm{i}\omega\tau)$, where ϵ_s denotes the static permittivity. Both the conductivity $\varsigma > 0$ and the relaxation time $\tau > 0$ are independent of ω. For an introduction to dispersion models for temporally dispersive matter, see Ref. 4 and references therein.

realizability known as the Kramers-Kronig relations:

$$\operatorname{Re}\epsilon(\omega) = \epsilon_\infty + \frac{2}{\pi}\mathcal{P}\int_0^\infty \frac{\omega' \operatorname{Im}\epsilon(\omega')}{\omega'^2-\omega^2}\,\mathrm{d}\omega' \tag{2.29}$$

$$\operatorname{Im}\epsilon(\omega) = -\frac{2\omega}{\pi}\mathcal{P}\int_0^\infty \frac{\operatorname{Re}\epsilon(\omega')-\epsilon_\infty}{\omega'^2-\omega^2}\,\mathrm{d}\omega' \tag{2.30}$$

Since the instantaneous response is non-unique from a modeling point of view, see Ref. 16, (2.29) and (2.30) are often phrased with $\epsilon_\infty = 1$. For isotropic media, the Kramers-Kronig relations can also be formulated in the refractive index $n(\omega) = (\epsilon(\omega)\mu(\omega))^{1/2}$, see Refs. 19 and 35.

When static conductivity $\varsigma > 0$ is present in the dielectric medium, (2.29) remains valid whereas the term $\varsigma/\omega\epsilon_0$ must be included on the right hand side of (2.30), see Ref. 28 and the discussion in Paper II, *i.e.*,

$$\operatorname{Im}\epsilon(\omega) = \frac{\varsigma}{\omega\epsilon_0} - \frac{2\omega}{\pi}\mathcal{P}\int_0^\infty \frac{\operatorname{Re}\epsilon(\omega')-\epsilon_\infty}{\omega'^2-\omega^2}\,\mathrm{d}\omega'.$$

This additional term refers to the contribution from a small semicircle enclosing the singularity at $\omega = 0$, *cf.*, the integration contour in Fig. 4.

A number of important conclusions can be deduced from the Kramers-Kronig relations. In particular, assuming that $\operatorname{Im}\epsilon(\omega)$ is sufficiently well-behaved in the absence of a conductivity term, yields, when sending $\omega \to 0+$, the summation rule

$$\operatorname{Re}\epsilon(0) = \epsilon_\infty + \frac{2}{\pi}\mathcal{P}\int_0^\infty \frac{\operatorname{Im}\epsilon(\omega')}{\omega'}\,\mathrm{d}\omega'. \tag{2.31}$$

From (2.30) and (2.31) and the passivity condition, it is concluded that the permittivity in the static limit is real-valued and larger or equal to ϵ_∞. This result is, among other things, important for the analysis of wave interaction with temporally dispersive matter in Paper II. Finally, note that $G(\omega) = \epsilon(\omega) - \epsilon_\infty$ also satisfies (2.26) provided it vanishes sufficiently fast at infinity, *i.e.*,

$$\int_0^\infty \epsilon(\mathrm{i}\omega) - \epsilon_\infty\,\mathrm{d}\omega = \int_0^\infty \operatorname{Im}\epsilon(\omega)\,\mathrm{d}\omega, \tag{2.32}$$

where the right hand side of (2.32) is non-negative due to passivity. Observe that this summation rule is not applicable to the conductivity model since then both the left and right hand sides of (2.32) diverge.

Meĭman's theorem on p. 5, and the fact that ϵ_∞ is real-valued, implies that $\epsilon(\omega)$ is nowhere zero in the upper half of the ω-plane. Hence, also the inverse of $\epsilon(\omega)$ is holomorphic in that half-plane, and (2.22) and (2.23) hold for $G(\omega) = \epsilon^{-1}(\omega) - \epsilon_\infty^{-1}$, *i.e.*,

$$\operatorname{Re}\epsilon^{-1}(\omega) = \epsilon_\infty^{-1} + \frac{2}{\pi}\mathcal{P}\int_0^\infty \frac{\omega' \operatorname{Im}\epsilon^{-1}(\omega')}{\omega'^2-\omega^2}\,\mathrm{d}\omega' \tag{2.33}$$

$$\operatorname{Im}\epsilon^{-1}(\omega) = -\frac{2\omega}{\pi}\mathcal{P}\int_0^\infty \frac{\operatorname{Re}\epsilon^{-1}(\omega')-\epsilon_\infty^{-1}}{\omega'^2-\omega^2}\,\mathrm{d}\omega' \tag{2.34}$$

Both (2.29) and (2.30) as well as (2.33) and (2.34) can be used to derive superconvergent summation rules in terms of the plasma frequency, see Refs. 2 and 20.[18] The reader should, however, be careful to consult Ref. 29 on this topic due to its many mistakes and absence of physical clarity.

A Gedankenexperiment associated with the Kramers-Kronig relations is presented in Ref. 17. Consider a pair of spectacles with, say, green glasses subject to a flashlight in a dark room. The light as a function of time is modeled as a δ-twinkle, *i.e.*,

$$\delta(t) = \frac{1}{2\pi} \int_{-\infty}^{\infty} \mathrm{e}^{\mathrm{i}\omega t} \, \mathrm{d}\omega. \tag{2.35}$$

The interpretation of (2.35) is that the δ-twinkle contains all frequencies in such a way that the waves interfere destructively except at the instant $t = 0$. Now, consider a pair of ideal green glasses which transmits green light in some region of the spectrum, but absorbs all other waves necessary for the mutual cancelation at time $t > 0$. Suppose there is no connection between the real and imaginary parts (*i.e.*, the refractive and absorptive properties) of the refractive index. Why then is it not possible to see in the dark with the green glasses? An explanation is provided by the Kramers-Kronig relations which state that the refractive index depends on ω in such a way that the transmitted waves in the green region obtain the right phase shifts necessary for the destructive interference at time $t > 0$. In fact, there is no green or any other colored glasses which simply absorb a part of the spectrum without possessing refraction.

An extension of Kramers-Kronig relations to heterogeneous media is presented in Ref. 46 based on Herglotz functions similar to $\omega(\epsilon(\omega) - \epsilon_\infty)$. Kramers-Kronig relations can also be derived for acoustic waves; the homogeneous case for fluid media is due to V. L. Ginzberg in Ref. 13.

3 Dispersion relations in scattering theory

Dispersion relations for scattering of acoustic and electromagnetic waves are briefly discussed in this section as an introduction to Papers I and III.[19] The ideas presented here follow the expositions in Refs. 34 and 47. Dispersion relations for partial waves, addressed in Refs. 34 and 35, are however excluded from the thesis since new results soon appear in a forthcoming paper. The basic theory of acoustic and electromagnetic waves is treated in Refs. 6 and 45. For an introduction to acoustic and electromagnetic scattering theory, see also Refs. 4, 30, 32 and 43.

[18] The term *superconvergence* is referred to the asymptotic behavior of the Hilbert transform (2.21) as $\omega \to \infty$ along the real axis, see Ref. 41. Superconvergent summation rules are often deduced from Kramers-Kronig relations and an additional physical requirement in the high frequency regime, *e.g.*, the assumption that the electromagnetic response of the medium under consideration is described by a Lorentz model, or equivalently, the damped harmonic oscillator in Sec. 2.2, for frequencies far above any resonances of the medium.

[19] The results in this section also hold for a larger class of symmetric hyperbolic systems including elastic waves, see Refs. 10 and 45.

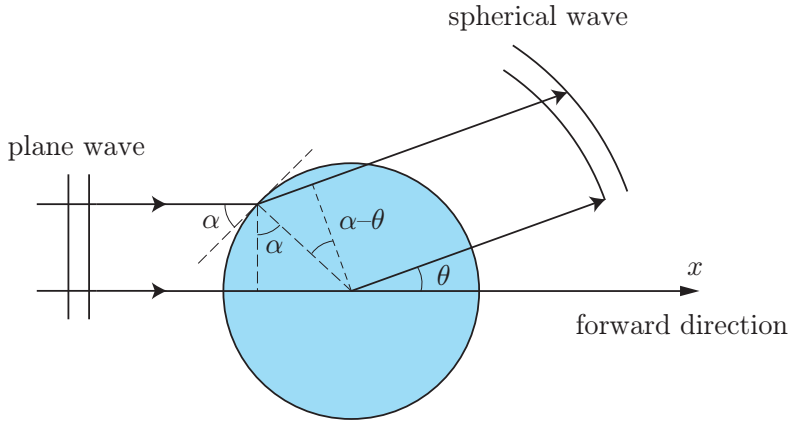

Figure 5: Geometry for non-forward scattering by a spherical symmetric target.

3.1 Non-forward dispersion relations

Non-forward dispersion relations deal with constraints on physical realizable measures for scattering of wave packages by a fixed obstacle. For simplicity, consider the spherical symmetric target of radius a in Fig. 5 subject to a plane wave excitation $f(\tau)$ of either acoustic or electromagnetic origin, *viz.*,

$$f(\tau) = \frac{1}{2\pi} \int_{-\infty}^{\infty} F(\omega) \mathrm{e}^{-\mathrm{i}\omega\tau/c} \, \mathrm{d}\omega, \tag{3.1}$$

where $\tau = ct - x$. Here, c denotes the phase velocity of the surrounding medium which is assumed to be lossless, isotropic and homogeneous.[20] For a fixed scattering angle θ, the path difference between a wave deflected at the surface of the scatterer and a reference wave in free space passing through the origin is, according to Fig. 5, $\Delta(\alpha) = a(\sin\alpha - \sin(\alpha - \theta))$. The maximal path difference hence occurs for $\alpha = \theta/2$ (just solve $\mathrm{d}\Delta(\alpha)/\mathrm{d}\alpha = 0$ to obtain $\alpha - \theta = \pm\alpha + 2\pi k$, where k is an integer, and use that $0 < \alpha < \pi/2$) with

$$\max_{0<\alpha<\pi/2} \Delta(\alpha) = 2a \sin\theta/2.$$

Thus, the shortest path for the scattered wave to reach any radial distance exterior to the scatterer is $2a\sin\theta/2$ shorter than the path taken through the origin.

Assume that $f(\tau) = 0$ for $\tau < 0$ (implying that $F(\omega)$ is holomorphic in the upper half of the ω-plane) in the sense that the incident wave front is determined by the equation $ct - x = 0$. Consequently, the scattered wave $h(\tau)$ at large distances does

[20] For both acoustic and electromagnetic waves, it is assumed that c exceeds the phase velocity of the scatterer if the latter is permeable; otherwise, the present analysis should be modified with the same technique used for the Dirichlet boundary condition in Paper III. An important difference in scattering of acoustic and electromagnetic waves is that in the former case, the phase velocity of the scatterer often exceeds c (*cf.*, a metal obstacle embedded in fluid medium such as water or air at normal pressure), while in the latter case, the surrounding medium is often free space and the opposite relation holds.

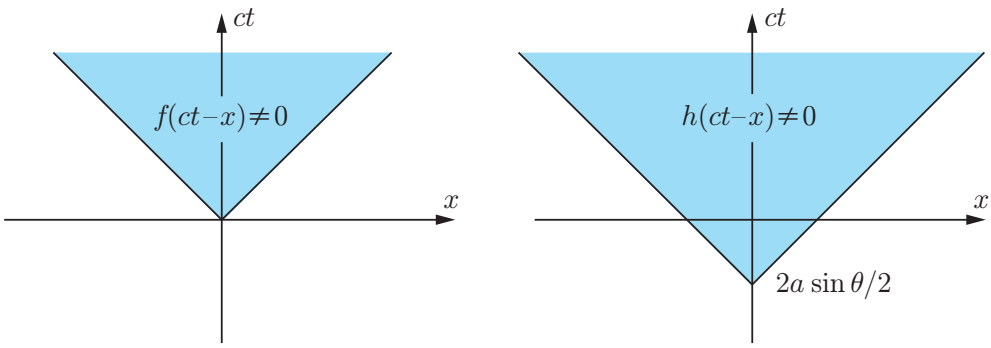

Figure 6: Light cones for the incident and scattered wave packages, $f(\tau)$ and $h(\tau)$, respectively, where $\tau = ct - x$.

not reach the radial distance x until $\tau > -2a \sin\theta/2$, which is illustrated by the light cones in Fig. 6. Introduce $H(\omega)$ as the Fourier transform of $h(\tau)$ analogous to (3.1), and let $S(\omega,\theta) = x\mathrm{e}^{-\mathrm{i}\omega x/c}H(\omega)/F(\omega)$ denote the associated scattering amplitude. Then, for a fixed scattering angle θ, it follows that $\mathrm{e}^{2\mathrm{i}\omega a/c\sin\theta/2}S(\omega,\theta)$ is holomorphic in the upper half of the ω-plane, since $F(\omega)$ is arbitrary and also holomorphic in that region.[21] However, $\mathrm{e}^{2\mathrm{i}\omega a/c\sin\theta/2}S(\omega,\theta)$ does not vanish at infinity, since for many boundary conditions in wave mechanics, $S(\omega,\theta) = \mathcal{O}(\omega)$ as $\omega \to \infty$ along the real axis. Thus, $S(\omega,\theta)/\omega^2$ rather than $S(\omega,\theta)$ vanishes sufficiently rapid at infinity, and $G(\omega) = \mathrm{e}^{2\mathrm{i}\omega a/c\sin\theta/2}S(\omega,\theta)/\omega^2$ inserted into (2.22) yields[22]

$$\mathrm{Re}\left\{\mathrm{e}^{2\mathrm{i}\omega a/c\sin\theta/2}\frac{S(\omega,\theta)}{\omega^2}\right\} = \frac{2}{\pi}\mathcal{P}\int_0^\infty \frac{\omega'}{\omega'^2-\omega^2}\,\mathrm{Im}\left\{\mathrm{e}^{2\mathrm{i}\omega' a/c\sin\theta/2}\frac{S(\omega',\theta)}{\omega'^2}\right\}\mathrm{d}\omega'. \tag{3.2}$$

The exponential factor $\mathrm{e}^{2\mathrm{i}\omega a/c\sin\theta/2}$ corresponds to a time delay of the light cone on the right hand side of Fig. 6 due to an essential singularity in $S(\omega,\theta)$ at infinity. In particular, the exponential factor reduces to $\mathrm{e}^{2\mathrm{i}\omega a/c}$ for scattering in the backward direction $\theta = \pi$. Note that (3.2) also can be formulated as a dispersion relation with two subtractions, *cf.*, the discussion in Sec. 2.5.

A drawback of (3.2) for $\theta \neq 0$ is that it depends on the choice of origin, and that the real and imaginary parts of $S(\omega,\theta)$ are mixed on both sides due to the exponential factor. In addition, the signs of the real and imaginary parts of $\mathrm{e}^{2\mathrm{i}\omega a/c\sin\theta/2}S(\omega,\theta)/\omega^2$ are indefinite, *i.e.*, they take both positive and negative values. There have been attempts, however unsuccessful, to regard $\mathrm{e}^{2\mathrm{i}\omega a/c\sin\theta/2}S(\omega,\theta)/\omega^2$ as a function of ω and $\zeta = 2\omega\sin\theta/2$ rather than ω and θ. In this case, the exponential factor becomes constant for a fixed ζ, and one seeks for a holomorphic continuation of this new function. The difficulties involved in such an extension is briefly addressed in Refs. 17 and 34.

Jung's theorem in Ref. 23 can be used to extend (3.2) to include scatterers of

[21] Here, the argument of the exponential factor $\mathrm{e}^{2\mathrm{i}\omega a/c\sin\theta/2}$ should be interpreted as $2\mathrm{i}\frac{\omega a}{c}\sin\frac{\theta}{2}$.

[22] The asymptotic behavior $S(\omega,\theta) = \mathcal{O}(\omega)$ as $\omega \to \infty$ is motivated by the forward direction $\theta = 0$. For non-forward scattering, (3.2) can also be formulated with other weight functions than $1/\omega^2$ which vanish slower at infinity.

arbitrary shape instead of just spherical symmetric targets. The theorem states that the radius of the smallest sphere circumscribing any scatterer of diameter D is less or equal to $\sqrt{6}D/4$, with equality if and only if the scatterer contains the vertices of a tetrahedron of edge lengths equal to D. Thus, the non-forward dispersion relation (3.2) also holds for scatterers of arbitrary shape if a in the exponents are replaced by any a_0 satisfying[23]

$$a_0 \geq \frac{\sqrt{6}}{4} D. \tag{3.3}$$

In particular, (3.2) subject to the static limit $\omega \to 0+$ yields (recall that $S(0,\theta) = \lim_{\omega\to 0+} S(\omega,\theta)$ is real-valued)

$$\frac{S(0,\theta)}{\omega^2} = \frac{2}{\pi}\int_0^\infty \frac{1}{\omega'^3}\,\mathrm{Im}\left\{\mathrm{e}^{2\mathrm{i}\omega' a_0/c\sin\theta/2} S(\omega',\theta)\right\}\,\mathrm{d}\omega', \tag{3.4}$$

where it has been assumed that $S(\omega,\theta)$ is continuous at $\omega = 0$ and sufficiently regular to exchange Cauchy's principal value and the static limit.[24] Thus, as a consequence of passivity and primitive causality, (3.4) holds for any a_0 satisfying (3.3) although the left hand side of (3.4) only depends on the static properties of the scatterer irrespectively of a_0.

3.2 Forward dispersion relations

The dispersion relation (3.2) becomes particularly useful when applied to the forward direction, *i.e.*, for the scattering angle $\theta = 0$. In this case, the exponential factor $\mathrm{e}^{2\mathrm{i}\omega a/c\sin\theta/2}$ vanishes, and (3.2) reduces to

$$\frac{S(\omega,0)}{\omega^2} = \frac{2}{\pi}\mathcal{P}\int_0^\infty \frac{\omega'}{\omega'^2-\omega^2}\,\frac{\mathrm{Im}\,S(\omega',0)}{\omega'^2}\,\mathrm{d}\omega'. \tag{3.5}$$

Relation (3.5) is given experimental significance by invoking the optical theorem, $\sigma_{\mathrm{ext}}(\omega) = 4\pi c/\omega\,\mathrm{Im}\,S(\omega,0)$, which states that the scattering amplitude in the forward direction solely determines the amount of extinction, *i.e.*, the combined effect of absorption and scattering in all directions. Here, $\sigma_{\mathrm{ext}}(\omega)$ denotes the extinction cross section defined as the sum of the scattered and absorbed power divided by the incident power flux. The optical theorem is common to many disparate scattering phenomena such as acoustic waves, electromagnetic waves, and elementary particles, see Refs. 34 and 35. A historical survey of the optical theorem from a century ago to modern applications is given in Ref. 33.

For many boundary conditions in wave mechanics, including the transmission problems for acoustic and electromagnetic waves, $S(\omega,0) = \mathcal{O}(\omega^2)$ as $\omega \to 0+$ along

[23] Of course, *a priori* knowledge of the geometry of the scatterer improves the bound on a_0. For example, for a sphere it is sufficient that a_0 is greater or equal to $D/2$, in contrast to (3.3) which yields the lower bound $0.61D$.

[24] For a non-spherical target, θ refers to the multi-variable (ϑ,ϕ) of the polar and azimuthal angles ϑ and ϕ, respectively.

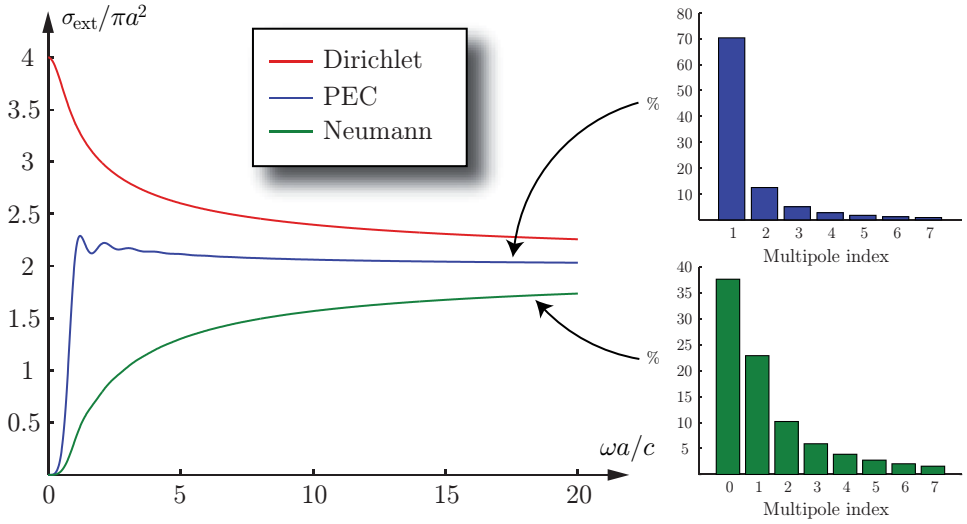

Figure 7: Partial wave decompositions of (3.6) for scattering of acoustic and electromagnetic waves by an impermeable sphere of radius a.

the real axis, and (3.5) implies[25]

$$\lim_{\omega\to 0+} \operatorname{Re} \frac{S(\omega,0)}{\omega^2} = \frac{1}{2\pi^2 c} \int_0^\infty \frac{\sigma_{\text{ext}}(\omega')}{\omega'^2}\, \mathrm{d}\omega'. \tag{3.6}$$

This forward dispersion relation is particularly useful since the extinction cross section per definition is non-negative and therefore the sign of the integrand is definite. In addition, both the integrand and the left hand side in (3.6) are experimentally significant, and the important variational results of D. S. Jones in Refs. 21 and 22 can be invoked. Recall that (3.6) holds for arbitrary scatterers since it does not contain any reference to either the shape or composition of the obstacle. Applications of this relation to various problems in theoretical physics involving wave interaction with matter are presented in the included papers. In particular, (3.6) is the starting point for the physical limitations on reciprocal antennas in Papers IV and V.

Scattering of acoustic (Dirichlet & Neumann) and electromagnetic (PEC) waves by an impermeable sphere of radius a is illustrated in Fig. 7. In the figure, the extinction cross section is depicted for both the perfectly electric conducting boundary condition, and the Neumann and Dirichlet problems for acoustic waves. In addition, statistics on the acoustic and electromagnetic partial wave decompositions of the integral in (3.6) are included on the right hand side of the figure.[26] From the statistics, it is seen that the integral in (3.6) is dominated by the lowest order multipole for both the PEC and Neumann boundary conditions. Note however the

[25]The extension to other weight functions than $1/\omega^2$ for a given static limit of $S(\omega,0)$ is addressed in a forthcoming paper.

[26]For an introduction to partial waves in scattering by impermeable spheres, see Ref. 44. Additional results on the interpretation of (3.6) in terms of partial waves, including a set of peculiar integral relations for the spherical Bessel and Hankel functions, will be presented in a forthcoming paper. For example, any passive and causal function $\epsilon = \epsilon(\kappa)$ satisfying the Kramers-Kronig

absence of a monopole (zeroth order rotationally symmetric multipole) term in the electromagnetic case due to a result by Brouwer in algebraic topology that a continuous tangential vector field on the unit sphere must vanish somewhere, or simplified, it is impossible to smoothly comb a hedgehog without leaving a bald spot or making a parting. The static limit of the Dirichlet condition is the major reason why the upper curve does not satisfy (3.6), see the discussion in Paper II. Furthermore, integration by parts in (3.6) becomes particularly useful when the curves in Fig. 7 *a priori* are known to be monotone. Then a similar identity to (3.6) with a definite sign in the integrand can be established for the derivative $\mathrm{d}\sigma_{\mathrm{ext}}(\omega)/\,\mathrm{d}\omega$. This technique is feasible for the Neumann problem, but obviously not for the PEC boundary condition due to its oscillatory character.

The fact that the extinction cross sections in Fig. 7 approach twice the projected area in the forward direction is known as the extinction paradox. From geometrical optics one naively expects that at short wavelengths a particle will remove as much energy as incident upon it. However, in this limit, geometrical optics is not applicable since the particle always will have edges in the neighborhood of which geometrical optics fails to be valid. The paradoxical character of the short wavelength limit is relieved by recalling that the observation is made at great distance far beyond where a shadow can be distinguished. For example, a meteorite in interstellar space between a star and one of our telescopes will remove twice the light incident upon it (when also deflected light at small angles is counted as scattered), while a flower pot in a window only removes the sunlight falling on it, and not twice this amount. For a discussion of the extinction paradox in terms of the physical optics approximation, see Refs. 4 and 43.

Epilogue

The following quote ends this General Introduction by emphasizing the importance of holomorphic functions in theoretical physics:

> *Thus, the beautiful mathematical theory of analytic continuation provides the key to a deeper understanding of some of the most beautiful phenomena displayed in the sky, and also manifested in so many other ways — through all scales of size — revealing the underlying unity of nature.*
>
> Herch Moysés Nussenzveig
>
> "Diffraction Effects in Semiclassical Scattering", Chapter XVI

relations (2.29) and (2.30) also satisfies the integral identity

$$\mathrm{Re}\sum_{l=1}^{\infty}(2l+1)\int_0^{\infty}\frac{\mathrm{j}_l(\kappa)(\kappa\epsilon^{1/2}\mathrm{j}_l(\kappa\epsilon^{1/2}))'-\epsilon(\kappa\mathrm{j}_l(\kappa))'\mathrm{j}_l(\kappa\epsilon^{1/2})}{\mathrm{h}_l(\kappa)(\kappa\epsilon^{1/2}\mathrm{j}_l(\kappa\epsilon^{1/2}))'-\epsilon(\kappa\mathrm{h}_l(\kappa))'\mathrm{j}_l(\kappa\epsilon^{1/2})}\frac{\mathrm{d}\kappa}{\kappa^4}=\pi\lim_{\kappa\to0+}\frac{\epsilon-1}{\epsilon+2},$$

where j_l and h_l denote the spherical Bessel and Hankel functions of the first kind, respectively. Here, $(\kappa\mathrm{f}_l(\kappa))'=\kappa\mathrm{f}_l'(\kappa)+\mathrm{f}_l(\kappa)$ for complex-valued κ with $\mathrm{f}_l'(\kappa)=l\mathrm{f}_l(\kappa)/\kappa-\mathrm{f}_{l+1}(\kappa)$, where f_l denotes any of j_l and h_l. Similar integral identities can be derived for scattering of acoustic waves.

References

[1] L. V. Ahlfors. *Complex Analysis.* McGraw-Hill, New York, second edition, 1966.

[2] M. Altarelli and D. Y. Smith. Superconvergence and sum rules for the optical constants: Physical meaning, comparison with experiment, and generalization. *Phys. Rev. B*, **9**(4), 1290–1298, 1974.

[3] C. M. Bender and S. A. Orszag. *Advanced Mathematical Methods for Scientists and Engineers.* McGraw-Hill, New York, 1978.

[4] C. F. Bohren and D. R. Huffman. *Absorption and Scattering of Light by Small Particles.* John Wiley & Sons, New York, 1983.

[5] H. J. Carlin and P. P. Civalleri. *Wideband circuit design.* CRC Press, Boca Raton, 1998.

[6] G. Dassios and R. Kleinman. *Low frequency scattering.* Oxford University Press, Oxford, 2000.

[7] R. de L. Kronig. On the theory of dispersion of X-rays. *J. Opt. Soc. Am.*, **12**(6), 547–557, 1926.

[8] P. A. M. Dirac. Classical theory of radiating electrons. *Proc. R. Soc. A*, **167**, 148–169, 1938.

[9] P. L. Duren. *Theory of H^p Spaces.* Dover Publications, New York, 2000.

[10] L. C. Evans. *Partial Differential Equations.* American Mathematical Society, Providence, Rhode Island, 1998.

[11] R. M. Fano. Theoretical limitations on the broadband matching of arbitrary impedances. *Journal of the Franklin Institute*, **249**(1,2), 57–83 and 139–154, 1950.

[12] J. B. Garnett. *Bounded Analytic Functions.* Springer-Verlag, New York, revised first edition, 2007.

[13] V. L. Ginzberg. Concerning the general relationship between absorption and dispersion of sound waves. *Sov. Phys. Acoust.*, **1**, 32–41, 1955.

[14] D. J. Griffiths. *Introduction to Electrodynamics.* Prentice-Hall, Inc., Englewood Cliffs, New Jersey, third edition, 1999.

[15] M. Gustafsson. *Wave Splitting in Direct and Inverse Scattering Problems.* PhD thesis, Lund University, Department of Electrical and Information Technology, P.O. Box 118, S-221 00 Lund, Sweden, 2000. http://www.eit.lth.se.

[16] M. Gustafsson. On the non-uniqueness of the electromagnetic instantaneous response. *J. Phys. A: Math. Gen.*, **36**, 1743–1758, 2003.

[17] R. Hagedorn. *Introduction to field theory and dispersion relations.* Pergamon, Oxford, 1964.

[18] L. Hörmander. *The Analysis of Linear Partial Differential Operators I.* Grundlehren der mathematischen Wissenschaften 256. Springer-Verlag, Berlin Heidelberg, 1983.

[19] J. D. Jackson. Introduction to dispersion relation techniques. In G. R. Screaton, editor, *Dispersion relations*, chapter 1, pages 1–63. Interscience Publishers, New York, 1960.

[20] J. D. Jackson. *Classical Electrodynamics.* John Wiley & Sons, New York, third edition, 1999.

[21] D. S. Jones. Low frequency electromagnetic radiation. *J. Inst. Maths. Applics.*, **23**(4), 421–447, 1979.

[22] D. S. Jones. Scattering by inhomogeneous dielectric particles. *Quart. J. Mech. Appl. Math.*, **38**, 135–155, 1985.

[23] H. W. E. Jung. Über die kleinste Kugel, die eine räumliche Figur einschliesst. *J. reine angew. Math.*, **123**, 241–257, 1901.

[24] H. Konig and J. Meixner. Lineare Systeme und lineare Transformationen. *Math. Nachr.*, **19**(2–3), 265–322, 1958.

[25] M. H. A. Kramers. La diffusion de la lumière par les atomes. *Atti. Congr. Int. Fis. Como*, **2**, 545–557, 1927.

[26] G. Kristensson. Condon's model on optical rotatory power and causality — a scientific trifle. Technical Report LUTEDX/(TEAT-7080)/1–23/(1999), Lund University, Department of Electrical and Information Technology, P.O. Box 118, S-221 00 Lund, Sweden, 1999. http://www.eit.lth.se.

[27] L. D. Landau and E. M. Lifshitz. *Statistical Physics, Part 1.* Butterworth-Heinemann, Linacre House, Jordan Hill, Oxford, third edition, 1980.

[28] L. D. Landau, E. M. Lifshitz, and L. P. Pitaevskiĭ. *Electrodynamics of Continuous Media.* Pergamon, Oxford, second edition, 1984.

[29] V. Lucarini, J. J. Saarinen, K.-E. Peiponen, and E. M. Vartiainen. *Kramers-Kronig Relations in Optical Materials Research.* Springer-Verlag, Berlin, 2005.

[30] P. A. Martin. *Multiple Scattering: Interaction of Time-Harmonic Waves with N Obstacles*, volume 107 of *Encyclopedia of Mathematics and its Applications.* Cambridge University Press, Cambridge, U.K., 2006.

[31] J. Meixner. Thermodynamische Erweiterung der Nachwirkungstheorie. *Zeitschrift für Physik A Hadrons and Nuclei*, **139**(1), 30–43, 1954.

[32] P. M. Morse and K. U. Ingard. *Theoretical Acoustics*. McGraw-Hill, New York, 1968.

[33] R. Newton. Optical theorem and beyond. *Am. J. Phys*, **44**, 639–642, 1976.

[34] R. G. Newton. *Scattering Theory of Waves and Particles*. Dover Publications, New York, second edition, 2002.

[35] H. M. Nussenzveig. *Causality and dispersion relations*. Academic Press, London, 1972.

[36] F. Rohrlich. *Classical charged particles: foundations of their theory*. Addison-Wesley, Reading, MA, USA, 1965.

[37] P. Roman. *Advanced quantum theory: an outline of the fundamental ideas*. Addison-Wesley, Reading, MA, USA, 1965.

[38] J. J. Sakurai. *Advanced quantum mechanics*. Addison-Wesley, Reading, MA, USA, 1967.

[39] I. Stakgold. *Green's Functions and Boundary Value Problems*. John Wiley & Sons, New York, 1979.

[40] J. R. Taylor. *Scattering theory: the quantum theory of nonrelativistic collisions*. Robert E. Krieger Publishing Company, Malabar, Florida, 1983.

[41] E. C. Titchmarsh. *Introduction to the Theory of Fourier Integrals*. Oxford University Press, Oxford, second edition, 1948.

[42] J. S. Toll. Causality and the Dispersion Relation: Logical Foundations. *Phys. Rev.*, **104**(6), 1760–1770, 1956.

[43] H. van de Hulst. *Light Scattering by Small Particles*. John Wiley & Sons, Inc., New York, 1957.

[44] V. V. Varadan, Y. Ma, V. K. Varadan, and A. Lakhtakia. Scattering of waves by spheres and cylinders. In V. V. Varadan, A. Lakhtakia, and V. K. Varadan, editors, *Field Representations and Introduction to Scattering*, Acoustic, Electromagnetic and Elastic Wave Scattering, chapter 4, pages 211–324. Elsevier Science Publishers, Amsterdam, 1991.

[45] V. V. Varadan and V. K. Varadan. Acoustic, electromagnetic and elastodynamics fields. In V. V. Varadan, A. Lakhtakia, and V. K. Varadan, editors, *Field Representations and Introduction to Scattering*, Acoustic, Electromagnetic and Elastic Wave Scattering, chapter 1, pages 1–35. Elsevier Science Publishers, Amsterdam, 1991.

[46] R. L. Weaver and Y.-H. Pao. Dispersion relations for linear wave propagation in homogeneous and inhomogeneous media. *J. Math. Phys.*, **22**(9), 1909–1918, 1981.

[47] D. Y. Wong. Dispersion relations and applications. In E. P. Wigner, editor, *Dispersion Relations and their Connection with Causality*, chapter 4, pages 68–96. Academic Press, New York, 1964. Proceedings of the International School of Physics "Enrico Fermi", Course XXIX, held at Verenna on Lake Como, Villa Monastero, July 15–August 3, 1963.

Physical limitations on broadband scattering by heterogeneous obstacles

Paper I

Christian Sohl, Mats Gustafsson, and Gerhard Kristensson

Based on: C. Sohl, M. Gustafsson, and G. Kristensson. Physical limitations on broadband scattering by heterogeneous obstacles. Technical Report LUTEDX/-(TEAT-7151)/1–25/(2006), Lund University.

Abstract

In this paper, new physical limitations on the extinction cross section and broadband scattering are investigated. A measure of broadband scattering in terms of the integrated extinction is derived for a large class of scatterers based on the holomorphic properties of the forward scattering dyadic. Closed-form expressions of the integrated extinction are given for the homogeneous ellipsoids and theoretical bounds are discussed for arbitrary heterogeneous scatterers. Finally, the theoretical results are illustrated by numerical computations for a series of generic scatterers.

1 Introduction

The relation between the extinction cross section and the forward scattering dyadic, nowadays known as the optical theorem, dates back to the work of Rayleigh more than a century ago [28]. Since then, the concept has fruitfully been extended to high-energy physics where it today plays an essential role in analyzing particle collisions [20]. This is one striking example of how results, with minor modifications, can be used in both electromagnetic and quantum mechanic scattering theory. Another example of such an analogy is presented in this paper, and it is believed that more analogies of this kind exist, see *e.g.*, the excellent books by Taylor [29] and Nussenzveig [22].

As far as the authors know, a broadband measure for scattering of electromagnetic waves was first introduced by Purcell [24] in 1969 concerning absorption and emission of radiation by interstellar dust. Purcell derived the integrated extinction for a very narrow class of scatterers via the Kramers-Kronig relations [17, pp. 279–283]. A slightly different derivation of the same result was done by Bohren and Huffman [4, pp. 116–117]. In both references it was noticed that the integrated extinction is proportional to the volume of the scatterer, with proportionality factor depending only on the shape and the long wavelength limit response of the scatterer. Based upon this observation, Bohren and Huffman conjecture [4, p. 117]:

> *Regardless of the shape of the particle, however, it is plausible on physical grounds that integrated extinction should be proportional to the volume of an arbitrary particle, where the proportionality factor depends on its shape and static dielectric function.*

Curiosity whether this supposition is true and the generalization of the results to a wider class of scatterers have been the main driving forces of the present study.

Physical limitations on scattering of electromagnetic waves play an important role in the understanding of wave interaction with matter. Specifically, numerous papers addressing physical limitations in antenna theory are found in the literature. Unfortunately, they are almost all restricted to the spherical geometry, deviating only slightly from the pioneering work of Chu [5] in 1948. In contrast to antenna theory, there are, however, few papers addressing physical limitations in scattering by electromagnetic waves. An invaluable exception is given by the fundamental work

Figure 1: Illustration of the scattering problem. The scatterer V is subject to a plane wave incident in the $\hat{\boldsymbol{k}}$-direction.

of Nussenzveig [21] in which both scattering by waves and particles are analyzed in terms of causality. Other exceptions of importance for the present paper are the Rayleigh scattering bounds derived by Jones [10, 11].

The results of Purcell mentioned above are generalized in several ways in this paper. The integrated extinction is proved to be valid for anisotropic heterogeneous scatterers of arbitrary shape. Specifically, this quantity is analyzed in detail for the ellipsoidal geometry. Several kinds of upper and lower bounds on broadband scattering for isotropic material models are presented. These limitations give a means of determining if an extinction cross section is realizable or not.

The paper is organized as follows: in Section 2, the integrated extinction is derived for a large class of scatterers based on the holomorphic properties of the forward scattering dyadic. Next, in Section 3, bounds on broadband scattering are discussed for arbitrary isotropic heterogeneous scatterers. In the following section, Section 4, some closed-form expressions of the integrated extinction are given. Moreover, in Section 5, numerical results on the extinction cross section are presented and compared with the theoretical bounds. Finally, some future work and possible applications are discussed in Section 6.

Throughout this paper, vectors are denoted in italic bold face, and dyadics in roman bold face. A hat (ˆ) on a vector denotes that the vector is of unit length.

2 Broadband scattering

The scattering problem considered in this paper is Fourier-synthesized plane wave scattering by a bounded heterogeneous obstacle of arbitrary shape, see Figure 1. The scatterer is modeled by anisotropic constitutive relations [17, Ch. XI] and assumed to be surrounded by free space. The analysis presented in this paper includes the perfectly electric conducting material model, as well as general temporal dispersion with or without a conductivity term.

2.1 The forward scattering dyadic

The scattering properties of V are described by the far field amplitude, $\boldsymbol{F}$, defined in terms of the scattered field, $\boldsymbol{E}_\mathrm{s}$, as [15, Sec. 2]

$$\boldsymbol{E}_\mathrm{s}(t,\boldsymbol{x}) = \frac{\boldsymbol{F}(\mathrm{c}_0 t - x, \hat{\boldsymbol{x}})}{x} + \mathcal{O}(x^{-2}) \quad \text{as } x \to\to \infty, \tag{2.1}$$

where c_0 is the speed of light in vacuum, and $\hat{\boldsymbol{x}} = \boldsymbol{x}/x$ with $x = |\boldsymbol{x}|$. The far field amplitude is related to the incident field, $\boldsymbol{E}_\mathrm{i}(\mathrm{c}_0 t - \hat{\boldsymbol{k}} \cdot \boldsymbol{x})$, which is impinging in the $\hat{\boldsymbol{k}}$-direction, via the linear and time-translational invariant convolution

$$\boldsymbol{F}(\tau, \hat{\boldsymbol{x}}) = \int_{-\infty}^{\infty} \mathbf{S}_\mathrm{t}(\tau - \tau', \hat{\boldsymbol{k}}, \hat{\boldsymbol{x}}) \cdot \boldsymbol{E}_\mathrm{i}(\tau') \, \mathrm{d}\tau'.$$

The dimensionless temporal scattering dyadic $\mathbf{S}_\mathrm{t}$ is assumed to be causal in the forward direction, $\hat{\boldsymbol{k}}$, in the sense that the scattered field cannot precede the incident field [21, pp. 15–16], *i.e.*,

$$\mathbf{S}_\mathrm{t}(\tau, \hat{\boldsymbol{k}}, \hat{\boldsymbol{k}}) = \mathbf{0} \quad \text{for } \tau < 0. \tag{2.2}$$

The Fourier transform of (2.1) evaluated in the forward direction is

$$\boldsymbol{E}_\mathrm{s}(k, x\hat{\boldsymbol{k}}) = \frac{\mathrm{e}^{\mathrm{i}kx}}{x} \mathbf{S}(k, \hat{\boldsymbol{k}}) \cdot \boldsymbol{E}_0 + \mathcal{O}(x^{-2}) \quad \text{as } x \to \infty,$$

where k is a complex variable in the upper half plane with $\operatorname{Re} k = \omega/\mathrm{c}_0$. Here, the amplitude of the incident field is $\boldsymbol{E}_0$, and the forward scattering dyadic, $\mathbf{S}$, is given by the Fourier representation

$$\mathbf{S}(k, \hat{\boldsymbol{k}}) = \int_{0^-}^{\infty} \mathbf{S}_\mathrm{t}(\tau, \hat{\boldsymbol{k}}, \hat{\boldsymbol{k}}) \mathrm{e}^{\mathrm{i}k\tau} \, \mathrm{d}\tau. \tag{2.3}$$

The imaginary part of k improves the convergence of (2.3) and extends the elements of $\mathbf{S}$ to holomorphic functions in the upper half plane for a large class of dyadics $\mathbf{S}_\mathrm{t}$. Recall that $\mathbf{S}(\mathrm{i}k, \hat{\boldsymbol{k}})$ is real-valued for real-valued k and $\mathbf{S}(\mathrm{i}k, \hat{\boldsymbol{k}}) = \mathbf{S}^*(-\mathrm{i}k^*, \hat{\boldsymbol{k}})$ [21, Sec. 1.3–1.4].

The scattering cross section σ_s and absorption cross section σ_a are defined as the ratio of the scattered and absorbed power, respectively, to the incident power flow density in the forward direction. The sum of the scattering and absorption cross sections is the extinction cross section,

$$\sigma_\mathrm{ext} = \sigma_\mathrm{s} + \sigma_\mathrm{a}.$$

The three cross sections are by definition real-valued and non-negative. The extinction cross section is related to the forward scattering dyadic, $\mathbf{S}$, via the optical theorem [20, pp. 18–20]

$$\sigma_\mathrm{ext}(k) = \frac{4\pi}{k} \operatorname{Im}\left\{ \hat{\boldsymbol{p}}_\mathrm{e}^* \cdot \mathbf{S}(k, \hat{\boldsymbol{k}}) \cdot \hat{\boldsymbol{p}}_\mathrm{e} \right\}. \tag{2.4}$$

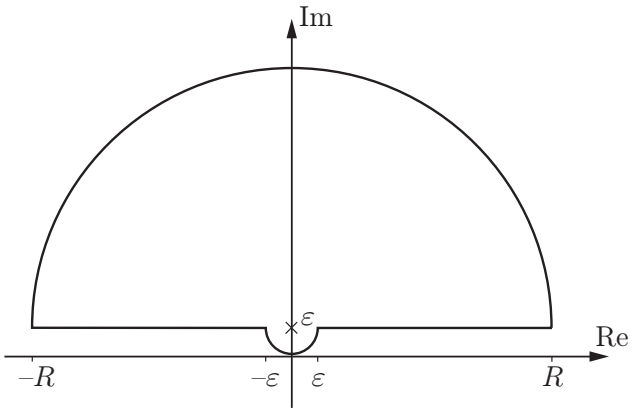

Figure 2: Integration contour used in the Cauchy integral theorem in (2.5).

Here, k is real-valued, and $\hat{\boldsymbol{p}}_{\mathrm{e}} = \boldsymbol{E}_0/|\boldsymbol{E}_0|$ is a complex-valued vector, independent of k, that represents the electric polarization, and, moreover, satisfies $\hat{\boldsymbol{p}}_{\mathrm{e}} \cdot \hat{\boldsymbol{k}} = 0$.

The holomorphic properties of $\mathbf{S}$ can be used to determine an integral identity for the extinction cross section. To simplify the notation, let $\varrho(k) = \hat{\boldsymbol{p}}_{\mathrm{e}}^* \cdot \mathbf{S}(k, \hat{\boldsymbol{k}}) \cdot \hat{\boldsymbol{p}}_{\mathrm{e}}/k^2$. The Cauchy integral theorem with respect to the contour in Figure 2 then yields

$$\varrho(\mathrm{i}\varepsilon) = \int_0^\pi \frac{\varrho(\mathrm{i}\varepsilon - \varepsilon \mathrm{e}^{\mathrm{i}\phi})}{2\pi} \, \mathrm{d}\phi + \int_0^\pi \frac{\varrho(\mathrm{i}\varepsilon + R\mathrm{e}^{\mathrm{i}\phi})}{2\pi} \, \mathrm{d}\phi + \int_{\varepsilon<|k|<R} \frac{\varrho(k + \mathrm{i}\varepsilon)}{2\pi \mathrm{i} k} \, \mathrm{d}k, \quad (2.5)$$

where k in the last integral on the right hand side is real-valued.

The left hand side of (2.5) and the integrand in the first integral on the right hand side are well-defined in the limit $\varepsilon \to 0$ and given by the long wavelength limit [15, p. 18]

$$\varrho(\mathrm{i}\varepsilon) = \frac{1}{4\pi} (\hat{\boldsymbol{p}}_{\mathrm{e}}^* \cdot \boldsymbol{\gamma}_{\mathrm{e}} \cdot \hat{\boldsymbol{p}}_{\mathrm{e}} + \hat{\boldsymbol{p}}_{\mathrm{m}}^* \cdot \boldsymbol{\gamma}_{\mathrm{m}} \cdot \hat{\boldsymbol{p}}_{\mathrm{m}}) + \mathcal{O}(\varepsilon) \quad \text{as } \varepsilon \to\!\to 0. \quad (2.6)$$

Here, $\hat{\boldsymbol{p}}_{\mathrm{m}} = \hat{\boldsymbol{k}} \times \hat{\boldsymbol{p}}_{\mathrm{e}}$ denotes the magnetic polarization and $\boldsymbol{\gamma}_{\mathrm{e}}$ and $\boldsymbol{\gamma}_{\mathrm{m}}$ are the electric and magnetic polarizability dyadics, respectively, see Appendix A for their explicit definitions. These dyadics are real-valued and symmetric. This result also includes the effect of a conductivity term [15, pp. 49–51].

The second term on the right hand side of (2.5) is assumed to approach zero and does not contribute in the limit $R \to \infty$. This is physically reasonable since the short wavelength response of a material is non-unique from a modeling point of view [8]. The assumption is also motivated by the extinction paradox [31, pp. 107–113], *i.e.*,

$$\varrho(k) = -\frac{A(\hat{\boldsymbol{k}})}{2\pi \mathrm{i} k} \left(1 + \mathcal{O}(|k|^{-1})\right) \quad \text{as } |k| \to \infty, \qquad \operatorname{Im} k \geq 0,$$

where A denotes the projected area in the forward direction.

In the last term on the right hand side of (2.5) it is assumed that ϱ is sufficiently regular to extend the contour to the real axis. Under this assumption, the real part

of (2.5) yields

$$\varrho(0) = \frac{1}{\pi}\int_{-\infty}^{\infty} \frac{\operatorname{Im}\varrho(k)}{k}\ \mathrm{d}k = \frac{1}{4\pi^2}\int_{-\infty}^{\infty} \frac{\sigma_{\mathrm{ext}}(k)}{k^2}\ \mathrm{d}k = \frac{1}{4\pi^3}\int_0^{\infty} \sigma_{\mathrm{ext}}(\lambda)\,\mathrm{d}\lambda, \qquad (2.7)$$

where we have used the optical theorem, (2.4). In this expression $\lambda = 2\pi/k$ is the vacuum wavelength.

In fact, the assumptions on ϱ can be relaxed, and the analysis can be generalized to certain classes of distributions [21, pp. 33–43]. However, the integral in (2.7) is classically well-defined for the examples considered in this paper. The relation (2.7) can also be derived using the Hilbert transform [30, Ch. V].

2.2 The integrated extinction

We are now ready to utilize the main result in the previous section. Moreover, the properties of the polarizability dyadics are exploited and different material models are discussed.

Insertion of the long wavelength limit (2.6) into (2.7) yields the integrated extinction

$$\int_0^{\infty} \sigma_{\mathrm{ext}}(\lambda)\ \mathrm{d}\lambda = \pi^2\left(\hat{\boldsymbol{p}}_{\mathrm{e}}^{*}\cdot\boldsymbol{\gamma}_{\mathrm{e}}\cdot\hat{\boldsymbol{p}}_{\mathrm{e}} + \hat{\boldsymbol{p}}_{\mathrm{m}}^{*}\cdot\boldsymbol{\gamma}_{\mathrm{m}}\cdot\hat{\boldsymbol{p}}_{\mathrm{m}}\right). \qquad (2.8)$$

Note that (2.8) is independent of any temporal dispersion, depending only on the long wavelength limit response of the scatterer in terms of $\boldsymbol{\gamma}_{\mathrm{e}}$ and $\boldsymbol{\gamma}_{\mathrm{m}}$. Closed-form expressions of $\boldsymbol{\gamma}_{\mathrm{e}}$ and $\boldsymbol{\gamma}_{\mathrm{m}}$ exist for the homogeneous ellipsoids, see Section 4. The polarizability dyadics for more general obstacles are summarized in Kleinman & Senior [15, p. 31].

For pure electric ($\boldsymbol{\gamma}_{\mathrm{m}} = \mathbf{0}$) and pure magnetic ($\boldsymbol{\gamma}_{\mathrm{e}} = \mathbf{0}$) scatterers, the integrated extinction depends only on $\hat{\boldsymbol{p}}_{\mathrm{e}}$ and $\hat{\boldsymbol{p}}_{\mathrm{m}}$, respectively, and hence not on $\hat{\boldsymbol{k}} = \hat{\boldsymbol{p}}_{\mathrm{e}} \times \hat{\boldsymbol{p}}_{\mathrm{m}}$. Moreover, the integrated extinction for a scatterer with isotropic polarizability dyadics, *i.e.*, $\boldsymbol{\gamma}_{\mathrm{e}} = \gamma_{\mathrm{e}}\mathbf{I}$ and $\boldsymbol{\gamma}_{\mathrm{m}} = \gamma_{\mathrm{m}}\mathbf{I}$, is independent of $\hat{\boldsymbol{p}}_{\mathrm{e}}$ and $\hat{\boldsymbol{p}}_{\mathrm{m}}$ as well as $\hat{\boldsymbol{k}}$.

An important model in many applications is the perfectly conducting case (PEC), which is formally obtained in the long wavelength limit by the limits [15, pp. 39–40]

$$\chi_{\mathrm{e}}(\boldsymbol{x}) \to \infty \quad \text{and} \quad \chi_{\mathrm{m}}(\boldsymbol{x}) \searrow -1. \qquad (2.9)$$

Since the long wavelength limit lacks a natural length scale it follows that the integrated extinction for any heterogeneous scatterer is proportional to the volume $|V| = \int_V \mathrm{dV}_{\boldsymbol{x}}$, where $\mathrm{dV}_{\boldsymbol{x}}$ is the volume measure with respect to $\boldsymbol{x}$ — a result conjectured by Bohren and Huffman [4, p. 117] for spherical scatterers. A brief derivation of this statement for anisotropic, heterogeneous material parameters is presented in Appendix A.

Randomly oriented scatterers are valuable in many applications [24]. The broadband scattering properties of an ensemble of randomly oriented scatterers is quantified by the averaged integrated extinction,

$$\int_0^{\infty} \bar{\sigma}_{\mathrm{ext}}(\lambda)\ \mathrm{d}\lambda = \frac{\pi^2}{3}\operatorname{tr}(\boldsymbol{\gamma}_{\mathrm{e}} + \boldsymbol{\gamma}_{\mathrm{m}}). \qquad (2.10)$$

An interesting variational result based on (2.10) states that among all isotropic, homogeneous scatterers of equal volume and susceptibilities, the spherical scatterer minimizes the averaged integrated extinction [10, Thm. 3].

3 Bounds on broadband scattering

The main result of Section 2.2 is now exploited. Firstly, upper and lower bounds on the integrated extinction utilizing the eigenvalue properties of the polarizability dyadics are established. These estimates are followed by two additional upper and lower bounds based on the results of Jones [10, 11].

3.1 Bandwidth estimates

Since the extinction cross section is non-negative, it is clear that for any wavelength interval $\Lambda \subset [0, \infty)$,

$$|\Lambda| \min_{\lambda \in \Lambda} \sigma(\lambda) \leq \int_{\Lambda} \sigma(\lambda) \ \mathrm{d}\lambda \leq \int_0^{\infty} \sigma_{\mathrm{ext}}(\lambda) \ \mathrm{d}\lambda, \tag{3.1}$$

where $|\Lambda|$ is the absolute bandwidth and σ denotes any of the extinction, scattering and absorption cross sections σ_{ext}, σ_{s}, and σ_{a}, respectively. This seemingly trivial estimate gives a fundamental limitation on the product between the bandwidth and the amplitude of the cross sections, see Fig. 7.

3.2 Increasing material parameters

An important variational result can be established for isotropic material parameters with the long wavelength limit response given by the electric and magnetic susceptibilities, $\chi_{\mathrm{e}}(\boldsymbol{x})$ and $\chi_{\mathrm{m}}(\boldsymbol{x})$, respectively. The result states that the integrated extinction increase monotonically with increasing $\chi_{\mathrm{e}}(\boldsymbol{x})$ and $\chi_{\mathrm{m}}(\boldsymbol{x})$ for each $\boldsymbol{x} \in \mathbb{R}^3$ [11, Thm. 1], *i.e.*,

$$\chi_{i1}(\boldsymbol{x}) \leq \chi_{i2}(\boldsymbol{x}), \quad \boldsymbol{x} \in \mathbb{R}^3 \quad \Longrightarrow \quad \int_0^{\infty} \sigma_{\mathrm{ext}1}(\lambda) \ \mathrm{d}\lambda \leq \int_0^{\infty} \sigma_{\mathrm{ext}2}(\lambda) \ \mathrm{d}\lambda, \tag{3.2}$$

where $i = \mathrm{e}, \mathrm{m}$. Recall that Kramers-Kronig relations [17, pp. 279–281] implies that $\chi_{\mathrm{e}}(\boldsymbol{x})$ and $\chi_{\mathrm{m}}(\boldsymbol{x})$ pointwise are non-negative, provided the conductivity is zero. If the conductivity of the scatterer is non-zero, the electric polarizability dyadic, $\boldsymbol{\gamma}_{\mathrm{e}}$, can be determined by letting the electric susceptibility becoming infinitely large [15, pp. 49–50]. As a consequence of (3.2), no heterogeneous scatterer has a larger integrated extinction than the corresponding homogeneous one with maximal susceptibility.

3.3 Eigenvalue estimates

The static polarizability dyadics $\boldsymbol{\gamma}_{\mathrm{e}}$ and $\boldsymbol{\gamma}_{\mathrm{m}}$ are real-valued and symmetric, and hence diagonalizable with real-valued eigenvalues $\gamma_{\mathrm{e}j}$ and $\gamma_{\mathrm{m}j}$ with $j = 1, 2, 3$, respectively,

ordered as $\gamma_{e1} \geq \gamma_{e2} \geq \gamma_{e3}$ and $\gamma_{m1} \geq \gamma_{m2} \geq \gamma_{m3}$. Since the right hand side of (2.8) is the Rayleigh quotients of $\boldsymbol{\gamma}_e$ and $\boldsymbol{\gamma}_m$, their largest and smallest eigenvalues bound (2.8) according to standard matrix theory,[1] *viz.*,

$$\pi^2(\gamma_{e3} + \gamma_{m3}) \leq \int_0^\infty \sigma_{ext}(\lambda)\ \mathrm{d}\lambda \leq \pi^2(\gamma_{e1} + \gamma_{m1}), \tag{3.3}$$

Equality on the left (right) hand side of (3.3) holds when $\hat{\boldsymbol{p}}_e$ is a unit eigenvector of $\boldsymbol{\gamma}_e$ with eigenvalue γ_{e3} (γ_{e1}) and $\hat{\boldsymbol{p}}_m$ simultaneously is a unit eigenvector of $\boldsymbol{\gamma}_m$ with eigenvalue γ_{m3} (γ_{m1}).

3.4 Scatterers of arbitrary shape

Broadband scattering in the sense of the integrated extinction is according to (3.3) directly related to the eigenvalues of the static polarizability dyadics. Lemma 2 in Jones [11] applied to (3.3) yields

$$\pi^2 \int_V \frac{\chi_e(\boldsymbol{x})}{\chi_e(\boldsymbol{x})+1} + \frac{\chi_m(\boldsymbol{x})}{\chi_m(\boldsymbol{x})+1}\ \mathrm{dV}_{\boldsymbol{x}} \leq \int_0^\infty \sigma_{ext}(\lambda)\ \mathrm{d}\lambda \leq \pi^2 \int_V \chi_e(\boldsymbol{x}) + \chi_m(\boldsymbol{x})\ \mathrm{dV}_{\boldsymbol{x}}. \tag{3.4}$$

The bounds in (3.4) are sharp in the sense that equality can be obtained as a limiting process for certain homogeneous ellipsoids, see Section 4.

The right hand side of (3.4) is bounded from above by $|V|\|\chi_e + \chi_m\|_\infty$, where $\|f\|_\infty = \sup_{\boldsymbol{x}\in V} |f(\boldsymbol{x})|$ denotes the supremum norm. As a consequence, the upper bound on the integrated extinction for any heterogeneous scatterer is less than or equal to the integrated extinction for the corresponding homogeneous scatterer with susceptibilities $\|\chi_e\|_\infty$ and $\|\chi_m\|_\infty$. This observation leads to the conclusion that there is no fundamental difference on the integrated extinction between scattering by heterogeneous and homogeneous obstacles.

For weak scatterers in the sense of the Born-approximation, $\|\chi_e + \chi_m\|_\infty \ll 1$, and (3.4) implies

$$\int_0^\infty \sigma_{ext}(\lambda)\ \mathrm{d}\lambda = \pi^2 \int_V \chi_e(\boldsymbol{x}) + \chi_m(\boldsymbol{x})\ \mathrm{dV}_{\boldsymbol{x}} + \mathcal{O}(\|\chi_e + \chi_m\|_\infty^2), \tag{3.5}$$

where the Taylor series expansion $1/(1+x) = 1 + \mathcal{O}(x)$ for $|x| < 1$ have been used. Note that (3.5) reduces to a particularly simple form for homogeneous scatterers.

3.5 Star-shaped scatterers

Due to (3.2), it is possible to derive upper bounds on the integrated extinction by applying the bounds to the corresponding homogeneous scatterer with susceptibilities $\|\chi_e\|_\infty$ and $\|\chi_m\|_\infty$. To this end, assume V is star-shaped in the sense that $K_V \neq \emptyset$, where K_V is the set of $\boldsymbol{x} \in V$ such that for all $\boldsymbol{y} \in V$ and $0 \leq s \leq 1$

[1] If the eigenvectors corresponding to the largest eigenvalues are the same for the electric and the magnetic cases, the bounds in (3.3) can be sharpened.

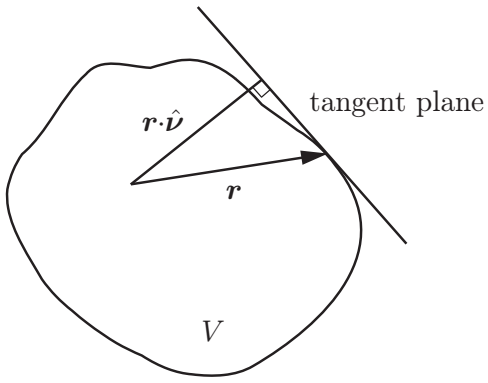

Figure 3: Geometry for the star-shape parametrization.

the straight line $\boldsymbol{x} + (1-s)\boldsymbol{y}$ is contained in V, *i.e.*, if it has an interior point from which its entire boundary can be seen. For a convex scatterer, $K_V = V$.

A refined upper bound on $\gamma_{\mathrm{e}1}$ and $\gamma_{\mathrm{m}1}$ [10, Thm. 5] applied to (3.3), also taking into account the shape of V, yields the inequality

$$\int_0^\infty \sigma_{\mathrm{ext}}(\lambda)\ \mathrm{d}\lambda \leq \pi^2 |V| \psi \left(\frac{\|\chi_{\mathrm{e}}\|_\infty}{\psi + \|\chi_{\mathrm{e}}\|_\infty} + \frac{\|\chi_{\mathrm{m}}\|_\infty}{\psi + \|\chi_{\mathrm{m}}\|_\infty} \right), \tag{3.6}$$

where the geometrical factor ψ is defined by

$$\psi = \frac{3}{|V|} \max_j \int_S \frac{(\hat{\boldsymbol{e}}_j \cdot \boldsymbol{r})^2}{\boldsymbol{r} \cdot \hat{\boldsymbol{\nu}}}\ \mathrm{dS}_{\boldsymbol{r}} \leq \frac{9}{|V|} \int_S \frac{r^2}{\boldsymbol{r} \cdot \hat{\boldsymbol{\nu}}}\ \mathrm{dS}_{\boldsymbol{r}}. \tag{3.7}$$

Here, $\hat{\boldsymbol{e}}_j$ denote mutually orthonormal vectors and $\mathrm{dS}_{\boldsymbol{r}}$ is the surface measure of S with respect to $\boldsymbol{r}$ (S is the bounding surface of V). The denominator in (3.7) is the distance from the tangent plane to the origin, see Figure 3. The upper bound in (3.7) is independent of the coordinate system orientation but depends on the location of the origin.

Furthermore, the right hand side of (3.6) is bounded from above by either $\|\chi_{\mathrm{e}}\|_\infty$ and $\|\chi_{\mathrm{m}}\|_\infty$ or ψ. The first case yields (3.4) for a homogeneous scatterer (material parameters $\|\chi_{\mathrm{e}}\|_\infty$ and $\|\chi_{\mathrm{m}}\|_\infty$), while the latter implies

$$\int_0^\infty \sigma_{\mathrm{ext}}(\lambda)\ \mathrm{d}\lambda \leq 2\pi^2 |V| \psi, \tag{3.8}$$

irrespectively of the material parameters of V. By comparing (3.4) with (3.8), it is clear that (3.8) provides the sharpest bound when $2\psi < \|\chi_{\mathrm{e}} + \chi_{\mathrm{m}}\|_\infty$. Note that (3.2) implies that it is possible to evaluate (3.7) for any surface circumscribing the scatterer V.

The geometrical factor for the oblate spheroid is $\psi = 3(4 + \xi^{-2})/5$ and for the prolate spheroid $\psi = 3(3 + 2\xi^{-2})/5$ (the origin at the center of the spheroid), where $\xi \in [0, 1]$ is the ratio of the minor to the major semi-axis. In particular, $\psi = 3$ for the sphere. The bound in (3.6) is isoperimetric since equality holds for the homogeneous sphere, see Section 4. The geometrical factor ψ for the circular cylinder of radius b and length ℓ is[2] $\psi = \max\{3 + 3b^2/\ell^2, 3 + \ell^2/2b^2\}$.

[2]This expression deviates from the result of Jones [10].

3.6 Jung's theorem

Jung's theorem [13] gives an optimal upper bound on the radius of a bounded subset $V \subset \mathbb{R}^3$ in terms of its diameter, $\operatorname{diam} V$. The theorem states that V is contained in the unique sphere of radius $R_V \leq \sqrt{6}/4 \operatorname{diam} V$, with equality if and only if the closure of V contains the vertices of a tetrahedron of edge lengths equal to $\operatorname{diam} V$. Since $\psi = 3$ for the sphere and $|V|$ is bounded from above by the volume of the sphere of radius R_V, (3.6) yields

$$\int_0^\infty \sigma_{\mathrm{ext}}(\lambda)\ \mathrm{d}\lambda \leq \frac{\pi^3 3\sqrt{6}}{8}(\operatorname{diam} V)^3 \left(\frac{\|\chi_{\mathrm{e}}\|_\infty}{3+\|\chi_{\mathrm{e}}\|_\infty} + \frac{\|\chi_{\mathrm{m}}\|_\infty}{3+\|\chi_{\mathrm{m}}\|_\infty} \right). \tag{3.9}$$

The right hand side of (3.9) can be estimated from above independently of the material parameters. We get

$$\int_0^\infty \sigma_{\mathrm{ext}}(\lambda)\ \mathrm{d}\lambda \leq \frac{\pi^3 3\sqrt{6}}{4}(\operatorname{diam} V)^3,$$

which is useful in cases where the right hand side of (3.8) diverges.

In this section, we have applied Jung's theorem to a sphere circumscribing the scatterer. There are, however, other choices of circumscribing surfaces that can be utilized [9].

4 Homogeneous ellipsoidal scatterers

For homogeneous, anisotropic ellipsoidal scatterers with susceptibility dyadics $\boldsymbol{\chi}_{\mathrm{e}}$ and $\boldsymbol{\chi}_{\mathrm{m}}$, closed-form expressions of $\boldsymbol{\gamma}_{\mathrm{e}}$ and $\boldsymbol{\gamma}_{\mathrm{m}}$ exist [12], *viz.*,

$$\boldsymbol{\gamma}_i = |V|\boldsymbol{\chi}_i \cdot (\mathbf{I} + \mathbf{L} \cdot \boldsymbol{\chi}_i)^{-1}, \quad i = \mathrm{e}, \mathrm{m} \tag{4.1}$$

where $\mathbf{L}$ and $\mathbf{I}$ are the depolarizing and unit dyadics in $\mathbb{R}^3$, respectively. In terms of the semi-axes a_j in the $\hat{\boldsymbol{e}}_j$-direction, the volume $|V| = 4\pi a_1 a_2 a_3/3$. The depolarizing dyadic has unit trace, and is real-valued and symmetric [32], and, hence, diagonalizable with real-valued eigenvalues. Its eigenvalues are the depolarizing factors L_j [6, 23]

$$L_j = \frac{a_1 a_2 a_3}{2} \int_0^\infty \frac{\mathrm{d}s}{(s+a_j^2)\sqrt{(s+a_1^2)(s+a_2^2)(s+a_3^2)}}, \quad j = 1, 2, 3. \tag{4.2}$$

The depolarizing factors satisfy $0 \leq L_j \leq 1$ and $\sum_j L_j = 1$.

Closed-form expressions of (4.2) exist in the special case of the ellipsoids of revolution, *i.e.*, the prolate and oblate spheroids. In terms of the eccentricity $e = \sqrt{1-\xi^2}$, where $\xi \in [0, 1]$ is the ratio of the minor to the major semi-axis, the depolarizing factors are (symmetry axis along the $\hat{\boldsymbol{e}}_3$-direction)

$$L_1 = L_2 = \frac{1}{4e^3}\left(2e - (1-e^2)\ln\frac{1+e}{1-e}\right), \qquad L_3 = \frac{1-e^2}{2e^3}\left(\ln\frac{1+e}{1-e} - 2e\right), \tag{4.3}$$

and

$$L_1 = L_2 = \frac{1-e^2}{2e^2}\left(-1 + \frac{\arcsin e}{e\sqrt{1-e^2}}\right), \qquad L_3 = \frac{1}{e^2}\left(1 - \frac{\sqrt{1-e^2}}{e}\arcsin e\right),$$

for the prolate and oblate spheroids, respectively. In particular, $L_j = 1/3$ for the sphere.

The integrated extinction for anisotropic homogeneous ellipsoidal scatterers is given by (4.1) inserted into (2.8). The result is

$$\int_0^\infty \sigma_{\text{ext}}(\lambda)\ \mathrm{d}\lambda = \pi^2|V| \sum_{i=\text{e,m}} \hat{\boldsymbol{p}}_i^* \cdot \boldsymbol{\chi}_i \cdot (\mathbf{I} + \mathbf{L}\cdot\boldsymbol{\chi}_i)^{-1} \cdot \hat{\boldsymbol{p}}_i. \tag{4.4}$$

For isotropic material parameters, $\boldsymbol{\chi}_\text{e} = \chi_\text{e}\mathbf{I}$ and $\boldsymbol{\chi}_\text{m} = \chi_\text{m}\mathbf{I}$, (4.4) reduces to

$$\int_0^\infty \sigma_{\text{ext}}(\lambda)\ \mathrm{d}\lambda = \pi^2|V| \sum_{j=1}^{3} \left(\frac{\kappa_{\text{e}j}\chi_\text{e}}{1+\chi_\text{e}L_j} + \frac{\kappa_{\text{m}j}\chi_\text{m}}{1+\chi_\text{m}L_j}\right), \tag{4.5}$$

where $\kappa_{\text{e}j} = |\hat{\boldsymbol{p}}_\text{e}\cdot\hat{\boldsymbol{e}}_j|^2$ and $\kappa_{\text{m}j} = |\hat{\boldsymbol{p}}_\text{m}\cdot\hat{\boldsymbol{e}}_j|^2$ are the polarization vectors projected onto the mutually orthonormal vectors $\hat{\boldsymbol{e}}_j$. Note that $\sum_j \kappa_{\text{e}j} = \sum_j \kappa_{\text{m}j} = 1$, and that the averaged integrated extinction is characterized by $\kappa_{\text{e}j} = \kappa_{\text{m}j} = 1/3$. For prolate and oblate spheroids, which are axially symmetric with respect to the $\hat{\boldsymbol{e}}_3$-axis, a plane wave incident at an angle θ to this axis, yields

$$\begin{cases} \kappa_{\text{e}1} + \kappa_{\text{e}2} = 1 \\ \kappa_{\text{e}3} = 0 \\ \kappa_{\text{m}1} + \kappa_{\text{m}2} = \cos^2\theta \\ \kappa_{\text{m}3} = \sin^2\theta \end{cases} \quad \text{(TE)} \qquad \begin{cases} \kappa_{\text{m}1} + \kappa_{\text{m}2} = 1 \\ \kappa_{\text{m}3} = 0 \\ \kappa_{\text{e}1} + \kappa_{\text{e}2} = \cos^2\theta \\ \kappa_{\text{e}3} = \sin^2\theta \end{cases} \quad \text{(TM)}$$

In the limit as the volume goes to zero, the integrated extinction vanishes for a scatterer with finite susceptibilities. To obtain a non-zero integrated extinction, the scatterer has either to be conducting or evaluated in the high-contrast limit, see *e.g.*, the PEC disk below. In the long wavelength PEC limit, see (2.9), the integrated extinction becomes

$$\int_0^\infty \sigma_{\text{ext}}(\lambda)\ \mathrm{d}\lambda = \pi^2|V| \sum_{j=1}^{3} \left(\frac{\kappa_{\text{e}j}}{L_j} - \frac{\kappa_{\text{m}j}}{1-L_j}\right). \tag{4.6}$$

The right hand side of (4.5) is bounded from above by χ_i and from below by $\chi_i/(1+\chi_i)$. The bounds in (3.4) are sharp in the sense that χ_i and $\chi_i/(1+\chi_i)$ are obtained at arbitrary precision for the infinite needle and disk of constant volume $|V|$, respectively. In fact, the upper bound holds for an infinite needle oriented along the $\hat{\boldsymbol{e}}_3$-direction ($L_1 + L_2 = 1$) with parallel polarization ($\kappa_{i3} = 1$). The corresponding equality for the lower bound holds for the infinite disk with unit normal vector $\hat{\boldsymbol{e}}_3$ ($L_3 = 1$) and parallel polarization ($\kappa_{i3} = 1$).

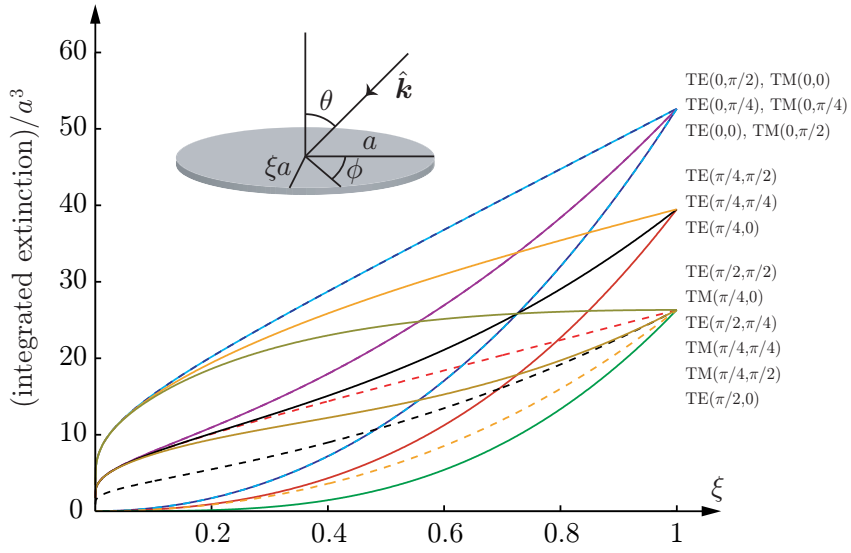

Figure 4: The integrated extinction (4.7) in units of a^3 as function of the semi-axis ratio ξ for the PEC elliptic disk. The notations TE(θ,ϕ) and TM(θ,ϕ) refer to the TE- and TM-polarizations for $\theta,\phi \in \{0,\pi/4,\pi/2\}$.

A simple example of (4.5) is given by the homogeneous sphere for which the integrated extinction is equal to $3\pi^2|V|\sum_i \chi_i/(\chi_i+3)$ independent of κ_{ej} and κ_{mj}, which also is the result of Bohren and Huffman for the non-magnetic case [4, p. 117]. In particular, the PEC limit (2.9) implies that the integrated extinction for the sphere is equal to $3\pi^2|V|/2$. Similar results for stratified dielectric spheres are obtained using recursive compositions of Möbius transformations. For the case of two layers, see Section 5.5.

The integrated extinction for the PEC elliptic disk is given by (4.6), and the integrals in (4.2), as the semi-axis a_3 approaches zero, are available in the literature [6, p. 507], [23]. The result is

$$\begin{cases} L_1/|V| = \dfrac{3}{4\pi a^3 e^2}\,(\mathrm{K}-\mathrm{E}) \\ L_2/|V| = \dfrac{3}{4\pi a^3 e^2}\,\big(\mathrm{E}/(1-e^2)-\mathrm{K}\big) \\ (L_3-1)/|V| = -\dfrac{3\mathrm{E}}{4\pi a^3(1-e^2)} \end{cases}$$

where a is the major semi-axis, and $\mathrm{E}=\mathrm{E}(e^2)$ and $\mathrm{K}=\mathrm{K}(e^2)$ are the complete elliptic integrals of first and second kind, respectively [1, p. 590]. We obtain

$$\int_0^\infty \sigma_{\mathrm{ext}}(\lambda)\ \mathrm{d}\lambda = \frac{4\pi^3 a^3}{3}\begin{cases} B\cos^2\phi + C\sin^2\phi - A\sin^2\theta & (\mathrm{TE}) \\ \big(B\sin^2\phi + C\cos^2\phi\big)\cos^2\theta & (\mathrm{TM}) \end{cases} \tag{4.7}$$

where θ and ϕ are the spherical angles of the incident direction, $\hat{\boldsymbol{k}}$. The factors A,

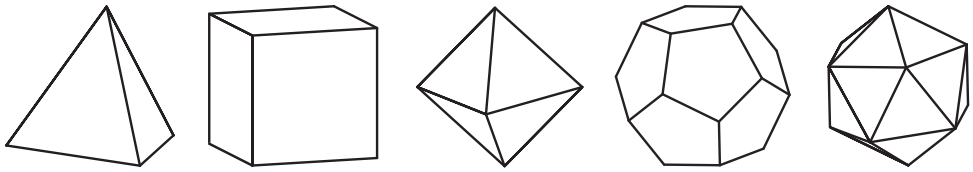

49.6$|V|$ 35.9$|V|$ 35.0$|V|$ 31.4$|V|$ 30.9$|V|$

Figure 5: The integrated extinctions for the Platonic solids based on MoM-calculations [25]. The Platonic solids are from left to right the tetrahedron, hexahedron, octahedron, dodecahedron and icosahedron, with 4, 6, 8, 12 and 20 faces, respectively.

B, and C are defined as

$$A = \frac{1-e^2}{\mathrm{E}}, \quad B = \frac{e^2(1-e^2)}{\mathrm{E}-(1-e^2)\mathrm{K}}, \quad C = \frac{e^2}{\mathrm{K}-\mathrm{E}}.$$

Note that the TM-polarization vanishes for $\theta = \pi/2$ independently of $\phi \in [0, 2\pi)$. The integrated extinction (4.7) can also be derived from the long wavelength limit of the T-matrix approach [3].

The integrated extinction in the right hand side of (4.7) as function of ξ is depicted in Figure 4. Note the degeneracy of the integrated extinction at the end points $\xi = 0$ and $\xi = 1$, corresponding to the PEC needle of length $2a$ and the PEC circular disk of radius a, respectively.

5 Numerical results

In this section, we illustrate the theoretical results obtained above by several numerical examples. Specifically, we calculate the extinction cross sections and the eigenvalues of the polarizability dyadics for a set of scatterers with isotropic material parameters. These results are then compared to the theoretical results presented in Sections 2, 3, and 4.

5.1 Platonic solids

Since the homogeneous Platonic solids are invariant under a set of appropriate point groups, their polarizability dyadics are isotropic. By (2.8) this implies that the integrated extinctions are independent of both polarization and incident direction. The five Platonic solids are depicted in Figure 5, see also Table 1, together with the integrated extinctions in the non-magnetic, high-contrast limit, *i.e.*, $\chi_{\mathrm{e}} \to \infty$.

A common lower bound on the integrated extinctions in Figure 5 is obtained by (4.5) for the volume-equivalent sphere. This lower bound is motivated by Jones' result [10, Thm. 3], and the fact that the polarizability dyadics are isotropic. The result is $14.80|V|$.

Platonic solids	$\gamma_e/\lvert V\rvert$	γ_e/a^3	**Int. ext.**	$\lvert V\rvert/a^3$
Tetrahedron	5.03	0.593	$49.6\lvert V\rvert$	$\sqrt{2}/12$
Hexahedron	3.64	3.64	$35.9\lvert V\rvert$	1
Octahedron	3.55	1.67	$35.0\lvert V\rvert$	$\sqrt{2}/3$
Dodecahedron	3.18	24.4	$31.4\lvert V\rvert$	$(15+7\sqrt{5})/4$
Icosahedron	3.13	6.83	$30.9\lvert V\rvert$	$5(3+\sqrt{5})/12$

Table 1: The eigenvalues γ_e and the integrated extinction for the Platonic solids in units of $|V|$ in the high-contrast limit $\chi_e \to \infty$. The last column gives the volume of the Platonic solids expressed in the edge length a.

Upper bounds on the integrated extinctions are given by the smallest circumscribing high-contrast spheres, which based on solid geometry are found to be $241.60|V|$, $80.54|V|$, $61.98|V|$, $44.62|V|$ and $48.96|V|$ for the tetrahedron, hexahedron, octahedron, dodecahedron and icosahedron, respectively, see (3.2). The upper and lower bounds are seen to be quite close to the numerical values presented in Figure 5, at least for the dodecahedron and icosahedron, which do not deviate much from the volume-equivalent sphere. Since the Platonic solids are star-shaped with respect to all interior points, a somewhat different set of upper bounds can be derived from (3.6).

5.2 Dielectric spheroids

The averaged extinction cross section, $\bar{\sigma}_{\text{ext}}$, as function of the radius ka for a prolate and oblate spheroid is illustrated in Figure 6. The solid curve depicts the averaged extinction cross section (equal to the extinction cross section) for the volume-equivalent sphere of radius a, and the dashed and dotted curves correspond to the prolate and oblate spheroids, respectively, of semi-axis ratio $\xi = 1/2$. The scatterers are non-magnetic with electric susceptibility $\chi_e = 1$. Note that the largest variation of the curves in Figure 6 occurs for the sphere due to the fact that its extinction cross section is independent of the polarization and the direction of incidence, which implies that no resonances are averaged out in contrast to the case for the prolate and oblate spheroids.

The numerically integrated averaged extinction cross sections for $ka \in [0, 20]$ agree within relative errors of 1.2% with the theoretical values $7.46|V|$ and $7.48|V|$ based on (4.5) for the prolate and oblate spheroids, respectively. The corresponding values for the sphere are 0.7% and $7.40|V|$. The calculations are based on the T-matrix approach [19].

According to Section 2, a lower bound on the averaged integrated extinctions for the spheroids is $7.40|V|$ corresponding to the volume-equivalent sphere. Based on (3.4), lower and upper bounds common to the three curves in Figure 6 are $4.93|V|$ and $9.87|V|$, respectively. Using the star-shaped bound (3.6), these upper bounds are improved to $8.57|V|$ and $8.17|V|$ for the prolate and the oblate spheroids, respectively. Both the lower and upper bounds are reasonable close to the theoretical

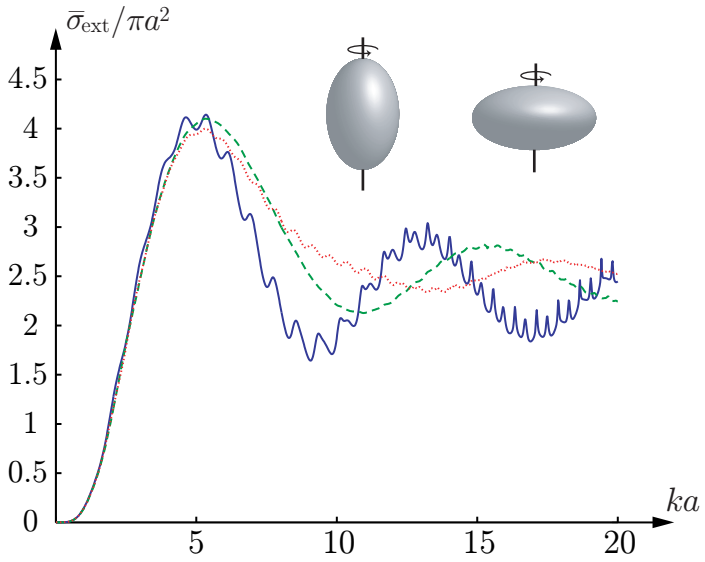

Figure 6: The averaged extinction cross section, $\bar{\sigma}_{\text{ext}}$, in units of πa^2 as function of ka for a prolate (dashed) and oblate (dotted) non-magnetic spheroid with electric susceptibility $\chi_{\text{e}} = 1$ and semi-axis ratio $\xi = 1/2$. The extinction cross section for the volume-equivalent sphere of radius a (solid) is included.

values.

5.3 Lorentz dispersive circular cylinder

The averaged extinction cross section, $\bar{\sigma}_{\text{ext}}$, as function of the frequency for a Lorentz dispersive circular cylinder is depicted in Figure 7. The ratio of the cylinder length ℓ to its radius b is $\ell/b = 2$. The cylinder is non-magnetic with electric susceptibility given by the Lorentz model [4, Sec. 9.1]

$$\chi_{\text{e}}(\omega) = \frac{\omega_{\text{p}}^2}{\omega_0^2 - \omega^2 - \text{i}\omega\nu},$$

where ω_{p} is the plasma frequency, ν the collision frequency and ω_0 the resonance frequency. Explicit values of ω_{p}, ω_0 and ν are $\omega_{\text{p}} = \omega_0 = 4\pi \cdot 10^9\,\text{rad/s}$, $\nu = 0.7 \cdot 10^9\,\text{rad/s}$, and $\omega_{\text{p}} = \omega_0 = 20\pi \cdot 10^9\,\text{rad/s}$, $\nu = 10^{10}\,\text{rad/s}$, respectively. The Lorentz parameters are chosen such that all three curves in the left figure have the same long wavelength susceptibility $\chi_{\text{e}} = \chi_{\text{e}}(0) = 1$. The first two curves with peaks at 2 GHz and 10 GHz depict the dispersive case, while the third for comparison illustrates the results for the non-dispersive case. The three curves in the left figure have the same integrated extinctions, since their long wavelength susceptibilities coincide. The calculation is based on the T-matrix approach [19].

A numerical calculation of the eigenvalues of the polarizability dyadic for the dielectric cylinder is performed by adopting the finite element method (FEM). The results are $0.773|V|$, $0.749|V|$, and $0.749|V|$. This result implies that the numerically

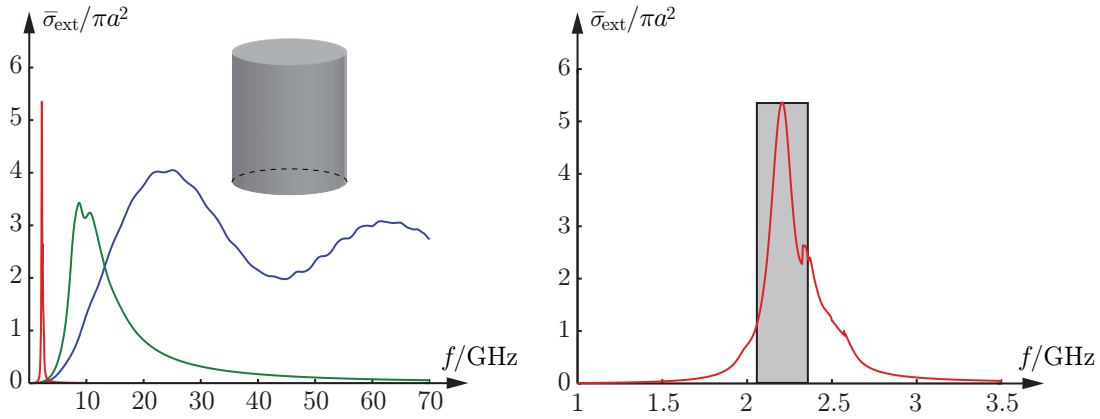

Figure 7: The averaged extinction cross section, $\bar{\sigma}_{\text{ext}}$, in units of πa^2 as function of the frequency in GHz for a non-magnetic Lorentz dispersive circular cylinder with volume-equivalent sphere of radius $a = 1\,\text{cm}$. The three curves in the left figure have the same long wavelength response $\chi_{\text{e}} = 1$. The first two curves with peaks at 2 GHz and 10 GHz are Lorentz dispersive, while the third curve is non-dispersive. The right figure is a close-up of the 2 GHz peak in the left figure.

computed averaged extinction cross section, $\bar{\sigma}_{\text{ext}}$, in (2.10) is $7.47|V|$. The numerically calculated integrated extinction in the interval $f \in [0, 70]\,\text{GHz}$ is $7.43|V|$ for the first, and $7.44|V|$ for the second curve in Figure 7.

Common lower and upper bounds on the integrated extinctions based on (3.4) are $4.94|V|$ and $9.87|V|$, respectively. A sharper lower bound is $7.40|V|$ corresponding to the volume-equivalent sphere. An upper bound can for comparison be obtained from (3.6). For $\ell/b = 2$ this implies $\psi = 5$ and the upper bound $8.23|V|$, which is sharper than the bound based on (3.4).

The figure on the right hand side of Figure 7 is a close-up of the 2 GHz peak. The boundary curve of the box corresponds to an artificial scatterer with averaged extinction cross section supported at the peak, *i.e.*, for an averaged extinction cross section that vanishes everywhere outside the box. The integrated extinction for the boundary curve of the box and the three curves in the left hand side of Figure 7 coincide.

5.4 Debye dispersive non-spherical raindrop

The averaged extinction cross section, $\bar{\sigma}_{\text{ext}}$, as function of the frequency for a falling raindrop is depicted in Figure 8. The axially symmetric drop is parameterized by the polar angle θ and the radial distance

$$r(\theta) = r_0 \left(1 + \sum_{k=0}^{10} c_k \cos k\theta \right),$$

where r_0 is determined from the condition of the volume-equivalence with the sphere of radius a, *i.e.*, $|V| = \frac{2\pi}{3} \int_0^\pi r^3(\theta) \sin\theta \;\, \mathrm{d}\theta$ with $|V| = 4\pi a^3/3$. The radius of

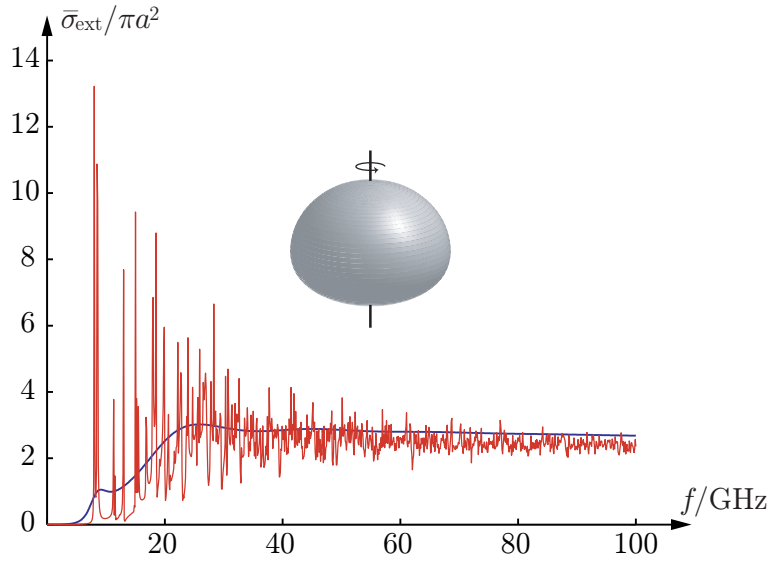

Figure 8: The averaged extinction cross section, $\bar{\sigma}_{\text{ext}}$, in units of πa^2 as function of the frequency in GHz for a raindrop of volume-equivalent radius $a = 2\,\text{mm}$. The smooth curve is for the Debye-model (5.1), while the oscillatory curve is for the non-dispersive case. The two curves have the same long wavelength response and therefore also the same integrated extinctions.

the volume-equivalent sphere used in Figure 8 is $a = 2\,\text{mm}$ with associated shape coefficients $c_0 = -0.0458$, $c_1 = 0.0335$, $c_2 = -0.1211$, $c_3 = 0.0227$, $c_4 = 0.0083$, $c_5 = -0.0089$, $c_6 = 0.0012$, $c_7 = 0.0021$, $c_8 = -0.0013$, $c_9 = -0.0001$ and $c_{10} = 0.0008$ [2]. The calculation is based on the T-matrix approach [19].

The smooth curve in Figure 8 is for the non-magnetic Debye model [4, Sec. 9.5]

$$\chi_{\text{e}}(\omega) = \chi_\infty + \frac{\chi_{\text{s}} - \chi_\infty}{1 - \text{i}\omega\tau}, \tag{5.1}$$

where τ is the relaxation time and χ_∞ and χ_{s} are the short and long wavelength susceptibilities, respectively. Pure water at 20°C is considered with $\chi_{\text{s}} = 79.2$, $\chi_\infty = 4.6$ and $\tau = 9.36\,\text{ps}$ [14, p. 43]. The curve with largest variation is for the non-dispersive case with an susceptibility identical to the long wavelength limit, χ_{s}, of (5.1).

Since the long wavelength susceptibilities coincide for the two curves in Figure 8, their integrated extinctions are equal according to (2.10). The eigenvalues of the polarizability dyadics for the raindrop can be obtained by numerical computations. A finite element method (FEM) computation gives the three eigenvalues: $2.43|V|$, $3.21|V|$, and $3.21|V|$, respectively. This result implies that the numerically computed averaged extinction cross section, $\bar{\sigma}_{\text{ext}}$, in (2.10) is $29.1|V|$. If we numerically integrate the average extinction cross section in Figure 8 over $f \in [0, 100]\,\text{GHz}$, we get $26.4|V|$ for the dispersive and $25.6|V|$ for the non-dispersive curve, respectively. The reason why the numerically integrated extinctions are about 10% below the FEM values is due to the finite integration interval.

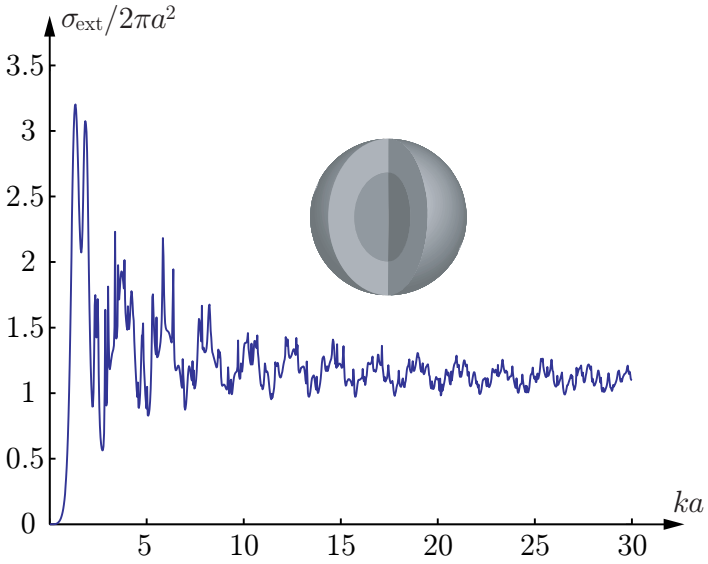

Figure 9: The extinction cross section, σ_{ext}, in units of $2\pi a^2$ as function of the radius ka for a dielectric stratified sphere with two layers of equal volume. The electric and magnetic susceptibilities are $\chi_{\text{e}1} = 2$ and $\chi_{\text{m}1} = 1$ for the core and $\chi_{\text{e}2} = 1$ and $\chi_{\text{m}2} = 2$ for the outer layer.

Lower and upper bounds on the integrated extinctions, given by (3.4), are $9.75|V|$ and $782|V|$, respectively, which are rather crude. A more accurate lower bound is given by the non-magnetic, volume-equivalent sphere with static susceptibilities $\chi_{\text{e}} = \chi_{\text{s}}$, for which (4.5) yields $28.5|V|$. The star-shaped bound in Section 3.5 is also applicable. The result for the raindrop is $32.15|V|$. We observe that both the lower and upper bounds approximate the true value very well.

5.5 Dielectric stratified sphere

Due to spherical symmetry, the polarizability dyadics of a stratified sphere are isotropic and easily computed by recursive applications of Möbius transformations. In particular, the integrated extinction for two layers with electric and magnetic susceptibilities $\chi_{\text{e}1}$ and $\chi_{\text{m}1}$ in the core, and $\chi_{\text{e}2}$ and $\chi_{\text{m}2}$ in the outer layer, respectively, is

$$\int_0^\infty \sigma_{\text{ext}}(\lambda)\ \mathrm{d}\lambda = 3\pi^2|V| \sum_{i=\text{e,m}} \frac{\chi_{i2}(\chi_{i1}+2\chi_{i2}+3)+\varsigma^3(2\chi_{i2}+3)(\chi_{i1}-\chi_{i2})}{(\chi_{i2}+3)(\chi_{i1}+2\chi_{i2}+3)+2\varsigma^3\chi_{i2}(\chi_{i1}-\chi_{i2})}, \quad (5.2)$$

where ς is the ratio of the inner to the outer radius. The special cases $\varsigma = 0$ and $\varsigma = 1$ correspond to homogeneous spheres with susceptibilities χ_{i2} and χ_{i1}, respectively, see Section 4. Moreover, both $\chi_{i1} = \chi_{i2}$ and $\chi_{i2} = 0$ yield the homogeneous sphere of susceptibility χ_{i1}, with the volume of the sphere being a fraction ς^3 of the volume $|V|$ in the latter case.

The extinction cross section, σ_{ext}, as function of the radius ka for the stratified sphere with two layers of equal volume, $\varsigma = 1/\sqrt[3]{2}$, is depicted in Figure 9. The

used susceptibilities are $\chi_{\mathrm{e}1} = 2$ and $\chi_{\mathrm{m}1} = 1$ in the core, and $\chi_{\mathrm{e}2} = 1$ and $\chi_{\mathrm{m}2} = 2$ in the outer layer. The calculations are based on the Mie-series approach [18]. Note that the curve in Figure 9 approaches twice the geometrical cross section area in the short wavelength limit. Compare this observation with the extinction paradox [31, pp. 107–108].

The numerically integrated extinction is $19.1|V|$ for $ka \in [0, 30]$ and $19.3|V|$ for $ka \in [0, 100]$, with relative errors of 1.7% and 0.5%, respectively, compared to the theoretical value $19.4|V|$ given by (5.2).

Lower and upper bounds on the integrated extinction based on the inequality in (3.2) are $14.8|V|$ and $23.7|V|$, respectively, corresponding to the volume-equivalent homogeneous sphere with minimal and maximal susceptibilities, $\inf_{\boldsymbol{x}\in V} \chi_i$ and $\sup_{\boldsymbol{x}\in V} \chi_i$, respectively. Note that this upper bound coincides with the one obtained from (3.6), but that both the lower and upper bounds based on (3.2) are sharper than the ones given by (3.4).

5.6 PEC circular disk

The integrated extinction for the PEC circular disk of radius a is given by (4.7) in the limit $\xi \to 1$. The result is

$$\int_0^\infty \sigma_{\mathrm{ext}}(\lambda)\ \mathrm{d}\lambda = \frac{8\pi^2 a^3}{3} \begin{cases} 1 + \cos^2\theta & (\mathrm{TE}) \\ \\ 2\cos^2\theta & (\mathrm{TM}) \end{cases} \tag{5.3}$$

The right hand side of (5.3) can also be derived from the long wavelength limit of the T-matrix approach [16].

The extinction cross section, σ_{ext}, as function of the radius ka for the PEC circular disk is depicted in Figure 10. The notations TE(θ) and TM(θ) refer to the TE- and TM-polarizations, respectively, and the stars denote the short wavelength limit $\cos\theta$ given by the extinction paradox [31, pp. 107–108]. Note the degeneracy of both polarizations for normal incidence, and that the extinction cross section vanishes identically for TM($\pi/2$). The calculation is based on the T-matrix approach [16].

To find the numerically integrated extinctions, the integration interval $ka \in [0, 15]$ does not suffice to get reasonable accuracy. However, by extending the integrand above $ka = 15$ by the expected short wavelength limit, we obtain relative errors of 0.5% compared to the exact results of (5.3).

The bounds discussed in Section 3 are not directly applicable to the PEC circular disk since the disk has zero volume. However, a crude upper bound is obtained by the circumscribing PEC sphere. The result is $1.5\pi^2$, in units of the volume of the circumscribing sphere. Compare this with the exact results of (5.3) in terms of the volume of the circumscribing sphere — the factor 1.5 for the circumscribing sphere is to be compared with $4/\pi \approx 1.27$ at $\theta = 0$ incidence.

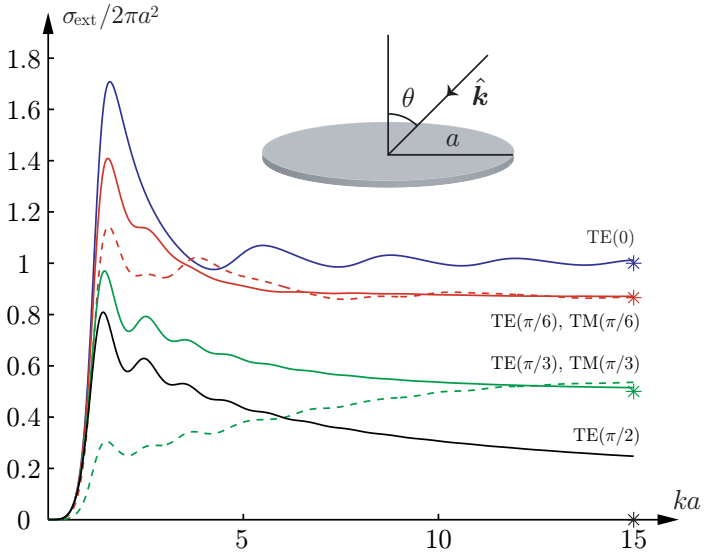

Figure 10: The extinction cross section, σ_{ext}, in units of $2\pi a^2$ as function of the radius ka for the PEC circular disk. The solid and dashed lines are for the TE- and TM-polarizations, respectively, and the stars denote the short wavelength limits $\cos\theta$.

5.7 PEC needle

The integrated extinction for the PEC needle of length $2a$ oriented along the $\hat{\boldsymbol{e}}_3$-direction is given by (4.3) and (4.6) in the limit $\xi \to 0$. The result is

$$\int_0^\infty \sigma_{\text{ext}}(\lambda)\ \mathrm{d}\lambda = \frac{4\pi^3 a^3}{3} \begin{cases} \mathcal{O}(\xi^2) & \text{(TE)} \\ \dfrac{\sin^2\theta}{\ln 2/\xi - 1} + \mathcal{O}(\xi^2) & \text{(TM)} \end{cases} \tag{5.4}$$

The right hand side of (5.4) can also be derived from the long wavelength limit of the T-matrix [3].

The integrated extinction (5.4) is seen to vanish for both polarizations in the limit $\xi \to 0$. Since the extinction cross section is non-negative, this implies that it vanishes almost everywhere except on a set of measure zero consisting of the denumerable resonances for which an integer multiple of $\lambda/2$ coincides with the length of the needle. This result is illustrated numerically in Figure 11, which shows the extinction cross section, σ_{ext}, for the PEC needle for the TM-polarization at normal incidence. Note that, due to symmetry, only resonances corresponding to ka equal to an odd multiple of $\pi/2$ are excited at normal incidence. The numerically integrated extinctions in Figure 11 agree well with (5.4). The relative errors are less than 0.5% with an integration interval $ka \in [0, 12]$ for the three curves.

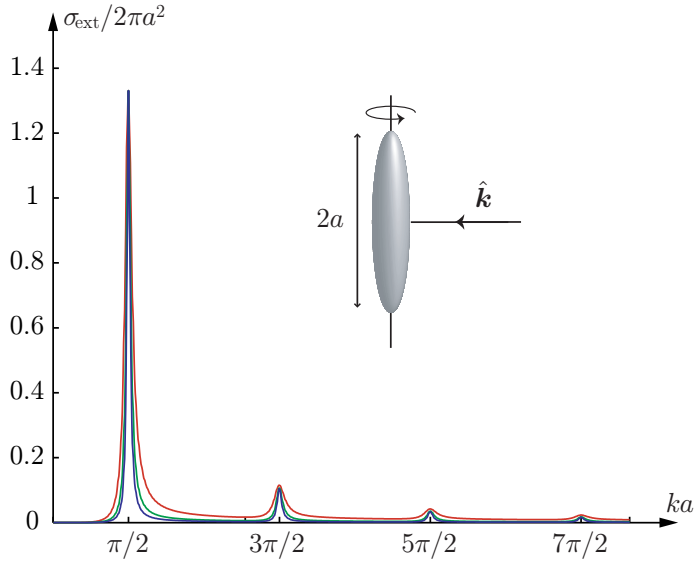

Figure 11: The extinction cross section, σ_{ext}, in units of $2\pi a^2$ as function of ka for the PEC needle of length $2a$. The needle is approximated by a prolate spheroid with semi-axis ratio 10^{-3} for the outermost, 10^{-5} for the intervening, and 10^{-7} for the innermost curve. The calculation is based on the T-matrix approach [3].

6 Concluding remarks

The integrated extinction is an example of what is referred to in modern physics as a dispersion relation [21]. The basic idea for the dispersion relations is that certain linear and causal physical quantities with known high-frequency (short wavelength) asymptotic are boundary values of holomorphic functions of one or more complex variables.

The major results of this paper are the proof and illustrations of the integrated extinction for linear, passive, and anisotropic scatterers. It is shown that the integrated extinction is monotonically increasing in the material properties. Moreover, the electric and magnetic material properties contribute equally to the integrated extinction. It is also shown that the integrated extinction is useful in deriving physical limitations on broadband scattering.

The integrated extinction is particularly important from an antenna point of view, since it generalizes the physical limitations on the antenna performance derived by Chu [5] for the smallest circumscribing sphere. These new limitations, which can be shown to relate bandwidth and directivity of any antenna in terms of volume and shape, are reported in [7]. The integrated extinction is also of great interest in applications to broadband scattering by artificial material models such as metamaterials. In this application, it provides physical limitations on scattering by general material models [27]. Moreover, the bounds presented in Section 3 may be of use to bound material parameters in inverse scattering problems. All these applications to material modeling and inverse scattering problems are currently under investigation, and will be reported in forthcoming papers.

Additional theoretical work on the integrated extinction also includes bi-anisotropy and diamagnetics, which will be reported elsewhere. Finally, it should be noted that the concept of the integrated extinction with minor changes also holds in linear acoustics [26].

Acknowledgments

The financial support by the Swedish Research Council is gratefully acknowledged.

Appendix A The polarizability dyadics

For an anisotropic scatterer modeled by the material dyadic $\boldsymbol{\tau}$ (electric susceptibility dyadic $\boldsymbol{\chi}_{\mathrm{e}}$ without a conductivity term, or magnetic susceptibility dyadic $\boldsymbol{\chi}_{\mathrm{m}}$), the total electric field $\boldsymbol{E}$ (similarly for the magnetic field $\boldsymbol{H}$) satisfies

$$\begin{cases} \nabla \times \boldsymbol{E}(\boldsymbol{x}) = \boldsymbol{0} \\ \nabla \cdot ((\boldsymbol{\tau}(\boldsymbol{x}) + \mathbf{I}) \cdot \boldsymbol{E}(\boldsymbol{x})) = 0 \end{cases} \quad \boldsymbol{x} \in \mathbb{R}^3$$

Here, $\boldsymbol{\tau}$ is assumed to be a symmetric dyadic at all points $\boldsymbol{x}$ and sufficiently regular to justify the operations below.

Decompose the total field $\boldsymbol{E}$ as $\boldsymbol{E}_j = E_0 \hat{\boldsymbol{e}}_j + \boldsymbol{E}_{\mathrm{s}j}$, where $j = 1, 2, 3$. The pertinent partial differential equation for the scattered field $\boldsymbol{E}_{\mathrm{s}j}$ is then

$$\begin{cases} \nabla \times \boldsymbol{E}_{\mathrm{s}j}(\boldsymbol{x}) = \boldsymbol{0} \\ \nabla \cdot ((\boldsymbol{\tau}(\boldsymbol{x}) + \mathbf{I}) \cdot \boldsymbol{E}_{\mathrm{s}j}(\boldsymbol{x})) = -E_0 \nabla \cdot (\boldsymbol{\tau}(\boldsymbol{x}) \cdot \hat{\boldsymbol{e}}_j) \end{cases} \quad \boldsymbol{x} \in \mathbb{R}^3 \tag{A.1}$$

together with the asymptotic condition $\boldsymbol{E}_{\mathrm{s}j}(\boldsymbol{x}) \to \mathcal{O}(|\boldsymbol{x}|^{-3})$ as $|\boldsymbol{x}| \to \infty$.

The first condition in (A.1) implies that there exists a potential Φ_j related to the scattered field as $\boldsymbol{E}_{\mathrm{s}j} = -\nabla \Phi_j$ satisfying

$$\begin{cases} \nabla \cdot ((\boldsymbol{\tau}(\boldsymbol{x}) + \mathbf{I}) \cdot \nabla \Phi_j(\boldsymbol{x})) = E_0 \nabla \cdot (\boldsymbol{\tau}(\boldsymbol{x}) \cdot \hat{\boldsymbol{e}}_j) \\ \Phi_j(\boldsymbol{x}) \to \mathcal{O}(|\boldsymbol{x}|^{-2}) \text{ as } |\boldsymbol{x}| \to \infty \end{cases} \quad \boldsymbol{x} \in \mathbb{R}^3 \tag{A.2}$$

This problem has a unique solution. The entries of the polarizability dyadic $\boldsymbol{\gamma}$ ($\boldsymbol{\gamma}_{\mathrm{e}}$ or $\boldsymbol{\gamma}_{\mathrm{m}}$ depending on whether the problem is electric or magnetic) is then ($i, j = 1, 2, 3$)

$$\hat{\boldsymbol{e}}_i \cdot \boldsymbol{\gamma} \cdot \hat{\boldsymbol{e}}_j = \frac{1}{E_0} \hat{\boldsymbol{e}}_i \cdot \int_{\mathbb{R}^3} \boldsymbol{\tau}(\boldsymbol{x}) \cdot \boldsymbol{E}_j(\boldsymbol{x}) \, \mathrm{dV}_{\boldsymbol{x}}. \tag{A.3}$$

Scale this solution by a factor α, *i.e.*, let $\boldsymbol{x} \longrightarrow \boldsymbol{x}' = \alpha \boldsymbol{x}$, with material dyadic $\boldsymbol{\tau}'(\boldsymbol{x}') = \boldsymbol{\tau}(\boldsymbol{x})$, and denote the solution to the new problem by $\Phi'_j(\boldsymbol{x}')$. The new problem then satisfies

$$\begin{cases} \nabla' \cdot \big((\boldsymbol{\tau}'(\boldsymbol{x}') + \mathbf{I}) \cdot \nabla' \Phi'_j(\boldsymbol{x}')\big) = E_0 \nabla' \cdot (\boldsymbol{\tau}'(\boldsymbol{x}') \cdot \hat{\boldsymbol{e}}_j) \\ \Phi'_j(\boldsymbol{x}') \to 0 \text{ as } |\boldsymbol{x}'| \to \infty \end{cases} \quad \boldsymbol{x}' \in \mathbb{R}^3$$

or in the unscaled coordinates

$$\begin{cases} \alpha^{-2}\nabla\cdot\big((\boldsymbol{\tau}(\boldsymbol{x})+\mathbf{I})\cdot\nabla\Phi_j'(\alpha\boldsymbol{x})\big) = E_0\alpha^{-1}\nabla\cdot(\boldsymbol{\tau}(\boldsymbol{x})\cdot\hat{\boldsymbol{e}}_j) \\ \Phi_j'(\alpha\boldsymbol{x})\to 0 \text{ as } |\boldsymbol{x}|\to\infty \end{cases} \qquad \boldsymbol{x}\in\mathbb{R}^3$$

Due to the unique solubility of the boundary value problem (A.2), $\Phi_j'(\boldsymbol{x}') = \alpha\Phi_j(\boldsymbol{x})$, and consequently $\boldsymbol{E}_j'(\boldsymbol{x}') = \boldsymbol{E}_j(\boldsymbol{x}) = \boldsymbol{E}_j(\boldsymbol{x}'/\alpha)$. The polarizability dyadic for the scaled problem then becomes

$$\hat{\boldsymbol{e}}_i\cdot\boldsymbol{\gamma}'\cdot\hat{\boldsymbol{e}}_j = \hat{\boldsymbol{e}}_i\cdot\int_{\mathbb{R}^3}\boldsymbol{\tau}'(\boldsymbol{x}')\cdot\boldsymbol{E}_j'(\boldsymbol{x}')\,\mathrm{dV}_{\boldsymbol{x}'} = \alpha^3\hat{\boldsymbol{e}}_i\cdot\int_{\mathbb{R}^3}\boldsymbol{\tau}(\boldsymbol{x})\cdot\boldsymbol{E}_j(\boldsymbol{x})\,\mathrm{dV}_{\boldsymbol{x}},$$

and we see that $\boldsymbol{\gamma}$ scales with the volume $|V|\sim\alpha^3$.

A.1 Symmetry

The polarizability dyadic $\boldsymbol{\gamma}$ is symmetric, since $\boldsymbol{\tau}$ is assumed symmetric at all points $\boldsymbol{x}$. In fact, from (A.3),

$$\hat{\boldsymbol{e}}_i\cdot\boldsymbol{\gamma}\cdot\hat{\boldsymbol{e}}_j = \hat{\boldsymbol{e}}_i\cdot\int_{\mathbb{R}^3}\boldsymbol{\tau}(\boldsymbol{x})\cdot\hat{\boldsymbol{e}}_j\,\mathrm{dV}_{\boldsymbol{x}} - \frac{1}{E_0}\hat{\boldsymbol{e}}_i\cdot\int_{\mathbb{R}^3}\boldsymbol{\tau}(\boldsymbol{x})\cdot\nabla\Phi_j(\boldsymbol{x})\,\mathrm{dV}_{\boldsymbol{x}}. \tag{A.4}$$

The last integral in (A.4) is rewritten as

$$\begin{aligned}
&\hat{\boldsymbol{e}}_i\cdot\int_{\mathbb{R}^3}\boldsymbol{\tau}(\boldsymbol{x})\cdot\nabla\Phi_j(\boldsymbol{x})\,\mathrm{dV}_{\boldsymbol{x}} \\
&= \int_{\mathbb{R}^3}\nabla\cdot(\hat{\boldsymbol{e}}_i\cdot\boldsymbol{\tau}(\boldsymbol{x})\Phi_j(\boldsymbol{x}))\,\mathrm{dV}_{\boldsymbol{x}} - \int_{\mathbb{R}^3}\nabla\cdot(\hat{\boldsymbol{e}}_i\cdot\boldsymbol{\tau}(\boldsymbol{x}))\,\Phi_j(\boldsymbol{x})\,\mathrm{dV}_{\boldsymbol{x}} \\
&= -\int_{\mathbb{R}^3}\nabla\cdot(\boldsymbol{\tau}(\boldsymbol{x})\cdot\hat{\boldsymbol{e}}_i)\,\Phi_j(\boldsymbol{x})\,\mathrm{dV}_{\boldsymbol{x}} \\
&= -\frac{1}{E_0}\int_{\mathbb{R}^3}\nabla\cdot((\boldsymbol{\tau}(\boldsymbol{x})+\mathbf{I})\cdot\nabla\Phi_i(\boldsymbol{x}))\,\Phi_j(\boldsymbol{x})\,\mathrm{dV}_{\boldsymbol{x}},
\end{aligned}$$

due to (A.2) provided $\boldsymbol{\tau}$ is symmetric at all points $\boldsymbol{x}$. Furthermore,

$$\begin{aligned}
&\hat{\boldsymbol{e}}_i\cdot\int_{\mathbb{R}^3}\boldsymbol{\tau}(\boldsymbol{x})\cdot\nabla\Phi_j(\boldsymbol{x})\,\mathrm{dV}_{\boldsymbol{x}} \\
&= -\frac{1}{E_0}\int_{\mathbb{R}^3}\nabla\cdot\{((\boldsymbol{\tau}(\boldsymbol{x})+\mathbf{I})\cdot\nabla\Phi_i(\boldsymbol{x}))\,\Phi_j(\boldsymbol{x})\}\,\mathrm{dV}_{\boldsymbol{x}} \\
&+ \frac{1}{E_0}\int_{\mathbb{R}^3}\nabla\Phi_j(\boldsymbol{x})\cdot((\boldsymbol{\tau}(\boldsymbol{x})+\mathbf{I})\cdot\nabla\Phi_i(\boldsymbol{x}))\,\mathrm{dV}_{\boldsymbol{x}} \\
&= \frac{1}{E_0}\int_{\mathbb{R}^3}\nabla\Phi_j(\boldsymbol{x})\cdot((\boldsymbol{\tau}(\boldsymbol{x})+\mathbf{I})\cdot\nabla\Phi_i(\boldsymbol{x}))\,\mathrm{dV}_{\boldsymbol{x}}.
\end{aligned}$$

The polarizability dyadic (A.4) therefore becomes

$$\hat{\boldsymbol{e}}_i\cdot\boldsymbol{\gamma}\cdot\hat{\boldsymbol{e}}_j = \hat{\boldsymbol{e}}_i\cdot\int_{\mathbb{R}^3}\boldsymbol{\tau}(\boldsymbol{x})\cdot\hat{\boldsymbol{e}}_j\,\mathrm{dV}_{\boldsymbol{x}} - \frac{1}{E_0^2}\int_{\mathbb{R}^3}\nabla\Phi_j(\boldsymbol{x})\cdot((\boldsymbol{\tau}(\boldsymbol{x})+\mathbf{I})\cdot\nabla\Phi_i(\boldsymbol{x}))\,\mathrm{dV}_{\boldsymbol{x}},$$

which clearly is symmetric in the indices i and j if $\boldsymbol{\tau}$ is symmetric at all points $\boldsymbol{x}$.

A.2 High-contrast limit

In the high-contrast limit, when the entries of the material dyadic become infinitely large independent of $\boldsymbol{x}$, the appropriate surface integral representation of the polarizability dyadic is [15, p. 22]

$$\hat{\boldsymbol{e}}_i \cdot \boldsymbol{\gamma} \cdot \hat{\boldsymbol{e}}_j = \frac{1}{E_0} \hat{\boldsymbol{e}}_i \cdot \sum_{n=1}^{N} \int_{S_n} (\hat{\boldsymbol{\nu}}(\boldsymbol{x}) \Phi_j(\boldsymbol{x}) - \boldsymbol{x} \hat{\boldsymbol{\nu}}(\boldsymbol{x}) \cdot \nabla \Phi_j(\boldsymbol{x})) \, \mathrm{dS}_{\boldsymbol{x}},$$

where S_n, $n = 1, 2, \ldots, N$ denote the bounding surfaces (outward-directed unit normal $\hat{\boldsymbol{\nu}}$) of the domain outside the material (we assume that $\boldsymbol{\tau}$ is compactly supported). Moreover, $\Psi_j(\boldsymbol{x}) = \Phi_j(\boldsymbol{x}) - E_0 x_j$, is the solution to ($n = 1, 2, \ldots, N$)

$$\begin{cases} \nabla^2 \Psi_j(\boldsymbol{x}) = 0, \quad \boldsymbol{x} \text{ outside } S_n \\ \displaystyle\int_{S_n} \hat{\boldsymbol{\nu}}(\boldsymbol{x}) \cdot \nabla \, \Psi_j(\boldsymbol{x})|_+ \, \mathrm{dS}_{\boldsymbol{x}} = 0 \\ \Psi_j(\boldsymbol{x}) \to -E_0 x_j + \mathcal{O}(|\boldsymbol{x}|^{-2}) \text{ as } |\boldsymbol{x}| \to \infty \end{cases}$$

With similar arguments as above, we find that the eigenvalues of the high-contrast polarizability dyadic also scale with the volume. For the relation with the capacitance concept, we refer to [15].

References

[1] M. Abramowitz and I. A. Stegun, editors. *Handbook of Mathematical Functions*. Applied Mathematics Series No. 55. National Bureau of Standards, Washington D.C., 1970.

[2] K. V. Beard and C. C. Chuang. A new model for the equilibrium shape of raindrops. *J. Atmos. Sci.*, **44**(11), 1509–1524, 1986.

[3] J. Björkberg and G. Kristensson. Electromagnetic scattering by a perfectly conducting elliptic disk. *Canad. J. Phys.*, **65**(7), 723–734, 1987.

[4] C. F. Bohren and D. R. Huffman. *Absorption and Scattering of Light by Small Particles*. John Wiley & Sons, New York, 1983.

[5] L. J. Chu. Physical limitations of omni-directional antennas. *Appl. Phys.*, **19**, 1163–1175, 1948.

[6] R. E. Collin. *Field Theory of Guided Waves*. IEEE Press, New York, second edition, 1991.

[7] M. Gustafsson, C. Sohl, and G. Kristensson. Physical limitations on antennas of arbitrary shape. *Proc. R. Soc. A*, **463**, 2007. doi:1098/rspa.2007.1893.

[8] M. Gustafsson. On the non-uniqueness of the electromagnetic instantaneous response. *J. Phys. A: Math. Gen.*, **36**, 1743–1758, 2003.

[9] F. John. Extremum problems with inequalities as subsidiary conditions. In O. E. Friedrichs, K. O. Neugebauer and J. J. Stoker, editors, *Studies and Essays: Courant Anniversary Volume*, pages 187–204. Wiley-Interscience, New York, 1948.

[10] D. S. Jones. Low frequency electromagnetic radiation. *J. Inst. Maths. Applics.*, **23**(4), 421–447, 1979.

[11] D. S. Jones. Scattering by inhomogeneous dielectric particles. *Quart. J. Mech. Appl. Math.*, **38**, 135–155, 1985.

[12] R. C. Jones. A generalization of the dielectric ellipsoid problem. *Phys. Rev.*, **68**(3–4), 93–96, 1945.

[13] H. W. E. Jung. Über die kleinste Kugel, die eine räumliche Figur einschliesst. *J. reine angew. Math.*, **123**, 241–257, 1901.

[14] U. Kaatze. Microwave dielectric properties of water. In A. Kraszewski, editor, *Microwave Aquametry*, chapter 2, pages 37–53. IEEE Press, New York, 1996.

[15] R. E. Kleinman and T. B. A. Senior. Rayleigh scattering. In V. V. Varadan and V. K. Varadan, editors, *Low and high frequency asymptotics*, volume 2 of *Acoustic, Electromagnetic and Elastic Wave Scattering*, chapter 1, pages 1–70. Elsevier Science Publishers, Amsterdam, 1986.

[16] G. Kristensson and P. C. Waterman. The T-matrix for acoustic and electromagnetic scattering by circular disks. *J. Acoust. Soc. Am.*, **72**(5), 1612–1625, 1982.

[17] L. D. Landau, E. M. Lifshitz, and L. P. Pitaevskiĭ. *Electrodynamics of Continuous Media*. Pergamon, Oxford, second edition, 1984.

[18] G. Mie. Beiträge zur Optik trüber Medien, speziell kolloidaler Metallösungen. *Ann. Phys. Leipzig*, **25**, 377–445, 1908.

[19] M. I. Mishchenko and L. D. Travis. Capabilities and limitations of a current FORTRAN implementation of the T-matrix method for randomly oriented, rotationally symmetric scatterers. *J. Quant. Spectrosc. Radiat. Transfer*, **60**(3), 309–324, 1998.

[20] R. G. Newton. *Scattering Theory of Waves and Particles*. Dover Publications, New York, second edition, 2002.

[21] H. M. Nussenzveig. *Causality and dispersion relations*. Academic Press, London, 1972.

[22] H. M. Nussenzveig. *Diffraction Effects in Semiclassical Scattering*. Cambridge University Press, Cambridge, U.K., 1992.

[23] J. A. Osborn. Demagnetizing factors of the general ellipsoid. *Phys. Rev.*, **67**, 351–357, 1945.

[24] E. M. Purcell. On the absorption and emission of light by interstellar grains. *J. Astrophys.*, **158**, 433–440, 1969.

[25] A. Sihvola, P. Ylä-Oijala, S. Järvenpää, and J. Avelin. Polarizabilities of Platonic solids. *IEEE Trans. Antennas Propagat.*, **52**(9), 2226–2233, 2004.

[26] C. Sohl, M. Gustafsson, and G. Kristensson. The integrated extinction for broadband scattering of acoustic waves. Technical Report LUTEDX/(TEAT-7156)/1–10/(2007), Lund University, Department of Electrical and Information Technology, P.O. Box 118, S-221 00 Lund, Sweden, 2007. http://www.eit.lth.se.

[27] C. Sohl, M. Gustafsson, and G. Kristensson. Physical limitations on metamaterials: Restrictions on scattering and absorption over a frequency interval. Technical Report LUTEDX/(TEAT-7154)/1–11/(2007), Lund University, Department of Electrical and Information Technology, P.O. Box 118, S-221 00 Lund, Sweden, 2007. http://www.eit.lth.se.

[28] J. W. Strutt. On the light from the sky, its polarization and colour. *Phil. Mag.*, **41**, 107–120 and 274–279, April 1871. Also published in Lord Rayleigh, Scientific Papers, volume I, Cambridge University Press, Cambridge, 1899.

[29] J. R. Taylor. *Scattering theory: the quantum theory of nonrelativistic collisions.* Robert E. Krieger Publishing Company, Malabar, Florida, 1983.

[30] E. C. Titchmarsh. *Introduction to the Theory of Fourier Integrals.* Oxford University Press, Oxford, second edition, 1948.

[31] H. van de Hulst. *Light Scattering by Small Particles.* John Wiley & Sons, Inc., New York, 1957.

[32] A. D. Yaghjian. Electric dyadic Green's functions in the source region. *Proc. IEEE*, **68**(2), 248–263, 1980.

Physical limitations on metamaterials: Restrictions on scattering and absorption over a frequency interval

Paper II

Christian Sohl, Mats Gustafsson, and Gerhard Kristensson

Based on: C. Sohl, M. Gustafsson, and G. Kristensson. Physical limitations on metamaterials: Restrictions on scattering and absorption over a frequency interval. Technical Report LUTEDX/(TEAT-7154)/1–11/(2007), Lund University.

Abstract

A limitation on the extinction cross section, valid for all scatterers satisfying some basic physical assumptions, is investigated. The physical limitation is obtained from the holomorphic properties of the forward scattering dyadic. The analysis focuses on the consequences for materials with negative permittivity and permeability, *i.e.*, metamaterials. From a broadband point of view, the limitations imply that there is no fundamental difference between metamaterials and ordinary materials with respect to scattering and absorption. The analysis is illustrated by three numerical examples of metamaterials modeled by temporal dispersion.

1 Introduction

Since the introduction of negative refractive index materials by V. G. Veselago in Ref. 14, there has been an enormous theoretical and experimental interest in the possibilities of such materials. These materials are often referred to as metamaterials, even though a metamaterial in general is a much broader concept of a structured material, and not necessarily composed of materials with negative permittivity and permeability values. Negative refractive index materials seem not to occur naturally, and if they can be manufactured, they possess extravagant properties promising for various physical applications, see Refs. 9 and 11, and references therein.

The scattering properties of obstacles consisting of metamaterials have been of considerable scientific interest during the last decade. Mostly canonical geometries, such as the spheres, see *e.g.*, Ref. 10, have been employed, and the design of scatterers that both increases and decreases the scattering properties have been reported.

The analysis presented in this paper show that, from a broadband point of view, the scattering and absorption properties of any material (not just metamaterials) that satisfy basic physical assumptions, are limited by the static electric and magnetic behavior of the composed materials. In particular, we show that, when these limitations are applied to low-frequency resonances on metamaterials, large scattering effects have to be traded for bandwidth. Specifically, the lower the resonance frequency, the higher its Q-factor. For a single frequency, metamaterials may possess exceptional characteristics, but, since bandwidth is essential, it is important to study metamaterials over a frequency interval, and with physically realistic dispersion models.

The results presented in this paper are independent of how the material that constitutes the scatterer is constructed or produced. This broad range of material models is a consequence of the fact that the analysis is solely based on the principles of energy conservation and causality applied to a set of linear and time-translational invariant constitutive relations.

The present paper is a direct application of the theory for broadband scattering introduced in Ref. 12. In addition to material modeling, the theory has also been applied successfully to physical limitations on arbitrary antennas in Refs. 1 and 3. The underlying mathematical description for broadband scattering is motivated by

the study of causality and dispersion relations in the scattering theory of waves and particles in Refs. 7 and 8.

2 Derivation of the integrated extinction

Consider a localized and bounded scatterer $V \subset \mathbb{R}^3$ of arbitrary shape. The dynamics of the material in V is modeled by the Maxwell equations with general heterogeneous and anisotropic constitutive relations. The constitutive relations are expressed in terms of the electric and magnetic susceptibility dyadics, $\boldsymbol{\chi}_\mathrm{e}$ and $\boldsymbol{\chi}_\mathrm{m}$, respectively. Due to the heterogeneous character of $\boldsymbol{\chi}_\mathrm{e}$ and $\boldsymbol{\chi}_\mathrm{m}$, V can be interpreted both as a single scatterer and as a set of multiple scatterers. The present analysis includes the perfectly conducting material model as well as general temporal dispersion with or without a conductivity term. The analysis can also be extended with minor changes to bianisotropic materials with the same conclusions drawn.

The direct scattering problem addressed in this paper is Fourier-synthesized plane wave scattering by V. Due to the linearity of the Maxwell equations, it is sufficient to consider monochromatic plane waves with time dependence $\mathrm{e}^{-\mathrm{i}\omega t}$. The incident wave is assumed to impinge in the $\hat{\boldsymbol{k}}$-direction with an electric field $\boldsymbol{E}_\mathrm{i}$ depending only on the difference $\tau = \mathrm{c}_0 t - \hat{\boldsymbol{k}} \cdot \boldsymbol{x}$, where $\boldsymbol{x}$ denotes the space variable. Introduce the far field amplitude $\boldsymbol{F}$ via $\boldsymbol{E}_\mathrm{s} = \boldsymbol{F}(\mathrm{c}_0 t - x, \hat{\boldsymbol{x}})/x + \mathcal{O}(x^{-2})$ as $x \to \infty$, where $\boldsymbol{E}_\mathrm{s}$ represents the scattered electric field. Under the assumption that the constitutive relations of V are linear and time-translational invariant, $\boldsymbol{F}$ is given by the convolution

$$\boldsymbol{F}(\tau, \hat{\boldsymbol{x}}) = \int_{-\infty}^{\infty} \mathbf{S}_\mathrm{t}(\tau - \tau', \hat{\boldsymbol{k}}, \hat{\boldsymbol{x}}) \cdot \boldsymbol{E}_\mathrm{i}(\tau') \, \mathrm{d}\tau'.$$

Here, $\mathbf{S}_\mathrm{t}$ is assumed to be primitive causal in the forward direction, *i.e.*, $\mathbf{S}_\mathrm{t}(\tau, \hat{\boldsymbol{k}}, \hat{\boldsymbol{k}}) = 0$ for $\tau < 0$, see Ref. 8. Furthermore, introduce the forward scattering dyadic $\mathbf{S}$ as the Fourier transform of $\mathbf{S}_\mathrm{t}$ evaluated in the forward direction, *i.e.*,

$$\mathbf{S}(k, \hat{\boldsymbol{k}}) = \int_{0^-}^{\infty} \mathbf{S}_\mathrm{t}(\tau, \hat{\boldsymbol{k}}, \hat{\boldsymbol{k}}) \mathrm{e}^{\mathrm{i}k\tau} \, \mathrm{d}\tau, \tag{2.1}$$

where $k = \omega/\mathrm{c}_0$. The extension of (2.1) to complex-valued k with $\operatorname{Im} k > 0$ improves the convergence of the integral and implies that $\mathbf{S}$ is holomorphic in the upper half of the complex k-plane. Recall that the cross symmetry relation $\mathbf{S}(k, \hat{\boldsymbol{k}}) = \mathbf{S}^*(-k^*, \hat{\boldsymbol{k}})$ is a direct consequence of such an extension.

Introduce $\boldsymbol{E}_0$ as the Fourier amplitude of the incident wave, and let $\hat{\boldsymbol{p}}_\mathrm{e} = \boldsymbol{E}_0/|\boldsymbol{E}_0|$ and $\hat{\boldsymbol{p}}_\mathrm{m} = \hat{\boldsymbol{k}} \times \hat{\boldsymbol{p}}_\mathrm{e}$ denote the associated electric and magnetic polarizations, respectively. Recall that $\boldsymbol{E}_0$ is subject to the constraint of transverse wave propagation, *i.e.*, $\boldsymbol{E}_0 \cdot \hat{\boldsymbol{k}} = 0$. Under the assumption that $\hat{\boldsymbol{p}}_\mathrm{e}$ and $\hat{\boldsymbol{p}}_\mathrm{m}$ are independent of k, it follows from the analysis above that also $\varrho(k) = \hat{\boldsymbol{p}}_\mathrm{e}^* \cdot \mathbf{S}(k, \hat{\boldsymbol{k}}) \cdot \hat{\boldsymbol{p}}_\mathrm{e}/k^2$ is holomorphic for $\operatorname{Im} k > 0$. Cauchy's integral theorem applied to ϱ then yields, see Ref. 12,

$$\varrho(\mathrm{i}\varepsilon) = \int_0^\pi \frac{\varrho(\mathrm{i}\varepsilon - \varepsilon \mathrm{e}^{\mathrm{i}\phi})}{2\pi} \, \mathrm{d}\phi + \int_0^\pi \frac{\varrho(\mathrm{i}\varepsilon + R\mathrm{e}^{\mathrm{i}\phi})}{2\pi} \, \mathrm{d}\phi + \int_{\varepsilon<|k|<R} \frac{\varrho(k + \mathrm{i}\varepsilon)}{2\pi \mathrm{i} k} \, \mathrm{d}k. \tag{2.2}$$

Here, it is assumed that ϱ is sufficiently regular to extend the contour to the real-axis in the last integral on the right hand side of (2.2). Relation (2.2) is subject to the limits $\varepsilon \to 0$ and $R \to \infty$.

The long wavelength limit of ϱ on the left hand side of (2.2) and the integrand in the first integral on the right hand side can be derived from a power series expansion of the Maxwell equations. The result is, see Ref. 4,

$$\varrho(\varepsilon) = \frac{1}{4\pi} \left(\hat{\boldsymbol{p}}_{\mathrm{e}}^{*} \cdot \boldsymbol{\gamma}_{\mathrm{e}} \cdot \hat{\boldsymbol{p}}_{\mathrm{e}} + \hat{\boldsymbol{p}}_{\mathrm{m}}^{*} \cdot \boldsymbol{\gamma}_{\mathrm{m}} \cdot \hat{\boldsymbol{p}}_{\mathrm{m}} \right) + \mathcal{O}(\varepsilon) \tag{2.3}$$

as $\varepsilon \to 0$, where $\boldsymbol{\gamma}_{\mathrm{e}}$ and $\boldsymbol{\gamma}_{\mathrm{m}}$ denote the electric and magnetic polarizability dyadics, respectively. For the appropriate definitions of $\boldsymbol{\gamma}_{\mathrm{e}}$ and $\boldsymbol{\gamma}_{\mathrm{m}}$, and some of their properties, see Ref. 12 and references therein.

The second integral on the right hand side of (2.2) vanishes in the limit as $R \to \infty$ according to the extinction paradox in Ref. 13. In terms of ϱ, a generalization of the extinction paradox states that $\varrho(k) = -A/(2\pi \mathrm{i} k) + \mathcal{O}(|k|^{-2})$ as $|k| \to \infty$. The constant A is real-valued since $\mathbf{S}(\mathrm{i}k, \hat{\boldsymbol{k}})$ is real-valued for real-valued k. For a large class of scatterers, A coincides with the projected area in the forward direction. The disappearance of the second integral on the right hand side of (2.2) is also supported by the fact that the high-frequency response of a material is non-unique from a modeling point of view, see Ref. 2.

From the details above, it is clear that the real part of (2.2) when subject to the limits $\varepsilon \to 0$ and $R \to \infty$, yields

$$\varrho(0) = \frac{1}{2}\varrho(0) + \frac{1}{8\pi^2} \int_{-\infty}^{\infty} \frac{\sigma_{\mathrm{ext}}(k)}{k^2} \, \mathrm{d}k, \tag{2.4}$$

where the optical theorem $\sigma_{\mathrm{ext}}(k) = 4\pi k \operatorname{Im} \varrho(k)$ has been invoked, see Ref. 12. Here, the extinction cross section σ_{ext} is defined as the sum of the scattered and absorbed power divided by the power flow density of the incident wave. Recall that the optical theorem is a direct consequence of energy conservation, see Ref. 7. Relation (2.3) inserted into (2.4) using the wavelength variable $\lambda = 2\pi/k$ finally yields

$$\int_0^{\infty} \sigma_{\mathrm{ext}}(\lambda) \, \mathrm{d}\lambda = \pi^2 \left(\hat{\boldsymbol{p}}_{\mathrm{e}}^{*} \cdot \boldsymbol{\gamma}_{\mathrm{e}} \cdot \hat{\boldsymbol{p}}_{\mathrm{e}} + \hat{\boldsymbol{p}}_{\mathrm{m}}^{*} \cdot \boldsymbol{\gamma}_{\mathrm{m}} \cdot \hat{\boldsymbol{p}}_{\mathrm{m}} \right). \tag{2.5}$$

The left hand side of (2.5) is referred to as the integrated extinction. For additional details on the derivation of (2.5), see Ref. 12.

Relation (2.5) is slightly modified when an isotropic conductivity term $\mathrm{i}\varsigma/\omega\epsilon_0$ is introduced in $\boldsymbol{\chi}_{\mathrm{e}}$ for some region of V, see Ref. 12. The scalar conductivity ς is non-negative and assumed independent of ω. In the presence of a conductivity term, the analysis in Ref. 4 shows that the right hand side of (2.5) should be evaluated in the limit as the eigenvalues of $\boldsymbol{\chi}_{\mathrm{e}}$ approach infinity independently of $\boldsymbol{\chi}_{\mathrm{m}}$. The perfectly conducting case is obtained as the eigenvalues of $\boldsymbol{\chi}_{\mathrm{m}}$ in addition approach -1.

Electric and magnetic material properties are seen to be treated on equal footing in (2.5), both in terms of polarization and material description. Furthermore,

the right hand side of (2.5) depends solely on the long wavelength limit or static response of V, while the left hand side is a dynamic quantity which unites the scattering and absorption properties of V. Recall that $\boldsymbol{\gamma}_\mathrm{e}$ and $\boldsymbol{\gamma}_\mathrm{m}$ only are functions of the geometry of V and the long wavelength susceptibilities $\boldsymbol{\chi}_\mathrm{e}(0) = \lim_{\omega\to 0}\boldsymbol{\chi}_\mathrm{e}(\omega)$ and $\boldsymbol{\chi}_\mathrm{m}(0) = \lim_{\omega\to 0}\boldsymbol{\chi}_\mathrm{m}(\omega)$. Here, $\boldsymbol{\chi}_\mathrm{e}(0)$ and $\boldsymbol{\chi}_\mathrm{m}(0)$ are real-valued in the case of vanishing conductivity. For heterogeneous structures, the long wavelength susceptibilities $\boldsymbol{\chi}_\mathrm{e}(0)$ and $\boldsymbol{\chi}_\mathrm{m}(0)$ also depend on the space variable $\boldsymbol{x}$.

In many applications, the scatterer is randomly oriented with respect to an ensamble of incident waves. For this purpose, the averaged extinction cross section $\bar{\sigma}_\mathrm{ext}$ is conviniently introduced by averaging (2.5) over the unit sphere in $\mathbb{R}^3$, *i.e.*,

$$\int_0^\infty \bar{\sigma}_\mathrm{ext}(\lambda)\ \mathrm{d}\lambda = \frac{\pi^2}{3}\,\mathrm{trace}(\boldsymbol{\gamma}_\mathrm{e}+\boldsymbol{\gamma}_\mathrm{m}). \tag{2.6}$$

For non-spherical particles, (2.6) provides a neat verification of (2.5) without specifying the orientation of V with respect to the incident wave, see Sec. 4.1.

3 Bounds on scattering and absorption

For applications to exotic material models such as metamaterials, it is beneficial to introduce the high-contrast polarizability dyadic $\boldsymbol{\gamma}_\infty$ as the limit of either $\boldsymbol{\gamma}_\mathrm{e}$ or $\boldsymbol{\gamma}_\mathrm{m}$ when the eigenvalues of $\boldsymbol{\chi}_\mathrm{e}(0)$ or $\boldsymbol{\chi}_\mathrm{m}(0)$ simultaneously become infinitely large. From the variational properties of $\boldsymbol{\gamma}_\mathrm{e}$ and $\boldsymbol{\gamma}_\mathrm{m}$ discussed in Ref. 12 and references therein, it follows that both $\boldsymbol{\gamma}_\mathrm{e}$ and $\boldsymbol{\gamma}_\mathrm{m}$ are bounded from above by $\boldsymbol{\gamma}_\infty$, *i.e.*,

$$\int_0^\infty \sigma_\mathrm{ext}(\lambda)\ \mathrm{d}\lambda \leq \pi^2\left(\hat{\boldsymbol{p}}_\mathrm{e}^*\cdot\boldsymbol{\gamma}_\infty\cdot\hat{\boldsymbol{p}}_\mathrm{e}+\hat{\boldsymbol{p}}_\mathrm{m}^*\cdot\boldsymbol{\gamma}_\infty\cdot\hat{\boldsymbol{p}}_\mathrm{m}\right). \tag{3.1}$$

The right hand side of (3.1) is independent of any material properties, depending only on the geometry and the orientation of V with respect to the incident wave. The right hand side can, independent of $\hat{\boldsymbol{p}}_\mathrm{e}$ and $\hat{\boldsymbol{p}}_\mathrm{m}$, further be estimated from above by the eigenvalues of $\boldsymbol{\gamma}_\infty$, see Ref. 12.

The integrated extinction can be used to derive various bounds and variational principles for broadband scattering. Since the extinction cross section σ_ext by definition is non-negative, the left hand side of (2.5) can be estimated from below as

$$|\Lambda|\inf_{\lambda\in\Lambda}\sigma(\lambda) \leq \int_\Lambda \sigma(\lambda)\ \mathrm{d}\lambda \leq \int_0^\infty \sigma_\mathrm{ext}(\lambda)\ \mathrm{d}\lambda, \tag{3.2}$$

where $\Lambda\subset[0,\infty)$ denotes an arbitrary wavelength interval with absolute bandwidth $|\Lambda|$. Here, σ represents any of the scattering, absorption and extinction cross sections, see Ref. 12 for their appropriate definitions. The quantity $|\Lambda|\inf_{\lambda\in\Lambda}\sigma(\lambda)$ in (3.2) is particularly useful for box-shaped limitations, *viz.*,

$$|\Lambda|\inf_{\lambda\in\Lambda}\sigma(\lambda) \leq \pi^2\left(\hat{\boldsymbol{p}}_\mathrm{e}^*\cdot\boldsymbol{\gamma}_\mathrm{e}\cdot\hat{\boldsymbol{p}}_\mathrm{e}+\hat{\boldsymbol{p}}_\mathrm{m}^*\cdot\boldsymbol{\gamma}_\mathrm{m}\cdot\hat{\boldsymbol{p}}_\mathrm{m}\right). \tag{3.3}$$

From (3.2) and (3.3) it is clear that the long wavelength limit response of V also provides upper bounds on scattering and absorption within any finite wavelength

interval Λ. Analogous to (3.1), the right hand side of (3.3) can also be estimated from above by $\boldsymbol{\gamma}_\infty$ and its eigenvalues. An important consequence of the fact that (2.5) and (3.3) only depend on the long wavelength limit response of V is that they are independent of any temporal dispersion.

The fact that (2.5) and (3.3) are independent of any temporal dispersion implies that there is no fundamental difference in scattering and absorption (in a broadband sense) between metamaterials and ordinary materials, as long as the static properties of the material are identical. In fact, it is well known that passive materials must be temporally dispersive since the Kramers-Kronig relations imply that $\boldsymbol{\chi}_\mathrm{e}(0)$ and $\boldsymbol{\chi}_\mathrm{m}(0)$ element-wise are non-negative in the absence of a conductivity term, see Ref. 5. Recall that the Kramers-Kronig relations are a direct consequence of primitive causality, see Ref. 8.

When an isotropic conductivity term $\mathrm{i}\varsigma/\omega\epsilon_0$ is present in $\boldsymbol{\chi}_\mathrm{e}$, the Kramers-Kronig relations must be modified due to the singular behavior of $\boldsymbol{\chi}_\mathrm{e}$. As mentioned above, the analysis in Ref. 4 shows that the introduction of such a term in $\boldsymbol{\chi}_\mathrm{e}$ implies that $\boldsymbol{\gamma}_\mathrm{e}$ should be substituted for $\boldsymbol{\gamma}_\infty$ in the right hand side of (2.5) and (3.3).

Two popular models for temporal dispersion for metamaterials are the Drude and Lorentz models, see (4.2) and Ref. 8, respectively. The Drude model is often preferred over the Lorentz model since it provides a wider bandwidth over which the eigenvalues of $\boldsymbol{\chi}_\mathrm{e}$ and $\boldsymbol{\chi}_\mathrm{m}$ attain values less than -1. However, based on the arguments above, it is uninteresting from the point of view of (2.5) and (3.3) which temporal dispersion model is used to characterize metamaterials as long as the model satisfies primitive causality.

In summary, the physical limitations on scattering and absorption discussed in Ref. 12 also hold for any metamaterials satisfying primitive causality. For a single frequency, metamaterials may possess extraordinary physical properties, but over any bandwidth they are with respect to scattering and absorption not different from materials with the eigenvalues of $\boldsymbol{\chi}_\mathrm{e}$ and $\boldsymbol{\chi}_\mathrm{m}$ non-negative.

4 Numerical synthesis of metamaterials

In this section, numerical results for three temporally dispersive scatterers are discussed in terms of the physical limitations in Sec. 3. The examples are chosen to provide a fictitious numerical synthesis of metamaterials. For convenience, the examples are restricted to isotropic material properties, *i.e.*, $\boldsymbol{\chi}_\mathrm{e} = \chi_\mathrm{e}\mathbf{I}$ and $\boldsymbol{\chi}_\mathrm{m} = \chi_\mathrm{m}\mathbf{I}$, where $\mathbf{I}$ denotes the unit dyadic. A similar example for the Lorentz dispersive cylinder is given in Ref. 12.

4.1 The Lorentz dispersive prolate spheroid

The averaged extinction cross section $\bar{\sigma}_\mathrm{ext}$ for a homogeneous and non-magnetic ($\chi_\mathrm{m} = 0$) prolate spheroid with semi-axis ratio $\xi = 1/2$ is depicted in Fig. 1. The prolate spheroid is temporally dispersive with electric susceptibility given by the

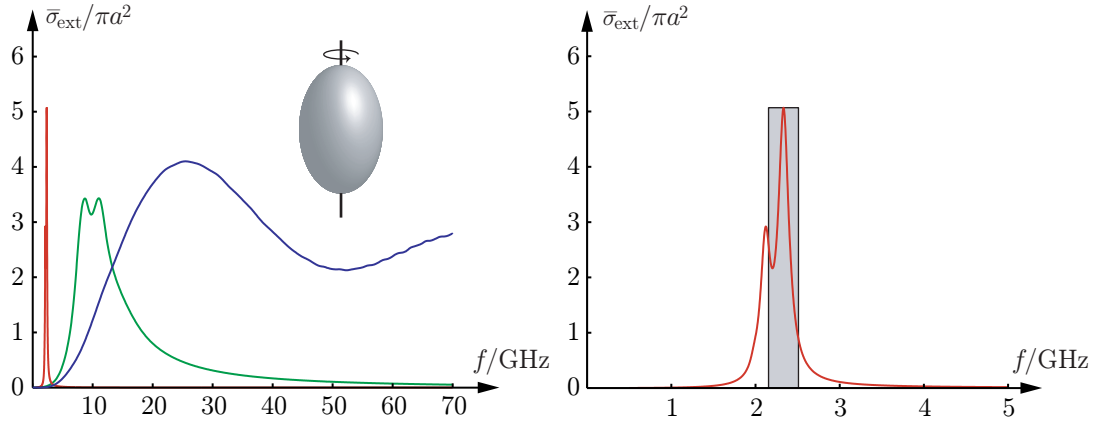

Figure 1: The averaged extinction cross section $\bar{\sigma}_{\text{ext}}$ as function of the frequency in GHz for a prolate spheroid with semi-axis ratio $\xi = 1/2$. Note the normalization with πa^2, where $a = 1\,\text{cm}$ denotes the radius of the volume-equivalent sphere.

Lorentz model, see Ref. 8,

$$\chi_{\text{e}}(\omega) = \frac{\omega_{\text{p}}^2}{\omega_0^2 - \omega^2 - \text{i}\omega\nu},$$

where $(\omega - \omega_0)\,\text{Re}\,\chi_{\text{e}}(\omega) \leq 0$ and $\text{Im}\,\chi_{\text{e}}(\omega) \geq 0$ for $\omega \in [0, \infty)$. Explicit values of ω_{p}, ω_0 and ν for the two curves with peaks at 2 GHz and 10 GHz are $\omega_{\text{p}} = \omega_0 = 4\pi \cdot 10^9\,\text{rad/s}$, $\nu = 7 \cdot 10^8\,\text{rad/s}$, and $\omega_{\text{p}} = \omega_0 = 20\pi \cdot 10^9\,\text{rad/s}$, $\nu = 10^{10}\,\text{rad/s}$, respectively. The third curve in the left figure corresponds to the non-dispersive case with $\chi_{\text{e}} = 1$, independent of ω. Since the three curves in the left figure have the same values of χ_{e} in the long wavelength limit, *i.e.*, $\chi_{\text{e}}(0) = 1$, it follows from (2.5) that their integrated extinctions coincide.

Closed-form expressions of the averaged integrated extinction (2.6) exist for the prolate and oblate spheroids, see Ref. 12. For a non-magnetic spheroid with semi-axis ratio ξ,

$$\int_0^\infty \bar{\sigma}_{\text{ext}}(\lambda)\,\text{d}\lambda = \frac{4\pi^3 a^3}{9} \sum_{j=1}^{3} \frac{1}{1 + L_j(\xi)}, \tag{4.1}$$

where $L_j(\xi)$ denote the associated depolarizing factors and a is the radius of the volume equivalent sphere. For a prolate spheroid with semi-axis ratio $\xi = 1/2$, the depolarizing factors are approximately given by $L_1(1/2) = L_2(1/2) = 0.4132$ and $L_3(1/2) = 0.1736$, see Ref. 12. For the prolate spheroid in Fig. 1, $a = 1\,\text{cm}$, and the right hand side of (4.1) is equal to $31.24\,\text{cm}^3$. The integrated extinction $31.24\,\text{cm}^3$ is also numerically confirmed with arbitrary precision for the three curves in Fig. 1.

The right figure in Fig. 1 is a close-up of the 2 GHz peak in the left figure. The shaded box represents a realization of an artificial scatterer with the averaged integrated extinction $31.24\,\text{cm}^3$ centered around the peak. The integrated extinction for the boundary curve of the box and the three curves in the left figure coincide. Note that the width of the box is approximately equal to the bandwidth of the

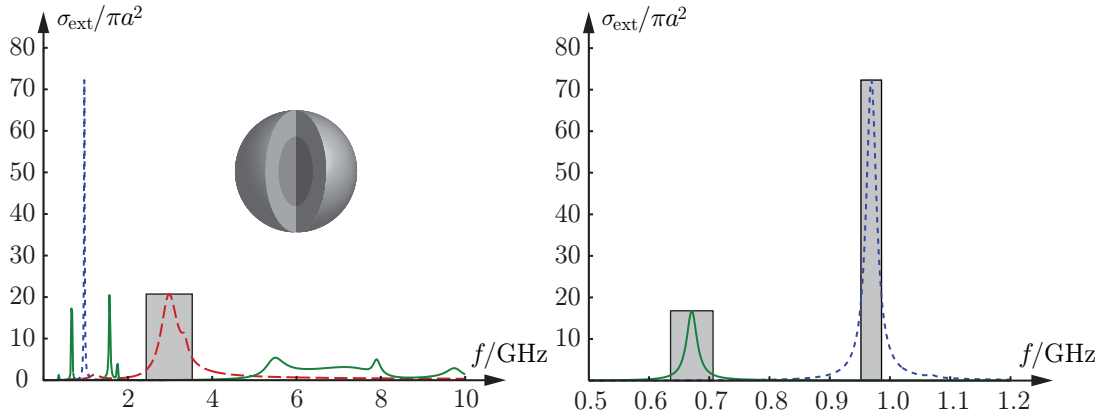

Figure 2: The extinction cross section σ_{ext} as function of the frequency in GHz for a stratified sphere which attains simultaneously negative values of the permittivity and the permeability. Note the normalization with the geometrical cross section πa^2, where $a = 1\,\text{cm}$ denotes the outer radius of the sphere.

peak when evaluated at half amplitude. The calculation in Fig. 1 is based on the implementation of the T-matrix approach in Ref. 6. For a similar example given by the Lorentz dispersive cylinder, see Ref. 12.

4.2 The Drude dispersive stratified sphere

The extinction cross section σ_{ext} for a stratified sphere with two layers of equal volume is depicted in Fig. 2. The stratified sphere is temporally dispersive with identical electric ($\ell = \text{e}$) and magnetic ($\ell = \text{m}$) material properties given by the Drude model

$$\chi_\ell(\omega) = \frac{\text{i}\varsigma}{\epsilon_0\omega(1 - \text{i}\omega\tau)}, \qquad \ell = \text{e}, \text{m}, \tag{4.2}$$

where $\varsigma > 0$ and $\tau > 0$. The real and imaginary parts of (4.2) read

$$\chi_\ell(\omega) = \frac{-\varsigma\tau}{\epsilon_0(1 + \omega^2\tau^2)} + \text{i}\frac{\varsigma}{\epsilon_0\omega(1 + \omega^2\tau^2)}. \tag{4.3}$$

Since $\text{Re}\,\chi_\ell(\omega) < 0$ for $\omega \in [0, \infty)$, the stratified sphere in Fig. 2 attains simultaneously negative values of the permittivity and the permeability. The calculation in Fig. 2 is based on a Möbius transformation applied to the classical Mie series expansion in Refs. 7 and 8.

The two curves in the upper figure with peaks at 0.97 GHz (dotted line) and 3.0 GHz (dashed line) correspond to a homogeneous sphere with identical material properties in the inner and outer layers. These two curves are characterized by the relaxation times $\tau = 10^{-8}\,\text{s}$ and $\tau = 10^{-9}\,\text{s}$, respectively, and with conductivity $\varsigma = 10\,\text{S/m}$ in both cases. For the third curve (solid line) with peaks at 0.67 GHz and 1.6 GHz, the material parameters of the outer layer are $\tau = 8{\cdot}10^{-9}\,\text{s}$ and $\varsigma = 10\,\text{S/m}$, while the inner layer is non-dispersive with $\chi_{\text{e}1} = 10$ and $\chi_{\text{m}1} = 0$ independent of ω. The lower figure provides a close-up of the peaks at 0.67 GHz and 0.97 GHz.

Closed-form expressions of the electric polarizability dyadic $\boldsymbol{\gamma}_{\mathrm{e}}$ exist for the stratified sphere, see Ref. 12. For a stratified sphere of two layers, the integrated extinction can be expressed as

$$\int_0^\infty \sigma_{\mathrm{ext}}(\lambda)\ \mathrm{d}\lambda = 4\pi^3 a^3 \sum_{\ell=\mathrm{e,m}} \frac{\chi_{\ell 2}(\chi_{\ell 1}+2\chi_{\ell 2}+3)+\zeta^3(2\chi_{\ell 2}+3)(\chi_{\ell 1}-\chi_{\ell 2})}{(\chi_{\ell 2}+3)(\chi_{\ell 1}+2\chi_{\ell 2}+3)+2\zeta^3\chi_{\ell 2}(\chi_{\ell 1}-\chi_{\ell 2})}, \quad (4.4)$$

where a denotes the outer radius, and $\chi_{\ell 1}$ and $\chi_{\ell 2}$ represent the long wavelength susceptibilities of the inner and outer layers, respectively. Furthermore, $\zeta \in [0,1]$ denotes the quotient between the inner and the outer radii.

Since (4.2) is characterized by a conductivity term which is singular at $\omega = 0$, the discussion above implies that the right hand side of (4.4) is subject to the limits $\chi_{\mathrm{e}2} \to \infty$ and $\chi_{\mathrm{m}2} \to \infty$. Based on this observation, it is concluded that the integrated extinction for all three curves in Fig. 2 coincide and are equal to $8\pi^3 a^3$ or $248.0\,\mathrm{cm}^3$, where $a = 1\,\mathrm{cm}$ has been used. In contrast to the limits $\chi_{\mathrm{e}1} \to \infty$ and $\chi_{\mathrm{m}1} \to \infty$, this result is independent of ζ as well as $\chi_{\mathrm{e}1}$ and $\chi_{\mathrm{m}1}$. Note that (2.3) and (2.5) yield that the integrated extinction $8\pi^3 a^3$ is equivalent to the long wavelength limit $\varrho(0) = 2a^3$. The integrated extinction $248.0\,\mathrm{cm}^3$ is numerically confirmed with arbitrary precision for the three curves in Fig. 2.

The physical limitation (3.3) is depicted by the shaded boxes in Fig. 2. These boxes correspond to artificial scatterers with extinction cross sections supported at the peaks 0.67 GHz, 0.97 GHz and 3.0 GHz. The integrated extinction of each box is equal to $248.0\,\mathrm{cm}^3$ and coincides with the integrated extinction for any other curve in the figure. From Fig. 2 it is seen how the width of the box increases as the peaks are suppressed in magnitude and shifted toward higher frequencies. Note that the tiny peaks at 0.36 GHz (solid line) and 1.2 GHz (dashed line) constitute a large part of the integrated extinction, thus implying that the peaks at 0.67 GHz and 3.0 GHz do not fit the boxes that well in comparison with the box centered at 0.97 GHz. Recall that the area of the boxes in Fig. 2 only depends on the properties of V in the long wavelength limit, and is hence independent of any temporal dispersion for $\omega > 0$.

The extinction cross section for a non-magnetic stratified sphere with two layers of equal volume is depicted in Fig. 3. The stratified sphere is temporally dispersive with electric susceptibility χ_{e} given by the Drude model (4.2). The two curves in the left figure with peaks at 0.96 GHz (dotted line) and 2.7 GHz (dashed line) correspond to the homogeneous case with identical material parameters in both layers: $\tau = 10^{-8}\,\mathrm{s}$ and $\tau = 10^{-9}\,\mathrm{s}$, respectively, with $\varsigma = 10\,\mathrm{S/m}$ in both cases. For the third curve with peak at 1.4 GHz (solid line), the material parameters of the outer layer is $\varsigma = 10\,\mathrm{S/m}$ and $\tau = 10^{-8}\,\mathrm{s}$, while the inner layer is non-dispersive with $\chi_{\mathrm{e}1} = 10$ independent of ω. The left figure in Fig. 3 is a close-up of the peaks at 0.96 GHz and 1.4 GHz with the associated box-shaped limitations.

Since the stratified sphere in Fig. 3 has the same electric long wavelength response as the scatterer in Fig. 2 but in addition is non-magnetic, it follows from (4.4) that the integrated extinction of the scatterer in Fig. 3 is half the integrated extinction of the scatterer in Fig. 2, *i.e.*, $4\pi^3 a^3$ or $124.0\,\mathrm{cm}^3$. This observation is a direct

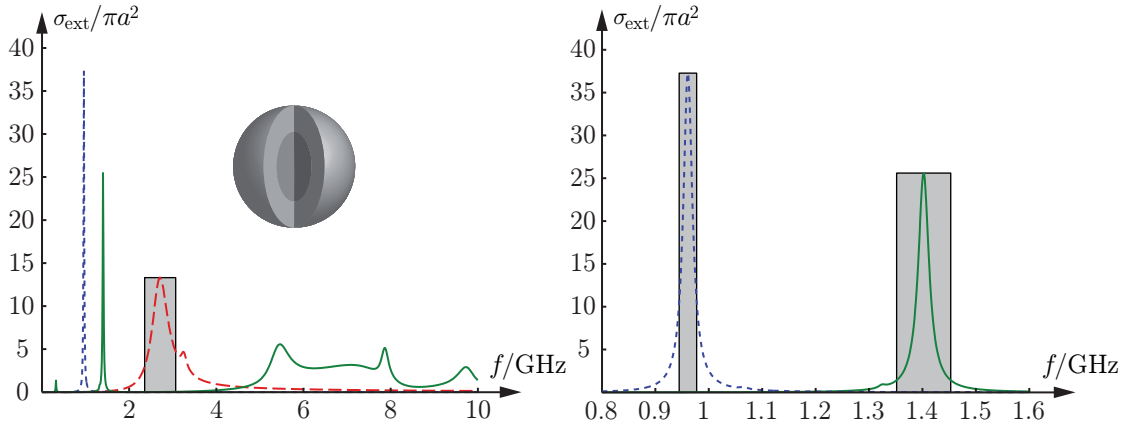

Figure 3: The extinction cross section σ_{ext} as function of the frequency in GHz for a non-magnetic stratified sphere which attain negative values of the permittivity. Note the normalization with the geometrical cross section πa^2, where $a = 1\,\text{cm}$ denotes the outer radius of the sphere.

consequence of the symmetry of (4.4) with respect to electric ($\ell = \text{e}$) and magnetic ($\ell = \text{m}$) material properties. The result is also supported by the fact that the amplitude of, say, the peak at 0.97 GHz in Fig. 2 is approximately twice as large as the corresponding peak at 0.96 GHz in Fig. 3.

5 Conclusions

The conclusions of the present paper are clear: independent of how the materials in the scatterer are defined and modeled by temporal dispersion (*i.e.*, irrespective of the sign of the permittivity and permeability), the holomorphic properties of the forward scattering dyadic imply that, from a broadband point of view, there is no fundamental difference in scattering and absorption between metamaterials and ordinary materials. For a single frequency, metamaterials may possess extraordinary properties, but with respect to any bandwidth such materials are no different from any other naturally formed substances as long as causality is obeyed. As a consequence, if metamaterials are used to lower the resonance frequency, this is done to the cost of an increasing Q-factor of the resonance. The present analysis includes materials modeled by anisotropy and heterogeneity, and can be extended to general bianisotropic materials as well. For example, the introduction of chirality does not contribute to the integrated extinction since all chiral effects vanish in the long wavelength limit.

It is believed that there are more physical quantities that apply to the theory for broadband scattering in Ref. 12. Thus far, the theory has been applied fruitfully to arbitrary antennas in Refs. 1 and 3 to yield physical limitations on antenna performance and information capacity. Similar broadband limitations on cloaking and invisibility using metamaterials and other exotic material models are currently under investigation.

Acknowledgment

The financial support by the Swedish Research Council is gratefully acknowledged. The authors are also grateful for fruitful discussions with Anders Karlsson at the Dept. of Electrical and Information Technology, Lund University, Sweden.

References

[1] M. Gustafsson, C. Sohl, and G. Kristensson. Physical limitations on antennas of arbitrary shape. *Proc. R. Soc. A*, **463**, 2007. doi:1098/rspa.2007.1893.

[2] M. Gustafsson. On the non-uniqueness of the electromagnetic instantaneous response. *J. Phys. A: Math. Gen.*, **36**, 1743–1758, 2003.

[3] M. Gustafsson, C. Sohl, and G. Kristensson. Physical limitations on antennas of arbitrary shape. Technical Report LUTEDX/(TEAT-7153)/1–37/(2007), Lund University, Department of Electrical and Information Technology, P.O. Box 118, S-221 00 Lund, Sweden, 2007. http://www.eit.lth.se.

[4] R. E. Kleinman and T. B. A. Senior. Rayleigh scattering. In V. V. Varadan and V. K. Varadan, editors, *Low and high frequency asymptotics*, volume 2 of *Acoustic, Electromagnetic and Elastic Wave Scattering*, chapter 1, pages 1–70. Elsevier Science Publishers, Amsterdam, 1986.

[5] L. D. Landau, E. M. Lifshitz, and L. P. Pitaevskiĭ. *Electrodynamics of Continuous Media*. Pergamon, Oxford, second edition, 1984.

[6] M. I. Mishchenko and L. D. Travis. Capabilities and limitations of a current FORTRAN implementation of the T-matrix method for randomly oriented, rotationally symmetric scatterers. *J. Quant. Spectrosc. Radiat. Transfer*, **60**(3), 309–324, 1998.

[7] R. G. Newton. *Scattering Theory of Waves and Particles*. Springer-Verlag, New York, 1982.

[8] H. M. Nussenzveig. *Causality and dispersion relations*. Academic Press, London, 1972.

[9] S. A. Ramakrishna. Physics of negative refractive index materials. *Reports on Progress in Physics*, **68**(2), 449–521, 2005.

[10] R. Ruppin. Extinction properties of a sphere with negative permittivity and permeability. *Solid State Commun.*, **116**, 411–415, 2000.

[11] D. R. Smith, J. B. Pendry, and M. C. K. Wiltshire. Metamaterials and negative refractive index. *Science*, **305**(5685), 788–792, 2004.

[12] C. Sohl, M. Gustafsson, and G. Kristensson. Physical limitations on broadband scattering by heterogeneous obstacles. Accepted for publication in J. Phys. A: Math. Theor., 2007.

[13] H. van de Hulst. *Light Scattering by Small Particles*. John Wiley & Sons, Inc., New York, 1957.

[14] V. G. Veselago. The electrodynamics of substances with simultaneously negative values of ϵ and μ. *Sov. Phys. Usp.*, **10**(4), 509–514, 1968.

The integrated extinction for broadband scattering of acoustic waves

Christian Sohl, Mats Gustafsson, and Gerhard Kristensson

Paper III

Based on: C. Sohl, M. Gustafsson, and G. Kristensson. The integrated extinction for broadband scattering of acoustic waves. Technical Report LUTEDX/(TEAT-7156)/1–10/(2007), Lund University.

Abstract

In this paper, physical limitations on scattering of acoustic waves over a frequency interval are discussed based on the holomorphic properties of the scattering amplitude in the forward direction. The result is given by a dispersion relation for the extinction cross section which yields an upper bound on the product of the extinction cross section and the associated bandwidth of any frequency interval. The upper bound is shown to depend only on the geometry and static material properties of the scatterer. The results are exemplified by permeable and impermeable scatterers with homogeneous and isotropic material properties.

1 Introduction

Linear acoustics with propagation and scattering of waves in air and water has been a subject of considerable interest for more than a century. Major contributions to the scattering theory of both acoustic and electromagnetic waves from bounded obstacles was provided by Rayleigh in a sequence of papers. From a theoretical point of view, scattering of acoustic waves share many features with electromagnetic and elastodynamic wave interaction. For a comprehensive introduction to linear acoustics, see, *e.g.*, Refs. 5 and 11.

The objective of this paper is to derive physical limitations on broadband scattering of acoustic waves. In more detail, the scattering problem discussed here involves how a scatterer of arbitrary shape perturbs some known incident field over a frequency interval. The analysis is based on a forward dispersion relation for the extinction cross section applied to a set of passive and linear constitutive relations. This forward dispersion relation, known as the integrated extinction, is a direct consequence of causality and energy conservation via the holomorphic properties of the scattering amplitude in the forward direction. As far as the authors knows, the integrated extinction was first introduced in Ref. 7 concerning absorption and emission of electromagnetic waves by interstellar dust. The analysis in Ref. 7, however, is restricted to homogeneous and isotropic spheroids. This narrow class of scatterers was generalized in Ref. 8 to include anisotropic and heterogenous obstacles of arbitrary shape.

The present paper is a direct application to linear acoustics of the physical limitations for scattering of electromagnetic waves introduced in Refs. 8 and 9. The broad usefulness of the integrated extinction is illustrated by its diversity of applications, see, *e.g.*, Ref. 9 for upper bounds on the bandwidth of metamaterials associated with electromagnetic interaction. The integrated extinction has also fruitfully been applied to antennas of arbitrary shape in Ref. 2 to establish physical limitations on directivity and bandwidth. The theory for broadband scattering of acoustic waves is motivated by the summation rules and the analogy with causality in the scattering theory for particles in Ref. 6.

In Sec. 2, the integrated extinction is derived based on the holomorphic properties of the scattering amplitude in the forward direction. The derivation is based on a exterior problem, and is hence independent of the boundary conditions imposed on

Figure 1: Illustration of the direct scattering problem: the scatterer V is subject to a plane wave $u_\mathrm{i} = \mathrm{e}^{\mathrm{i}k\hat{\boldsymbol{k}}\cdot\boldsymbol{x}}$ impinging in the $\hat{\boldsymbol{k}}$-direction. The incident field is perturbed by V and a scattered field u_s is detected in the $\hat{\boldsymbol{x}}$-direction.

the scatterer. The effect of various boundary conditions are discussed in Sec. 3, and there applied to the results in Sec. 2. In the final section, Sec. 4, the main results of the paper are summarized and possible applications of the integrated extinction are discussed.

2 The integrated extinction

Consider a time-harmonic plane wave $u_\mathrm{i} = \mathrm{e}^{\mathrm{i}k\hat{\boldsymbol{k}}\cdot\boldsymbol{x}}$ (complex excess pressure) with time dependence $\mathrm{e}^{-\mathrm{i}\omega t}$ impinging on a bounded, but not necessary simply connected, scatterer $V \subset \mathbb{R}^3$ of arbitrary shape, see Figure 1. The plane wave is impinging in the $\hat{\boldsymbol{k}}$-direction, and $\boldsymbol{x}$ denotes the position vector with respect to some origin. The scatterer V is assumed to be linear and time-translational invariant with passive material properties modeled by general anisotropic and heterogeneous constitutive relations. The analysis includes the impermeable case as well as transmission problems with or without losses. The scatterer V is embedded in the exterior region $\mathbb{R}^3 \setminus \overline{V}$, which is assumed to be a compressible homogeneous and isotropic fluid characterized by the wave number $k = \omega/c$. The material properties of $\mathbb{R}^3 \setminus \overline{V}$ are assumed to be lossless and independent of time.

Let $u = u_\mathrm{i} + u_\mathrm{s}$ denote the total field in $\mathbb{R}^3 \setminus \overline{V}$, where the time-dependent physical excess pressure p is related to u via $p = \mathrm{Re}\{u\mathrm{e}^{-\mathrm{i}\omega t}\}$. The scattered field u_s represents the disturbance of the field in the presence of V. It satisfies the Helmholtz equation in the exterior of V, see Ref. 11, *i.e.*,

$$\nabla^2 u_\mathrm{s} + k^2 u_\mathrm{s} = 0, \qquad \boldsymbol{x} \in \mathbb{R}^3 \setminus \overline{V}. \tag{2.1}$$

The boundary condition imposed on u_s at large distances $x = |\boldsymbol{x}|$ is the Sommerfeld radiation condition

$$\lim_{x\to\infty} x\left(\frac{\partial u_\mathrm{s}}{\partial x} - \mathrm{i}k u_\mathrm{s}\right) = 0, \tag{2.2}$$

which is assumed to hold uniformly in all directions $\hat{\boldsymbol{x}} = \boldsymbol{x}/x$. The condition (2.2) establishes the outgoing character of u_s, and provides a condition for a well-posed

exterior boundary value problem. For a discussion of various boundary conditions imposed on V, see Sec. 3.

From the integral representations in Ref. 10 it is clear that every solution to (2.1) satisfying (2.2) has an asymptotic behavior of an outgoing spherical wave, *i.e.*,

$$u_{\mathrm{s}} = \frac{\mathrm{e}^{\mathrm{i}kx}}{x} S(k, \hat{\boldsymbol{x}}) + \mathcal{O}(x^{-2}) \quad \text{as } x \to \infty.$$

The scattering amplitude S is independent of x and describes the interaction of V with the incident field. From a time-domain description of the problem it follows that S is the Fourier transform of some temporal scattering amplitude S_{t}. Assume S_{t} is causal in the forward direction in the sense that $S_{\mathrm{t}}(\tau, \hat{\boldsymbol{k}}, \hat{\boldsymbol{k}}) = 0$ for $\tau < 0$, where $\tau = ct - \hat{\boldsymbol{k}} \cdot \boldsymbol{x}$. Based on this condition, the Fourier transform of S_{t} reduces to an integral over $\tau > 0$, *i.e.*,

$$S(k, \hat{\boldsymbol{k}}) = \int_0^\infty S_{\mathrm{t}}(\tau, \hat{\boldsymbol{k}}, \hat{\boldsymbol{k}}) \mathrm{e}^{\mathrm{i}k\tau} \, \mathrm{d}\tau. \tag{2.3}$$

The convergence of (2.3) is improved by extending its domain of definition to complex-valued k with $\operatorname{Im} k > 0$. Such an extension defines a holomorphic function S in the upper half plane $\operatorname{Im} k > 0$, see Sec. 1 in Ref. 6. Note that S in general is not a holomorphic function at infinity for $\operatorname{Im} k > 0$ in the absence of the causality condition.

The description of broadband scattering is simplified by introducing a weighted function ϱ of the scattering amplitude in the forward direction. For this purpose, let ϱ denote the holomorphic function

$$\varrho(k) = S(k, \hat{\boldsymbol{k}})/k^2, \qquad \operatorname{Im} k > 0.$$

Since S_{t} is real-valued it follows from (2.3) that ϱ is real-valued on the imaginary axis, and that it satisfies the cross symmetry $\varrho(-k^*) = \varrho^*(k)$ (the star denotes complex conjugation) for complex-valued k. Assume that ϱ vanishes uniformly as $|k| \to \infty$ for $\operatorname{Im} k \geq 0$. This assumption is justified by the argument that the high-frequency response of a material is non-unique from a modeling point of view. The assumption is also supported by the extinction paradox $\operatorname{Im} \varrho(k) = \mathcal{O}(k^{-1})$ as $k \to \infty$ for real-valued k, see Ref. 8 and references therein.

An important measure of the total energy that V extracts from the incident field in the form of radiation or absorption is given by the extinction cross section σ_{ext}. The extinction cross section is related to ϱ via the optical theorem, see Ref. 6,

$$\sigma_{\mathrm{ext}} = 4\pi k \operatorname{Im} \varrho, \tag{2.4}$$

where $k \in [0, \infty)$. The optical theorem is a direct consequence of energy conservation (or probability in the scattering theory of the Schrödinger equation) and states that the total energy removed from the incident field is solely determined by $\operatorname{Im} \varrho$. The extinction cross section is commonly decomposed into the scattering cross section σ_{s} and the absorption cross section σ_{a}, *i.e.*,

$$\sigma_{\mathrm{ext}} = \sigma_{\mathrm{s}} + \sigma_{\mathrm{a}}. \tag{2.5}$$

Here, σ_s and σ_a are defined as the scattered and absorbed power divided by the incident power flux. The scattering and absorption cross sections are related to u_s and u on the boundary ∂V via, see Ref. 1,

$$\sigma_\mathrm{s} = \frac{4\pi}{k} \operatorname{Im} \int_{\partial V} u_\mathrm{s}^* \frac{\partial u_\mathrm{s}}{\partial n} \, \mathrm{d}S, \qquad \sigma_\mathrm{a} = \frac{4\pi}{k} \operatorname{Im} \int_{\partial V} u \frac{\partial u^*}{\partial n} \, \mathrm{d}S,$$

where the normal derivative $\partial/\partial n$ is evaluated with respect to the outward pointing unit normal vector. In the permeable and lossy case, the absorption cross section σ_a represents the total energy absorbed by V. For a lossless scatterer, $\sigma_\mathrm{a} = 0$.

Under the assumption that ϱ vanishes uniformly as $|k| \to \infty$ for $\operatorname{Im} k \geq 0$, it follows from the analysis in Ref. 6 that ϱ satisfies the Hilbert transform or the Plemelj formulae

$$\operatorname{Re} \varrho(k') = \frac{1}{\pi} \mathcal{P} \int_{-\infty}^{\infty} \frac{\operatorname{Im} \varrho(k)}{k - k'} \, \mathrm{d}k, \tag{2.6}$$

where k' is real-valued and $\mathcal{P}$ denotes Cauchy's principal value. It is particularly interesting to evaluate (2.6) in the static limit. For this purpose, assume that $\operatorname{Re} \varrho(k') = \mathcal{O}(1)$ and $\operatorname{Im} \varrho(k') = \mathcal{O}(k')$ as $k' \to 0$, and that ϱ is sufficiently regular to interchange the principal value and the static limit. Based on these assumptions, (2.4) yields

$$\lim_{k \to 0} \operatorname{Re} \varrho(k) = \frac{2}{\pi} \int_0^{\infty} \frac{\operatorname{Im} \varrho(k)}{k} \, \mathrm{d}k, \tag{2.7}$$

where it has been used that $\operatorname{Im} \varrho(k) = -\operatorname{Im} \varrho(-k)$ for real-valued k. The optical theorem (2.4) inserted into (2.7) finally yields

$$\int_0^{\infty} \frac{\sigma_\mathrm{ext}(k)}{k^2} \, \mathrm{d}k = 2\pi^2 \lim_{k \to 0} \operatorname{Re} \varrho(k). \tag{2.8}$$

The left hand side of (2.8) is referred to as the integrated extinction. The identity provides a forward dispersion relation for the extinction cross section as a direct consequence of causality and energy conservation. In fact, due to the lack of any length scale in the static limit as $k \to 0$, the right hand side of (2.8) is proportional to the volume of V. Furthermore, the right hand side of (2.8) depends only on the static properties of V, and is presented in Sec. 3 for a large class of homogeneous and isotropic scatterers.

The weak assumptions imposed on ϱ in the derivation above is summarized as follows: $\varrho(k) \to 0$ uniformly as $|k| \to \infty$ for $\operatorname{Im} k \geq 0$, and $\operatorname{Re} \varrho(k) = \mathcal{O}(1)$ and $\operatorname{Im} \varrho(k) = \mathcal{O}(k)$ as $k \to 0$ for real-valued k. In general, the integrated extinction (2.8) is not valid if any of these assumptions are violated, as illustrated in Sec. 3.3. In fact, the requirements above can be relaxed by the introduction of the Plemelj formulae for distributions. The integrated extinction (2.8) can also be derived using Cauchy's integral theorem, see Ref. 8.

The integrated extinction (2.8) may be used to establish physical limitations on broadband scattering by acoustic waves. Since σ_ext is defined as the sum of the scattered and absorbed power divided by the incident power flux, it is by definition

non-negative. Hence, the left hand side of (2.8) is estimated from below by

$$|K| \min_{k\in K} \frac{\sigma(k)}{k^2} \leq \int_K \frac{\sigma(k)}{k^2}\, \mathrm{d}k \leq \int_0^\infty \frac{\sigma_{\mathrm{ext}}(k)}{k^2}\, \mathrm{d}k, \tag{2.9}$$

where $|K|$ denotes the absolute bandwidth of any $K \subset [0,\infty)$, and σ represents either σ_{ext}, σ_{s} or σ_{a}. By combining the left hand side of (2.9) with the right hand side of (2.8), one obtain the fundamental inequality

$$|K| \min_{k\in K} \frac{\sigma(k)}{k^2} \leq 2\pi^2 \lim_{k\to 0} \mathrm{Re}\, \varrho(k). \tag{2.10}$$

The interpretation of (2.10) is that it yields an upper bound on the absolute bandwidth $|K|$ for a given scattering and/or absorption cross section $\min_{k\in K} \sigma(k)/k^2$. From (2.10), it is seen that the static limit of $\mathrm{Re}\, \varrho$ bounds the total amount of power extracted by V within K. The electromagnetic analogy to (2.10) is, *inter alia*, central for establishing upper bounds on the performance of antennas of arbitrary shape, see Ref. 2.

3 The effect of various boundary conditions

In this section, the static limit $\lim_{k\to 0} \mathrm{Re}\, \varrho$ is examined for various boundary conditions and applied to the integrated extinction (2.8). For this purpose, V is assumed to be homogeneous and isotropic with sufficiently smooth boundary ∂V to guarantee the existence of boundary values in the classical sense.

3.1 The Neumann or acoustically hard problem

The Neumann or acoustically hard problem corresponds to an impermeable scatterer with boundary condition $\partial u/\partial n = 0$ for $\boldsymbol{x} \in \partial V$. The physical interpretation of the Neumann boundary condition is that the velocity field on ∂V is zero since no local displacements are admitted. From the fact that u_{s} only exists in $\mathbb{R}^3 \setminus \overline{V}$, it follows that the corresponding scattered field in the time-domain cannot precede the incident field in the forward direction, *i.e.*, the causality condition imposed on S_{t} in Sec. 2 is valid for the Neumann problem. The static limit of S is derived in Refs. 1 and 3 from a power series expansion of u_{i} and u_{s}. The result in terms of $\mathrm{Re}\, \varrho$ reads

$$\lim_{k\to 0} \mathrm{Re}\, \varrho(k) = \frac{1}{4\pi}(\hat{\boldsymbol{k}} \cdot \boldsymbol{\gamma}_{\mathrm{m}} \cdot \hat{\boldsymbol{k}} - |V|), \tag{3.1}$$

where $|V|$ denotes the volume of V. Here, $\boldsymbol{\gamma}_{\mathrm{m}}$ models the scattering of acoustic waves in the low frequency limit. In analogy with the corresponding theory for electromagnetic waves in Ref. 8, $\boldsymbol{\gamma}_{\mathrm{m}}$ is termed the magnetic polarizability dyadic. The magnetic polarizability dyadic is proportional to $|V|$, and closed-form expressions of $\boldsymbol{\gamma}_{\mathrm{m}}$ exist for the ellipsoids.

An expression of the integrated extinction for the Neumann problem is obtained by inserting (3.1) into (2.8), *viz.*,

$$\int_0^\infty \frac{\sigma_{\text{ext}}(k)}{k^2}\,\mathrm{d}k = \frac{\pi}{2}(\hat{\boldsymbol{k}}\cdot\boldsymbol{\gamma}_{\text{m}}\cdot\hat{\boldsymbol{k}} - |V|). \tag{3.2}$$

Note that (3.2) is independent of $\hat{\boldsymbol{k}}$ when $\boldsymbol{\gamma}_{\text{m}}$ is isotropic, *i.e.*, $\boldsymbol{\gamma}_{\text{m}} = \gamma_{\text{m}}\mathbf{I}$ where $\mathbf{I}$ denotes the unit dyadic, corresponding to a scatterer which is invariant under certain point groups, see Ref. 8 and references therein. The product $\hat{\boldsymbol{k}}\cdot\boldsymbol{\gamma}_{\text{m}}\cdot\hat{\boldsymbol{k}}$ on the right hand side of (3.2) can be estimated from above by the largest eigenvalue of $\boldsymbol{\gamma}_{\text{m}}$, and associated upper bounds on these eigenvalues are extensively discussed in Ref. 8. The static limit of $\operatorname{Re}\varrho$ in (3.1) can also be inserted into the right hand side of (2.10) to yield an upper bound on the scattering and absorption properties of V within any finite interval K.

The integrated extinction (3.2) takes a particularly simple form for the sphere. In this case, $\boldsymbol{\gamma}_{\text{m}}$ is isotropic with $\gamma_{\text{m}} = 3|V|/2$, see Refs. 3 and 8, and the right hand side of (3.2) is reduced to $\pi|V|/4$. This result for the sphere has numerically been verified using the classical Mie-series expansion in Ref. 5.

3.2 The transmission or acoustically permeable problem

In addition to the exterior boundary value problem (2.1) and (2.2), the transmission or acoustically permeable problem is defined by the interior requirement that $\nabla^2 u_{\text{s}} + k_\star^2 u_{\text{s}} = 0$ for $\boldsymbol{x} \in V$ with the induced boundary conditions $u^+ = u^-$ and $\rho_\delta \partial u^+/\partial n = \partial u^-/\partial n$. Here, $k_\star = \omega/c_\star$ denotes the wave number in V, and u^+ and u^- represents the limits of u from $\mathbb{R}^3 \setminus \overline{V}$ and V, respectively. The quantity ρ_δ is related to the relative mass density $\rho_{\text{rel}} = \rho_\star/\rho$ via $\rho_\delta = \rho_{\text{rel}}/(1 - \mathrm{i}\omega\delta_\star\kappa_\star)$, where $\kappa_\star$ and $\rho_\star$ denotes the compressibility and the mass density of V, respectively. The compressibility represents the relative volume reduction per unit increase in surface pressure. The conversion of mechanical energy into thermal energy due to losses in V are modeled by the compressional viscosity $\delta_\star > 0$, which represents the rate of change of mass per unit length. In the lossless case, $\delta_\star = 0$, the phase velocity is $c_\star = 1/\sqrt{\kappa_\star\rho_\star}$ and $\rho_\delta = \rho_{\text{rel}}$.

The causality condition introduced in Sec. 2 is valid for the transmission problem provided $\operatorname{Re} c_\star < c$, *i.e.*, when the incident field precedes the scattered field in the forward direction. Unless V does not fulfill this requirement, ϱ is not holomorphic for $\operatorname{Im} k > 0$ and the analysis in Sec. 2 does not hold. Hence, the integrated extinction (2.8) is not valid if $\operatorname{Re} c_\star \geq c$. This defect can partially be justified by replacing the definition of ϱ by $\varrho = \mathrm{e}^{2\mathrm{i}ka} S(k, \hat{\boldsymbol{k}})/k^2$, where $a > 0$ is sufficiently large to guarantee the existence of causality in the forward direction. The compensating factor $\mathrm{e}^{2\mathrm{i}ka}$ corresponds to a time-delayed scattered field, and for homogenous and isotropic scatterers, a sufficient condition for a is $2a > \operatorname{diam} V$, where $\operatorname{diam} V$ denotes the diameter of V. A drawback of the introduction of the factor $\mathrm{e}^{2\mathrm{i}ka}$ in the definition of ϱ is that the optical theorem no longer can be identified in the derivation. Instead, the integrated extinction for scatterers which not obey the causality

condition reduce to integral identities for Re ϱ and Im ϱ. Unfortunately, in this case the integrands have not a definite sign and therefore the estimate (2.10) is not valid.

The static limit of the scattering amplitude S for the transmission problem is derived in Refs. 1 and 3. The result in terms of Re ϱ reads

$$\lim_{k\to 0} \operatorname{Re} \varrho(k) = \frac{1}{4\pi}((\kappa_{\mathrm{rel}} - 1)|V| - \hat{\boldsymbol{k}} \cdot \boldsymbol{\gamma}(\rho_{\mathrm{rel}}^{-1}) \cdot \hat{\boldsymbol{k}}), \tag{3.3}$$

where $\kappa_{\mathrm{rel}} = \kappa_\star/\kappa$ denotes the relative compressibility of V, and $\boldsymbol{\gamma}$ represents the general polarizability dyadic. In the derivation of (3.3), it has been used that possible losses $\delta_\star > 0$ in V do not contribute in the static limit of Re ϱ, which motivates that the argument in $\boldsymbol{\gamma}$ is ρ_{rel} rather than ρ_δ. Analogous to $\boldsymbol{\gamma}_{\mathrm{m}}$, the general polarizability dyadic is proportional to $|V|$, and closed-form expressions for $\boldsymbol{\gamma}$ exist for the ellipsoids, see Refs. 1, 3 and 8. From the properties of $\boldsymbol{\gamma}$ and $\boldsymbol{\gamma}_{\mathrm{m}}$ in the references above, it follows that $\boldsymbol{\gamma}(\rho_{\mathrm{rel}}^{-1}) \to -\boldsymbol{\gamma}_{\mathrm{m}}$ as $\rho_{\mathrm{rel}} \to \infty$, and hence the static limit of Re ϱ reduces to (3.1) for the Neumann problem as $\kappa_{\mathrm{rel}} \to 0+$ and $\rho_{\mathrm{rel}} \to \infty$. Another interesting limit corresponding to vanishing mass density in V is given by $\boldsymbol{\gamma}(\rho_{\mathrm{rel}}^{-1}) \to \boldsymbol{\gamma}_{\mathrm{e}}$ as $\rho_{\mathrm{rel}} \to 0+$, where $\boldsymbol{\gamma}_{\mathrm{e}}$ is termed the electric polarizability dyadic in analogy with the low frequency scattering of electromagnetic waves, see Refs. 1, 3 and 8.

The integrated extinction for the transmission problem is given by (3.3) inserted into (2.8). The result is

$$\int_0^\infty \frac{\sigma_{\mathrm{ext}}(k)}{k^2}\, \mathrm{d}k = \frac{\pi}{2}((\kappa_{\mathrm{rel}} - 1)|V| - \hat{\boldsymbol{k}} \cdot \boldsymbol{\gamma}(\rho_{\mathrm{rel}}^{-1}) \cdot \hat{\boldsymbol{k}}), \tag{3.4}$$

Note that (3.4) is independent of any losses $\delta_\star > 0$, and that the directional character of the integrated extinction only depends on the relative mass density ρ_{rel}. For $\rho_{\mathrm{rel}} \to 1$, *i.e.*, identical mass densities in V and $\mathbb{R}^3 \setminus \overline{V}$, the integrated extinction is independent of the incident direction $\hat{\boldsymbol{k}}$, depending only on the relative compressibility κ_{rel}. Furthermore, the integrated extinction (3.2) vanishes in the limit as $\kappa_{\mathrm{rel}} \to 1$ and $\rho_{\mathrm{rel}} \to 1$, corresponding to identical material properties in V and $\mathbb{R}^3 \setminus \overline{V}$. Due to the non-negative character of the extinction cross section, this limit implies that $\sigma_{\mathrm{ext}} = 0$ independent of the frequency as expected. Analogous to the Neumann problem, (3.4) is also independent of the incident direcion $\hat{\boldsymbol{k}}$ for scatterers with $\boldsymbol{\gamma} = \gamma \mathbf{I}$ for some real-valued γ. The product $\hat{\boldsymbol{k}} \cdot \boldsymbol{\gamma} \cdot \hat{\boldsymbol{k}}$ on the right hand side of (3.4) is estimated from above by the largest eigenvalue of $\boldsymbol{\gamma}$, and associated upper bounds on these eigenvalues are discussed in Ref. 8. The static limit of Re ϱ in (3.1) can also be inserted into the right hand side of (2.10) to yield an upper bound on the scattering and absorption properties of V over any finite interval K.

For the isotropic and homogenous sphere, $\gamma = 3|V|(1 - \rho_{\mathrm{rel}})/(2\rho_{\mathrm{rel}} + 1)$, and the right hand side of (3.3) is independent of the incident direction as required by symmetry. Also this result for the sphere has been verified numerically to arbitrary precision using the classical Mie-series expansion.

3.3 Boundary conditions with contradictions

The integrated extinction (2.8) and the analysis in Sec. 2 are not applicable to the Dirichlet or acoustically soft problem with $u = 0$ for $\boldsymbol{x} \in \partial V$. The physical interpretation of the Dirichlet boundary condition is that the scatterer offers no resistance to pressure. The Dirichlet problem defines an impermeable scatterer for which u_s only exist in $\mathbb{R}^3 \setminus \overline{V}$. Hence, the causality condition introduced in Sec. 2 is valid. However, the assumption that $\operatorname{Re} \varrho(k) = \mathcal{O}(1)$ as $k \to 0$ for real-valued k is not valid in this case. Instead, Refs. 1 and 3 suggest that

$$\operatorname{Re} \varrho(k) = \mathcal{O}(k^{-2}) \quad \text{as } k \to 0$$

for real-valued k. The conclusion is therefore that the integrated extinction (2.8) is not valid for the Dirichlet problem.

The same conclusion also holds for the Robin problem with impedance boundary condition $\partial u/\partial n + \mathrm{i}k\nu u = 0$ for $\boldsymbol{x} \in \partial V$. The Robin problem models an intermediate behavior between the Dirichlet and Neumann problems, see Ref. 1. The real-valued constant ν is related to the exterior acoustic impedance η (defined by the ratio of the excess pressure and the normal velocity on ∂V) via $\eta\nu = \sqrt{\rho/\kappa}$, where κ and ρ denotes the compressibility and mass density of $\mathbb{R}^3 \setminus \overline{V}$, respectively. In the limits $\nu \to 0+$ and $\nu \to \infty$, the Robin problem reduces to the Neumann and Dirichlet problems, respectively. For the Robin problem, the static limit of $\operatorname{Re} \varrho$ for $\nu \neq 0$ reads, see Refs. 1 and 3,

$$\operatorname{Re} \varrho(k) = \mathcal{O}(k^{-1}) \quad \text{as } k \to 0$$

for real-valued k. Hence, the assumption in Sec. 2 that $\operatorname{Re} \varrho(k) = \mathcal{O}(1)$ as $k \to 0$ is not valid for the Robin problem either. The question whether a similar identity to the integrated extinction exists for the Dirichlet and Robin problems with other weight functions than $1/k^2$ in (2.8), is addressed in a forthcoming paper.

4 Conclusion

The static limits of $\operatorname{Re} \varrho$ in Sec. 3 can be used in (2.10) to establish physical limitations on the amount of energy a scatterer can extract from a known incident field in any frequency interval $K \subset [0, \infty)$. Both absorbed and radiated energy is taken into account. From the analysis of homogeneous and isotropic scatterers in Sec. 3, it is clear that the integrated extinction holds for both Neumann and transmission problems. However, the present formulation of the integrated extinction fails for the Dirichlet and Robin problems since the assumption in Sec. 2 that $\operatorname{Re} \varrho(k) = \mathcal{O}(1)$ as $k \to 0$ for real-valued k is violated for these boundary conditions. In fact, the eigenvalues of the polarizability dyadics $\boldsymbol{\gamma}$, $\boldsymbol{\gamma}_\mathrm{e}$ and $\boldsymbol{\gamma}_\mathrm{m}$ are easily calculated using the finite element method (FEM). Some numerical results of these eigenvalues are presented in Refs. 8 and 9 together with comprehensive illustrations of the integrated extinction for electromagnetic waves.

The integrated extinction (2.8) can also be used to establish additional information on the inverse scattering problem of linear acoustics. One advantage of the integrated extinction is that it only requires measurements of the scattering amplitude in the forward direction. The theory may also be used to obtain additional insights into the possibilities and limitations of manufactured materials such as acoustic metamaterials in Ref. 4. However, the main importance of the integrated extinction (2.8) is that it provides a fundamental knowledge of the physical processes involved in wave interaction with matter over any bandwidth. It is also crucial to the understanding of the physical effects imposed on a system by the first principles of causality and energy conservation.

Acknowledgment

The financial support by the Swedish Research Council is gratefully acknowledged. The authors are also grateful for fruitful discussions with Anders Karlsson at the Dept. of Electrical and Information Technology, Lund University, Sweden.

References

[1] G. Dassios and R. Kleinman. *Low frequency scattering.* Oxford University Press, Oxford, 2000.

[2] M. Gustafsson, C. Sohl, and G. Kristensson. Physical limitations on antennas of arbitrary shape. *Proc. R. Soc. A*, **463**, 2007. doi:1098/rspa.2007.1893.

[3] R. E. Kleinman and T. B. A. Senior. Rayleigh scattering. In V. V. Varadan and V. K. Varadan, editors, *Low and high frequency asymptotics*, volume 2 of *Acoustic, Electromagnetic and Elastic Wave Scattering*, chapter 1, pages 1–70. Elsevier Science Publishers, Amsterdam, 1986.

[4] J. Li and C. T. Chan. Double-negative acoustic metamaterial. *Phys. Rev. E*, **70**(5), 055602, 2004.

[5] P. M. Morse and K. U. Ingard. *Theoretical Acoustics.* McGraw-Hill, New York, 1968.

[6] H. M. Nussenzveig. *Causality and dispersion relations.* Academic Press, London, 1972.

[7] E. M. Purcell. On the absorption and emission of light by interstellar grains. *J. Astrophys.*, **158**, 433–440, 1969.

[8] C. Sohl, M. Gustafsson, and G. Kristensson. Physical limitations on broadband scattering by heterogeneous obstacles. Accepted for publication in J. Phys. A: Math. Theor., 2007.

[9] C. Sohl, M. Gustafsson, and G. Kristensson. Physical limitations on metamaterials: Restrictions on scattering and absorption over a frequency interval. Technical Report LUTEDX/(TEAT-7154)/1–11/(2007), Lund University, Department of Electrical and Information Technology, P.O. Box 118, S-221 00 Lund, Sweden, 2007. http://www.eit.lth.se.

[10] S. Ström. Introduction to integral representations and integral equations for time-harmonic acoustic, electromagnetic and elastodynamic wave fields. In V. V. Varadan, A. Lakhtakia, and V. K. Varadan, editors, *Field Representations and Introduction to Scattering*, Acoustic, Electromagnetic and Elastic Wave Scattering, chapter 2, pages 37–141. Elsevier Science Publishers, Amsterdam, 1991.

[11] V. V. Varadan and V. K. Varadan. Acoustic, electromagnetic and elastodynamics fields. In V. V. Varadan, A. Lakhtakia, and V. K. Varadan, editors, *Field Representations and Introduction to Scattering*, Acoustic, Electromagnetic and Elastic Wave Scattering, chapter 1, pages 1–35. Elsevier Science Publishers, Amsterdam, 1991.

Physical limitations on antennas of arbitrary shape

Mats Gustafsson, Christian Sohl, and Gerhard Kristensson

Paper IV

Based on: M. Gustafsson, C. Sohl, and G. Kristensson. Physical limitations on antennas of arbitrary shape. Technical Report LUTEDX/(TEAT-7153)/1–36/(2007), Lund University.

Abstract

In this paper, physical limitations on bandwidth, realized gain, Q-factor, and directivity are derived for antennas of arbitrary shape. The product of bandwidth and realizable gain is shown to be bounded from above by the eigenvalues of the long wavelength high-contrast polarizability dyadics. These dyadics are proportional to the antenna volume and easily determined for an arbitrary geometry. Ellipsoidal antenna volumes are analyzed in detail and numerical results for some generic geometries are presented. The theory is verified against the classical Chu limitations for spherical geometries, and shown to yield sharper bounds for the ratio of the directivity and the Q-factor for non-spherical geometries.

1 Introduction

The concept of physical limitations for electrically small antennas was first introduced more than half a century ago in Refs. 3 and 24, respectively. Since then, much attention has been drawn to the subject and numerous papers have been published, see Ref. 12 and references therein. Unfortunately, almost all these papers are restricted to the sphere via the spherical vector wave expansions, deviating only slightly from the pioneering ideas introduced in Ref. 3.

The objective of this paper is to derive physical limitations on bandwidth, realized gain, Q-factor, and directivity for antennas of arbitrary shape. The limitations presented here generalize in many aspects the classical results by Chu. The most important advantage of the new limitations is that they no longer are restricted to the sphere but instead hold for arbitrary antenna volumes. In fact, the smallest circumscribing sphere is far from optimal for many antennas, *cf.*, the dipole and loop antennas in Sec. 8. Furthermore, the new limitations successfully separate the electric and magnetic material properties of the antennas and quantify them in terms of their polarizability dyadics.

The new limitations introduced here are also important from a radio system point of view. Specifically, they are based on the bandwidth and realizable gain as well as the Q-factor and the directivity. The interpretation of the Q-factor in terms of the bandwidth is still subject to some research, see Ref. 25. Moreover, the new limitations permit the study of polarization effects and their influence on the antenna performance. An example of such an effect is polarization diversity for applications in MIMO communication systems.

The present paper is a direct application of the physical limitations for broadband scattering introduced in Refs. 19 and 20, where the integrated extinction is related to the long wavelength polarizability dyadics. The underlying mathematical description is strongly influenced by the consequences of causality and the summation rules and dispersion relations in the scattering theory for the Schrödinger equation, see Refs. 16, 17 and 22.

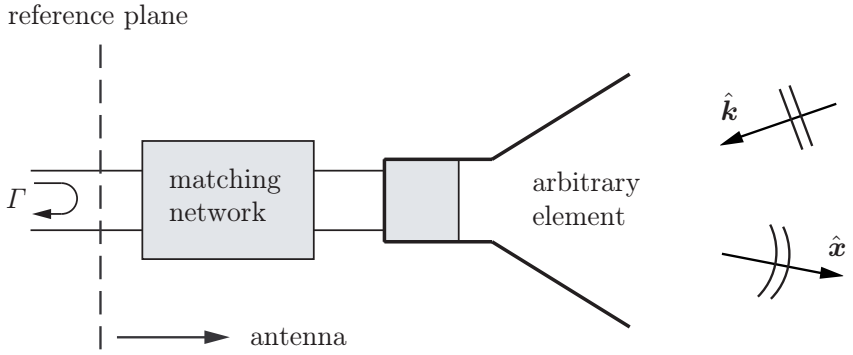

Figure 1: Illustration of a hypothetic antenna subject to an incident plane-wave in the $\hat{\boldsymbol{k}}$-direction.

2 Scattering and absorption of antennas

The present theory is inspired by the general scattering formalism of particles and waves in Refs. 16 and 22. In fact, based on the assumptions of linearity, time-translational invariance and causality there is no fundamental difference between antennas and properly modeled scatterers. This kind of fruitful equivalence between antenna and scattering theory has already been encountered in the literature, *cf.*, the limitations on the absorption efficiency in Ref. 2 and its relation to minimum scattering antennas. Without loss of generality, the integrated extinction and the theory introduced in Ref. 19 can therefore be argued to also hold for antennas of arbitrary shape. In contrast to Ref. 19, the present paper focuses on the absorption cross section rather than scattering properties.

For this purpose, consider an antenna of arbitrary shape surrounded by free space and subject to a plane-wave excitation impinging in the $\hat{\boldsymbol{k}}$-direction, see Fig. 1. The antenna is assumed to be lossless with respect to ohmic losses and satisfy the fundamental principles of linearity, time-translational invariance and causality. The dynamics of the antenna is modeled by the Maxwell equations with general reciprocal anisotropic constitutive relations. The constitutive relations are expressed in terms of the electric and magnetic susceptibility dyadics, $\boldsymbol{\chi}_{\mathrm{e}}$ and $\boldsymbol{\chi}_{\mathrm{m}}$, respectively, which are functions of the material properties of the antenna.

The assumption of a lossless antenna is not severe since the analysis can be modified to include ohmic losses, see the discussion in Sec. 9. In fact, ohmic losses are important for small antennas, and taking such effects into account, suggest that the lossless antenna is more advantageous than the corresponding antenna with ohmic losses. Recall that $\boldsymbol{\chi}_{\mathrm{e}}$ and $\boldsymbol{\chi}_{\mathrm{m}}$ also depend on the angular frequency ω of the incident plane-wave in the presence of losses.

The bounding volume V of the antenna is of arbitrary shape with the restriction that the complete absorption of the incident wave is contained within V. The bounding volume is naturally delimited by a reference plane or a port at which a unique voltage and current relation can be defined, see Fig. 1. The present definition of the antenna structure includes the matching network and is of the same kind as

the descriptions in Refs. 3 and 25. The reflection coefficient Γ at the port is due to the unavoidable impedance mismatch of the antenna over a given wavelength interval, see Ref. 5. The present analysis is restricted to single port antennas with a scalar (single) reflection coefficient. The extension to multiple ports is commented briefly in Sec. 9.

For any antenna, the scattered electric field $\boldsymbol{E}_\mathrm{s}$ in the forward direction $\hat{\boldsymbol{k}}$ can be expressed in terms of the forward scattering dyadic $\mathbf{S}$ as, see Appendix A,

$$\boldsymbol{E}_\mathrm{s}(k, x\hat{\boldsymbol{k}}) = \frac{\mathrm{e}^{\mathrm{i}kx}}{x}\mathbf{S}(k, \hat{\boldsymbol{k}}) \cdot \boldsymbol{E}_0 + \mathcal{O}(x^{-2}) \quad \text{as } x \to \infty. \tag{2.1}$$

Here, $\boldsymbol{E}_0$ denotes the Fourier amplitude of the incident field $\boldsymbol{E}_\mathrm{i}(\mathrm{c}_0 t - \hat{\boldsymbol{k}}\cdot\boldsymbol{x})$, and k is a complex variable with $\operatorname{Re} k = \omega/\mathrm{c}_0$ and $\operatorname{Im} k \geq 0$. For a large class of antennas, the elements of $\mathbf{S}$ are holomorphic in k and Cauchy's integral theorem can be applied to

$$\varrho(k) = \frac{1}{k^2}\hat{\boldsymbol{p}}_\mathrm{e}^* \cdot \mathbf{S}(k, \hat{\boldsymbol{k}}) \cdot \hat{\boldsymbol{p}}_\mathrm{e}, \quad k \in \mathbb{C}. \tag{2.2}$$

Here, $\hat{\boldsymbol{p}}_\mathrm{e} = \boldsymbol{E}_0/|\boldsymbol{E}_0|$ denotes the electric polarization, which is assumed to be independent of k.[1] The complex-valued function (2.2) is referred to as the extinction volume and it provides a holomorphic extension of the extinction cross section to $\operatorname{Im} k \geq 0$, see Appendix A.

A dispersion relation or summation rule for the extinction cross section can be derived in terms of the electric and magnetic polarizability dyadics $\boldsymbol{\gamma}_\mathrm{e}$ and $\boldsymbol{\gamma}_\mathrm{m}$, respectively. The derivation is based on energy conservation via the optical theorem in Refs. 16 and 22. The optical theorem $\sigma_\mathrm{ext} = 4\pi k \operatorname{Im} \varrho$ and the asymptotic behavior of the extinction volume ϱ in the long wavelength limit, $|k| \to 0$, are the key building blocks in the derivation. The result is the integrated extinction

$$\int_0^\infty \sigma_\mathrm{ext}(\lambda)\ \mathrm{d}\lambda = \pi^2(\hat{\boldsymbol{p}}_\mathrm{e}^* \cdot \boldsymbol{\gamma}_\mathrm{e} \cdot \hat{\boldsymbol{p}}_\mathrm{e} + \hat{\boldsymbol{p}}_\mathrm{m}^* \cdot \boldsymbol{\gamma}_\mathrm{m} \cdot \hat{\boldsymbol{p}}_\mathrm{m}), \tag{2.3}$$

where the magnetic (or cross) polarization $\hat{\boldsymbol{p}}_\mathrm{m} = \hat{\boldsymbol{k}} \times \hat{\boldsymbol{p}}_\mathrm{e}$ has been introduced. The functional dependence on $\hat{\boldsymbol{k}}$ and $\hat{\boldsymbol{p}}_\mathrm{e}$ is for simplicity suppressed from the argument on the left hand side of (2.3). Note that (2.3) also can be formulated in $k = 2\pi/\lambda$ via the transformation $\sigma_\mathrm{ext}(\lambda) \to 2\pi\sigma_\mathrm{ext}(2\pi/k)/k^2$. For details on the derivation of (2.3) and definition of the extinction cross section σ_ext and the polarizability dyadics $\boldsymbol{\gamma}_\mathrm{e}$ and $\boldsymbol{\gamma}_\mathrm{m}$, see Appendix A and B. The integrated extinction applied to scattering problems is exploited in Ref. 19.

It is already at this point important to notice that the right hand side of (2.3) only depends on the long wavelength limit or static response of the antenna, while the left hand side is a dynamic quantity which includes the absorption and scattering properties of the antenna. Furthermore, electric and magnetic properties are seen to be treated on equal footing in (2.3), both in terms of material properties and polarization description.

[1] Observe that the assumption that $\hat{\boldsymbol{p}}_\mathrm{e}$ is independent of k does not imply that the polarization of the antenna in Fig. 1 is frequency independent.

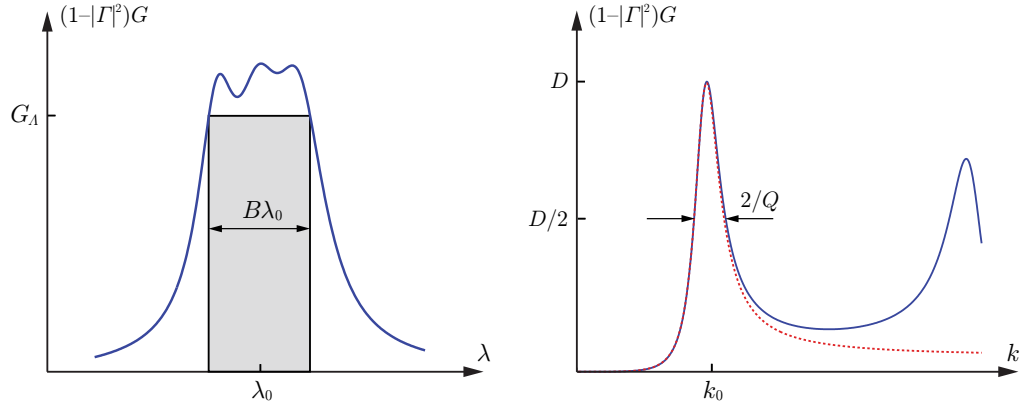

Figure 2: Illustration of the two types of physical limitations considered in this paper: $G_\Lambda B$ represented by the shaded box (left figure) and D/Q related to the dotted resonance model (right figure).

The antenna parameters of importance in this paper are the partial gain G and the partial directivity D, see Appendix E and Ref. 13. In general, both G and D depend on the incident direction $\hat{\boldsymbol{k}}$ and the electric polarization $\hat{\boldsymbol{p}}_{\mathrm{e}}$ as well as the wave number k. In addition, the partial realized gain, $(1-|\Gamma|^2)G$, depends on the reflection coefficient Γ. In the forthcoming analysis, the relative bandwidth B, the Q-factor, and the associated center wavelength λ_0 are naturally introduced as intrinsic parameters in the sense that neither of them depend on $\hat{\boldsymbol{k}}$ or $\hat{\boldsymbol{p}}_{\mathrm{e}}$ for a given single port antenna.

Two different types of bounds on the first resonance of an antenna are addressed in this paper, see Fig. 2. The bounds relate the integral (2.3) of two generic integrands to the polarizability dyadics. The bound on the partial realized gain, $(1-|\Gamma|^2)G$, in the left figure takes the form of a box, *i.e.*, it estimates the integral with the bandwidth times the partial realized gain. The bound in the right figure utilizes the classical resonance shape of the integrand giving a bound expressed in terms of the partial directivity and the associated Q-factor.

3 Limitations on bandwidth and gain

From the definition of the extinction cross section σ_{ext} it is clear that it is non-negative and bounded from below by the absorption cross section σ_{a}. For an unmatched antenna, σ_{a} is reduced by the reflection loss $1-|\Gamma|^2$ according to $\sigma_{\mathrm{a}} = (1-|\Gamma|^2)\sigma_{\mathrm{a0}}$, where σ_{a0} denotes the absorption cross section or partial effective area for the corresponding perfectly matched antenna, see Refs. 18 and 13. The absorption cross section σ_{a0} is by reciprocity related to the partial antenna directivity D as $D = 4\pi\sigma_{\mathrm{a0}}/\lambda^2$, see Ref. 18. Thus, for any wavelength $\lambda \in [0,\infty)$,

$$\sigma_{\mathrm{ext}} \geq \sigma_{\mathrm{a}} = (1-|\Gamma|^2)\sigma_{\mathrm{a0}} = \frac{1}{4\pi}(1-|\Gamma|^2)\lambda^2 D. \tag{3.1}$$

Recall that D depends on the electric polarization $\hat{\boldsymbol{p}}_{\mathrm{e}}$ as well as the incident direction $\hat{\boldsymbol{k}}$. In the present case of no ohmic losses, the partial gain G coincides with the partial directivity D.

Introduce the wavelength interval $\mathit{\Lambda} = [\lambda_1, \lambda_2]$ with center wavelength $\lambda_0 = (\lambda_2 + \lambda_1)/2$ and associated relative bandwidth

$$B = 2\frac{\lambda_2 - \lambda_1}{\lambda_2 + \lambda_1} = 2\frac{k_1 - k_2}{k_2 + k_1},$$

where $0 < B \leq 2$ and $k = 2\pi/\lambda \in K$ denotes the angular wave number in $K = [k_2, k_1]$. Thus, for any wavelength interval $\mathit{\Lambda}$, the estimate $\sigma_{\mathrm{ext}} \geq \sigma_{\mathrm{a}}$ in (3.1) yields

$$\int_0^\infty \sigma_{\mathrm{ext}}(\lambda)\ \mathrm{d}\lambda \geq \int_{\mathit{\Lambda}} \sigma_{\mathrm{a}}(\lambda)\ \mathrm{d}\lambda = \frac{1}{4\pi}\int_{\mathit{\Lambda}} (1 - |\mathit{\Gamma}|^2)\lambda^2 G(\lambda)\ \mathrm{d}\lambda, \tag{3.2}$$

where $D = G$ is used.[2]

In order to simplify the notation, introduce $G_\Lambda = \inf_{\lambda\in\mathit{\Lambda}}(1 - |\mathit{\Gamma}|^2)G$ as the minimum partial realized gain over the wavelength interval $\mathit{\Lambda}$. Following this notation, the integral on the right hand side of (3.2) can be estimated from below as

$$\int_{\mathit{\Lambda}} (1 - |\mathit{\Gamma}|^2)\lambda^2 G(\lambda)\ \mathrm{d}\lambda \geq G_\Lambda \int_{\mathit{\Lambda}} \lambda^2\ \mathrm{d}\lambda = \lambda_0^3 G_\Lambda B\left(1 + \frac{B^2}{12}\right). \tag{3.3}$$

Without loss of generality, the factor $1 + B^2/12$ can be estimated from below by unity. This estimate is also supported by the fact that $B \ll 2$ in many applications. Based upon this observation, (2.3), (3.2) and (3.3) can be summarized to yield the following limitation on the product $G_\Lambda B$ valid for any antenna satisfying the general assumptions stated in Sec. 2:

$$G_\Lambda B \leq \frac{4\pi^3}{\lambda_0^3}(\hat{\boldsymbol{p}}_{\mathrm{e}}^* \cdot \boldsymbol{\gamma}_{\mathrm{e}} \cdot \hat{\boldsymbol{p}}_{\mathrm{e}} + \hat{\boldsymbol{p}}_{\mathrm{m}}^* \cdot \boldsymbol{\gamma}_{\mathrm{m}} \cdot \hat{\boldsymbol{p}}_{\mathrm{m}}). \tag{3.4}$$

Relation (3.4) is one of the main results of this paper. Note that the factor $4\pi^3/\lambda_0^3$ neatly can be expressed as $k_0^3/2$ in terms of the angular wave number $k_0 = 2\pi/\lambda_0$.

The estimate $1 + B^2/12 \geq 1$ in (3.3) is motivated by the simple form of (3.4). In broadband applications, B is in general not small compared to unity, and the higher order term in B should be included on the left hand side of (3.4).

The right hand side of (3.4) depends on both $\hat{\boldsymbol{p}}_{\mathrm{e}}$ and $\hat{\boldsymbol{k}} = \hat{\boldsymbol{p}}_{\mathrm{e}} \times \hat{\boldsymbol{p}}_{\mathrm{m}}$, as well as the long wavelength limit (static limit with respect to $k = 2\pi/\lambda$) material properties and shape of the antenna. It is indeed surprising that it is just the long wavelength limit properties of the antenna that bound the product $G_\Lambda B$ in (3.4). Since $\boldsymbol{\gamma}_{\mathrm{e}}$ and $\boldsymbol{\gamma}_{\mathrm{m}}$ are proportional to the volume V of the antenna, see Ref. 19, it follows from (3.4) that the upper bound on the product $G_\Lambda B$ is directly proportional to V/λ_0^3 or $k_0^3 a^3$, where a denotes the radius of the volume-equivalent sphere.

[2]The equality sign on the left hand side in (3.2) is motivated by the broadband absorption efficiency introduced in (3.7).

In many antenna applications it is desirable to bound the product $G_\Lambda B$ independently of the material properties. For this purpose, introduce the high-contrast polarizability dyadic $\boldsymbol{\gamma}_\infty$ as the limit of either $\boldsymbol{\gamma}_\mathrm{e}$ or $\boldsymbol{\gamma}_\mathrm{m}$ when the elements of $\boldsymbol{\chi}_\mathrm{e}$ or $\boldsymbol{\chi}_\mathrm{m}$ in the long wavelength limit simultaneously approach infinity.[3] Note that this definition implies that $\boldsymbol{\gamma}_\infty$ is independent of any material properties, depending only on the geometry of the antenna. From the variational properties of $\boldsymbol{\gamma}_\mathrm{e}$ and $\boldsymbol{\gamma}_\mathrm{m}$ discussed in Ref. 19 and references therein, it follows that both $\boldsymbol{\gamma}_\mathrm{e}$ and $\boldsymbol{\gamma}_\mathrm{m}$ are bounded from above by $\boldsymbol{\gamma}_\infty$. Hence, (3.4) yields

$$G_\Lambda B \leq \frac{4\pi^3}{\lambda_0^3}(\hat{\boldsymbol{p}}_\mathrm{e}^* \cdot \boldsymbol{\gamma}_\infty \cdot \hat{\boldsymbol{p}}_\mathrm{e} + \hat{\boldsymbol{p}}_\mathrm{m}^* \cdot \boldsymbol{\gamma}_\infty \cdot \hat{\boldsymbol{p}}_\mathrm{m}). \tag{3.5}$$

The introduction of the high-contrast polarizability dyadic $\boldsymbol{\gamma}_\infty$ in (3.5) is the starting point of the analysis below.

The high-contrast polarizability dyadic $\boldsymbol{\gamma}_\infty$ is real-valued and symmetric, and consequently diagonalizable with real-valued eigenvalues. Let $\gamma_1 \geq \gamma_2 \geq \gamma_3$ denote the three eigenvalues. Based on the constraint $\hat{\boldsymbol{p}}_\mathrm{e} \cdot \hat{\boldsymbol{p}}_\mathrm{m} = 0$, which is a consequence of the free space plane-wave excitation, the right hand side of (3.5) can be estimated from above as

$$\sup_{\hat{\boldsymbol{p}}_\mathrm{e} \cdot \hat{\boldsymbol{p}}_\mathrm{m} = 0} G_\Lambda B \leq \frac{4\pi^3}{\lambda_0^3}(\gamma_1 + \gamma_2). \tag{3.6}$$

The interpretation of the operator $\sup_{\hat{\boldsymbol{p}}_\mathrm{e} \cdot \hat{\boldsymbol{p}}_\mathrm{m} = 0}$ is polarization matching, *i.e.*, the polarization of the antenna coincides with the polarization of the incident wave. In the case of non-magnetic antennas, $\boldsymbol{\gamma}_\mathrm{m} = \mathbf{0}$, the second eigenvalue γ_2 in (3.6) vanishes. Hence, the right hand side of (3.6) can be improved by at most a factor of two by utilizing magnetic materials. Note that the upper bounds in (3.5) and (3.6) coincide when $\boldsymbol{\gamma}_\infty$ is isotropic.

Since γ_1 and γ_2 only depend on the long wavelength properties of the antenna, they can easily be calculated for arbitrary geometries using either the finite element method (FEM) or the method of moments (MoM). Numerical results of γ_1 and γ_2 for the Platonic solids, the rectangular parallelepiped and some classical antennas are presented in Secs. 7 and 8. Important variational properties of γ_j are discussed in Ref. 19 and references therein. The influence of supporting ground planes and the validity of the method of images for high-contrast polarizability calculations are presented in Appendix C.

The estimate in (3.2) can be improved based on a priori knowledge of the scattering properties of the antenna. In fact, $\sigma_\mathrm{ext} \geq \sigma_\mathrm{a}$ in (3.1) may be replaced by $\sigma_\mathrm{ext} = \sigma_\mathrm{a}/\eta$, where $0 < \eta \leq 1$ denotes the absorption efficiency of the antenna, see Ref. 2. For most antennas at the resonance frequency, $\eta \leq 1/2$, but exceptions from this rule of thumb exist. In particular, minimum scattering antennas (MSA) defined by $\eta = 1/2$ yield an additional factor of two on the right hand side of (3.1). The inequality in (3.2) can be replaced by the equality

$$\int_\Lambda \sigma_\mathrm{ext}(\lambda)\ \mathrm{d}\lambda = \widetilde{\eta}^{-1} \int_\Lambda \sigma_\mathrm{a}(\lambda)\ \mathrm{d}\lambda. \tag{3.7}$$

[3]Recall that $\boldsymbol{\chi}_\mathrm{e}$ and $\boldsymbol{\chi}_\mathrm{m}$ are real-valued in the long wavelength limit. In the case of finite or infinite conductivity, see Appendix B.

The constant $\widetilde{\eta}$ is bounded from above by the absorption efficiency via $\widetilde{\eta} \leq \sup_{\lambda\in\Lambda} \eta$, and provides a broadband generalization of the absorption efficiency. If $\widetilde{\eta}$ is invoked in (3.2), the right hand side of the inequalities (3.4), (3.5), and (3.6) are sharpened by the multiplicative factor $\widetilde{\eta}$.

4 Limitations on Q-factor and directivity

Under the assumption of N non-interfering resonances characterized by the real-valued angular wave numbers k_n, a multiple resonance model for the absorption cross section is

$$\sigma_{\mathrm{a}}(k) = 2\pi \sum_{n=1}^{N} \varrho_n \frac{Q_n k_n}{1 + Q_n^2 (k/k_n - k_n/k)^2/4}, \tag{4.1}$$

where k is assumed real-valued and ϱ_n are positive weight functions satisfying $\sum_n \varrho_n = \varrho(0)$. Here, the Q-factor of the resonance at k_n is denoted by Q_n, and for $Q_n \gg 1$, the associated relative half-power bandwidth is $B_n \sim 2/Q_n$, see Fig. 3. Recall that $Q_n \geq 1$ is consistent with $0 < B_n \leq 2$. For the resonance model (4.1), one can argue that Q_n in fact coincides with the corresponding antenna Q-factor in Appendix F when the relative bandwidth $2/Q_n$ is based on the half-power threshold, see also Refs. 6 and 25. In the case of strongly interfering resonances, the model (4.1) either has to be modified or the estimates in Sec. 3 have to be used.

The absorption cross section is the imaginary part, $\sigma_{\mathrm{a}} = 4\pi k \operatorname{Im} \varrho_{\mathrm{a}}$, of the function

$$\varrho_{\mathrm{a}}(k) = \sum_{n=1}^{N} \varrho_n \frac{\mathrm{i} Q_n k_n/(2k)}{1 - \mathrm{i} Q_n \left(k/k_n - k_n/k\right)/2}, \tag{4.2}$$

for real-valued k. The function $\varrho_{\mathrm{a}}(k)$ is holomorphic for $\operatorname{Im} k > 0$ and has a symmetrically distributed pair of poles for $\operatorname{Im} k < 0$, see Fig. 3. The integrated absorption cross section is

$$\frac{1}{4\pi^2} \int_{-\infty}^{\infty} \frac{\sigma_{\mathrm{a}}(k)}{k^2} \, \mathrm{d}k = \varrho_{\mathrm{a}}(0) = \widetilde{\eta} \varrho(0) \leq \varrho(0), \tag{4.3}$$

where $\varrho(0)$ is given by the long wavelength limit (A.4).

For antennas with a dominant first resonance at $k = k_1$, it follows from (3.1) and (4.1) that the partial realized gain G satisfies

$$(1 - |\Gamma|^2) G = \frac{k^2 \sigma_{\mathrm{a}}}{\pi} \leq \varrho(0) \frac{2k^2 Q k_1}{1 + Q^2 (k/k_1 - k_1/k)^2/4}, \tag{4.4}$$

where $\varrho_1 \leq \varrho(0)$ has been used. The right hand side of (4.4) reaches its maximum value $\varrho(0) 2k_1^3 Q/(1 - Q^{-2})$ at $k_0 = k_1(1 - 2Q^{-2})^{-1/2}$ or $k_0 = k_1 + \mathcal{O}(Q^{-2})$ as $Q \to \infty$. Hence, k_0 is a good approximation to k_1 if $Q \gg 1$. For a lossless antenna which is perfectly matched at $k = k_0$, the partial realized gain $(1 - |\Gamma|^2)G$ coincides with the partial directivity D. Under this assumption, (4.4) yields $D/Q \leq \varrho(0) 2k_1^3/(1 - Q^{-2})$ which further can be estimated from above as

$$\frac{D}{Q} \leq \frac{k_0^3}{2\pi} \left(\hat{\boldsymbol{p}}_{\mathrm{e}}^* \cdot \boldsymbol{\gamma}_{\mathrm{e}} \cdot \hat{\boldsymbol{p}}_{\mathrm{e}} + \hat{\boldsymbol{p}}_{\mathrm{m}}^* \cdot \boldsymbol{\gamma}_{\mathrm{m}} \cdot \hat{\boldsymbol{p}}_{\mathrm{m}} \right), \tag{4.5}$$

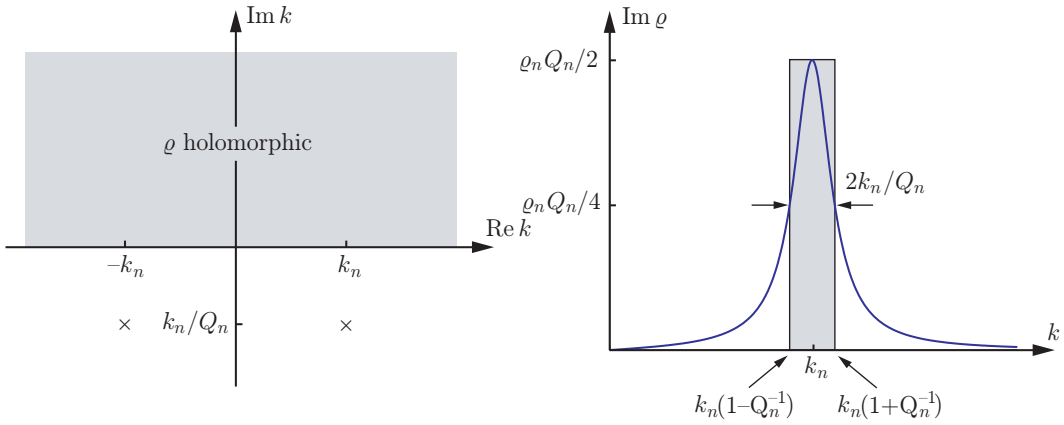

Figure 3: The symmetrically distributed pair of poles (×) of the extinction volume ϱ in the complex k-plane (left figure) and the corresponding single resonance model of $\mathrm{Im}\,\varrho$ when $Q_n \gg 1$ (right figure).

where (A.4) have been used. Relation (4.5) together with (3.5) constitute the main results of this paper.

Analogous to (3.5) and (3.6), it is clear that (4.5) can be estimated from above by the high-contrast polarizability dyadic $\boldsymbol{\gamma}_\infty$ and the associated eigenvalues γ_1 and γ_2, *viz.*,

$$\sup_{\hat{\boldsymbol{p}}_\mathrm{e}\cdot\hat{\boldsymbol{p}}_\mathrm{m}=0} \frac{D}{Q} \leq \frac{k_0^3}{2\pi}(\gamma_1+\gamma_2). \tag{4.6}$$

Here, (4.6) is subject to polarization matching and therefore independent of the electric and magnetic polarizations, $\hat{\boldsymbol{p}}_\mathrm{e}$ and $\hat{\boldsymbol{p}}_\mathrm{m}$, respectively. Note that the upper bounds in (4.5) and (4.6) only differ from the corresponding results in (3.5) and (3.6) by a factor of π, *i.e.*, $G_\Lambda B \leq \pi C$ and $D/Q \leq C$. Hence, it is sufficient to consider either the $G_\Lambda B$ bound or the D/Q bound for a specific antenna. The estimates (4.5) and (4.6) can be improved by the multiplicative factor $\widetilde{\eta}$ if a priori knowledge of the scattering properties of the antenna (3.7) is invoked in (4.4).

The resonance model for the absorption cross section in (4.1) is also directly applicable to the theory of broadband scattering in Ref. 19. In that reference, (4.1) can be used to model absorption and scattering properties and yield new limitations on broadband scattering.

5 Comparison with Chu and Chu-Fano

In this section, the bounds on $G_\Lambda B$ and D/Q subject to matched polarizations, *i.e.*, inequalities (3.6) and (4.6), are compared with the corresponding results by Chu and Fano in Refs. 3 and 5, respectively.

5.1 Limitations on Q-factor and directivity

The classical limitations derived by Chu in Ref. 3 relate the Q-factor and the directivity D to the quantity $k_0 a$ of the smallest circumscribing sphere. Using the notation of Secs. 3 and 4, the classical result by Chu for an omni-directional antenna (for example in the azimuth plane) reads

$$\sup_{\hat{\boldsymbol{p}}_{\mathrm{e}}\cdot\hat{\boldsymbol{p}}_{\mathrm{m}}=0} \frac{D}{Q} \leq \frac{3}{2}\frac{k_0^3 a^3}{k_0^2 a^2 + 1} = \frac{3}{2} k_0^3 a^3 + \mathcal{O}(k_0^5 a^5) \quad \text{as } k_0 a \to 0. \tag{5.1}$$

In the general case of both TE- and TM-modes, (5.1) must be modified, see Ref. 12, *viz.*,

$$\sup_{\hat{\boldsymbol{p}}_{\mathrm{e}}\cdot\hat{\boldsymbol{p}}_{\mathrm{m}}=0} \frac{D}{Q} \leq \frac{6 k_0^3 a^3}{2 k_0^2 a^2 + 1} = 6 k_0^3 a^3 + \mathcal{O}(k_0^5 a^5) \quad \text{as } k_0 a \to 0. \tag{5.2}$$

Note that (5.2) differs from (5.1) by approximately a factor of four when $k_0 a \ll 1$.

The bounds in (5.1) and (5.2) should be compared with the corresponding result in Sec. 4 for the sphere. For a sphere of radius a, the eigenvalues γ_1 and γ_2 are degenerated and equal to $4\pi a^3$, see Sec. 6. Insertion of $\gamma_1 = \gamma_2 = 4\pi a^3$ into (4.6) yields $\sup_{\hat{\boldsymbol{p}}_{\mathrm{e}}\cdot\hat{\boldsymbol{p}}_{\mathrm{m}}=0} D/Q \leq C$, where the constant C is given by

$$C = 4 k_0^3 a^3, \qquad C = 2 k_0^3 a^3, \qquad C = k_0^3 a^3. \tag{5.3}$$

The three different cases in (5.3) correspond to both electric and magnetic material properties ($C = 4k_0^3 a^3$), pure electric material properties ($C = 2k_0^3 a^3$), and pure electric material properties with a priori knowledge of minimum scattering characteristics ($C = k_0^3 a^3$ with $\widetilde{\eta} = 1/2$), respectively. Note that the third case in (5.3) more generally can be expressed as $C = 2k_0^3 a^3 \widetilde{\eta}$ for any broadband absorption efficiency $0 < \widetilde{\eta} \leq 1$. The bounds in (5.2) and (5.3) are comparable although the new limitations (5.3) are sharper. In the omni-directional case, (5.1) provides a sharper bound than (5.3), except for the pure electric case with absorption efficiency $\widetilde{\eta} < 3/4$.

5.2 Limitations on bandwidth and gain

The limitation (3.6) should also be compared with the result of Chu when the Fano theory of broadband matching is used. The Fano theory includes the impedance variation over the frequency interval to yield limitations on the bandwidth, see Ref. 5. For a resonance circuit model, the Fano theory yields that the relation between B and Q is, see Ref. 6,

$$B \leq \frac{\pi}{Q \ln 1/|\Gamma|}. \tag{5.4}$$

The reflection coefficient Γ is due to mismatch of the antenna. It is related to the standing wave ratio SWR as $|\Gamma| = (\mathrm{SWR} - 1)/(1 + \mathrm{SWR})$.

Introduce Q_{s} as the Q-factor of the smallest circumscribing sphere with $1/Q_{\mathrm{s}} = k_0^3 a^3 + \mathcal{O}(k_0^5 a^5)$ as $k_0 a \to 0$ for omni-directional antennas. Under this assumption, it

follows from (5.1) that $\sup_{\hat{\boldsymbol{p}}_\mathrm{e}\cdot\hat{\boldsymbol{p}}_\mathrm{m}=0} D \leq 3Q/2Q_\mathrm{s}$. Insertion of this inequality into (5.4) then yields

$$\sup_{\hat{\boldsymbol{p}}_\mathrm{e}\cdot\hat{\boldsymbol{p}}_\mathrm{m}=0} G_\Lambda B \leq \frac{3\pi}{2}\frac{1-|\Gamma|^2}{\ln 1/|\Gamma|}k_0^3a^3. \tag{5.5}$$

For a given k_0a, the right hand side of (5.5) is monotone in $|\Gamma|$ and bounded from above by $3\pi k_0^3a^3$. However, note that the Chu-Fano limitation (5.5) is restricted to omni-directional antennas with $k_0a \ll 1$.

Inequality (5.5) should be compared with the corresponding result in Sec. 3 for the smallest circumscribing sphere. Since the upper bounds (3.6) and (4.6) only differ by a factor of π, *i.e.*, $\sup_{\hat{\boldsymbol{p}}_\mathrm{e}\cdot\hat{\boldsymbol{p}}_\mathrm{m}=0} G_\Lambda B \leq C'$ and $\sup_{\hat{\boldsymbol{p}}_\mathrm{e}\cdot\hat{\boldsymbol{p}}_\mathrm{m}=0} D/Q \leq C$ where $C' = \pi C$, it follows from (5.3) that

$$C' = 4\pi k_0^3a^3, \qquad C' = 2\pi k_0^3a^3, \qquad C' = \pi k_0^3a^3. \tag{5.6}$$

The three cases in (5.3) correspond to both electric and magnetic material properties ($C' = 4\pi k_0^3a^3$), pure electric material properties ($C' = 2\pi k_0^3a^3$), and pure electric material properties with a priori knowledge of minimum scattering characteristics ($C' = \pi k_0^3a^3$), respectively.

The limitations on $G_\Lambda B$ based on (5.6) are comparable with (5.5) for most reflections coefficients $|\Gamma|$. For $|\Gamma| < 0.65$ the Chu-Fano limitation (5.5) provides a slightly sharper bound on $G_\Lambda B$ than (5.6) for pure electric materials. However, recall that the spherical geometry gives an unfavorable comparison with the present theory, since for many antennas the eigenvalues γ_1 and γ_2 are reduced considerably compared with the smallest circumscribing sphere, *cf.*, the dipole in Sec. 8.1 and the loop antenna in Sec. 8.2.

6 Ellipsoidal geometries

Closed-form expressions of $\boldsymbol{\gamma}_\mathrm{e}$ and $\boldsymbol{\gamma}_\mathrm{m}$ exist for the ellipsoidal geometries, see Ref. 19, *viz.*,

$$\boldsymbol{\gamma}_\mathrm{e} = V\boldsymbol{\chi}_\mathrm{e}\cdot(\mathbf{I}+\mathbf{L}\cdot\boldsymbol{\chi}_\mathrm{e})^{-1}, \qquad \boldsymbol{\gamma}_\mathrm{m} = V\boldsymbol{\chi}_\mathrm{m}\cdot(\mathbf{I}+\mathbf{L}\cdot\boldsymbol{\chi}_\mathrm{m})^{-1}. \tag{6.1}$$

Here, $\mathbf{I}$ denotes the unit dyadic and $V = 4\pi a_1a_2a_3/3$ is the volume of ellipsoid in terms of the semi-axes a_j. The depolarizability dyadic $\mathbf{L}$ is real-valued and symmetric, and hence diagonalizable with real-valued eigenvalues. The eigenvalues of $\mathbf{L}$ are the depolarizing factors L_j, given by

$$L_j = \frac{a_1a_2a_3}{2}\int_0^\infty \frac{\mathrm{d}s}{(s+a_j^2)\sqrt{(s+a_1^2)(s+a_2^2)(s+a_3^2)}}, \quad j=1,2,3. \tag{6.2}$$

The depolarizing factors L_j satisfy $0 \leq L_j \leq 1$ and $\sum_j L_j = 1$. The semi-axes a_j are assumed to be ordered such that $L_1 \leq L_2 \leq L_3$. Closed-form expressions of (6.2) in terms of the semi-axis ratio $\xi = (\min_j a_j)/(\max_j a_j)$ exist for the ellipsoids of revolution, *i.e.*, the prolate spheroids ($L_2 = L_3$) and the oblate spheroids ($L_1 = L_2$), see Appendix G.

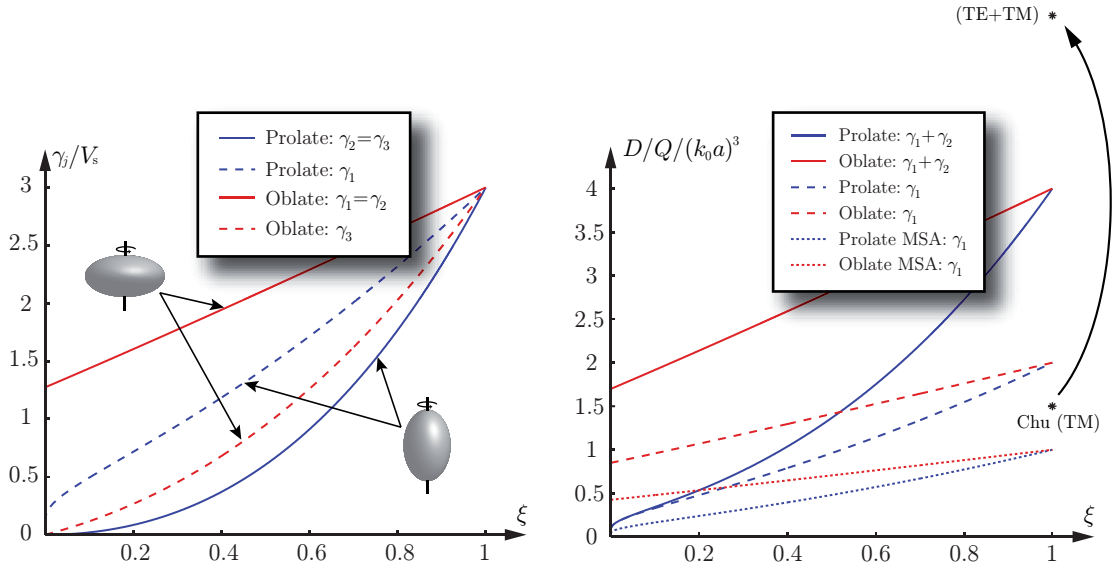

Figure 4: The eigenvalues $\gamma_1 \geq \gamma_2 \geq \gamma_3$ (left figure) and the quotient D/Q (right figure) for the prolate and oblate spheroids as function of the semi-axis ratio ξ. Note the normalization with the volume $V_s = 4\pi a^3/3$ of the smallest circumscribing sphere.

The high-contrast polarizability dyadic $\boldsymbol{\gamma}_\infty$ is given by (6.1) as the elements of $\boldsymbol{\chi}_e$ or $\boldsymbol{\chi}_m$ simultaneously approach infinity. From (6.1) it is clear that the eigenvalues of $\boldsymbol{\gamma}_\infty$ are given by $\gamma_j = V/L_j$. For the prolate and oblate spheroids, V is neatly expressed in terms of the volume $V_s = 4\pi a^3/3$ of the smallest circumscribing sphere. The results are $V = \xi^2 V_s$ and $V = \xi V_s$ for the prolate and oblate spheroids, respectively. The eigenvalues γ_1 and γ_2 for the prolate and oblate spheroids are depicted in the left figure in Fig. 4. Note that the curves for the oblate spheroid approach $4/\pi$ in the limit as $\xi \to 0$, see Appendix G. The corresponding limiting value for the curves as $\xi \to 1$ is 3.

The general bound on $G_\Lambda B$ for arbitrary ellipsoidal geometries is obtained by inserting (6.1) into (3.4), *i.e.*,

$$G_\Lambda B \leq \frac{4\pi^3 V}{\lambda_0^3} \left(\hat{\boldsymbol{p}}_e^* \cdot \boldsymbol{\chi}_e \cdot (\mathbf{I} + \mathbf{L} \cdot \boldsymbol{\chi}_e)^{-1} \cdot \hat{\boldsymbol{p}}_e + \hat{\boldsymbol{p}}_m^* \cdot \boldsymbol{\chi}_m \cdot (\mathbf{I} + \mathbf{L} \cdot \boldsymbol{\chi}_m)^{-1} \cdot \hat{\boldsymbol{p}}_m \right). \quad (6.3)$$

Independent of both material properties and polarization effects, the right hand side of (6.3) can be estimated from above in analogy with (3.6). The result is

$$\sup_{\hat{\boldsymbol{p}}_e \cdot \hat{\boldsymbol{p}}_m = 0} G_\Lambda B \leq \frac{4\pi^3 V}{\lambda_0^3} \left(\frac{1}{L_1} + \frac{1}{L_2} \right). \quad (6.4)$$

In the non-magnetic case, the second term on the right hand side of (6.3) and (6.4) vanishes. For the prolate and oblate spheroids, the closed-form expressions of L_j in Appendix G can be introduced to yield explicit upper bounds on $G_\Lambda B$.

The corresponding results for the quotient D/Q are obtained from the observation that $G_\Lambda B \leq \pi C$ is equivalent to $D/Q \leq C$, see Sec. 4. For the general case

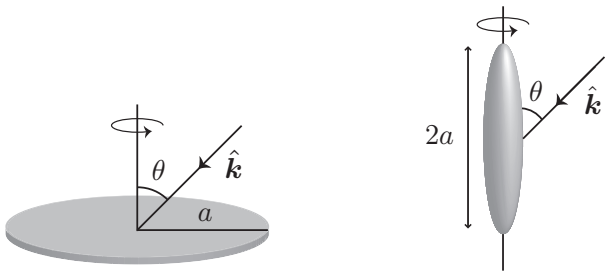

circular disk circular needle

Figure 5: Geometry of the circular disk and needle.

including polarization and material properties, (6.3) yields

$$\frac{D}{Q} \leq \frac{k_0^3 V}{2\pi} \left(\hat{\boldsymbol{p}}_{\mathrm{e}}^* \cdot \boldsymbol{\chi}_{\mathrm{e}} \cdot (\mathbf{I} + \mathbf{L} \cdot \boldsymbol{\chi}_{\mathrm{e}})^{-1} \cdot \hat{\boldsymbol{p}}_{\mathrm{e}} + \hat{\boldsymbol{p}}_{\mathrm{m}}^* \cdot \boldsymbol{\chi}_{\mathrm{m}} \cdot (\mathbf{I} + \mathbf{L} \cdot \boldsymbol{\chi}_{\mathrm{m}})^{-1} \cdot \hat{\boldsymbol{p}}_{\mathrm{m}} \right). \tag{6.5}$$

Analogous to (6.4), the restriction to matched polarizations for the quotient D/Q reads

$$\sup_{\hat{\boldsymbol{p}}_{\mathrm{e}} \cdot \hat{\boldsymbol{p}}_{\mathrm{m}} = 0} \frac{D}{Q} \leq \frac{k_0^3 V}{2\pi} \left(\frac{1}{L_1} + \frac{1}{L_2} \right). \tag{6.6}$$

The upper bound in (6.6) is depicted in the right figure in Fig. 4 for the prolate and oblate spheroids. The solid curves correspond to combined electric and magnetic material properties, while the dashed curves represent the pure electric case. The non-magnetic minimum scattering case ($\widetilde{\eta} = 1/2$) is given by the dotted curves. Note that the three curves in the right figure vanish for the prolate spheroid as $\xi \to 0$. The corresponding limiting values for the oblate spheroid are $16/3\pi$, $8/3\pi$ and $4/3\pi$, see Appendix G.

The curves depicted in the right figure in Fig. 4 should be compared with the classical results for the sphere in (5.1) and (5.2). The omni-directional bound (5.1) and its generalization (5.2) are marked in Fig. 4 by Chu (TE) and (TE+TM), respectively. From the figure, it is clear that (6.6) provides a sharper bound than (5.2). For omni-directional antennas, (5.1) is slightly sharper than (6.6) for the sphere, but when a priori knowledge of minimum scattering characteristics ($\widetilde{\eta} = 1/2$) is used, the reversed conclusion holds. Recall that the classical results in Sec. 5.1 are restricted to the sphere, in contrast to the theory introduced in this paper.

Based on the results in Appendix G, it is interesting to evaluate (6.4) in the limit as $\xi \to 0$. This limit corresponds to the axially symmetric needle and circular disk in Fig. 5. For a needle of length $2a$ with semi-axis $\xi \ll 1$, (G.3) inserted into (6.4) yields

$$G_\Lambda B \leq \frac{16\pi^4 a^3}{3\lambda_0^3} \frac{f(\theta)}{\ln 2/\xi - 1} + \mathcal{O}(\xi^2) \quad \text{as } \xi \to 0. \tag{6.7}$$

Here, $f(\theta) = \sin^2\theta$ for the TE- and TM-polarizations in the case of both electric and magnetic material properties. In the non-magnetic case, $f(\theta) = 0$ for the TE- and $f(\theta) = \sin^2\theta$ for the TM-polarization. Note that the $\sin^2\theta$ term in (6.7) and

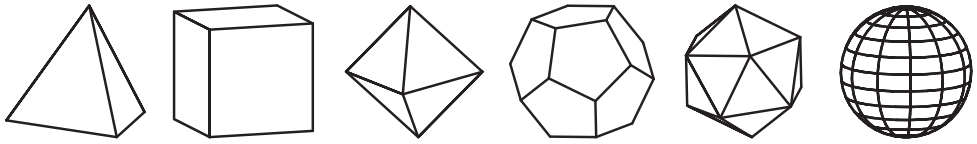

$5.029V$	$3.644V$	$3.551V$	$3.178V$	$3.130V$	$3V$
(0.205)	(0.445)	(0.377)	(0.704)	(0.632)	(1)

Figure 6: The eigenvalues γ (upper row) for the five Platonic solids and the sphere. The number in parenthesis are γ in units of $4\pi a^3$, where a denotes the radius of the smallest circumscribing sphere.

the logarithmic singularity in the denominator agree with the radiation pattern and the impedance of the dipole antenna in Sec. 8.1, see Ref. 4.

The corresponding result for the circular disk of radius a is non-vanishing in the limit as $\xi \to 0$, *viz.*,

$$G_\Lambda B \leq \frac{64\pi^3 a^3}{3\lambda_0^3} f(\theta). \tag{6.8}$$

Here, $f(\theta) = 1 + \cos^2\theta$ for the TE- and TM-polarizations in the case of both electric and magnetic material properties. In the non-magnetic case, $f(\theta) = 1$ for the TE- and and $f(\theta) = \cos^2\theta$ for the TM-polarization. Note the direct application of (6.8) for planar spiral antennas.

7 The high-contrast polarizability dyadic

In this section, some numerical results of $\boldsymbol{\gamma}_\infty$ are presented and analyzed in terms of the physical limitations discussed in Sec. 3.

7.1 The Platonic solids

Since the Platonic solids are invariant under appropriate point groups, see Ref. 11, their corresponding high-contrast polarizability dyadics $\boldsymbol{\gamma}_\infty$ are isotropic, *i.e.*, $\boldsymbol{\gamma}_\infty = \gamma_\infty \mathbf{I}$, where $\mathbf{I}$ denotes the unit dyadic in $\mathbb{R}^3$. Let $\gamma = \gamma_j$ represent the eigenvalues of $\boldsymbol{\gamma}_\infty$ for $j = 1, 2, 3$. The Platonic solids are depicted in Fig. 6 together with the eigenvalues γ in terms of the volume V of the solids. The five Platonic solids are from left to right the tetrahedron, hexahedron, octahedron, dodecahedron and icosahedron, with 4, 6, 8, 12 and 20 facets, respectively. Included in the figure are also γ in units of $4\pi a^3$, where a denotes the radius of the smallest circumscribing sphere. This comparison with the smallest circumscribing sphere is based on straightforward calculations which is further discussed in Sec. 7.2. The numerical values of γ in Fig. 6 are based on Method of Moments (MoM) calculations, see Ref. 19 and references therein.

Since the upper bound in (3.6) is linear in γ, it follows that among the Platonic solids, the tetrahedron provides the largest upper bound on $G_\Lambda B$ for a given volume

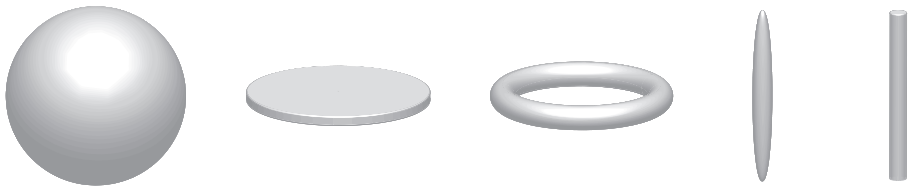

(1) (0.42) (0.24) (0.050) (0.056)

Figure 7: The eigenvalue γ_1 in units of $4\pi a^3$, where a denotes the radius of the smallest circumscribing sphere. The prolate spheroid, the circular ring and the circular cylinder correspond to the generalized semi-axis ratio $\xi = 10^{-3}$.

V. The eigenvalues γ in Fig. 6 are seen to approach $3V$ as the number of facets increases. This observation is confirmed by the variational principle discussed in Ref. 19, which states that for a given volume the sphere minimizes the trace of $\boldsymbol{\gamma}_\infty$ among all isotropic high-contrast polarizability dyadics. Hence, a lower bound on γ is given by the sphere for which $\gamma = 3V$.

For matched polarizations, the eigenvalues in Fig. 6 can directly be applied to (3.6) to yield an upper bound on the performance of any antenna circumscribed by a given Platonic solid. For example, the non-magnetic tetrahedron yields $G_\Lambda B \leq 624V/\lambda_0^3$ or $G_\Lambda B \leq 0.19$ for $V = 1\,\mathrm{cm}^3$ and center frequency $\mathrm{c}_0/\lambda_0 = 2\,\mathrm{GHz}$. The corresponding bound on the quotient D/Q differ only by a factor of π, *i.e.*, $D/Q \leq 0.059$.

It is interesting to note that the pertinent point group symmetries of the Platonic solids are preserved if their geometries are altered appropriately. Such symmetric changes yield a large class of geometries for which $\boldsymbol{\gamma}_\infty$ is isotropic and the upper bound on $G_\Lambda B$ is independent of the polarization. This observation together with the fact that the variational principle discussed above also can be applied to arbitrary isotropic high-contrast polarizability dyadics, are particularly interesting from a MIMO-perspective, see Ref. 9 and references therein.

7.2 Comparison with the sphere

From the discussion of the polarizability dyadics in Ref. 19, it is clear that both γ_1 and γ_2 are directly proportional to the volume of the antenna with a purely geometry dependent proportionality factor. For the circular disk, it follows from Appendix G that even though the volume of the disk vanishes, the eigenvalues γ_1 and γ_2 are non-zero. This result is due to the fact that the geometry dependent proportionality factors $1/L_1$ and $1/L_2$ approach infinity in the limit as the semi-axis ratio approaches zero. In other words, it is not sufficient to only consider the volume part of γ_1 and γ_2 to draw conclusions of the potential in antenna performance for a given volume. In addition, also the shape dependent proportionality factor must be taken into account.

Motivated by the discussion above, it is interesting to compare γ_1 and γ_2 for the different geometries discussed in Secs. 7 and 8, and in Ref. 7. The comparison refers

to the smallest circumscribing sphere with radius a, for which γ_1 and γ_2 are equal to $4\pi a^3$, see Ref. 7. For this purpose, introduce $\gamma_1/4\pi a^3$, which, in the case of pure electric material properties, yields a direct measure of the antenna performance in terms of (3.6) and (4.6). The main question addressed in this section is therefore: how much antenna performance can be gained for a given geometry by instead utilizing the full volume of the smallest circumscribing sphere?

In Fig. 7, the goodness number $\gamma_1/4\pi a^3$ are presented for the sphere, circular disk, toroidal ring, and prolate and cylindrical needles, respectively. The generalized semi-axis ratio[4] for the toroidal ring and the prolate and cylindrical needles are $\xi = 10^{-3}$. The values for the prolate needle and the toroidal ring are given by (G.3) and (H.5), respectively, while the cylindrical needle is based on FEM simulation for the dipole antenna in Sec. 8.1. The value for the circular disk is $4/3\pi \approx 0.42$ given by (G.4).

The results in Fig. 7 should be compared with the corresponding values in Fig. 6 for the Platonic solids. For example, it is seen that the potential of utilizing the tetrahedron is about 20.5% compared to the smallest circumscribing sphere. Since the high-contrast polarizability dyadics $\boldsymbol{\gamma}_\infty$ are isotropic for the Platonic solids and the sphere, it follows that the results in Fig. 6 also hold for the second and third eigenvalues, γ_2 and γ_3, respectively. This is however not the case for the geometries depicted in Fig. 7 since the circular disk, toroidal ring, and the prolate and cylindrical needles have no isotropic high-contrast polarizability dyadics. For the circular disk and the toroidal ring, γ_1 and γ_2 are equal, and therefore yield the same results as in Fig. 7 for combined electric and magnetic material properties.

In Fig. 7, it is seen that the physical limitations on $G_\Lambda B$ and D/Q for any two-dimensional antenna confined to the circular disk corresponds to about 42% of the potential to utilize the full sphere. This result is rather surprising since, in contrast to the sphere, the circular disk has zero volume. In other words, there is only a factor of $1/0.42 \approx 2.4$ to gain in antenna performance by utilizing three-dimensions compared to two for a given maximum dimension a of the antenna. Since the prolate and cylindrical needles vanish in the limit as the semi-axis ratio approaches zero, the performance of any one-dimensional antenna restricted to the line is negligible as compared to the performance of an antenna in the sphere.

Since γ_1 and γ_2 in the right hand side of (3.6) and (4.6) are determined from separate electric and magnetic problems in the long wavelength limit, see Appendix B, it is clear that electric and magnetic material properties, and hence also γ_1 and γ_2, can be combined separately. For example, any antenna with magnetic properties confined to the circular disk and electric properties confined to the toroidal ring has a potential which is $100(0.42 + 0.24) = 66\%$ of the sphere with no magnetic material properties present.

[4]The generalized semi-axis ratio for the cylindrical needle and the toroidal ring are defined by $\xi = b/a$, where a and b are given in Figs. 9 and 11, respectively.

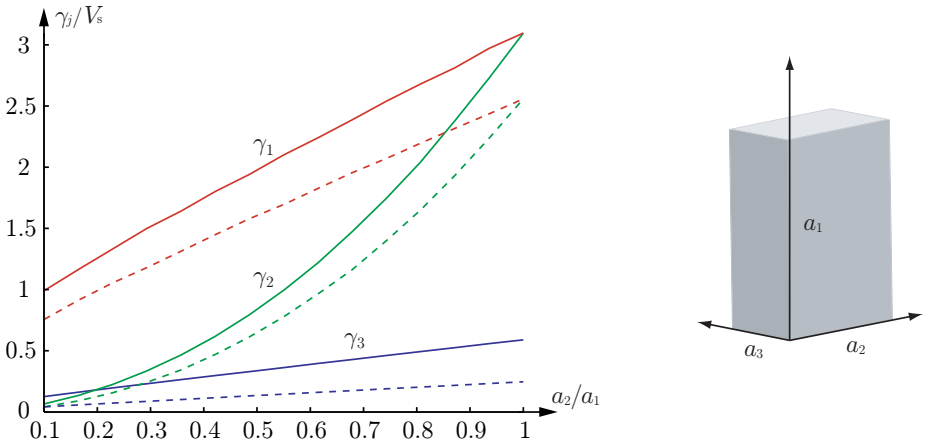

Figure 8: The eigenvalues γ_1, γ_2 and γ_3 as function of the ratio a_2/a_1 for a rectangular parallelepiped of edge lengths a_1, a_2 and a_3. The solid curves are for $a_1/a_3 = 5$ and the dotted curve is for $a_1/a_3 = 10$. Note the normalization with the volume $V_s = \pi a_1^3/6$ of the sphere of radius $a_1/2$.

7.3 The rectangular parallelepiped

The rectangular parallelepiped is a generic geometry that can be used to model, *e.g.*, mobile phones, laptops, and PDAs. The eigenvalues γ_1, γ_2 and γ_3 for a rectangular parallelepiped with edge lengths a_1, a_2 and a_3 are shown in Fig. 8 as a function of the ratio a_2/a_1. The solid and dotted curves correspond to $a_1/a_3 = 5$ and $a_1/a_3 = 10$, respectively. The eigenvalues are ordered $\gamma_1 \geq \gamma_2 \geq \gamma_3$ and the principal axes of the eigenvalues γ_i correspond to the directions parallel to a_i if $a_1 \geq a_2 \geq a_3$. The eigenvalues degenerate if the lengths of the corresponding edges coincide.

The performance of any non-magnetic antenna inscribed in the parallelepiped is limited as shown by (3.5) with $\boldsymbol{\gamma}_m = \mathbf{0}$. Specifically, the limitations on antennas polarized in the a_i direction are given by the eigenvalue, γ_i. Obviously, it is advantageous to utilize the longest dimension of the parallelepiped for the polarization of single port antennas. The limitation (3.5) also quantifies the degradation in using the other directions for the polarization. This is useful for the understanding of fundamental limitations and synthesis of MIMO antennas.

For example, a typical mobile phone is approximately 10 cm high, 5 cm wide, and 1 cm to 2 cm thick. The corresponding eigenvalues γ_1, γ_2 and γ_3 for $a_1 = 10$ cm are seen in Fig. 8 for $a_3 = 2$ cm (solid lines) and $a_3 = 1$ cm (broken lines). The distribution of the eigenvalues γ_1, γ_2 and γ_3 quantifies the trade off between pattern and polarization diversity for multiple antennas systems in the mobile phone. Pattern diversity utilizes the largest eigenvalue but requires an increased directivity at the cost of bandwidth (3.5). Similarly, polarization diversity utilizes at least two eigenvalues. It is observed that it is advantageous to use polarization and pattern diversity for $a_2 \approx a_1$ and $a_2 \ll a_1$, respectively. For a mobile phone where $a_2 \approx a_1/2$, either pattern diversity or a combined pattern and polarization diversity as linear combinations of the a_1 and a_2 directions can be used. Moreover, note that magnetic

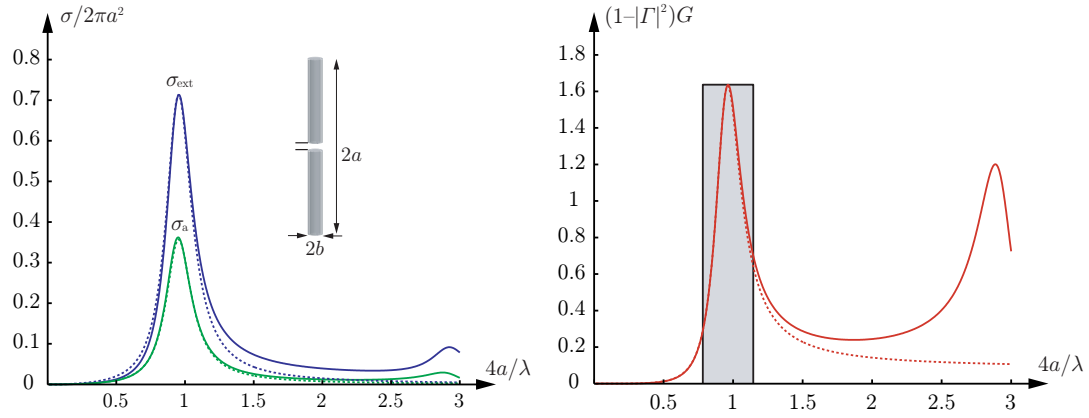

Figure 9: The extinction and absorption cross sections (left figure) and the realized gain (right figure) for a cylindrical dipole antenna with axial ratio $b/a = 10^{-3}$. The different curves correspond to Hallén's integral equation (solid curves), directivity and Q-factor limitation (4.6) (dashed curves), and gain and bandwidth limitation (3.6) (shaded box).

materials, increase the bound (3.5) and offer additional possibilities.

8 Analysis of some classical antennas

In this section, numerical simulations of some classical antennas are presented and analyzed in terms of the physical limitations discussed in Sec. 3.

8.1 The dipole antenna

The cylindrical dipole antenna is one of the simplest and most well known antennas. Here, the MoM solution of the Hallén's integral equation in Ref. 10 together with a gap feed model is used to determine the cross sections and impedance for a cylindrical dipole antenna with axial ratio $b/a = 10^{-3}$. The extinction and absorption cross sections and the realized gain are depicted in Fig. 9. The antenna is resonant at $2a \approx 0.48\lambda$ with directivity $D = 1.64$ and radiation resistance $73\,\Omega$. The half-power bandwidth is $B = 25\%$ and the corresponding Q-factor is estimated to $Q = 8.3$ by numerical differentiation of the impedance, see Ref. 25. The absorption efficiency η is depicted in Fig. 10. It is observed that $\eta \approx 0.5$ at the resonance frequency and $\widetilde{\eta} = 0.52$ for $0 \leq 4a/\lambda \leq 3$.

The MoM solution is also used to determine the forward scattering properties of the antenna. The forward scattering is represented by the extinction volume ϱ in Fig. 10. Recall that $\varrho(0)$ and $\operatorname{Im}\varrho$ directly are related to the polarizability dyadics and the extinction cross section, see Sec. 3.

Moreover, since $\operatorname{Re}\varrho \approx 0$ at the resonance frequency, it follows that the real-valued part of the forward scattering is negligible at this frequency. This observation is important in the understanding of the absorption efficiency of antennas, see Ref. 2.

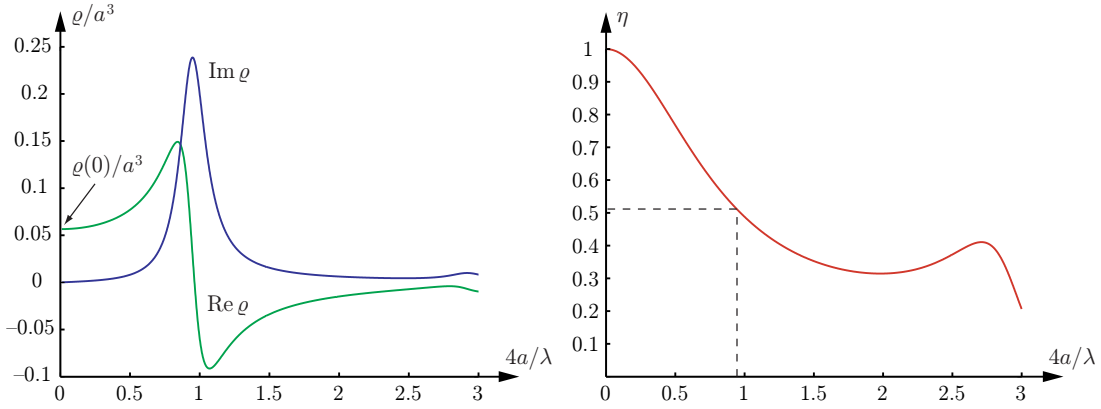

Figure 10: The extinction volume ϱ (left figure) and the absorption efficiency η (right figure) as function of $4a/\lambda$ for the dipole antenna.

FEM simulations are used to determine the polarizability dyadic and the eigenvalues of the cylindrical region in Fig. 9. The eigenvalue γ_1, corresponding to a polarization along the dipole, is $\gamma_1 = 0.71a^3$ and the other eigenvalues $\gamma_2 = \gamma_3$ are negligible. The result agrees with the integrated extinction (2.3) of the MoM solution within 2% for $0 \leq 4a/\lambda \leq 3$.

The eigenvalues $\gamma_1 = 0.71a^3$ and $\gamma_2 = 0$ inserted into (4.6) give physical limitations on the quotient D/Q of any resonant antenna confined to the cylindrical region, *i.e.*,

$$\sup_{\hat{\boldsymbol{p}}_\mathrm{e}\cdot\hat{\boldsymbol{p}}_\mathrm{m}=0} \frac{D}{Q} \leq \widetilde{\eta}\frac{k_0^3\gamma_1}{2\pi} \approx 0.39\widetilde{\eta}. \tag{8.1}$$

The corresponding bound on the Q-factor is $Q \geq 8.1$, if $D = 1.64$ and $\widetilde{\eta} = 0.52$ are used. In Fig. 9, it is observed that the single resonance model (dashed curves) with $Q = 8.5$ is a good approximation of the cross sections and realized gain. The corresponding half-power bandwidth is 24%. The eigenvalue γ_1 also gives a limitation on the product $G_\Lambda B$ in (3.6) as illustrated with the rectangular region in the right figure for an arbitrary minimum scattering antenna ($\widetilde{\eta} = 0.5$). The realized gain $G_\Lambda = 1.64$ gives the relative bandwidth $B = 38\%$.

It is also illustrative to compare the physical limitations with the MoM simulation for a short dipole. The resonance frequency of the dipole is reduced to $2a \approx 0.2\lambda$ with an inductive loading of $5\,\mu$H connected in series with the dipole. The MoM impedance computations of the short dipole give the half-power bandwidth $B = 1.4\%$ and the radiation resistance $8\,\Omega$. The D/Q bound (4.6) gives $Q \geq 110$ for the directivity $D = 1.52$ and an absorption efficiency $\widetilde{\eta} = 1/2$ corresponding to the half-power bandwidth $B \leq 1.8\%$.

Obviously, the simple structure of the dipole and the absence of broadband matching networks make the resonance model favorable. The limitation (4.6) is in excellent agreement with the performance of the dipole antenna for the absorption efficiency $\widetilde{\eta} = 0.52$, *i.e.*, $Q \geq 8.1$ from (4.6) compared to $Q = 8.3$ from the MoM solution. The $G_\Lambda B$ bound overestimates the bandwidth, but a broadband matching network can be used to enhance the bandwidth of the dipole, see Ref. 5.

Observe that the dipole antenna has a circumscribing sphere with $ka \approx 1.5$ and is not considered electrically small according to the Chu limitations in Ref. 3. The corresponding limit for the $2a \approx 0.2\lambda_0$ dipole ($ka \approx 0.63$ and $D = 1.52$) is $Q \geq 5.6$ and the half-power bandwidth of $36\% \gg 1.4\%$. In conclusion, the dipole utilizes the cylindrical region very efficiently but obviously not the spherical region.

8.2 The loop antenna

The magnetic counterpart to the dipole antenna in Sec. 8.1 is the loop antenna. The geometry of the loop antenna is conveniently described in toroidal coordinates, see Sec. H. Laplace's equation separates in the toroidal coordinate system and hence permits an explicit calculation of the high-contrast polarizability dyadic $\boldsymbol{\gamma}_\infty$. In this section the attention is restricted to the loop antenna of vanishing thickness and non-magnetic material properties. Under the assumptions of vanishing thickness, the analysis in Sec. H yields closed-form expressions of the eigenvalues γ_1, γ_2 and γ_3. Recall that the loop antenna coincides with the magnetic dipole in the long wavelength limit $a/\lambda \ll 1$.

In order to quantify the vanishing thickness limit, introduce the semi-axis ratio $\xi = b/a$, where a and b denote the axial and cross section radii, respectively, see Fig. 11. The three eigenvalues $\gamma_1 = \gamma_2$ and γ_3 are seen to vanish in the limit $\xi \to 0$. However, γ_1 and γ_2 vanish slower than γ_3, see Sec. H. The eigenvalues in the limit $\xi \to 0$ inserted into (4.5) yields

$$\frac{D}{Q} \leq \pi k_0^3 a^3 \frac{f(\theta)}{\ln 2/\xi - 1} + \mathcal{O}(\xi^2) \quad \text{as } \xi \to 0, \tag{8.2}$$

where $f(\theta) = 1$ for the TE- and $f(\theta) = \cos^2\theta$ for the TM-polarization. Here, $\theta \in [0, \pi]$ is the polar angle measured from the z-axis of symmetry in Fig. 11. Note that the logarithmic singularity in (8.2) is the same as for the dipole antenna, see Sec. H. Since the axial radius a is the only length scale that is present in the loop antenna in the limit $\xi \to 0$, it is natural that γ_1, γ_2, and γ_3 are proportional to a^3, see Appendix B.

By comparing the discussion above with the results in Ref. 7 and Sec. 8.1, it is concluded that there is a strong equivalence between the electric and magnetic dipoles. For the most advantageous polarization the upper bound on $G_\Lambda B$ is a factor of $3\pi/2$ larger for the loop antenna compared to the electric dipole.

The results are exemplified for a self-resonant loop with $k_0 a = 1.1$ and a capacitively loaded loop, $C = 10\,\text{pF}$, with $k_0 a = 0.33$, both with $\xi = 0.01$. The corresponding limitations (4.6) are $D/Q \leq 0.95\bar{\eta}$ and $D/Q \leq 0.025\bar{\eta}$, respectively. The MoM is used to determine the impedance and realized gain of the loop antenna with a gap feed at $\phi = 0$, see Fig. 11. The Q-factor of the self-resonant antenna is estimated to $Q = 5$ from numerical differentiation of the impedance, see Ref. 25. The corresponding main beam is in the $\hat{\boldsymbol{z}}$-direction with a directivity $D = 2.36$ giving $D/Q = 0.47$. Similarly, the tuned loop has $Q \approx 164$ and $D = 1.43$ in $\theta = 90^\circ$ and $\phi = 90^\circ$ giving $D/Q \approx 0.0086$.

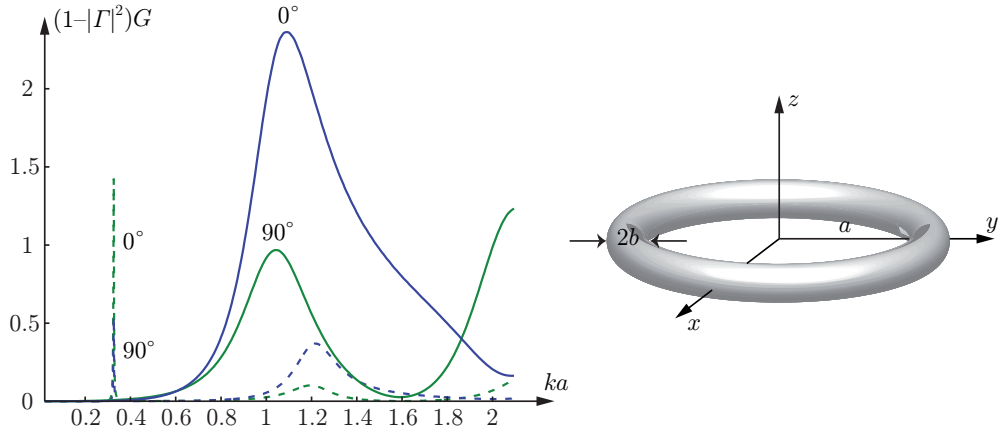

Figure 11: The realized partial gain of two loop antennas for $\theta = 0°, 90°$. One self resonant ($ka \approx 1$) and one capacitively tuned to $ka \approx 1/3$.

It is observed that the physical limitations (4.6) of the loops agree well with the MoM results. This difference can be reduced by introducing the appropriate absorption efficiency in the physical limitation. The corresponding results for the Chu limitation are $D/Q \leq 2.3$ for $k_0 a = 1.1$ and $D/Q \leq 0.18$ for $k_0 a = 0.33$, where the combined TE- and TM-case have been used as the loops are not omnidirectional, see Refs. 3 and 12.

8.3 Conical antennas

The bandwidth of a dipole antenna increases with the thickness of the antenna. The bandwidth can also be increased with conical dipoles, *i.e.*, the biconical antenna. The corresponding conical monopole and discone antennas are obtained by replacing one of the cones with a ground plane, see Ref. 21.

In Fig. 12, the eigenvalues $\gamma_x = \gamma_y$ and γ_z, corresponding to horizontal and vertical polarizations, respectively, are shown as a function of the ground plane radius, b, for the conical monopoles with angles $\theta = 10°$ and $30°$. The eigenvalues are normalized with a^3, where a is the height of the cone. It is observed that the eigenvalues increase with the radius, b, of the ground plane and the cone angle θ. This is a general result as the polarizability dyadic is non-decreasing with increasing susceptibilities, see Ref. 19.

The horizontal eigenvalues $\gamma_x = \gamma_y$ are dominated by the ground plane and increase approximately as b^3 according to the polarizability of the circular disk, see Appendix C. The vertical eigenvalue γ_z approaches $\gamma_{bz}/2$ as $b \to \infty$, where γ_{bz} denotes the vertical eigenvalue of the corresponding biconical antenna.

It is interesting to compare the D/Q estimate (4.6) for the biconical antenna and conical monopole antenna with a large but finite ground plane. The vertical eigenvalue γ_z of the conical monopole antenna is approximately half of the corresponding eigenvalue of the biconiocal antenna and the Q-factors of the two antennas are similar. The physical limitation on the directivity in the $\theta = 90°$ direction of

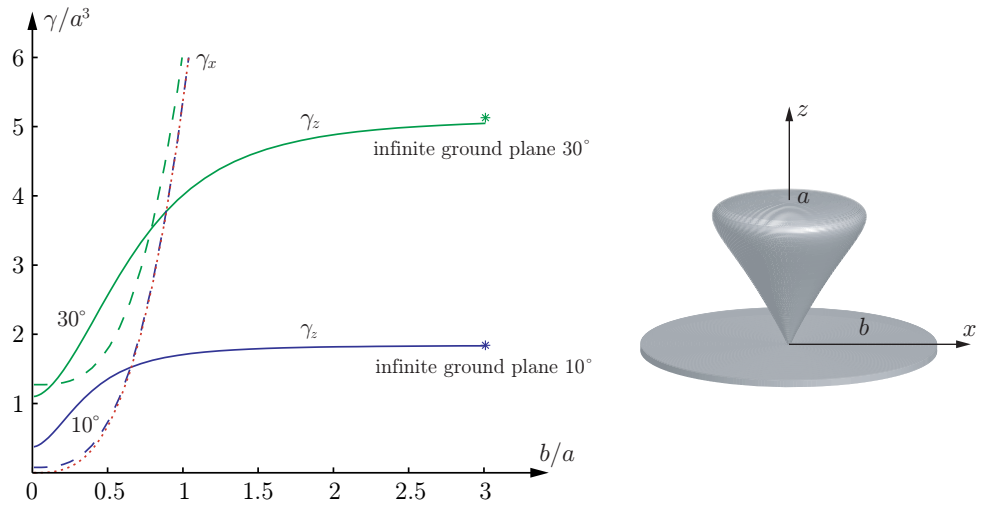

Figure 12: The vertical and horizontal eigenvalues γ_z and γ_x as function of the radius b for a biconical antenna of half vertex angle 10° and 30°, respectively.

the conical monopole is hence half of the directivity of the corresponding biconical antenna. This might appear contradictory as it is well known that the maximal directivity of a monopole is approximately twice the directivity of the corresponding dipole. However, the $\theta = 90°$ direction is on the border between the illuminated and the shadow regions. The integral representation of the far field shows that the induced ground-plane currents do not contribute to the far field in this direction, implying that the directivity is reduced a factor of four as suggested by the physical limitations, see Appendix D.

The rapid increase in $\gamma_x = \gamma_y$ with the radius of the ground plane suggests that it is advantageous to utilize the polarization in the theses directions. This is done by the discone antenna that has an omnidirectional pattern with a maximal directivity above $\theta = 90°$.

9 Conclusion and future work

In this paper, physical limitations on reciprocal antennas of arbitrary shape are derived based on the holomorphic properties of the forward scattering dyadic. The results are very general in the sense that the underlying analysis solely depends on energy conservation and the fundamental principles of linearity, time-translational invariance, and causality. Several deficiencies and drawbacks of the classical limitations of Chu and Wheeler in Refs. 3 and 24 are overcomed with this new formulation. The main advantages of the new limitations are at least fivefold: 1) they hold for arbitrary antenna geometries; 2) they are formulated in the gain and bandwidth as well as the directivity and the Q-factor; 3) they permit study of polarization effects such as diversity in applications for MIMO communication systems; 4) they successfully separate electric and magnetic antenna properties in terms of the intrinsic material parameters; 5) they are isoperimetric from a practical point of view

in the sense that for some geometries, physical antennas can be realized which yield equality in the limitations.

The main results of the present theory are the limitations on the partial realized gain and partial directivity in (3.4) and (4.5), respectively. Since the upper bounds in (3.4) and (4.5) are proportional to $k_0^3 a^3$, where a denotes the radius of, say, the volume equivalent sphere, it is clear that no broadband electrically small antennas exist unless gain or directivity is sacrificed for bandwidth or Q-factor. This is also the main conclusion in Ref. 12, but there presented on more vague grounds. Furthermore, the present theory suggests that, in addition to electric material properties, also magnetic materials could be invoked in the antenna design to increase the performance, *cf.*, the ferrite loaded loop antenna in Ref. 4.

In contrast to the classical results by Chu and Wheeler in Refs. 3 and 24, these new limitations are believed to be isoperimetric in the sense that the bounds hold for some physical antenna. A striking example of the intrinsic accuracy of the theory is illustrated by the dipole antenna in Sec. 8.1. In fact, many wire antennas are believed to be close to the upper bounds since these antennas make effective use of their volumes.

It is important to remember that a priori knowledge of the absorption efficiency $\eta = \sigma_{\mathrm{a}}/\sigma_{\mathrm{ext}}$ can sharpen the bounds in (3.4) and (4.5), *cf.*, the half-wave dipole antenna in Sec. 8.1 for which $\widetilde{\eta} \approx 1/2$ is used. Similarly, a priori knowledge of the radiation efficiency, η_{r}, can be used to improve the estimate in (3.2) using $G = \eta_{\mathrm{r}} D$.

The performance of an arbitrary antenna can be compared with the upper bounds in Secs. 3 and 4 using either the method of moments (MoM) or the finite difference time domain method (FDTD). For such a comparison, it is beneficial to determine the integrated extinction and compare the result using (2.3) rather than (3.4) and (4.5). The reason for this is that the full absorption and scattering properties are contained within (2.3) in contrast to (3.4) and (4.5). In fact, (2.3) is the fundamental physical relation and should be the starting point of much analysis.

In addition to the broadband absorption efficiency $\widetilde{\eta}$, several implications of the present theory remains to investigate. Future work include the effect of non-simple connected geometries (array antennas) and its relation to capacitive coupling, and additional analysis of classical antennas. From a wireless communication point of view it is also interesting to investigate the connection between the present theory and the concept of correlation and capacity in MIMO communication systems. Some of the problems mentioned here will be addressed in forthcoming papers.

Acknowledgment

The financial support by the Swedish Research Council and the SSF Center for High Speed Wireless Communication are gratefully acknowledged. The authors are also grateful for fruitful discussions with Anders Karlsson and Anders Derneryd at Dept. of Electrical and Information Technology, Lund University, Sweden.

Appendix A Details on the derivation of (2.3)

Consider a plane-wave excitation $\boldsymbol{E}_{\mathrm{i}}(\mathrm{c}_0 t - \hat{\boldsymbol{k}} \cdot \boldsymbol{x})$ incident in the $\hat{\boldsymbol{k}}$-direction, see Fig. 1. In the far field region, the scattered electric field $\boldsymbol{E}_{\mathrm{s}}$ is described by the far field amplitude $\boldsymbol{F}$ as

$$\boldsymbol{E}_{\mathrm{s}}(t, \boldsymbol{x}) = \frac{\boldsymbol{F}(\mathrm{c}_0 t - x, \hat{\boldsymbol{x}})}{x} + \mathcal{O}(x^{-2}) \quad \text{as } x \to \infty, \tag{A.1}$$

where c_0 denotes the speed of light in vacuum, and $\hat{\boldsymbol{x}} = \boldsymbol{x}/x$ with $x = |\boldsymbol{x}|$. The far field amplitude $\boldsymbol{F}$ in the forward direction $\hat{\boldsymbol{k}}$ is assumed to be causal and related to the incident field $\boldsymbol{E}_{\mathrm{i}}$ via the linear and time-translational invariant convolution

$$\boldsymbol{F}(\tau, \hat{\boldsymbol{k}}) = \int_{-\infty}^{\tau} \mathbf{S}_{\mathrm{t}}(\tau - \tau', \hat{\boldsymbol{k}}, \hat{\boldsymbol{k}}) \cdot \boldsymbol{E}_{\mathrm{i}}(\tau') \, \mathrm{d}\tau'.$$

Here, $\tau = \mathrm{c}_0 t - x$ and $\mathbf{S}_{\mathrm{t}}$ is the appropriate dimensionless temporal dyadic.

Introduce the forward scattering dyadic $\mathbf{S}$ as the Fourier transform of $\mathbf{S}_{\mathrm{t}}$ evaluated in the forward direction, *i.e.*,

$$\mathbf{S}(k, \hat{\boldsymbol{k}}) = \int_{0^-}^{\infty} \mathbf{S}_{\mathrm{t}}(\tau, \hat{\boldsymbol{k}}, \hat{\boldsymbol{k}}) \mathrm{e}^{\mathrm{i}k\tau} \, \mathrm{d}\tau, \tag{A.2}$$

where k is complex-valued with $\operatorname{Re} k = \omega/\mathrm{c}_0$. Recall that $\mathbf{S}(\mathrm{i}k, \hat{\boldsymbol{k}})$ is real-valued for real-valued k and that the crossing symmetry $\mathbf{S}(k, \hat{\boldsymbol{k}}) = \mathbf{S}^*(-k^*, \hat{\boldsymbol{k}})$ holds for complex-valued k. For a large class of temporal dyadics $\mathbf{S}_{\mathrm{t}}$, the elements of $\mathbf{S}$ are holomorphic in the upper half plane $\operatorname{Im} k > 0$.

From the analysis above, it follows that the Fourier transform of (A.1) in the forward direction reads

$$\boldsymbol{E}_{\mathrm{s}}(k, x\hat{\boldsymbol{k}}) = \frac{\mathrm{e}^{\mathrm{i}kx}}{x} \mathbf{S}(k, \hat{\boldsymbol{k}}) \cdot \boldsymbol{E}_0 + \mathcal{O}(x^{-2}) \quad \text{as } x \to \infty,$$

where $\boldsymbol{E}_0$ is the Fourier amplitude of the incident field. Introduce the extinction volume $\varrho(k) = \hat{\boldsymbol{p}}_{\mathrm{e}}^* \cdot \mathbf{S}(k, \hat{\boldsymbol{k}}) \cdot \hat{\boldsymbol{p}}_{\mathrm{e}}/k^2$, where $\hat{\boldsymbol{p}}_{\mathrm{e}} = \boldsymbol{E}_0/|\boldsymbol{E}_0|$ and $\hat{\boldsymbol{p}}_{\mathrm{m}} = \hat{\boldsymbol{k}} \times \hat{\boldsymbol{p}}_{\mathrm{e}}$ denote the electric and magnetic polarizations, respectively. Since the elements of $\mathbf{S}$ are holomorphic in k for $\operatorname{Im} k > 0$, it follows that also the extinction volume ϱ is a holomorphic function in the upper half plane. The Cauchy integral theorem with respect to the contour in Fig. 13 then yields

$$\varrho(\mathrm{i}\varepsilon) = \int_0^{\pi} \frac{\varrho(\mathrm{i}\varepsilon - \varepsilon \mathrm{e}^{\mathrm{i}\phi})}{2\pi} \, \mathrm{d}\phi + \int_0^{\pi} \frac{\varrho(\mathrm{i}\varepsilon + R\mathrm{e}^{\mathrm{i}\phi})}{2\pi} \, \mathrm{d}\phi + \int_{\varepsilon<|k|<R} \frac{\varrho(k + \mathrm{i}\varepsilon)}{2\pi \mathrm{i} k} \, \mathrm{d}k. \tag{A.3}$$

Here, it is assumed that the extinction volume ϱ is sufficiently regular to extend the contour to the real-axis in the last integral on the right hand side of (A.3). Relation (A.3) is subject to the limits as $\varepsilon \to 0$ and $R \to \infty$.

The left hand side of (A.3) and the integrand in the first integral on the right hand side are well-defined in the limit as $\varepsilon \to 0$. For a sufficiently regular ϱ in the vicinity of the origin, the analysis in Ref. 14 yield

$$\varrho(\mathrm{i}\varepsilon) = \frac{1}{4\pi} (\hat{\boldsymbol{p}}_{\mathrm{e}}^* \cdot \boldsymbol{\gamma}_{\mathrm{e}} \cdot \hat{\boldsymbol{p}}_{\mathrm{e}} + \hat{\boldsymbol{p}}_{\mathrm{m}}^* \cdot \boldsymbol{\gamma}_{\mathrm{m}} \cdot \hat{\boldsymbol{p}}_{\mathrm{m}}) + \mathcal{O}(\varepsilon) \quad \text{as } \varepsilon \to 0. \tag{A.4}$$

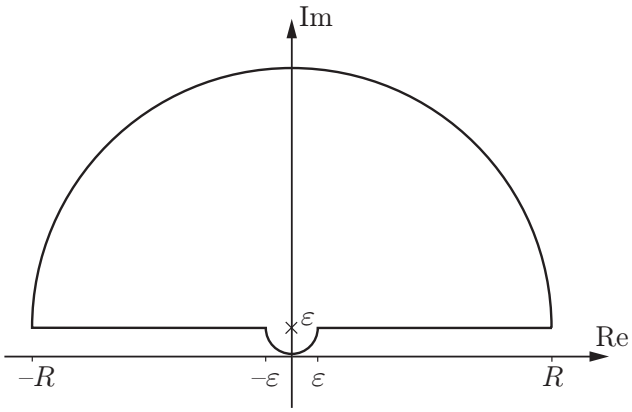

Figure 13: Integration contour in the complex k-plane used in (A.3).

Here, $\boldsymbol{\gamma}_{\mathrm{e}}$ and $\boldsymbol{\gamma}_{\mathrm{m}}$ denote the electric and magnetic polarizability dyadics in Appendix B. Since the short wavelength response of a material is non-unique from a modeling point of view, see Ref. 8, the second term on the right hand side of (A.3) is assumed to approach zero in the limit $R \to \infty$. In fact, for a large class of temporal dyadics $\mathbf{S}_{\mathrm{t}}$, the integrand $\varrho(\mathrm{i}\varepsilon + R\mathrm{e}^{\mathrm{i}\phi})/2\pi$ is proportional to the projected area A in the forward direction, *viz.*,

$$\varrho(k) = -\frac{A(\hat{\boldsymbol{k}})}{2\pi \mathrm{i}k} + \mathcal{O}(|k|^{-2}) \quad \text{as } |k| \to \infty, \qquad \operatorname{Im} k \geq 0. \tag{A.5}$$

The asymptotic behavior (A.5) is known as the extinction paradox, see Ref. 23. The constant A is real-valued since $\mathbf{S}(\mathrm{i}k, \hat{\boldsymbol{k}})$ is real-valued for real-valued k.

In order to proceed, the scattering, absorption and extinction cross sections are introduced. The scattering cross section σ_{s} and absorption cross section σ_{a} are defined as the ratio of the scattered and absorbed power, respectively, to the incident power flow density in the forward direction. The sum of the scattering and absorption cross sections is the extinction cross section $\sigma_{\mathrm{ext}} = \sigma_{\mathrm{s}} + \sigma_{\mathrm{a}}$. The three cross sections σ_{s}, σ_{a} and σ_{ext} are by definition real-valued and non-negative. The principle of energy conservation takes the form as a relation between the extinction volume ϱ and the extinction cross section. The relation is known as the optical theorem, see Refs. 16 and 22,

$$\sigma_{\mathrm{ext}}(k) = 4\pi k \operatorname{Im} \varrho(k), \tag{A.6}$$

where k is real-valued.

In summary, the real part of (A.3) subject to the limits $\varepsilon \to 0$ and $R \to \infty$ yields

$$\varrho(0) = \frac{1}{\pi} \int_{-\infty}^{\infty} \frac{\operatorname{Im} \varrho(k)}{k} \, \mathrm{d}k. \tag{A.7}$$

The optical theorem (A.6) applied to (A.7) then implies

$$\varrho(0) = \frac{1}{4\pi^2} \int_{-\infty}^{\infty} \frac{\sigma_{\mathrm{ext}}(k)}{k^2} \, \mathrm{d}k = \frac{1}{4\pi^3} \int_{0}^{\infty} \sigma_{\mathrm{ext}}(\lambda) \, \mathrm{d}\lambda, \tag{A.8}$$

where the wavelength $\lambda = 2\pi/k$ has been introduced. Hence, invoking (A.4) finally yields the integrated extinction

$$\int_0^\infty \sigma_{\text{ext}}(\lambda)\ \mathrm{d}\lambda = \pi^2 \left(\hat{\boldsymbol{p}}_{\text{e}}^* \cdot \boldsymbol{\gamma}_{\text{e}} \cdot \hat{\boldsymbol{p}}_{\text{e}} + \hat{\boldsymbol{p}}_{\text{m}}^* \cdot \boldsymbol{\gamma}_{\text{m}} \cdot \hat{\boldsymbol{p}}_{\text{m}}\right). \tag{A.9}$$

In fact, the already weak assumptions on the extinction volume ϱ in the analysis above can be relaxed via the introduction of certain classes of distributions, see Ref. 17.

Appendix B The polarizability dyadics

Let $\boldsymbol{\tau}$ denote a finite material dyadic ($\boldsymbol{\chi}_{\text{e}}$ without a conductivity term, or $\boldsymbol{\chi}_{\text{m}}$) with compact support. The entries of the polarizability dyadic $\boldsymbol{\gamma}$ ($\boldsymbol{\gamma}_{\text{e}}$ or $\boldsymbol{\gamma}_{\text{m}}$ depending on whether the problem is electric or magnetic) are defined as the volume integral

$$\hat{\boldsymbol{e}}_i \cdot \boldsymbol{\gamma} \cdot \hat{\boldsymbol{e}}_j = \frac{1}{E_0} \hat{\boldsymbol{e}}_i \cdot \int_{\mathbb{R}^3} \boldsymbol{\tau}(\boldsymbol{x}) \cdot \boldsymbol{E}_j(\boldsymbol{x})\ \mathrm{dV}_{\boldsymbol{x}}, \qquad i,j = 1,2,3. \tag{B.1}$$

Here, the total field $\boldsymbol{E}$ has been decomposed as $\boldsymbol{E}_j = E_0 \hat{\boldsymbol{e}}_j + \boldsymbol{E}_{\text{s}j}$ with respect to the mutually orthonormal vectors $\hat{\boldsymbol{e}}_j$. In the electric and magnetic cases, $\boldsymbol{E}$ represents the electric and magnetic field, respectively.

In the high-contrast limit, when the entries of $\boldsymbol{\tau}$ simultaneously approach infinity uniformly in $\boldsymbol{x}$, the pertinent definition of the high-contrast polarizability dyadic $\boldsymbol{\gamma}_\infty$ is, see Ref. 14,

$$\hat{\boldsymbol{e}}_i \cdot \boldsymbol{\gamma}_\infty \cdot \hat{\boldsymbol{e}}_j = \frac{1}{E_0} \hat{\boldsymbol{e}}_i \cdot \sum_{n=1}^{N} \int_{\mathrm{S}_n} \left(\hat{\boldsymbol{\nu}}(\boldsymbol{x}) \Phi_j(\boldsymbol{x}) - \boldsymbol{x} \hat{\boldsymbol{\nu}}(\boldsymbol{x}) \cdot \nabla \Phi_j(\boldsymbol{x})\right)\ \mathrm{dS}_{\boldsymbol{x}}. \tag{B.2}$$

The surface integral representation (B.2) holds for N disjunct bounding surfaces S_n with outward-directed unit normal vectors $\hat{\boldsymbol{\nu}}$. The potential $\Psi_j(\boldsymbol{x}) = \Phi_j(\boldsymbol{x}) - E_0 x_j$ is for each $n = 1, 2, \ldots, N$ the solution to the boundary value problem

$$\begin{cases} \nabla^2 \Psi_j(\boldsymbol{x}) = 0, \quad \boldsymbol{x} \text{ outside } \mathrm{S}_n \\ \displaystyle\int_{\mathrm{S}_n} \hat{\boldsymbol{\nu}}(\boldsymbol{x}) \cdot \nabla \Psi_j(\boldsymbol{x}) \mid_+ \ \mathrm{dS}_{\boldsymbol{x}} = 0 \\ \Psi_j(\boldsymbol{x}) \to -E_0 x_j + \mathcal{O}(|\boldsymbol{x}|^{-2}) \quad \text{as } |\boldsymbol{x}| \to \infty \end{cases}$$

The presence of a finite or infinite conductivity term in $\boldsymbol{\chi}_{\text{e}}$ is discussed in Ref. 14. The conclusion is that the electric polarizability dyadic $\boldsymbol{\gamma}_{\text{e}}$ should be replaced by $\boldsymbol{\gamma}_\infty$ independently of the real-part of $\boldsymbol{\chi}_{\text{e}}$ when a conductivity term is present. This may at first seem contradictory, since there is no continuity in the limit as the conductivity vanishes.

In Ref. 19, the polarizability dyadic $\boldsymbol{\gamma}$ is proved to be symmetric provided $\boldsymbol{\tau}$ is symmetric at all points $\boldsymbol{x}$. The dyadic $\boldsymbol{\gamma}$ is real-valued, and hence diagonalizable with real-valued eigenvalues. The corresponding set of orthogonal eigenvectors are

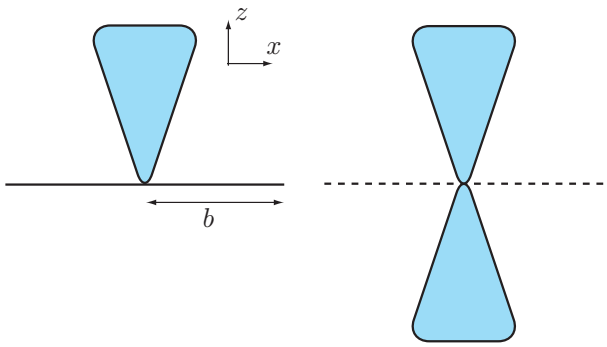

Figure 14: Illustration of an arbitrary antenna volume supported by a ground plane (left figure) and its corresponding mirror object (right figure).

the principal axes of the obstacle under consideration. The principal axes are particularly easy to determine for obstacles with continuous or discrete symmetries, *e.g.*, the ellipsoids and the Platonic solids in Sec. 7.1.

An important property of $\boldsymbol{\gamma}$ which is proved in Ref. 19, is that it is proportional to the volume of the support of $\boldsymbol{\tau}$. This is a direct consequence of the absence of any length scales in the long wavelength limit.

Appendix C Supporting ground planes

Supporting ground planes are central structures in many antenna applications. Consider an arbitrary volume, modeling the antenna, situated above a supporting ground plane of finite or infinite extent, see Fig. 14. To simplify the terminology, use monopole to denote object with a ground plane and dipole to denote the object together with its mirror object. The ground plane is assumed to be a circular disk of radius b with vanishing thickness. Since $\boldsymbol{\gamma}_\infty$ is independent of any coordinate representation, let the ground plane be given by $z = 0$.

For a polarization parallel with the ground plane, *i.e.*, spanned by $\hat{\boldsymbol{e}}_x$ and $\hat{\boldsymbol{e}}_y$, it is clear from the results in Appendix B of the circular disk that the contribution to $\boldsymbol{\gamma}_\infty$ from the ground plane is large. Indeed, a circular ground plane of radius b yields $\gamma_{\mathrm{x}} = \gamma_{\mathrm{y}} = 16b^3/3$, where γ_{x} and γ_{y} denote the eigenvalues of $\boldsymbol{\gamma}_\infty$ corresponding to the $\hat{\boldsymbol{e}}_x$ and $\hat{\boldsymbol{e}}_y$ directions, respectively (G.4).

The polarizability of the monopole for an electric polarization parallel with the $\hat{\boldsymbol{e}}_z$-direction has one contribution from the charge distribution on the object $z > 0$ and one part from the charge distribution on the ground plane $z = 0$. The contribution from the ground plane vanishes in (B.2) since $z = 0$. For a ground plane of infinite extent the method of images is applicable to determine the charge distribution for $z > 0$. In this method, the ground plane is replaced with a copy of the object placed in the mirror position of the object, *i.e.*, the dipole. The charge distribution is odd in z and the charge distribution for $z > 0$ is identical in the monopole and dipole cases. The polarizability of the dipole is hence exactly twice the polarizability of the corresponding monopole.

The difference between the finite and infinite ground planes is negligible as long as the charge distribution on the monopole can be approximated by the charge distribution in the corresponding dipole case.

Appendix D Directivity along ground planes

The integral representation of the far-field can be used to analyze the directivity of antennas in directions along the supporting ground plane. The pertinent integral representation reads

$$\boldsymbol{F}(\hat{\boldsymbol{r}}) = \frac{\mathrm{i}kZ_0}{4\pi} \int_S \hat{\boldsymbol{r}} \times (\boldsymbol{J}(\boldsymbol{x}) \times \hat{\boldsymbol{r}}) \mathrm{e}^{-\mathrm{i}k\hat{\boldsymbol{r}}\cdot\boldsymbol{x}} \, \mathrm{dS}_{\boldsymbol{x}}, \tag{D.1}$$

where $\boldsymbol{J}$ and Z_0 denote the induced current and the free space impedance, respectively.

Consider a monopole, *i.e.*, an object on a large but finite ground plane, at $z = 0$ with $\hat{\boldsymbol{e}}_z$ as a symmetry axis, see Fig. 14. The far-field of the monopole (D.1) can be written as a sum of one integral over the ground plane and one integral over the object. Let S_+ and S_0 denote the corresponding surfaces of the object and the ground plane, respectively. Assume that the ground plane is sufficiently large such that the currents on the monopole can be approximated with the currents on the corresponding dipole case for $z > 0$. Moreover, assume that the current is rotationally symmetric and that the current in the ϕ-direction is negligible giving an omni-directional radiation pattern. Hence, it is sufficient to consider the far-field pattern in the $\hat{\boldsymbol{r}} = \hat{\boldsymbol{e}}_x$-direction.

The induced currents on the ground plane are in the radial direction giving the term $\hat{\boldsymbol{e}}_x \times (\boldsymbol{J}(\boldsymbol{x}) \times \hat{\boldsymbol{e}}_x) = \hat{\boldsymbol{e}}_y J_\rho(\rho) \sin\phi$ in (D.1). It is seen that the currents on the ground plane does not contribute to the far field as

$$\boldsymbol{F}(\hat{\boldsymbol{e}}_x) = \hat{\boldsymbol{e}}_y \frac{\mathrm{i}k\eta}{4\pi} \int_{S_0} \mathrm{e}^{-\mathrm{i}k\rho\cos\phi} J_\rho(\rho) \sin\phi\rho \, \mathrm{d}\phi \, \mathrm{d}\rho = \boldsymbol{0}. \tag{D.2}$$

The contribution from the currents on the object can be analyzed with the method of images. From (D.2), it is seen the it is only the currents in the $\hat{\boldsymbol{e}}_z$-direction that contributes to the far field, *i.e.*,

$$\boldsymbol{F}(\hat{\boldsymbol{e}}_x) = \hat{\boldsymbol{e}}_z \frac{\mathrm{i}k\eta}{4\pi} \int_{S_+} \mathrm{e}^{-\mathrm{i}k\rho\cos\phi} J_z(\rho, z) \, \mathrm{dS}, \tag{D.3}$$

where $J_z\hat{\boldsymbol{e}}_z = \hat{\boldsymbol{e}}_x \times (\boldsymbol{J} \times \hat{\boldsymbol{e}}_x)$. The method of images shows that J_z is even in z so the z-directed currents above and below the ground plane give equal contributions to the far field. The directivity of the monopole antenna is hence a quarter of the directivity of the corresponding dipole antenna in the $\hat{\boldsymbol{e}}_x$-direction.

Appendix E Definition of some antenna terms

The following definitions of antenna terms are based on the IEEE standard 145-1993 in Ref. 13. The definitions refer to the electric polarization $\hat{\boldsymbol{p}}_{\mathrm{e}}$ (co-polarization)

rather than the magnetic polarization $\hat{\boldsymbol{p}}_{\mathrm{m}} = \hat{\boldsymbol{k}} \times \hat{\boldsymbol{p}}_{\mathrm{e}}$ (cross-polarization). The antennas are assumed to reciprocal, *i.e.*, they have similar properties as transmitting and receiving devices.

Absolute gain $G(\hat{\boldsymbol{k}})$. The absolute gain is the ratio of the radiation intensity in a given direction to the intensity that would be obtained if the power accepted by the antenna was radiated isotropically.

Partial gain $G(\hat{\boldsymbol{k}}, \hat{\boldsymbol{p}}_{\mathrm{e}})$. The partial gain in a given direction is the ratio of the part of the radiation intensity corresponding to a given polarization to the radiation intensity that would be obtained if the power accepted by the antenna was radiated isotropically. The absolute gain is equal to the sum of the partial gains for two orthogonal polarizations, *i.e.*, $G(\hat{\boldsymbol{k}}) = G(\hat{\boldsymbol{k}}, \hat{\boldsymbol{p}}_{\mathrm{e}}) + G(\hat{\boldsymbol{k}}, \hat{\boldsymbol{p}}_{\mathrm{m}})$.

Realized gain $G(\hat{\boldsymbol{k}}, \Gamma)$. The realized gain is the absolute gain of an antenna reduced by the losses due to impedance mismatch of the antenna, *i.e.*, $G(\hat{\boldsymbol{k}}, \Gamma) = (1 - |\Gamma|^2) G(\hat{\boldsymbol{k}})$.

Partial realized gain $G(\hat{\boldsymbol{k}}, \hat{\boldsymbol{p}}_{\mathrm{e}}, \Gamma)$. The partial realized gain is the partial gain for a given polarization reduced by the losses due to impedance mismatch of the antenna, *i.e.*, $G(\hat{\boldsymbol{k}}, \hat{\boldsymbol{p}}_{\mathrm{e}}, \Gamma) = (1 - |\Gamma|^2) G(\hat{\boldsymbol{k}}, \hat{\boldsymbol{p}}_{\mathrm{e}})$.

Absolute directivity $D(\hat{\boldsymbol{k}})$. The absolute directivity is the ratio of the radiation intensity in a given direction to the radiation intensity averaged over all directions. The averaged radiation intensity is equal to the total power radiated divided by 4π.

Partial directivity $D(\hat{\boldsymbol{k}}, \hat{\boldsymbol{p}}_{\mathrm{e}})$. The partial directivity in a given direction is the ratio of that part of the radiation intensity corresponding to a given polarization to the radiation intensity averaged over all directions. The averaged radiation intensity is equal to the total power radiated divided by 4π.

Absorption cross section $\sigma_{\mathrm{a}}(\hat{\boldsymbol{k}}, \hat{\boldsymbol{p}}_{\mathrm{e}}, \Gamma)$. The absorption cross section for a given polarization and incident direction is the ratio of the absorbed power in the antenna to the incident power flow density when subject to a plane-wave excitation. For a perfectly matched antenna, the absorption cross section coincides with the partial effective area.

Scattering cross section $\sigma_{\mathrm{s}}(\hat{\boldsymbol{k}}, \hat{\boldsymbol{p}}_{\mathrm{e}}, \Gamma)$. The scattering cross section for a given polarization and incident direction is the ratio of the scattered power by the antenna to the incident power flow density when subject to a plane-wave excitation.

Extinction cross section $\sigma_{\mathrm{ext}}(\hat{\boldsymbol{k}}, \hat{\boldsymbol{p}}_{\mathrm{e}}, \Gamma)$. The extinction cross section for a given polarization and incident direction is the sum of the absorbed and scattered power of the antenna to the incident power flow density when subject to a plane-wave excitation, *i.e.*, $\sigma_{\mathrm{ext}}(\hat{\boldsymbol{k}}, \hat{\boldsymbol{p}}_{\mathrm{e}}, \Gamma) = \sigma_{\mathrm{a}}(\hat{\boldsymbol{k}}, \hat{\boldsymbol{p}}_{\mathrm{e}}, \Gamma) + \sigma_{\mathrm{s}}(\hat{\boldsymbol{k}}, \hat{\boldsymbol{p}}_{\mathrm{e}}, \Gamma)$.

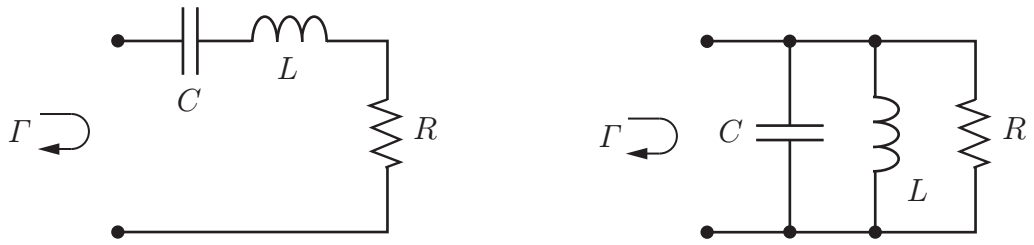

Figure 15: The RCL circuits corresponding to the plus (left figure) and minus (right figure) signs in (F.1).

Absorption efficiency[5] $\eta(\hat{\boldsymbol{k}}, \hat{\boldsymbol{p}}, \Gamma)$**.** The absorption efficiency of an antenna for a given polarization and incident direction is the ratio of the absorbed power to the total absorbed and scattered power when subject to a plane-wave excitation, *i.e.*, $\eta(\hat{\boldsymbol{k}}, \hat{\boldsymbol{p}}_\mathrm{e}, \Gamma) = \sigma_\mathrm{a}(\hat{\boldsymbol{k}}, \hat{\boldsymbol{p}}_\mathrm{e}, \Gamma)/\sigma_\mathrm{ext}(\hat{\boldsymbol{k}}, \hat{\boldsymbol{p}}_\mathrm{e}, \Gamma)$.

Quality factor Q**.** The quality factor of a resonant antenna is the ratio of 2π times the energy stored in the fields excited by the antenna to the energy radiated and dissipated per cycle. For electrically small antennas, it is equal to one-half the magnitude of the ratio of the incremental change in impedance to the corresponding incremental change in frequency at resonance, divided by the ratio of the antenna resistance to the resonant frequency.

Appendix F Q-factor and bandwidth

The quality factor, or Q-factor, is often used to estimate the bandwidth of an antenna. It is defined as the ratio of the energy stored in the reactive field to the radiated energy, *i.e.*, $Q = 2\omega \max(W_\mathrm{m}, W_\mathrm{e})/P$, see Appendix E and Refs. 6 and 25. Here, W_e and W_m denote the stored electric and magnetic energies, respectively, P is the dissipated power, and $\omega = kc_0$ the angular frequency. At the resonance, $k = k_0$, there are equal amounts of stored electric and magnetic energy, *i.e.*, $W_\mathrm{e} = W_\mathrm{m}$.

For many applications it is sufficient to model the antenna as a simple RCL resonance circuit around the resonance frequency. The reflection coefficient Γ of the antenna is then given by

$$\Gamma = \frac{Z(k) - R}{Z(k) + R} = \pm \frac{1 - (k/k_0)^2}{1 - (k/k_0)^2 - 2\mathrm{i}k/(k_0 Q)} \tag{F.1}$$

where Z denotes the frequency dependent part of the impedance, and the plus and minus signs in (F.1) correspond to the series and parallel circuits in Fig. 15, respectively. The reflection coefficient Γ is holomorphic in the upper half plane $\mathrm{Im}\,\omega > 0$ and characterized by the poles

$$k = \pm k_0 \sqrt{1 - Q^{-2}} - \mathrm{i}k_0/Q, \tag{F.2}$$

[5]This term is not defined in Ref. 13; the present definition is instead based on Ref. 2.

which are symmetrically distributed with respect to the imaginary axis.

The bandwidth of the resonances in (F.2) depends on the threshold level of the reflection coefficient. The relative bandwidths of half-power, $|\Gamma|^2 \leq 0.5$, is given by $B \approx 2/Q$. The corresponding losses due to the antenna mismatch are calculated from

$$1 - |\Gamma|^2 = \frac{1}{1 + Q^2(k/k_0 - k_0/k)^2/4}. \tag{F.3}$$

The definition of the Q-factor in terms of the quotient between stored and radiated energies is however not adequate for the present analysis. This is because the decomposition of the total energy into the stored and dissipated parts is a fundamentally difficult task. As noted in Refs. 6 and 25, the Q-factor at the resonance frequency $k = k_0$ can instead be determined by differentiating the reflection coefficient or impedance, *i.e.*,

$$\left|\frac{\partial \Gamma}{\partial k}\right| = \frac{1}{2R}\left|\frac{\partial Z}{\partial k}\right| = \frac{Q}{k_0}, \tag{F.4}$$

where the derivatives in (F.4) are evaluated at $k = k_0$. Relation (F.4) is exact for the single resonance circuit and is also a good approximation for multiple resonance models if Q is sufficiently large. In Sec. (4), a multiple resonance model is considered for the extinction volume ϱ introduced in Appendix A. The multiple resonance model is obtained by superposition of single resonance terms with poles of the type (F.2).

Appendix G The depolarizing factors

For the ellipsoids of revolution, *i.e.*, the prolate and oblate spheroids, closed-form expressions of (6.2) exist in terms of the semi-axis ratio $\xi \in [0, 1]$. The result for the prolate spheroid is ($a_2 = a_3$)

$$\begin{cases} L_1(\xi) = \dfrac{\xi^2}{2(1-\xi^2)^{3/2}}\left(\ln\dfrac{1+\sqrt{1-\xi^2}}{1-\sqrt{1-\xi^2}} - 2\sqrt{1-\xi^2}\right) \\ L_2(\xi) = L_3(\xi) = \dfrac{1}{4(1-\xi^2)^{3/2}}\left(2\sqrt{1-\xi^2} - \xi^2 \ln\dfrac{1+\sqrt{1-\xi^2}}{1-\sqrt{1-\xi^2}}\right) \end{cases} \tag{G.1}$$

while for the oblate spheroid ($a_1 = a_2$)

$$\begin{cases} L_1(\xi) = L_2(\xi) = \dfrac{\xi^2}{2(1-\xi^2)}\left(-1 + \dfrac{\arcsin\sqrt{1-\xi^2}}{\xi\sqrt{1-\xi^2}}\right) \\ L_3(\xi) = \dfrac{1}{1-\xi^2}\left(1 - \dfrac{\xi \arcsin\sqrt{1-\xi^2}}{\sqrt{1-\xi^2}}\right) \end{cases} \tag{G.2}$$

The depolarizing factors (G.1) and (G.2) are depicted in Fig. 16. Note that (G.1) and (G.2) differ in indices from the depolarizing factors in Ref. 19 due to the order relation $L_1 \leq L_2 \leq L_3$ assumed in Sec. 6 in this paper.

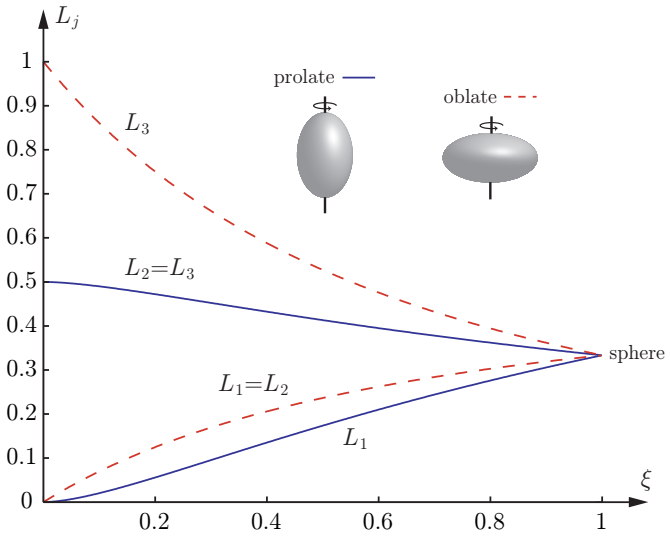

Figure 16: The depolarizing factors for the prolate (solid) and oblate (dashed) spheroids as function of the semi-axis ratio ξ. Note the degeneracy for the sphere.

Introduce the eigenvalues $\gamma_j(\xi) = V(\xi)/L_j(\xi)$ of the high-contrast polarizability dyadic. In terms of the radius a of the smallest circumscribing sphere, the spheroidal volume $V(\xi)$ is given by $\xi^2 4\pi a^3/3$ and $\xi 4\pi a^3/3$ for the prolate and oblate spheroids, respectively. For the analysis in Sec. 6, the limit of $\gamma_j(\xi)$ as $\xi \to 0$ is particular interesting, corresponding to the circular needle for the prolate spheroid and the circular disk for the oblate spheroid. The result for the circular needle reads

$$\begin{cases} \gamma_1(\xi) = \dfrac{4\pi a^3}{3} \dfrac{1}{\ln 2/\xi - 1} + \mathcal{O}(\xi^2) \\ \gamma_2(\xi) = \gamma_3(\xi) = \mathcal{O}(\xi^2) \end{cases} \qquad \text{as } \xi \to 0 \tag{G.3}$$

while for the circular disk,

$$\begin{cases} \gamma_1(\xi) = \gamma_2(\xi) = \dfrac{16a^3}{3} + \mathcal{O}(\xi) \\ \gamma_3(\xi) = \mathcal{O}(\xi) \end{cases} \qquad \text{as } \xi \to 0 \tag{G.4}$$

Closed-form expressions of (6.2) can also be evaluated for the elliptic needle and disk in terms of the complete elliptic integrals of the first and second kind, see Ref. 19.

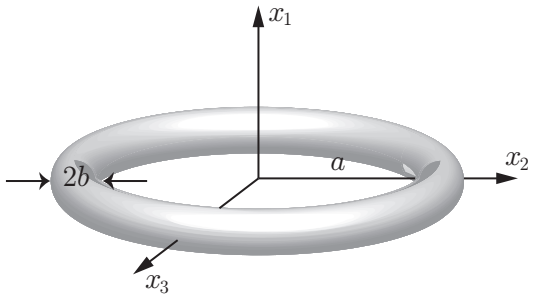

Figure 17: The toroidal ring and the Cartesian coordinate system (x_1, x_2, x_3).

Appendix H The toroidal ring

The general solution to Laplace's equation for the electrostatic potential ψ in toroidal coordinates[6] is, see Ref. 15,

$$\psi(u,v,\phi) = \sqrt{\cosh v - \cos u} \sum_{n,m=0}^{\infty} (a_m \cos m\phi + b_m \sin m\phi) \cdot (c_m \cos nu + d_m \sin nu) \left(A_{mn} \mathrm{P}^m_{n-\frac{1}{2}}(\cosh v) + B_{mn} \mathrm{Q}^m_{n-\frac{1}{2}}(\cosh v) \right),$$

where $\mathrm{P}^m_{n-1/2}$ and $\mathrm{Q}^m_{n-1/2}$ are the ring functions of the first and second kinds, respectively, see Ref. 1. The toroidal ring of axial radius a and cross section radius b is given by the surface $v = v_0$, see Fig. 17. Introduce the semi-axis ratio $\xi \in [0,1]$ as the quotient $\xi = b/a = 1 \cosh v_0$.

In this appendix, the eigenvalues of the high-contrast polarizability dyadic are derived for the loop antenna in Sec. 8.2 of vanishing thickness. Due to rotational symmetry in the x_1x_2-plane, the analysis is reduced to two exterior boundary value problems defined by the region $v \in [0, v_0]$ and $u, \phi \in [0, 2\pi)$. Due to the singular behavior of $\mathrm{Q}^m_{n-1/2}(\cosh v)$ as $v \to 0$ it is required that $B_{mn} = 0$. In addition, the electrostatic potential must vanish at infinity, *i.e.*, $\psi(u,v,\phi) \to 0$ when $u, v \to 0$ simultaneously. On the surface of the toroidal ring the two different boundary conditions of interest are, $\psi(u, v_0, \phi) = x_1$ and $\psi(u, v_0, \phi) = x_3$, see Appendix B. The following representations of the Cartesian coordinates in terms of $\mathrm{Q}^m_{n-1/2}$ are

[6]The toroidal coordinate system (u,v,ϕ) is defined in terms of the Cartesian coordinates (x_1, x_2, x_3) as

$$x_1 = \frac{\zeta \sinh v \cos\phi}{\cosh v - \cos u}, \qquad x_2 = \frac{\zeta \sinh v \sin\phi}{\cosh v - \cos u}, \qquad x_2 = \frac{\zeta \sin u}{\cosh v - \cos u},$$

where $u, \phi \in [0, 2\pi)$ and $v \in [0, \infty)$. The toroidal ring of axial radius a and cross section radius b is described by the surface $v = v_0$, where $a = \zeta \coth v_0$ and $b = \zeta / \sinh v_0$. Note that the present notation (u,v,ϕ) differs from (η, μ, ϕ) in Ref. 15.

proved to be useful:

$$\begin{cases} x_1 = -\dfrac{\zeta\sqrt{8}\cos\phi}{\pi}\sqrt{\cosh v_0 - \cos u}\displaystyle\sum_{n=0}^{\infty}\varepsilon_n \mathrm{Q}^1_{n-\frac{1}{2}}(\cosh v_0)\cos nu \\ x_3 = \dfrac{\zeta\sqrt{8}}{\pi}\sqrt{\cosh v_0 - \cos u}\displaystyle\sum_{n=1}^{\infty} n\mathrm{Q}_{n-\frac{1}{2}}(\cosh v_0)\sin nu \end{cases} \tag{H.1}$$

Two different boundary value problems are associated with the loop antenna in Sec. 8.2 depending on whether the magnetic polarization $\hat{\boldsymbol{p}}_{\mathrm{m}}$ is parallel or orthogonal to the x_3-axis. The solution of these boundary value problems are then closely related to the components of the electric polarizability dyadic. Only the case when the thickness of the toroidal ring vanishes, *i.e.*, when $\xi \to 0$ or equivalently $v_0 \to \infty$, is treated here.

H.1 Magnetic polarization perpendicular to the x_3-axis

A magnetic polarization $\hat{\boldsymbol{p}}_{\mathrm{m}}$ perpendicular to the x_3-axis is via the plane-wave condition $\hat{\boldsymbol{k}} = \hat{\boldsymbol{p}}_{\mathrm{e}} \times \hat{\boldsymbol{p}}_{\mathrm{m}}$ equivalent to the electric polarization $\hat{\boldsymbol{p}}_{\mathrm{e}}$ parallel with the x_3-axis. A straightforward calculation to this problem can be proved to yield

$$\psi(u,v,\phi) = \frac{\zeta\sqrt{8}}{\pi}\sqrt{\cosh v - \cos u}\sum_{n=1}^{\infty} n\frac{\mathrm{Q}_{n-\frac{1}{2}}(\cosh v_0)}{\mathrm{P}_{n-\frac{1}{2}}(\cosh v_0)}\mathrm{P}_{n-\frac{1}{2}}(\cosh v)\sin nu.$$

In terms of the normal derivative $\partial\psi/\partial\nu$ evaluated at $v = v_0$, the third eigenvalue of $\boldsymbol{\gamma}_\infty$ is given by

$$\gamma_3 = 2\pi\int_0^{2\pi} x_3\frac{\partial\psi(u,v_0,\phi)}{\partial\nu}\frac{\zeta^2\sinh v_0}{(\cosh v_0 - \cos u)^2}\,\mathrm{d}u \tag{H.2}$$

By insertion of (H.1) into (H.2), the asymptotic behavior of γ_3 in the limit $\xi \to 0$, or equivalently $v_0 \to \infty$, can be proved to be ($\zeta \to a$ as $v_0 \to \infty$)

$$\gamma_3 = \mathcal{O}(\xi^2) \quad \text{as } \xi \to 0. \tag{H.3}$$

Hence, the third eigenvalue γ_3 of the high-contrast polarizability dyadic vanishes as the thickness of the toroidal ring approaches zero.

H.2 Magnetic polarization parallel with the x_3-axis

The solution to the boundary value problem with the magnetic polarization $\hat{\boldsymbol{p}}_{\mathrm{m}}$ parallel with the x_3-axis, *i.e.*, $\hat{\boldsymbol{p}}_{\mathrm{e}}$ perpendicular to the x_1-axis, is

$$\psi(u,v,\phi) = -\frac{\zeta\sqrt{8}\cos\phi}{\pi}\sqrt{\cosh v - \cos u}\sum_{n=0}^{\infty}\varepsilon_n\frac{\mathrm{Q}^1_{n-\frac{1}{2}}(\cosh v_0)}{\mathrm{P}^1_{n-\frac{1}{2}}(\cosh v_0)}\mathrm{P}^1_{n-\frac{1}{2}}(\cosh v)\cos nu,$$

where $\varepsilon_n = 2 - \delta_{n0}$ is the Neumann factor. In terms of the normal derivative $\partial\psi/\partial\nu$ evaluated at $v = v_0$, the first and second eigenvalues of $\boldsymbol{\gamma}_\infty$ are

$$\gamma_1 = \gamma_2 = \int_0^{2\pi} \int_0^{2\pi} x_1 \frac{\partial\psi(u, v_0, \phi)}{\partial\nu} \frac{\zeta^2 \sinh v_0}{(\cosh v_0 - \cos u)^2} \, \mathrm{d}\phi \, \mathrm{d}u, \tag{H.4}$$

where x_1 as function of u and ϕ is given by (H.1). The asymptotic behavior of (H.4) as $\xi \to 0$, or equivalently $v_0 \to \infty$, can be proved to be ($\zeta \to a$ as $v_0 \to \infty$)

$$\gamma_1 = \gamma_2 = \frac{2\pi^2 a^3}{\ln 2/\xi - 1} + \mathcal{O}(\xi^2) \quad \text{as } \xi \to 0. \tag{H.5}$$

Note that (H.5) vanishes slower than (H.3) as $\xi \to 0$ due to the logarithmic singularity.

References

[1] M. Abramowitz and I. A. Stegun, editors. *Handbook of Mathematical Functions.* Applied Mathematics Series No. 55. National Bureau of Standards, Washington D.C., 1970.

[2] J. B. Andersen and A. Frandsen. Absorption efficiency of receiving antennas. *IEEE Trans. Antennas Propagat.*, **53**(9), 2843–2849, 2005.

[3] L. J. Chu. Physical limitations of omni-directional antennas. *Appl. Phys.*, **19**, 1163–1175, 1948.

[4] R. S. Elliott. *Antenna Theory and Design.* IEEE Press, New York, 2003. Revised edition.

[5] R. M. Fano. Theoretical limitations on the broadband matching of arbitrary impedances. *Journal of the Franklin Institute*, **249**(1,2), 57–83 and 139–154, 1950.

[6] M. Gustafsson and S. Nordebo. Bandwidth, Q-factor, and resonance models of antennas. *Progress in Electromagnetics Research*, **62**, 1–20, 2006.

[7] M. Gustafsson, C. Sohl, and G. Kristensson. Physical limitations on antennas of arbitrary shape. *Proc. R. Soc. A*, **463**, 2007. doi:1098/rspa.2007.1893.

[8] M. Gustafsson. On the non-uniqueness of the electromagnetic instantaneous response. *J. Phys. A: Math. Gen.*, **36**, 1743–1758, 2003.

[9] M. Gustafsson and S. Nordebo. Characterization of MIMO antennas using spherical vector waves. *IEEE Trans. Antennas Propagat.*, **54**(9), 2679–2682, 2006.

[10] E. Hallén. *Theoretical investigations into the transmitting and receiving qualities of antennae*, volume 11, No. 4 of *Nova acta Regiae Societatis Scientarium Upsaliensis IV*. Almqvist & Wiksell, Stockholm, 1938. ISSN 0029-5000; Ser. 4, 11:4.

[11] M. Hamermesh. *Group theory and its application to physical problems*. Dover Publications, New York, 1989.

[12] R. C. Hansen. *Electrically small, superdirective, and superconductive antennas*. John Wiley & Sons, New Jersey, 2006.

[13] IEEE Standard Definitions of Terms for Antennas, 1993. IEEE Std 145-1993. ISBN 1-55937-317-2.

[14] R. E. Kleinman and T. B. A. Senior. Rayleigh scattering. In V. V. Varadan and V. K. Varadan, editors, *Low and high frequency asymptotics*, volume 2 of *Acoustic, Electromagnetic and Elastic Wave Scattering*, chapter 1, pages 1–70. Elsevier Science Publishers, Amsterdam, 1986.

[15] P. M. Morse and H. Feshbach. *Methods of Theoretical Physics*, volume 2. McGraw-Hill, New York, 1953.

[16] R. G. Newton. *Scattering Theory of Waves and Particles*. Springer-Verlag, New York, 1982.

[17] H. M. Nussenzveig. *Causality and dispersion relations*. Academic Press, London, 1972.

[18] S. Silver. *Microwave Antenna Theory and Design*, volume 12 of *Radiation Laboratory Series*. McGraw-Hill, New York, 1949.

[19] C. Sohl, M. Gustafsson, and G. Kristensson. Physical limitations on broadband scattering by heterogeneous obstacles. Accepted for publication in J. Phys. A: Math. Theor., 2007.

[20] C. Sohl, M. Gustafsson, and G. Kristensson. Physical limitations on metamaterials: Restrictions on scattering and absorption over a frequency interval. Technical Report LUTEDX/(TEAT-7154)/1–11/(2007), Lund University, Department of Electrical and Information Technology, P.O. Box 118, S-221 00 Lund, Sweden, 2007. http://www.eit.lth.se.

[21] W. L. Stutzman and G. A. Thiele. *Antenna Theory and Design*. John Wiley & Sons, New York, second edition, 1998.

[22] J. R. Taylor. *Scattering theory: the quantum theory of nonrelativistic collisions*. Robert E. Krieger Publishing Company, Malabar, Florida, 1983.

[23] H. van de Hulst. *Light Scattering by Small Particles*. John Wiley & Sons, Inc., New York, 1957.

[24] H. A. Wheeler. Fundamental limitations of small antennas. *Proc. IRE*, **35**(12), 1479–1484, 1947.

[25] A. D. Yaghjian and S. R. Best. Impedance, bandwidth, and Q of antennas. *IEEE Trans. Antennas Propagat.*, **53**(4), 1298–1324, 2005.

A survey of isoperimetric limitations on antennas

Christian Sohl, Mats Gustafsson, and Gerhard Kristensson

Paper V

Based on: C. Sohl, M. Gustafsson, and G. Kristensson. A survey of isoperimetric limitations on antennas. Technical Report LUTEDX/(TEAT-7157)/1–9/(2007), Lund University.

Abstract

In this paper, physical limitations on antennas are presented based on the holomorphic properties of the forward scattering dyadic. As a direct consequence of causality and energy conservation, a forward dispersion relation for the extinction cross section is established, and isoperimetric inequalities for the partial realized gain and partial directivity are derived for antennas of arbitrary shape. Closed-form expressions for the prolate and oblate spheroids are compared with Chu's classical result for the sphere, and the effect of invoking metamaterials in the antenna design is discussed. The theory is illustrated by numerical simulations of a monopole antenna with a finite ground plane.

1 Introduction

Two questions of fundamental nature are addressed in this paper. For an arbitrary geometry, what is the upper bound on the performance of any antenna enclosed by this volume? Can electrically small broadband antennas exist unless directive properties are sacrificed for bandwidth? The history of these questions traces back to Chu and Wheeler in Refs. 1 and 9 more than half a century ago. Since then, much attention has drawn to the subject and numerous papers have been published, see Ref. 4 for a recent summary of the field. However, as far as the authors know, few successful attempts have been made to solve these problems rigorously for other geometries than the sphere. This restriction is mainly due to the failure of extending the spherical vector waves to form a set of orthogonal eigenfunctions on non-spherical surfaces. In this paper, physical limitations on antennas are presented which apply to arbitrary geometries without introducing orthogonal eigenfunctions.

The present paper is based on Refs. 2, 3 and 7, and the forward dispersion relation for the extinction cross section in Ref. 6. The theory has also successfully been applied to metamaterials in Ref. 8 to yield physical limitations on scattering and absorption by artificial materials over a frequency interval. The underlying mathematical description is influenced by the theory of dispersion relations for scattering of waves and particles in Ref. 5.

2 Physical limitations on $G_K B$ and D/Q

It is advantageous to picture the schematic antenna in Fig. 1 from a scattering point of view, *i.e.*, consider an antenna of arbitrary shape surrounded by free space and subject to a plane wave with time dependence $\mathrm{e}^{-\mathrm{i}\omega t}$ impinging in the $\hat{\boldsymbol{k}}$-direction. The material of the antenna is assumed to be lossless and satisfy the principles of reciprocity, linearity and time-translational invariance. The material properties are modeled by general anisotropic and heterogeneous constitutive relations in terms of the electric and magnetic susceptibility dyadics $\boldsymbol{\chi}_{\mathrm{e}}$ and $\boldsymbol{\chi}_{\mathrm{m}}$, respectively. The bounding volume of the antenna is naturally delimited by a reference plane at which a unique voltage and current relation is defined, see Fig. 1. Note that the present

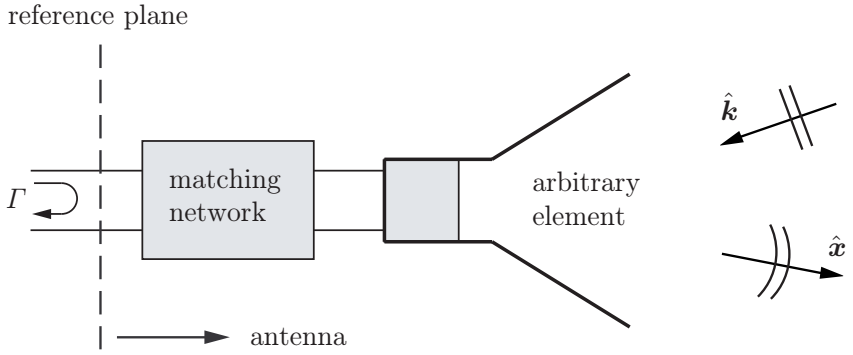

Figure 1: Illustration of a hypothetic antenna subject to a plane wave impinging in the $\hat{\boldsymbol{k}}$-direction. The incident wave is perturbed by the antenna and a scattered field is detected in the $\hat{\boldsymbol{x}}$-direction.

analysis is restricted to single port antennas with a frequency dependent scalar reflection coefficient Γ.

The scattered field caused by an incident plane wave with Fourier amplitude $\boldsymbol{E}_0$ and electric polarization $\hat{\boldsymbol{p}}_\mathrm{e} = \boldsymbol{E}_0/|\boldsymbol{E}_0|$ has the asymptotic behavior of an outgoing spherical wave, see Ref. 8, *i.e.*,

$$\boldsymbol{E}_\mathrm{s} = \frac{\mathrm{e}^{\mathrm{i}kx}}{x}\mathbf{S}(k,\hat{\boldsymbol{x}})\cdot\boldsymbol{E}_0 + \mathcal{O}(x^{-2}) \quad \text{as } x\to\infty,$$

where $\boldsymbol{x}$ denotes the position vector with respect to some origin, and $\hat{\boldsymbol{x}} = \boldsymbol{x}/x$ with $x = |\boldsymbol{x}|$. Here, $\mathbf{S}$ is independent of x and represents the scattering dyadic in the $\hat{\boldsymbol{x}}$-direction. Introduce the scattering cross section σ_s and the absorption cross section σ_a as the scattered and absorbed power divided by the incident power flow density, respectively. The principle of energy conservation then takes the form of a relation between the extinction cross section $\sigma_\mathrm{ext} = \sigma_\mathrm{s} + \sigma_\mathrm{a}$ and the imaginary part of the complex-valued function $\varrho = \hat{\boldsymbol{p}}_\mathrm{e}^*\cdot\mathbf{S}(k,\hat{\boldsymbol{k}})\cdot\hat{\boldsymbol{p}}_\mathrm{e}/k^2$. This relation is known as the optical theorem and states that $\sigma_\mathrm{ext} = 4\pi k\,\mathrm{Im}\,\varrho$ for $k\in[0,\infty)$.

Since the inverse Fourier transform of $\mathbf{S}$ is causal in the forward direction with respect to time ordered events, *i.e.*, the forward scattered field cannot precede the incident field, it can be shown that ϱ is a holomorphic function of k for $\mathrm{Im}\,k > 0$. Based on the optical theorem and the static limit of ϱ as $k\to 0$, Plemelj's formulae in Ref. 5 can be used to derive a forward dispersion relation for the extinction cross section. The result is

$$\int_0^\infty \frac{\sigma_\mathrm{ext}(k)}{k^2}\,\mathrm{d}k = \frac{\pi}{2}\sum_{i=\mathrm{e,m}}\hat{\boldsymbol{p}}_i^*\cdot\boldsymbol{\gamma}_i\cdot\hat{\boldsymbol{p}}_i, \tag{2.1}$$

where $\hat{\boldsymbol{p}}_\mathrm{m} = \hat{\boldsymbol{k}}\times\hat{\boldsymbol{p}}_\mathrm{e}$, and $\boldsymbol{\gamma}_\mathrm{e}$ and $\boldsymbol{\gamma}_\mathrm{m}$ denotes the electric and magnetic polarizability dyadics, respectively. For details on the derivation of (2.1) including definitions of the pertinent boundary value problems for $\boldsymbol{\gamma}_\mathrm{e}$ and $\boldsymbol{\gamma}_\mathrm{m}$, see Refs. 2 and 6.

The forward dispersion relation (2.1) can be used to establish upper bounds on the partial realized gain G and the relative bandwidth B of the schematic antenna

in Fig. 1. In fact, for any finite interval $K \subset [0, \infty)$,

$$\int_0^\infty \frac{\sigma_{\text{ext}}(k)}{k^2}\,\mathrm{d}k \geq \int_K \frac{\sigma_{\text{a}}(k)}{k^2}\,\mathrm{d}k = \pi \int_K (1-|\Gamma|^2)\frac{G(k)}{k^4}\,\mathrm{d}k, \tag{2.2}$$

where $1-|\Gamma|^2$ represents the impedance mismatch of the antenna. In the last equality, it has been used that the absorption cross section is related to the partial realized gain as $\sigma_{\text{a}} = \pi(1-|\Gamma|^2)G/k^2$, see Ref. 2. The estimate in (2.2) is generally not isoperimetric but can be sharpened by *a priori* information of the scattering properties of the antenna. For this purpose, introduce the quantity

$$\eta_K = \int_K \frac{\sigma_{\text{a}}(k)}{k^2}\,\mathrm{d}k \Big/ \int_K \frac{\sigma_{\text{ext}}(k)}{k^2}\,\mathrm{d}k\,, \tag{2.3}$$

which is related to the absorption efficiency $\eta = \sigma_{\text{a}}/\sigma_{\text{ext}}$ via $\eta_K \leq \sup_{k\in K}\eta$. In particular, minimum scattering antennas defined by $\sup_{k\in K}\eta = 1/2$ contribute with at most an additional factor two on the right hand side of the inequality in (2.2).

Introduce the minimum partial realized gain $G_K = \inf_{k\in K}(1-|\Gamma|^2)G$ and the relative bandwidth $B = \int_K \mathrm{d}k/k_0$, where k_0 denotes the center wave number in K. Then the integral on the right hand side of (2.2) is estimated from below by

$$\int_K (1-|\Gamma|^2)\frac{G(k)}{k^4}\,\mathrm{d}k \geq G_K \int_K \frac{\mathrm{d}k}{k^4} = \frac{G_K B}{k_0^3}\frac{1+B^2/12}{(1-B^2/4)^3} \geq \frac{G_K B}{k_0^3}. \tag{2.4}$$

The inequality on the right hand side of (2.4) is motivated by the fact that $B \ll 1$ in many applications. Based on this observation, (2.2) and (2.4) inserted into (2.1) yields the fundamental inequality

$$G_K B \leq \frac{k_0^3}{2}\sum_{i=\text{e,m}} \hat{\boldsymbol{p}}_i^* \cdot \boldsymbol{\gamma}_i \cdot \hat{\boldsymbol{p}}_i. \tag{2.5}$$

The corresponding physical limitation for the partial directivity D and the Q-factor Q is obtained from a resonance model for the absorption cross section, see Ref. 2. Under the assumption of a perfectly matched antenna at $k = k_0$, the upper bound on D/Q differs only by a factor π from (2.5), *viz.*,

$$\frac{D}{Q} \leq \frac{k_0^3}{2\pi}\sum_{i=\text{e,m}} \hat{\boldsymbol{p}}_i^* \cdot \boldsymbol{\gamma}_i \cdot \hat{\boldsymbol{p}}_i. \tag{2.6}$$

Recall that G_K and D both depend on the incident direction $\hat{\boldsymbol{k}}$ and the electric polarization $\hat{\boldsymbol{p}}_{\text{e}}$.

It is intriguing that it is just the static response of the antenna that bound the quantities $G_K B$ and D/Q. From the right hand side of (2.5) and (2.6), it is clear that the upper bounds on $G_K B$ and D/Q are independent of any coupling between electric and magnetic effects. Instead, electric and magnetic properties are seen to be treated on equal footing both in terms of material parameters and polarization description. For non-magnetic materials, *i.e.*, $\boldsymbol{\gamma}_{\text{m}} = \mathbf{0}$, the sum on the right hand

sides of (2.5) and (2.6) is simplified to only include electric quantities. Moreover, since both $\boldsymbol{\gamma}_{\mathrm{e}}$ and $\boldsymbol{\gamma}_{\mathrm{m}}$ are proportional to the volume V of the antenna, it follows that the bounds in (2.5) and (2.6) scale as $k_0^3 a^3$, where a denotes the radius of, say, the volume-equivalent sphere.

In many antenna applications, it is desirable to bound $G_K B$ and D/Q independently of both polarization states and material parameters. For this purpose, introduce the high-contrast polarizability dyadics $\boldsymbol{\gamma}_\infty$ as the limit of either $\boldsymbol{\gamma}_{\mathrm{e}}$ or $\boldsymbol{\gamma}_{\mathrm{m}}$ when the elements of $\boldsymbol{\chi}_{\mathrm{e}}$ and $\boldsymbol{\chi}_{\mathrm{m}}$ become infinite large. From the variational properties of $\boldsymbol{\gamma}_{\mathrm{e}}$ and $\boldsymbol{\gamma}_{\mathrm{m}}$ discussed in Ref. 6, it then follows that

$$\sup_{\hat{\boldsymbol{p}}_{\mathrm{e}}\cdot\hat{\boldsymbol{p}}_{\mathrm{m}}=0} G_K B \leq \frac{k_0^3}{2}(\gamma_1+\gamma_2), \qquad \sup_{\hat{\boldsymbol{p}}_{\mathrm{e}}\cdot\hat{\boldsymbol{p}}_{\mathrm{m}}=0} \frac{D}{Q} \leq \frac{k_0^3}{2\pi}(\gamma_1+\gamma_2), \tag{2.7}$$

where γ_1 and γ_2 denote the largest and second largest eigenvalue of $\boldsymbol{\gamma}_\infty$, respectively. The interpretation of (2.7) is polarization matching, *i.e.*, the polarization of the antenna coincides with the polarization of the incident wave. For non-magnetic material parameters, γ_2 vanishes in (2.7), and the upper bounds on $G_K B$ and D/Q are sharpened by at most a factor of two. Recall that γ_1 and γ_2 are easily calculated for arbitrary geometries using either the finite element method (FEM) or the method of moments (MoM).

3 Comparison with classical limitations

Closed-form expressions of γ_1 and γ_2 exist for the homogeneous ellipsoids, *viz.*, $\gamma_1 = V/L_1$ and $\gamma_2 = V/L_2$, where L_1 and L_2 denotes the smallest and second smallest depolarizing factor, respectively. The depolarizing factors satisfy $0 \leq L_j \leq 1$ and $\sum_j L_j = 1$ and are defined by

$$L_j = \frac{a_1 a_2 a_3}{2} \int_0^\infty \frac{\mathrm{d}s}{(s+a_j^2)\sqrt{(s+a_1^2)(s+a_2^2)(s+a_3^2)}}, \qquad j=1,2,3. \tag{3.1}$$

Closed-form expressions of (3.1) in terms of the semi-axis ratio $\xi = \min_j a_j / \max_j a_j$ exist for the ellipsoids of revolution, *i.e.*, the prolate ($L_2 = L_3$) and oblate ($L_1 = L_2$) spheroids.

The eigenvalues γ_1, γ_2 and γ_3 (smallest eigenvalue $\gamma_3 = V/L_3$) are depicted in Fig. 2 for the prolate and oblate spheroids as function of ξ. The solid curves on the right hand side of Fig. 2 correspond to the combined electric and magnetic case, while the dashed curves represent pure electric material parameters. Non-magnetic material parameters with minimum scattering characteristics, *i.e.*, $\sup_{k\in K} \eta = 1/2$, is depicted by the dotted curves. In fact, the three curves for the prolate spheroid in the right figure vanish as $\xi \to 0$, while the corresponding curves for the oblate spheroid approach $16/3\pi$, $8/3\pi$, and $4/3\pi$, respectively.

A simple example of the upper bound on D/Q in (2.7) is given by the sphere of radius a for which $\gamma_1 = \gamma_2 = 4\pi a^3$. In this case, D/Q is bounded from above by $4k_0^3 a^3$, which is sharper than the classical limitation $6k_0^3 a^3$ when both TE- and

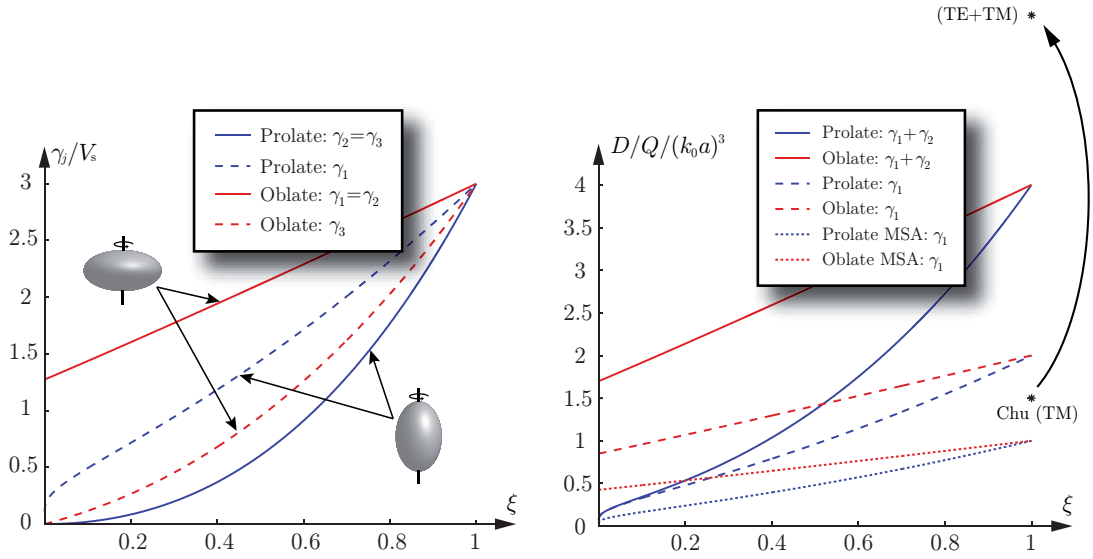

Figure 2: The eigenvalues γ_j (left figure) and the quotient D/Q (right figure) for the prolate and oblate spheroids as function of the semi-axis ratio ξ. Note the normalization with the volume V_s of the smallest circumscribing sphere.

TM-polarizations are present, see Ref. 4. For omni-directional antennas with non-magnetic material parameters, the upper bound on D/Q is still slightly sharper than Chu's limit $3k_0^3a^3/2$ in Ref. 1 when minimum scattering characteristics (MSA) are assumed. Recall however that the classical results $6k_0^3a^3$ and $3k_0^3a^3/2$ are restricted to the sphere in the limit as $k_0a \to 0$, which is not the case for the theory set forth in this paper.

4 The effect of metamaterials

The fact that (2.5) and (2.6) are independent of any temporal dispersion implies that there is no difference in the upper bounds of G_KB and D/Q if metamaterials are invoked in the antenna design instead of ordinary materials with identical static material parameters. In fact, it is well known that passive metamaterials are temporal dispersive since the Kramers-Kronig relations imply that $\lim_{\omega\to 0+} \boldsymbol{\chi}_{\mathrm{e}}(\omega)$ and $\lim_{\omega\to 0+} \boldsymbol{\chi}_{\mathrm{m}}(\omega)$ elementwise are non-negative in the absence of a conductivity term, see Ref. 8. When an isotropic conductivity term $i\varsigma/\omega\epsilon_0$ (scalar conductivity $\varsigma > 0$ independent of ω) is present in $\boldsymbol{\chi}_{\mathrm{e}}$, the Kramers-Kronig relations is modified due to the singular behavior of $\boldsymbol{\chi}_{\mathrm{e}}$ in the static limit. In the presence of a conductivity term, the analysis in Ref. 8 shows that the right hand side of (2.5) and (2.6) instead should be evaluated in the limit as the eigenvalues of $\boldsymbol{\chi}_{\mathrm{e}}$ approach infinity independently of $\boldsymbol{\chi}_{\mathrm{m}}$. Metamaterials may have the ability to lower the resonance frequency, but from the point of view of maximizing G_KB and D/Q, such materials are believed to be of limited use.

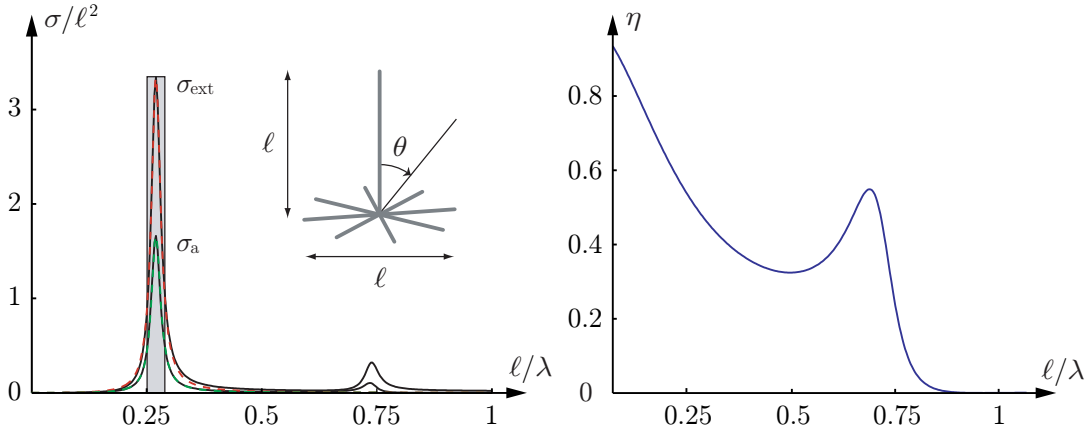

Figure 3: The extinction and absorption cross section for the monopole antenna (left figure) and the corresponding absorption efficiency (right figure). The different curves in the left figure correspond to a MoM solution (solid curves), Q-factor approximation (dashed curves), and limitation on the extinction cross section (shaded box).

5 A numerical example: the monopole antenna

The monopole antenna in Fig. 3 with a wire ground plane is used to illustrate the physical limitations introduced in Sec. 2. A monopole antenna behaves similar to a dipole antenna and the method of images can be used to analyze the antenna if the ground plane is sufficiently large, see Ref. 3. Here, a monopole antenna with height ℓ and ground plane radius $\ell/2$ is considered. The wires are cylindrical with radius $2.5 \cdot 10^{-5}\ell$. A MoM solution together with a gap feed model is used to determine the cross sections and impedance of the antenna.

The antenna is first considered as a passive scatterer loaded with $25\,\Omega$ in the gap feed. The extinction and absorption cross sections for an incident wave polarized matched at $\theta = 90^\circ$ are depicted in the left figure in Fig. 3. It is observed that the antenna is resonant for $\ell \approx 0.27\lambda$, where $\lambda = 2\pi/k$ denotes the wavelength in free space. The corresponding absorption efficiency is depicted on the right hand side of Fig. 3. It is observed that $\eta \approx 0.5$ at the resonance frequency, with $\eta_K \approx 0.5$ for $\ell/\lambda \in [0, 1]$. Note that the rather small ground plane gives a dipole-like radiation pattern at the quarter wavelength resonance.

The maximal gain, the partial gain at $\theta = 90^\circ$, and the partial realized gain at $\theta = 90^\circ$ for the antenna are depicted in the left figure in Fig. 4. At the resonance frequency, it is observed that the gain (and directivity) is 1.52 and that the radiation resistance is $25\,\Omega$. The Q-factor is estimated to $Q = 22$ by numerical differentiation of the reflection coefficient. The MoM solution is also used to determine the forward scattering properties of the antenna in terms of the extinction volume ϱ on the right hand side of Fig. 4.

The physical limitations in (2.7) require calculation of the eigenvalues γ_1 and γ_2. An electrostatic MoM simulation of the monopole antenna with a ground plane in

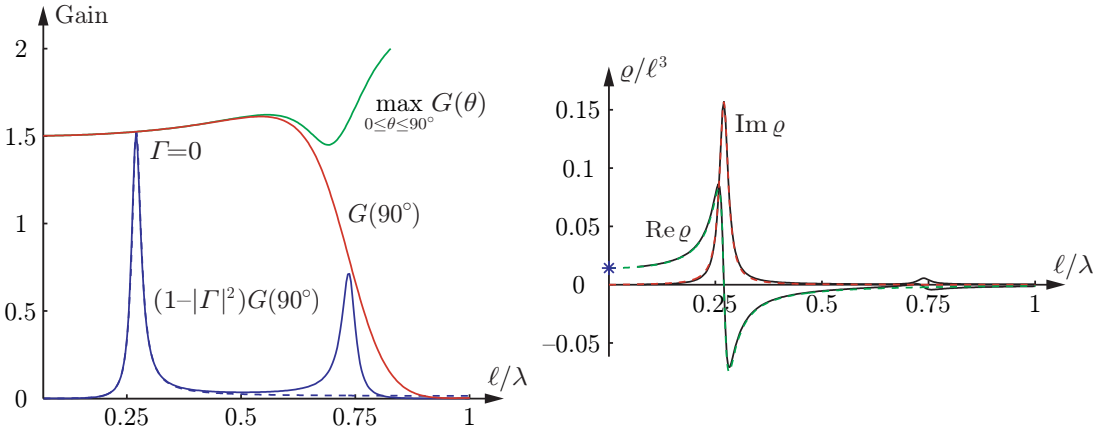

Figure 4: The maximal gain, the partial gain at $\theta = 90^\circ$, and the partial realized gain at $\theta = 90^\circ$ (left figure), and the extinction volume ϱ (right figure) for the monopole antenna. The different curves in the right figure correspond to a MoM solution (solid curves) and Q-factor approximation (dashed curves). The low frequency estimates of the monopole antenna with wire ground plane is indicated by the cross.

the form of a circular disk yields $\gamma_1 = 0.2\ell^3$ and hence $Q \geq 19$ if $D = 1.52$ and $\eta_K = 0.5$ are used in (2.7). Note that γ_2 vanishes from the upper bounds in (2.7) since no magnetic materials are present. As the circular ground plane contains more material than the wire ground plane it is clear that γ_1 for the monopole antenna with wire ground plane is smaller than γ_1 for the corresponding antenna with circular disk ground plane, *cf.*, the variational results in Ref. 6. The eigenvalue γ_1 for the monopole with the wire ground plane can either be determined by an electrostatic MoM solution or estimated by the forward dispersion relation (2.1). The latter method yields $\gamma_1 \geq 0.18\ell^3$, and assuming $\gamma_1 = 0.18\ell^3$ in (2.7) implies $Q \geq 22$.

In Figs. 3 and 4 it is observed that the single resonance model (dashed curves) with $Q = 22$ is a good approximation of the cross sections, extinction volume, and partial realized gain. Note also that the dipole antenna has a circumscribing sphere with $ka > 1$ and is therefore not considered electrically small according to the classical limitations in Ref. 1. In summary, the monopole antenna with wire ground plane show excellent agreement with the theory introduced in Sec. 2.

6 Conclusion

In this paper, physical limitations on reciprocal antennas of arbitrary shape are presented based on the holomorphic properties of the forward scattering dyadic. Upper bounds on $G_K B$ and D/Q are derived in terms of the electric and magnetic polarizability dyadics, $\boldsymbol{\gamma}_{\mathrm{e}}$ and $\boldsymbol{\gamma}_{\mathrm{m}}$, respectively. Since these bounds are proportional to the volume of the antenna, it is clear that for electrically small antennas, partial realized gain or partial directivity must be sacrificed for bandwidth or Q-factor. Based on the limitations, it is also concluded that metamaterials and other exotic

material models do not contribute to the upper bounds of $G_K B$ and D/Q in any larger extent than naturally formed substances.

The inequalities introduced in this paper are isoperimetric in the sense that equality in (2.5) and (2.6) hold for some physical antennas. For example, it is well known that the impedance of a cylindrical dipole antenna posses a reversed logarithmic singularity as the radius of the cylinder vanishes. In Ref. 2, this singularity is shown to coincide with the corresponding behavior of γ_1 for the prolate spheroid as $\xi \to 0$. In fact, numerical simulations of the dipole antenna in Ref. 3 show excellent agreement with the bounds presented in this paper. The present limitations are believed to be isoperimetric for a large class of antennas if *a priori* information of η_K from antenna simulations is taken into account.

The analysis in this paper generalizes in many aspects the classical results by Chu and Wheeler in Refs. 1 and 9. The main advantages of the new formulation are sixfold: 1) they hold for arbitrary geometries; 2) they are formulated both in terms of gain and bandwidth as well as directivity and Q-factor; 3) they include polarization effects with applications to diversity in MIMO communication; 4) they successfully separate electric and magnetic antenna properties in terms of the nature of the intrinsic materials; 5) they are isoperimetric; 6) *a priori* information about the scattering characteristics in the form of η_K improves the bounds.

Acknowledgment

The financial support by the Swedish Research Council and the SSF Center for High Speed Wireless Communication are gratefully acknowledged.

References

[1] L. J. Chu. Physical limitations of omni-directional antennas. *Appl. Phys.*, **19**, 1163–1175, 1948.

[2] M. Gustafsson, C. Sohl, and G. Kristensson. Physical limitations on antennas of arbitrary shape. *Proc. R. Soc. A*, **463**, 2007. doi:1098/rspa.2007.1893.

[3] M. Gustafsson, C. Sohl, and G. Kristensson. Physical limitations on antennas of arbitrary shape. Technical Report LUTEDX/(TEAT-7153)/1–37/(2007), Lund University, Department of Electrical and Information Technology, P.O. Box 118, S-221 00 Lund, Sweden, 2007. http://www.eit.lth.se.

[4] R. C. Hansen. *Electrically small, superdirective, and superconductive antennas.* John Wiley & Sons, New Jersey, 2006.

[5] H. M. Nussenzveig. *Causality and dispersion relations.* Academic Press, London, 1972.

[6] C. Sohl, M. Gustafsson, and G. Kristensson. Physical limitations on broadband scattering by heterogeneous obstacles. Accepted for publication in J. Phys. A: Math. Theor., 2007.

[7] C. Sohl, M. Gustafsson, and G. Kristensson. The integrated extinction for broadband scattering of acoustic waves. Technical Report LUTEDX/(TEAT-7156)/1–10/(2007), Lund University, Department of Electrical and Information Technology, P.O. Box 118, S-221 00 Lund, Sweden, 2007. http://www.eit.lth.se.

[8] C. Sohl, M. Gustafsson, and G. Kristensson. Physical limitations on metamaterials: Restrictions on scattering and absorption over a frequency interval. Technical Report LUTEDX/(TEAT-7154)/1–11/(2007), Lund University, Department of Electrical and Information Technology, P.O. Box 118, S-221 00 Lund, Sweden, 2007. http://www.eit.lth.se.

[9] H. A. Wheeler. Fundamental limitations of small antennas. *Proc. IRE*, **35**(12), 1479–1484, 1947.

A scattering and absorption identity for metamaterials — experimental results and comparison with theory

Christian Sohl, Christer Larsson, Mats Gustafsson, and Gerhard Kristensson

Paper VI

Based on: C. Sohl, C. Larsson, M. Gustafsson, and G. Kristensson. A scattering and absorption identity for metamaterials — experimental results and comparison with theory. Technical Report LUTEDX/(TEAT-7158)/1–9/(2007), Lund University.

Abstract

In this paper, measurements are presented on the combined effect of scattering and absorption of electromagnetic waves by a fabricated sample of metamaterial. This engineered composite material, designed as a planar array of inductive and capacitive resonators, is commonly referred to in the literature as a negative permittivity metamaterial. A scattering and absorption identity based on the holomorphic properties of the forward scattering dyadic are presented and compared with extinction measurements in the frequency interval $[3.2, 19.5]$ GHz. The experimental results are shown to be in good agreement with the theory.

1 Introduction

Since the contemporary discoveries of the equations in Refs. 4 and 9 which nowadays are termed the Kramers-Kronig relations, dispersion relation techniques have been applied successfully to disparate wave phenomena to reveal the underlying structure of wave interaction with matter. There are at least two main advantages of dispersion relations for the analysis of wave propagation in matter: i) they provide a consistency check of measured or calculated quantities, and ii) they may be used to verify whether a given model or an experimental outcome is causal or not. In addition, dispersion relations can be used to establish non-trivial relationships between various physical quantities, *cf.*, the fundamental bounds on scattering and absorption in Ref. 15. A comprehensive review of dispersion relations in material modeling and scattering theory is presented in Ref. 16.

The optical theorem relates the extinction cross section, *i.e.*, the measure of the effective area of absorption and scattering, to the forward scattering dyadic, see Refs. 11 and 12. As a consequence, the magnitude and phase of the scattered field in a single direction solely determines the extinction properties of the scatterer. In a series of papers in Refs. 15, 17 and 18, the use of a forward dispersion relation is exploited by invoking the optical theorem. In particular, it is established that the extinction cross section integrated over all frequencies is related to the static polarizability dyadics of the scatterer. This result is rather intriguing, and one of its many applications on antennas in Refs. 5 and 6 shows great potential. The present paper provides a first experimental verification of these new findings.

Although, the theory of broadband extinction of acoustic and electromagnetic waves by now is well established, and numerical simulations show excellent agreement with the theory, its experimental verification is of scientific importance. Moreover, scattering measurements in the forward direction offer several new experimental challenges to master. To circumvent the weak signal strength of the scattered field in comparison with the incident field, the present paper utilizes the idea that, for a specific class of targets, the scattered field in the forward and backward directions are identical.

The design of the engineered composite material used in this paper is similar to the structure reported in Ref. 14. As far as the authors know, the present paper is the first attempt to experimentally determine forward scattering properties of

metamaterials. In addition, the results provide an experimental verification of the theory governing the physical limitations in Refs. 15 and 18.

2 A forward dispersion relation

Consider the direct scattering problem of a plane electromagnetic wave $\boldsymbol{E}_0 \mathrm{e}^{\mathrm{i}\omega\hat{\boldsymbol{k}}\cdot\boldsymbol{x}/\mathrm{c}_0}$ with time dependence $\mathrm{e}^{-\mathrm{i}\omega t}$ impinging in the $\hat{\boldsymbol{k}}$-direction on a bounded scatterer surrounded by free space (c_0 is the phase velocity in free space). The material of the scatterer is modeled by a set of linear and passive constitutive relations which satisfy primitive causality and are independent of time, *i.e.*, no material ageing. The scattering properties in the $\hat{\boldsymbol{x}}$-direction for an arbitrary frequency $f = \omega/2\pi$ and a fixed polarization $\boldsymbol{E}_0/|\boldsymbol{E}_0|$ is quantified by the differential cross section, see Ref. 2,

$$\frac{\mathrm{d}\sigma}{\mathrm{d}\Omega}(\hat{\boldsymbol{k}}, \hat{\boldsymbol{x}}) = \frac{|\mathbf{S}(\hat{\boldsymbol{k}}, \hat{\boldsymbol{x}}) \cdot \boldsymbol{E}_0|^2}{|\boldsymbol{E}_0|^2}. \tag{2.1}$$

Here, the scattering dyadic $\mathbf{S}$ is expressed in terms of the scattered electric field $\boldsymbol{E}_\mathrm{s}$ as

$$\mathbf{S}(\hat{\boldsymbol{k}}, \hat{\boldsymbol{x}}) \cdot \boldsymbol{E}_0 = \lim_{x\to\infty} x\mathrm{e}^{-\mathrm{i}\omega x/\mathrm{c}_0} \boldsymbol{E}_\mathrm{s}(\hat{\boldsymbol{k}}, \boldsymbol{x}),$$

where $x = |\boldsymbol{x}|$ denotes the magnitude of the position vector $\boldsymbol{x}$, and $\hat{\boldsymbol{x}} = \boldsymbol{x}/x$. In particular, (2.1) evaluated in the backward direction $\hat{\boldsymbol{x}} = -\hat{\boldsymbol{k}}$ yields the well-known monostatic radar cross section (RCS) in Ref. 8.

The scattering cross section σ_s is defined as the total scattered power in all directions divided by the incident power flux. It is obtained by integrating (2.1) over the unit sphere with respect to $\hat{\boldsymbol{x}}$, *i.e.*,

$$\sigma_\mathrm{s}(\hat{\boldsymbol{k}}) = \int \frac{\mathrm{d}\sigma}{\mathrm{d}\Omega}(\hat{\boldsymbol{k}}, \hat{\boldsymbol{x}})\ \mathrm{d}\Omega. \tag{2.2}$$

Here, $\mathrm{d}\Omega = \sin\theta\,\mathrm{d}\theta\,\mathrm{d}\phi$ denotes the differential solid angle in terms of the polar and azimuthal variables $\theta \in [0, \pi]$ and $\phi \in [0, 2\pi)$, respectively. Based on (2.2), the extinction cross section $\sigma_\mathrm{ext} = \sigma_\mathrm{s} + \sigma_\mathrm{a}$ is defined as the sum of the scattering and absorption cross sections, where the latter is a measure of the absorbed power in the scatterer. The extinction cross section can also be determined from the forward scattering dyadic via the optical theorem

$$\sigma_\mathrm{ext}(\hat{\boldsymbol{k}}) = \frac{2\mathrm{c}_0}{f} \operatorname{Im}\left\{ \frac{\boldsymbol{E}_0^* \cdot \mathbf{S}(\hat{\boldsymbol{k}}, \hat{\boldsymbol{k}}) \cdot \boldsymbol{E}_0}{|\boldsymbol{E}_0|^2} \right\}, \tag{2.3}$$

where an asterisk denotes the complex conjugate. The relation (2.3) can be applied to a wide range of wave phenomenon including acoustic waves, electromagnetic waves, and elementary particles, see Refs. 12 and 16.

From the integral representations in Ref. 19 or the discussion in Ref. 13, it follows that for a non-magnetic, planar, and infinitely thin scatterer subject to a plane wave

impinging at normal incidence, the scattering dyadic in the forward and backward directions are identical *i.e.*,

$$\mathbf{S}(\hat{\boldsymbol{k}}, \hat{\boldsymbol{k}}) \cdot \boldsymbol{E}_0 = \mathbf{S}(\hat{\boldsymbol{k}}, -\hat{\boldsymbol{k}}) \cdot \boldsymbol{E}_0. \tag{2.4}$$

The interpretation of (2.4) is that it enables extinction measurements to be carried out by only observing the scattered field in the backward direction. Of course, both the magnitude and phase of $\boldsymbol{E}_{\mathrm{s}}(\hat{\boldsymbol{k}}, -x\hat{\boldsymbol{k}})$ as $x \to \infty$ have to be identified. In particular, (2.4) implies that the differential cross section in the forward and backward directions are equal.

A dispersion relation for the combined effect of scattering and absorption of electromagnetic waves is derived in Ref. 15 from the holomorphic properties of the forward scattering dyadic. The result is a summation rule for the extinction cross section valid for any linear and time-translational invariant scatterer obeying passivity and primitive causality. In the absence of magnetic properties in the static limit, the summation rule reads

$$\frac{\mathrm{c}_0}{4\pi^3} \int_0^\infty \frac{\sigma_{\mathrm{ext}}(f)}{f^2} \, \mathrm{d}f = \frac{\boldsymbol{E}_0^* \cdot \boldsymbol{\gamma}_{\mathrm{e}} \cdot \boldsymbol{E}_0}{4\pi |\boldsymbol{E}_0|^2}, \tag{2.5}$$

where the frequency dependence has been made explicit in the argument of the extinction cross section. Observe that the right hand side of (2.5) only depends on the static properties of the scatterer via the electric polarizability dyadic $\boldsymbol{\gamma}_{\mathrm{e}}$. This dyadic is defined in Refs. 3 and 15 together with closed-form expressions for the prolate and oblate spheroids and other generic geometries.

According to Ref. 7, the right hand side of (2.5) is equal to the static limit $\varrho(0)$ of the extinction volume

$$\varrho(f) = \frac{\mathrm{c}_0^2}{4\pi^2 f^2} \frac{\boldsymbol{E}_0^* \cdot \mathbf{S}(\hat{\boldsymbol{k}}, \hat{\boldsymbol{k}}) \cdot \boldsymbol{E}_0}{|\boldsymbol{E}_0|^2}. \tag{2.6}$$

This quantity satisfies $\operatorname{Re} \varrho = \mathcal{H}(\operatorname{Im} \varrho)$ and $\operatorname{Im} \varrho = -\mathcal{H}(\operatorname{Re} \varrho)$, where $\mathcal{H}$ denotes the Hilbert transform in Refs. 16 and 20. The imaginary part of ϱ is related to the optical theorem via $\sigma_{\mathrm{ext}}(f) = 8\pi^2 f \operatorname{Im} \varrho(f)/\mathrm{c}_0$. The fact that σ_{ext} is non-negative implies that the left hand side of (2.5) can be estimated from below by the corresponding integral over the arbitrary frequency interval $[f_1, f_2]$, *viz.*,

$$\frac{\mathrm{c}_0}{4\pi^3} \int_{f_1}^{f_2} \frac{\sigma(f)}{f^2} \, \mathrm{d}f \leq \frac{\mathrm{c}_0}{4\pi^3} \int_0^\infty \frac{\sigma_{\mathrm{ext}}(f)}{f^2} \, \mathrm{d}f = \varrho(0), \tag{2.7}$$

where σ denotes any of σ_{ext}, σ_{s} and σ_{a}. The interpretation of (2.7) is that there is only a limited amount of scattering and absorption available in the range $[f_1, f_2]$, *cf.*, the physical limitations on broadband scattering in Refs. 15 and 18. This means that the total amount of scattering and absorption is bounded from above by the static limit $\varrho(0)$ of the extinction volume.

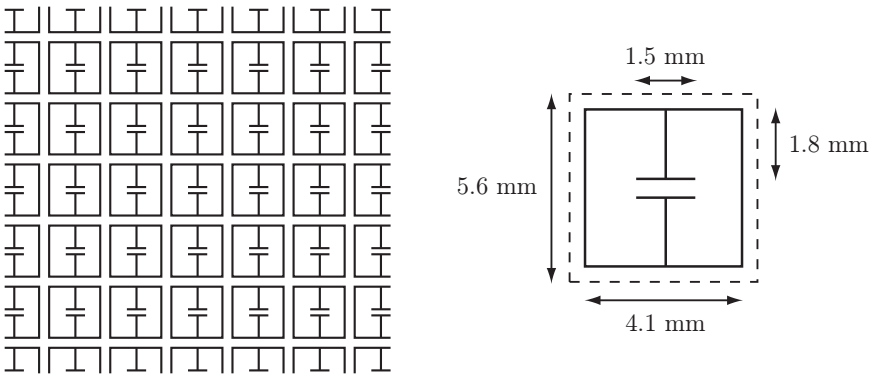

Figure 1: The pattern of the fabricated sample (left figure) and the geometry of the square unit cell (right figure). The line width of the printed circuit board is 0.1 mm.

3 Measurements on metamaterials

In this section, extinction measurements by a fabricated sample of metamaterial are presented. The sample design and experimental setup are described, and the outcome of the measurements is compared with the theoretical results in Sec. 2.

3.1 Sample design and experimental setup

The fabricated sample is designed as a single-layer planar array of inductive and capacitive resonators tuned for resonance at 8.5 GHz. It consists of 29×29 unit cells supported by a square FR4 substrate of edge length $a = 140$ mm and thickness 0.3 mm, see Fig. 1. The dielectric constant of the substrate varies between 4.2 and 4.4 in the frequency interval $[3.2, 19.5]$ GHz, with an overall loss factor less than 0.02. The design of the sample is similar to the structure addressed in Ref. 14.

Measurements were performed in the anechoic chamber at Saab Bofors Dynamics in Linköping, Sweden. The fabricated sample was mounted on an expanded polystyrene sample holder placed on a pylon. The chamber was set up for RCS measurements with dual polarized ridged circular waveguide horns positioned at a distance of 3.55 m from the sample, see Fig. 2. An Agilent Performance Network Analyzer (PNA) was used for the measurements, and the transmitted waveform was a continuous wave without online hard or software gating. The original frequency interval $[2, 20]$ GHz was reduced to $[3.2, 19.5]$ GHz due to range domain filtering of the data. The latter frequency interval was sampled with 7246 equidistant points corresponding to an unambiguous range of 66.7 m sufficient to avoid influence of room reverberations.

Calibration was performed using a metal plate with the same outer dimensions as the sample depicted in Fig. 2. The metal plate was also used to align the experimental setup using the specular reflection of the metal plate. The sample was measured, the background was subtracted coherently, and the data were calibrated. The data were then transformed to the range domain, where the response from the

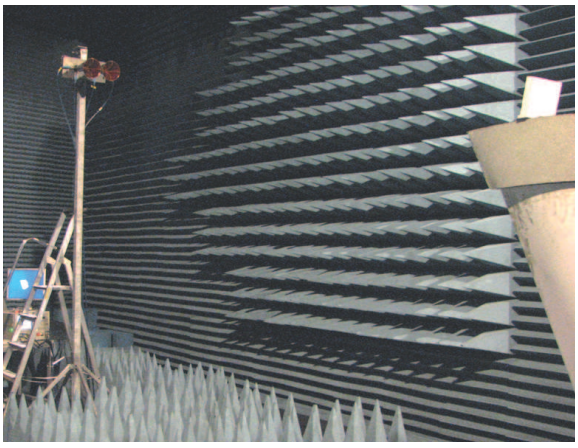

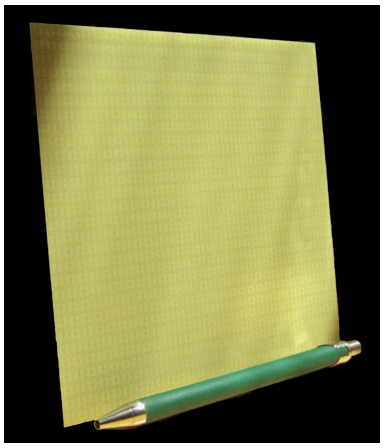

Figure 2: The experimental setup in the anechoic chamber (left figure) and the fabricated sample with 29×29 unit cells supported by a square FR4 substrate of edge length 140 mm (right figure).

sample was selected from the range profile using a 1.1 m spatial gate. Finally, the selected data was transformed back to the frequency domain.

3.2 Measurement results and comparison with theory

The measured RCS is depicted by the solid line on the left hand side in Fig. 3. In the figure, the first resonance at $f_0 \approx 8.5\,\mathrm{GHz}$ is observed as well as an increase in RCS with frequency, consistent with the specular reflection of the sample. As the sample is non-magnetic and sufficiently thin, the forward scattering dyadic is approximated by the scattering dyadic in the backward direction according to (2.4). In particular, this approximation is used to calculate the extinction cross section σ_{ext} via the optical theorem (2.3). The extinction cross section is depicted on the right hand side in Fig. 3. From the figure it is seen that σ_{ext} is non-negative confirming the validity of (2.4) since phase deviations in the scattering dyadic introduce significant errors in the extinction cross section.

The forward scattering dyadic is also used to determine the extinction volume ϱ, see (2.6), on the left hand side in Fig. 4. Here, it is observed that the real part of ϱ vanishes at the resonance frequency $f_0 \approx 8.5\,\mathrm{GHz}$, whereas the imaginary part of ϱ attains its maximum value. Note that the frequency scaling in (2.6) amplifies the noise in the measurements for low frequencies as noted in the figure. Finally, the function $\zeta(f) = 2\,\mathrm{Im}\,\varrho(f)/\pi f$, corresponding to the integrand in (2.5), is depicted on the right hand side in Fig. 4 with additional noise amplification for low frequencies. The shaded area on the right hand side is estimated by numerical integration to $26.0\,\mathrm{cm}^3$ and indicated by the dot in the left figure. Since ζ is non-negative, the value $26.0\,\mathrm{cm}^3$ yields a lower bound on $\varrho(0)$ according to (2.7). Obviously, $\varrho(0)$ is underestimated by the integral as the integrand does not vanish outside the frequency interval $[3.2, 19.5]\,\mathrm{GHz}$, *cf.*, the properties of holomorphic functions in Ref. 1.

According to the variational results in Ref. 15, $\varrho(0)$ is bounded from above by

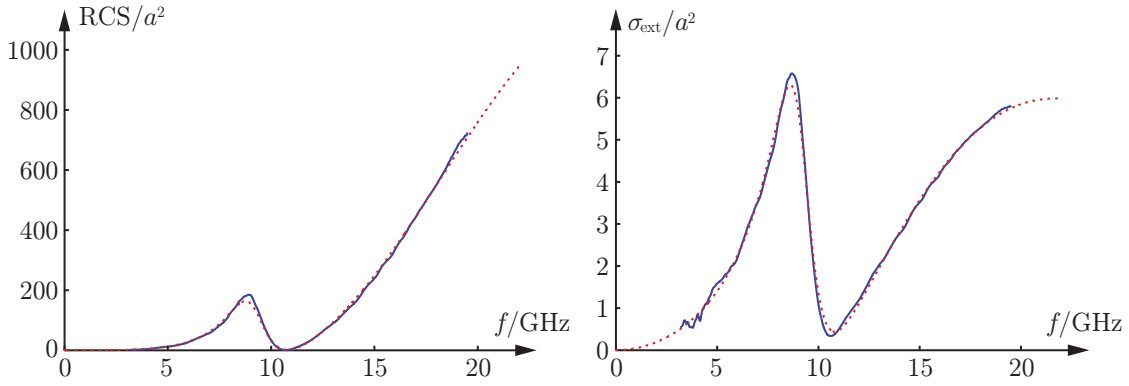

Figure 3: The monostatic radar cross section (left figure) and the extinction cross section (right figure) in units of the projected area a^2 in the forward direction. The solid lines correspond to measured data whereas the dashed lines are based on the approximation (3.1).

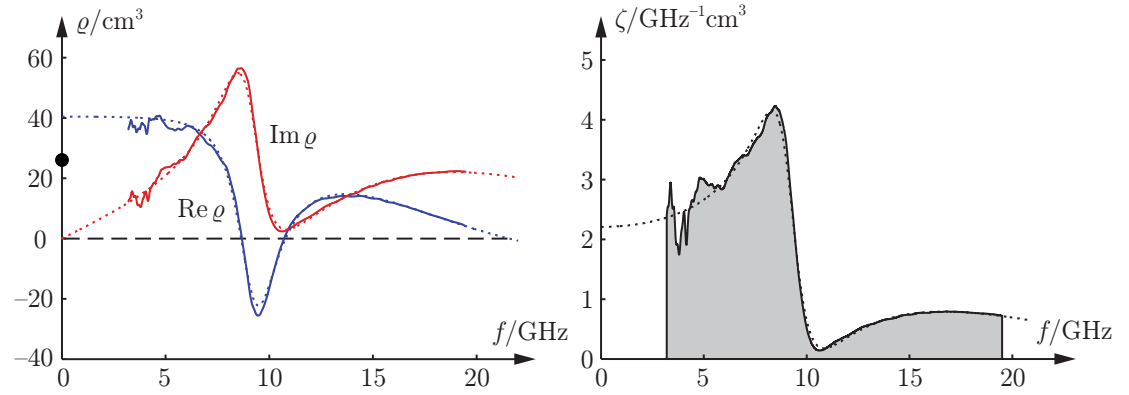

Figure 4: The extinction volume (left figure) and $\zeta(f) = 2\,\mathrm{Im}\,\varrho(f)/\pi f$ (right figure). The solid lines correspond to measured data whereas the dashed lines are based on the approximation (3.1). The shaded area on the right hand side is marked with a dot in the left figure.

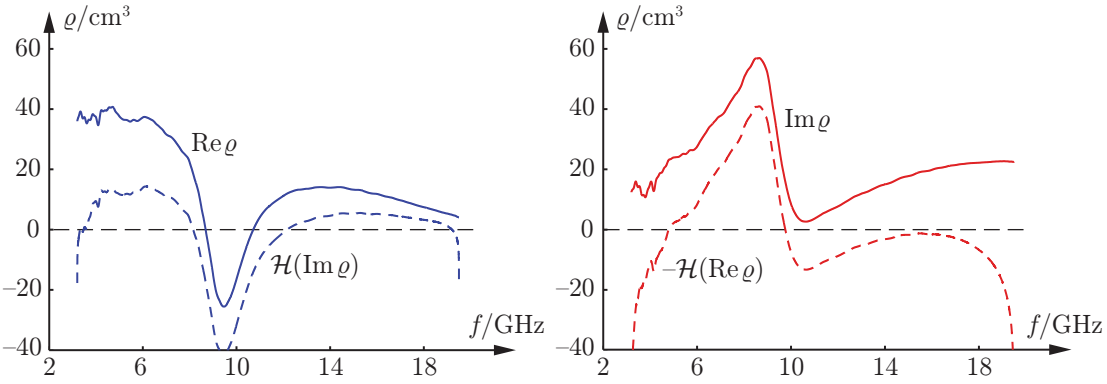

Figure 5: The real and imaginary parts of the extinction volume (solid lines) and the corresponding reconstructed quantities using the Hilbert transform $\mathcal{H}$ (dashed lines).

the corresponding quantity for a thin square metal plate with edge length 140 mm. Based on the method of moments, this static limit for the metal plate is computed to 222 cm^3. The upper bound should also be compared with the corresponding value 412 cm^3 for the smallest circumscribing circular disk of radius $140/\sqrt{2}$ mm, *cf.*, the closed-form expressions of $\varrho(0)$ in Ref. 15. As the upper bound 222 cm^3 is too rude, more appropriate techniques for estimating $\varrho(0)$ should be invoked. A possible such technique is given by the Hilbert transform $\mathcal{H}$ as depicted in Fig. 5. In the figure, it is observed that $\mathcal{H}(\mathrm{Im}\,\varrho)$ and $-\mathcal{H}(\mathrm{Re}\,\varrho)$ resemble the overall frequency dependence of the real and imaginary parts of ϱ, respectively. However, it is clear from the figure that the finite frequency interval of the measured data limits its usefulness.

Another feasible technique to approximate ϱ is the use of meromorphic functions with roots and zeros in the lower half of the complex f-plane. Numerical tests using the algorithm in Ref. 10 indicate that it is sufficient to consider rational functions with numerator and denominator of second and fourth degree, respectively, to approximate ϱ over $[3.2, 19.5]$ GHz.[1] Such functions can be represented by the sum of two Lorentzian terms according to

$$\varrho_{\mathrm{appr}}(f) = \sum_{n=1}^{2} \varrho_n \frac{f_n^2 + \mathrm{i} f \nu_n}{f_n^2 + 2\mathrm{i} f f_n / Q_n - f^2}. \tag{3.1}$$

The approximation (3.1) is depicted by the dotted lines in Fig. 4. Here, $f_1 = 9.3\,\mathrm{GHz}$, $Q_1 = 7.8$, $\varrho_1 = 4.6\,\mathrm{cm}^3$, $\nu_1 = -27\,\mathrm{GHz}$, $f_2 = 20\,\mathrm{GHz}$, $Q_2 = 1.6$, $\varrho_2 = 36\,\mathrm{cm}^3$, and $\nu_2 = 3.6\,\mathrm{GHz}$. Note that $\varrho_{\mathrm{appr}}(0) = \varrho_1 + \varrho_2 \approx 40\,\mathrm{cm}^3$. The approximation ϱ_{appr} is also used to extrapolate the RCS and the extinction volume in Fig. 3 as depicted by the dotted lines. Recall that $\zeta(f) = \mathcal{O}(1)$ as $f \to 0$ is supported by the static limit of the extinction cross section for a lossy target, see Ref. 3.

[1]The algorithm in Ref. 10 is implemented in the Signal Processing Toolbox in Matlab under the command `invfreqs`.

4 Conclusions

This paper reports on measurements of the extinction cross section and the extinction volume for a fabricated sample of metamaterial. It is found that the extinction cross section integrated over the frequency interval $[3.2, 19.5]$ GHz yields a lower bound on the static limit of the extinction volume according to (2.7). As already pointed out in Ref. 18, there is no fundamental difference between metamaterials and naturally formed substances as far as scattering and absorption quantified by the forward dispersion relation (2.5) is concerned. Similar measurements of the extinction volume for split ring resonators will be presented in a forthcoming paper. Forward scattering measurements with bulk material targets introduce new experimental challenges that will be addressed in the future.

Acknowledgments

The financial support by the Swedish Research Council is gratefully acknowledged. The authors also thank Saab Bofors Dynamics, Linköping, Sweden, and in particular Carl-Gustaf Svensson and Mats Andersson for generous hospitality and practical assistance throughout the measurement campaign.

References

[1] L. V. Ahlfors. *Complex Analysis*. McGraw-Hill, New York, second edition, 1966.

[2] C. F. Bohren and D. R. Huffman. *Absorption and Scattering of Light by Small Particles*. John Wiley & Sons, New York, 1983.

[3] G. Dassios and R. Kleinman. *Low frequency scattering*. Oxford University Press, Oxford, 2000.

[4] R. de L. Kronig. On the theory of dispersion of X-rays. *J. Opt. Soc. Am.*, **12**(6), 547–557, 1926.

[5] M. Gustafsson, C. Sohl, and G. Kristensson. Physical limitations on antennas of arbitrary shape. *Proc. R. Soc. A*, **463**, 2007. doi:1098/rspa.2007.1893.

[6] M. Gustafsson, C. Sohl, and G. Kristensson. Physical limitations on antennas of arbitrary shape. Technical Report LUTEDX/(TEAT-7153)/1–37/(2007), Lund University, Department of Electrical and Information Technology, P.O. Box 118, S-221 00 Lund, Sweden, 2007. http://www.eit.lth.se.

[7] R. E. Kleinman and T. B. A. Senior. Rayleigh scattering. In V. V. Varadan and V. K. Varadan, editors, *Low and high frequency asymptotics*, volume 2 of *Acoustic, Electromagnetic and Elastic Wave Scattering*, chapter 1, pages 1–70. Elsevier Science Publishers, Amsterdam, 1986.

[8] E. F. Knott, J. F. Shaeffer, and M. T. Tuley. *Radar Cross Section*. SciTech Publishing Inc., 5601 N. Hawthorne Way, Raleigh, NC 27613, 2004.

[9] M. H. A. Kramers. La diffusion de la lumière par les atomes. *Atti. Congr. Int. Fis. Como*, **2**, 545–557, 1927.

[10] E. C. Levi. Complex-curve fitting. *IRE Trans. on Automatic Control*, **4**, 37–44, 1969.

[11] R. Newton. Optical theorem and beyond. *Am. J. Phys*, **44**, 639–642, 1976.

[12] R. G. Newton. *Scattering Theory of Waves and Particles*. Dover Publications, New York, second edition, 2002.

[13] G. T. Ruck, D. E. Barrick, W. D. Stuart, and C. K. Krichbaum. *Radar Cross-Section Handbook*, volume 1. Plenum Press, New York, 1970.

[14] D. Schurig, J. J. Mock, and D. R. Smith. Electric-field-coupled resonators for negative permittivity metamaterials. *Appl. Phys. Lett.*, **88**, 041109, 2006.

[15] C. Sohl, M. Gustafsson, and G. Kristensson. Physical limitations on broadband scattering by heterogeneous obstacles. Accepted for publication in J. Phys. A: Math. Theor., 2007.

[16] C. Sohl. *Dispersion Relations for Extinction of Acoustic and Electromagnetic Waves*. Licentiate thesis, Lund University, Department of Electrical and Information Technology, P.O. Box 118, S-221 00 Lund, Sweden, 2007. http://www.eit.lth.se.

[17] C. Sohl, M. Gustafsson, and G. Kristensson. The integrated extinction for broadband scattering of acoustic waves. Technical Report LUTEDX/(TEAT-7156)/1–10/(2007), Lund University, Department of Electrical and Information Technology, P.O. Box 118, S-221 00 Lund, Sweden, 2007. http://www.eit.lth.se.

[18] C. Sohl, M. Gustafsson, and G. Kristensson. Physical limitations on metamaterials: Restrictions on scattering and absorption over a frequency interval. Technical Report LUTEDX/(TEAT-7154)/1–11/(2007), Lund University, Department of Electrical and Information Technology, P.O. Box 118, S-221 00 Lund, Sweden, 2007. http://www.eit.lth.se.

[19] S. Ström. Introduction to integral representations and integral equations for time-harmonic acoustic, electromagnetic and elastodynamic wave fields. In V. V. Varadan, A. Lakhtakia, and V. K. Varadan, editors, *Field Representations and Introduction to Scattering*, Acoustic, Electromagnetic and Elastic Wave Scattering, chapter 2, pages 37–141. Elsevier Science Publishers, Amsterdam, 1991.

[20] E. C. Titchmarsh. *Introduction to the Theory of Fourier Integrals*. Oxford University Press, Oxford, second edition, 1948.